Aix-Marseille Université
École **P**olytechnique **U**niversitaire de **M**arseille
IUSTI - UMR CNRS 7343 -

THÈSE

pour obtenir le grade de
DOCTEUR D'AIX-MARSEILLE UNIVERSITÉ
Discipline : Mécanique et Énergétique
Ecole Doctorale 353: Sciences pour l'Ingénieur
présentée et soutenue publiquement par

Marcos Rojas Cárdenas
le 13 Septembre 2012

Temperature Gradient Induced Rarefied Gas Flow

Le jury est composé de:

Rapporteur	Yogesh B. Gianchandani, Michigan University
Rapporteur	Gian Luca Morini, Universitá di Bologna
Examinateur	Aldo Frezzotti, Politecnico Di Milano
Examinateur	Juergen Brandner, Karlsruher Institut fur Technologie
Examinateur	Lounes Tadrist, Aix Marseille Université
Co-directeur de thése	Pierre Perrier, Aix Marseille Université
Directeur de thése	Irina Graur, Aix Marseille Université
Invité	J. Gilbert Méolans, Aix Marseille Université

Temperature Gradient Induced Rarefied Gas Flow

Marcos Rojas Cárdenas

Ecole polytechnique Universitaire de Marseille

Department of Mechanics and Energetics

Aix - Marseille University

A thesis submitted for the degree of

Doctor of Philosophy

September 2012

“Then he began to pity the great fish that he had hooked. He is wonderful and strange and who knows how old he is, he thought. Never have I had such a strong fish nor one who acted so strangely. Perhaps he is too wise to jump. He could ruin me by jumping or by a wild rush. But perhaps he has been hooked many times before and he knows that this is how he should make his fight. He cannot know that it is only one man against him, nor that it is an old man. But what a great fish he is and what will he bring in the market if the flesh is good. He took the bait like a male and he pulls like a male and his fight has no panic in it. I wonder if he has any plans or if he is just as desperate as I am?”

The old man and the sea
Ernest Hemingway
1952

“Autrefois, car il me semble qu'il y a plutôt des années que des semaines, j'étais un homme comme un autre homme. Chaque jour, chaque heure, chaque minute avait son idée. Mon esprit, jeune et riche, était plein de fantaisies. Il s'amusait à me les dérouler les unes après les autres, sans ordre et sans fin, brodant d'inépuisable arabesques cette rude et mince étoffe de la vie. C'étaient des jeunes filles, de splendides chapes d'évêques, de batailles gagnées, des théâtres plein de bruit et de lumière, et puisse encore des jeunes filles et de sombres promenades sous les larges bras des marronniers. C'était toujours fête dans mon imagination. Je pouvais penser à ce que je voulais, j'étais libre.”

Le Dernier Jour d'un Condamné
Victor Hugo
1829

Acknowledgements

This investigation was conducted in the frame of the Gas Flows in Micro Electro Mechanical Systems project (GASMEMS). My main host institution was the Laboratoire IUSTI UMR7343, Ecole Polytechnique Universitaire de Marseille of the Aix-Marseille University in France, where my work was supervised by Irina Graur, Pierre Perrier and J. Gilbert Méolans. My second host institution was the Advanced Operations and Engineering Services in the Netherlands, where my work was supervised by Gennady Markelov.

The research leading to these results has received funding from the European Communitys Seventh Framework Program (FP7/2007-2013 under grant agreement n 215504).

Abstract

This thesis presents the study and analysis of rarefied gas flows induced by thermal transpiration. Thermal transpiration refers to the macroscopic movement of rarefied gas generated by a temperature gradient. The main aspect of this work is centered around the measurement of the mass flow rate engendered by subjecting a micro-tube to a temperature gradient along its axis. In this respect, an original experimental apparatus and an original time-dependent experimental methodology was developed. The experimental results for the initial stationary thermal transpiration mass flow rate and for the final zero-flow thermal molecular parameters were compared with the results obtained from the numerical solution of the Shakhov model kinetic equation and the direct simulation Monte Carlo method.

Résumé

Ce manuscrit présente l'étude et l'analyse d'écoulements de gaz raréfiés, induits par la transpiration thermique. Le terme de transpiration thermique désigne le mouvement macroscopique d'un gaz raréfié engendré par l'effet du seul gradient de température. L'aspect principal de ce travail est centré autour de la mesure du débit stationnaire déclenché en soumettant un micro tube à un gradient de température appliqué le long de son axe. On a développé cet effet un appareillage expérimental original ainsi qu'une méthodologie expérimentale novatrice basée sur la dépendance du phénomène, analysé dans son ensemble, à l'égard du temps. Les résultats obtenus pour le débit stationnaire initial de transpiration thermique et pour les paramètres thermo-moléculaires caractérisant l'équilibre final de débit nul, ont été comparés aux résultats obtenus numériquement par la résolution de l'équation cinétique modéle de Shakhov et par la méthode de simulation directe de Monte-Carlo.

Contents

List of Figures

Nomenclature

Roman Symbols

a	fitting coefficient axial temperature distribution
$A_{T,L}$	fitting coefficient semi-empirical formula
A	section of the tube
b	fitting coefficient axial temperature distribution
$B_{T,L}$	fitting coefficient semi-empirical formula
$\overline{c}$	mean thermal speed
C	thermal velocity
c	velocity vector
C_T	fitting coefficient semi-empirical formula
c_1, c_2, c_3	velocity components
c_r	relative velocity
D	diameter of the tube
d	molecular diameter
dc	phase space elementary volume
D_{ext}	external diameter of the micro-tube
dr	physical space elementary volume

$\mathbf{F}$	external force
f	single particle distribution function
F_L	fitting coefficient semi-empirical formula
f_0^M	absolute Maxwellian distribution function
f_{loc}^M	local Maxwellian distribution function
f^{BGK}	BGK-model distribution function
f^{mod}	model distribution function
f^S	S-model distribution function
G	reduced flow rate independent from the rarefaction
G_0	reduced thermal transpiration mass flow rate
$G(\alpha)$	slip coefficient function
G_{iso}	reduced Poiseuille mass-flow rate
G_p	Poiseuille coefficient
G^*	reduced flow rate dependent from the rarefaction
G_T	Thermal Transpiration coefficient
H	H function
$J(f, f_1)$	collision integral
k_B	boltzmann constant
l	intermolecular distance or mean molecular spacing
L	characteristic length of the system
L_t	length of the micro-tube
$\dot{M}$	mass flow rate
m	mass

$\dot{M}_p$	isothermal mass flow rate
$\dot{M}_T$	thermal transpiration mass flow rate
$\dot{M}_{T_c}$	thermal transpiration mass flow rate in the cold-side reservoir
$\dot{M}_{T_h}$	thermal transpiration mass flow rate in the hot-side reservoir
N	number of molecules
n	molecular number density
$\mathbf{n}$	vector normal to the surface
p	pressure
P_{ij}	stress tensor
p_{c_f}	final equilibrium pressure in the cold-side reservoir
p_c	pressure in the cold-side reservoir
p_{h_f}	final equilibrium pressure in the hot-side reservoir
p_h	pressure in the hot-side reservoir
p_i	pressure at the beginning of the experiment
$\mathbf{q}$	heat flux
Q	generic macroscopic quantity
$\mathbf{r}$	position vector
R	specific gas constant
S	surface
T	temperature
t	time
t_0	starting time of the experiment
T_{av}	average temperature

T_c temperature in the cold-side reservoir

t_f time at the final equilibrium stage

T_h temperature in the hot-side reservoir

t^* transitional time

$\mathbf{u}$ bulk velocity

V_B big volume of known dimensions

V_c volume of the cold-side reservoir

V_h volume of the hot-side reservoir

V_t test volume

x, y, z coordinates in physical space

Greek Symbols

α accommodation coefficient

δ rarefaction parameter

δ_p isothermal rarefaction parameter

δ_T non-isothermal rarefaction parameter

ν collision frequency

γ thermal molecular pressure exponent

κ thermal conductivity

λ molecular mean free path

ψ collision invariants

ρ density

$\sigma d\Omega$ differential cross-section

τ characteristic time

tau_0 sitting time of a molecule over a surface

τ_c characteristic time in the cold-side reservoir

τ_h characteristic time in the hot-side reservoir

μ viscosity

$\overline{\nu}$ mean collision rate

Subscripts

L Liang coefficient

T Takaishi and Sensui coefficient

Acronyms

BE Boltzmann equation

BGK Bhatnagar-Gross-Kook model

CDG capacitance diaphragm gauge

CH cell height

CW cell width

DSMC Direct simulation Monte Carlo

DTM time step

DVM discrete velocity method

ES ellipsoidal statistical model

HS hard-sphere model

Kn Knudsen number

NS Navier-Stokes equation

PV pressure variation with time

PVS pressure variation speed

R	kernel function
S	Shakov model
tp	thermocouple
TPD	thermal molecular pressure difference
TPR	thermal molecular pressure ratio
TS	Takaishi and Sensui
VHS	variable hard-sphere model
VSS	variable soft-sphere model
vmp	most probable velocity

Résumé en français

Ecoulement d'un gaz raréfié induit par gradient thermique: la transpiration thermique

Présentation du phénomène

La transpiration thermique désigne le mouvement macroscopique qui se produit dans un gaz raréfié sous la seule influence d'un gradient de temperature établi le long de la paroi solide du conduit. Le gaz se déplace dans la direction du gradient de température, de la zone la plus froide vers la zone la plus chaude. Aux extrémités du conduit se trouvent généralement deux réservoirs respectivement maintenus à la température d'entrée et de sortie du conduit. Entre ces deux réservoirs n'existe aucune différence de pressions initiales ni aucune différence de constitutions chimiques. Ce fait physique dont la description phénoménologique peut paraitre assez simple se révèle en fait dune nature assez complexe. Il est donc intéressant d'approfondir l'ensemble des aspects de l'interaction gaz/surface qui sont à l'oeuvre dans la mise en mouvement du gaz qui semble engendré principalement par un échange de quantité de mouvement entre le fluide et la paroi du conduit.

Maxwell [1879] écrit à ce sujet que "la vitesse (du gaz le long de la paroi) et la contrainte tangentielle correspondante sont liées aux inégalités de températures le long de la surface du solide (contenant le gaz) qui donnent naissance à une force entrainant le gaz le long de la surface des zones les plus froides vers les zones les plus chaudes". Recemment Sone [2007] reprit à son compte ce concept en le développant un peu. Il précisa avec pertinence que le bilan de quantité de mouvement échangé entre un élément de surface de paroi et les molécules d'une particule fluide montrait l'existence d'une force résultante appliquée au gaz dans la direction du gradient thermique. Il en résulte l'apparition d'un écoulement et l'existence d'un débit massique. Les résultats théoriques de Maxwell et Sone obtenus sur la base d'une approche cinétique identifie donc lexistence d'une force qui engendre le déplacement du gaz. Dans le panorama actuel de l'état de l'art on voit peu d'études sur la physique qui est à l'oeuvre dans le déplacement du gaz sous l'action de la force crée par la transpiration thermique. Ce qui a été

principalement étudié à ce jour, c'est la phase finale d'équilibre qui s'établit au terme de la phase transitoire: le débit massique net s'annule alors sous les effets antagonistes du gradient de température et d'un différentiel final de pression crée par le mouvement du fluide pendant la phase transitoire, entre le réservoir de sortie et le réservoir dentrée.

Reynolds [1879] découvrit expérimentalement ce phénomène en imposant deux températures différentes entre deux régions (réservoirs) de dimensions finies, séparées par une plaque de matériaux poreux. La plaque assurait, à travers ses pores, un état de raréfaction du gaz dont toute l'importance sera explicitée plus loin. Au terme de ces expériences Reynods constata que dans l'état final où le débit s'annule, la pression du gaz dans la zone la plus chaude était plus élevée que la pression dans la zone la plus froide. Cette phase d'équilibre final, caractérisée par un débit nul fut comprise et expliquée pour la première fois par Knudsen en 1909. Knudsen [1909] eut l'intuition que c'est l'écoulement engendré initialement par la transpiration thermique (c'est à dire par le seul gradient thermique) qui crée une différence de pression entre les deux régions. Ensuite cette différence de pression induite crée un contre écoulement de type Poiseuille qui se superpose à l'écoulement de transpiration thermique initial et qui dans l'état "d'équilibre final" le compense complétement. Finalement, à ce stade ultime, le débit net s'annule. Cet état d'équilibre final à débit nul a été largement étudié dans la littérature, donnant lieu à plusieurs publications.

Motivations de cette étude

Dans ce travail nous introduisons une nouvelle approche expérimentale avec laquelle nous analysons le mouvement macroscopique du gaz: ce mouvement induit par transpiration thermique se développe dans un micro tube connecté à deux réservoirs. Nous obtenons ainsi des résultats pour les débits stationnaires générés par la transpiration thermique. Ces résultats sont obtenus en utilisant une méthode expérimentale basée sur la technique dite à "Volumes Constants". Comme on le sait cette méthode a été mise au point pour des écoulements isothermes stationnaires. Elle n'avait jamais été adaptée pour ce type découlements.

Loriginalité méthodologique de notre approche tient aussi à ce qu'elle englobe

l'aspect instationnaire du phénomène, prenant en compte et décrivant aussi l'étape transitoire qui conduit d'un phénomène initial stationnaire jusqu'à létape finale d'un "équilibre à débit nul". On suit ainsi, et l'on illustre aussi, l'intuition de Knudsen qui comme on l'a vu précedemment, avait pressenti la nature de cet écoulement transitoire entre deux états stationnaires. Ainsi donc la phase initiale de l'étude permet la mesure du débit stationnaire de transpiration thermique, pleinement établi et non perturbé. Mais l'étude déborde très largement cette phase initiale, vers une étude instationnaire, qui permettra notamment de mieux definir la phase initiale.

Concrétement les mesures concernent le suivi de l'évolution temporelle de la pression dans les réservoirs d'entrée et de sortie d'un micro-tube. La mesure démarre juste après qu'un événement extérieur modifiant le circuit survienne comme un déclencheur. C'est la fermeture d'une vanne qui, limitant le volume des réservoirs, permet qu'une variation de pression se produise dans les réservoirs d'entrée et de sortie. Elle permet du même coup le début de la mesure. Dès lors nous pouvons détecter l'écoulement engendré par la transpiration thermique à travers un seul micro-tube, le long duquel un gradient de température axial est imposé. Dans la première phase nous pouvons notamment en déduire la mesure du débit stationnaire de transpiration thermique. Comme on l'a évoqué plus haut, l'investigation permet ensuite de suivre le déplacement du gaz dans la phase transitoire jusqu'á l'état final de débit nul.

Nous pouvons ainsi obtenir des résultats plus généraux conduisant à d'importantes informations sur un microsystème fluidique actionné par un gradient de température. Nous avons ainsi introduit dans ce travail un approfondissement de la connaissance de la physique qui gouverne l'évolution temporelle de l'écoulement déclenché par la transpiration thermique.

Désormais nous pouvons envisager une large analyse de l'évolution des paramètres thermiques pendant la phase transitoire de l'écoulement. Ce travail a été entrepris ici, à travers l'étude de la pression p, de la vitesse de variation dp/dt de cette pression, mesurées dans les réservoirs, à travers aussi l'étude des temps caractéristiques régissant cette évolution.

De plus nous avons montré que le méthode expérimentale mise en oeuvre permettait une extraction très précise des paramètres régissant l'équilibre final de débit nul: on a ainsi analysé le "rapport des pressions thermiques d'équilibre" (thermal molecular pressure ratio, TPR), la différence des pressions thermiques d'équilibre (thermal molecular pressure difference, TPD) et enfin l'exposant γ du rapport des pressions d'équilibre (thermal molecular pressure exponent). Les résultats obtenus à l'équilibre final ont été comparés à d'autres résultats expérimentaux obtenus dans la littérature.

En fin nous avons validé nos résultats concernant le débit stationnaire de transpiration thermique ainsi que les paramètres caractérisant l'état final de débit nul, en les comparant aux résultats numériques correspondants, obtenus par diverses métodes: nous avons utilisé notamment pour cela la simulation directe Monte-Carlo (DSMC) et la version linéarisée de l'equation cinťique modèle de Shakhov (S-model).

Propriétés fondamentales de l'état des fluides utilisés: le gaz dilué

Importance et définition du gaz dilué. Les recherches expérimentales et numériques rapportées ici ont été conduites pour des gaz dits raréfiés et plus précisèment dans des régimes d'écoulement allant d'un régime moléculaire libre proche jusqu'au régime de glissement. Avant de définir les paramètres qui caractérisent la raréfaction d'un gaz il est essentiel de définir le gaz dilué car les conditions de "dilution" constituent la base sur laquelle la théorie ciétique est fondée. C'est sur de tels gaz que nous travaillons: cést pourquoi nous introduisons ces concepts au début de de la présentation détaillée du travail. La principale condition que doit respecter le fluide pour être considéré comme un gas dilué est que sa distance intermoléculaire moyenne (ou encore son espacement intermoléculaire moyen) qui est bien entendu la moyenne des distances entre deux molécules les plus proches, doit être grande par rapport au diamètre moléculaire.

$$d/l << 1, \tag{1}$$

où l est defini approximativement á partir du nombre de molécules contenues dans

une sphère, soit

$$l = n^{1/3}, \tag{2}$$

oú n est le nombre de molécules par unité de volume, c'est à dire la densité numérique.

Dans un gaz dilué, la probabilité pour que se produise une collision binaire (impliquant seulement deux molécules) est très grande devant celles relatives aux collisions impliquant plus de deux partenaires. Dans la construction de la théorie cinétique classique (notamment dans l'établissement de l'équation de Boltzmann) la gaz est supposé dilué et seules les collisions binaires sont prises en compte. Nous allons maintenant introduire les conditions qui permettent d'estimer le degré de raréfaction d'un gaz et le régime d'écoulement dans lequel il se meut. Pour ce faire nous allons introduire le nombre de Knudsen qui exprime le rapport entre le libre parcours moyen λ et la dimension caractéristique du système L (généralement la plus petite de ses dimensions géomètriques)

$$Kn = \lambda/L. \tag{3}$$

Le libre parcours moyen moléculaire est la distance moyenne parcourue par une molécules entre deux collisions moléculaires successives. Il est défini dans un fluide au repos (où dans le repère du centre de masse de la particule fluide) c'est pourquoi il peut être formellement défini comme le produit de la vitesse moyenne d'agitation thermique c, multiplié par le temps moyen entre collisions, ou divisé par la fréquence moyenne de collisions par molécule ν, soit

$$\lambda = \bar{c}/\bar{\nu}. \tag{4}$$

Il est évidemment difficile de mesurer directement la vitesse thermique moyenne où la fréquence moyenne de collision par molécule, mais le libre parcours moyen peut aussi être exprimé à l'aide de paramétres macroscopiques physiques tels que la pression, la température et la viscosité. Cette expression (dépendant du modèle d'interaction inter-moléculaire) est donnée et utilisée dans le Chapitre 5.

L'utilisation du nombre de Knudsen. Le nombre de Knudsen précédement introduit sert d'indicateur pour classer les différents états de raréfaction du gaz.

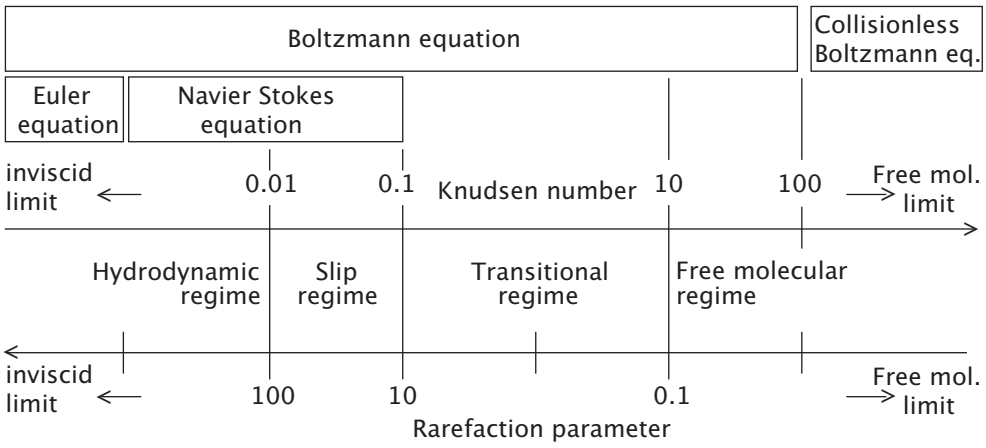

Figure 1: Schèma du spectre des régimes de rarefaction suivant le nombre de Knudsen

Avant de décrire le spectre de ces états de raréfaction, il convient de préciser la nature de cette raréfacion. On voit bien que puisqu'elle est caractérisée par un rapport où intervient la dimension du systéme elle n'est pas seulement liée (et inversement proportionnelle) à la densité numérique du fluide mais aussi et surtout au nombre de molécules présentes dans le système considéré. On verra aussi qu'elle est un bon indicateurs de l'importance relative de certains effets de paroi sur le fluide. Ainsi définis les états de raréfaction du fluide constituent un spectre dans lequel on distingue généralement quatre régimes principaux. Soit encore, du plus raréfié (correspondant aux nombres de Knudsen les plus forts) aux moins raréfié (correspondant aux nombres de Knudsen les plus faibles): le régime moléculaire libre, le régime transitionnel, le régime de glissement et le régime hydrodynamique (voir Figure 1).

Le cas limite du régime moléculaire libre où le fluide est fortement raréfié et ne peut plus être traité comme un milieu macroscopiquement continu, correspond asymptotiquement à un nombre de Knudsen tendant vers l'infini. Le cas limite du régime hydrodynamique où les hypothèses du milieu continu sont totalement valides, correspond asymptotiquement à un nombre de Knudsen tendant vers zéro.

Dans les cas où les hypothèses du milieu continu sont vérifiées, l'écoulement peut-être traité en utilisant les équations de conservation macroscopiques telles que

les équations de Navier-Stokes. Ces équations peuvent fournir des informations détaillées sur les paramètres macroscopiques du fluide en écoulement, tels que la pression, la température, où la vitesse du gaz. L'approche continue est considérée comme fondée jusqu'à des nombres de Knudsen de l'ordre de 0.2 (Bird [1995]) oú 0.3 suivant les auteurs, c'est à dire pour le régime hydrodynamique et pour le régime de glissement.

En régime hydrodynamique (approximativement $Kn < 0.01$) le libre parcours moyen est très faible devant la dimension caractéristique du système. Le nombre de collisions est très élevé et l'on peut considérer qu'en tout point le fluide atteint un équilibre local. Dans ce régime on peut considérer le fluide comme un milieu macroscopiquement continu composé de particules de fluide macroscopiques élémentaires. Dans ce contexte en utilisant les équations de Navier-Stokes, il est donc possible d'obtenir directement les paramètres macroscopiques du fluide qui ne dépendent que des variables d'espace et de temps, qui sont les variables indépendantes du système.

En régime de glissement (c'est à dire pour des nombres de Knudsen définis par $0.01 < Kn < 0.3$), les hypothèses du milieu continue restent valables pour lessentiel mais pour obtenir une bonne description macroscopique les équations de Navier-Stokes doivent être associées à des conditions de paroi faisant apparaitre une vitesse de glissement tangente à la paroi et un saut de température entre le solide et le gaz qui est à son contact. Pour prolonger la validité de l'équation continue il faut donc renoncer au conditions limites classiques d'adhérence (pour la vitesse) et de continuité (pour la température).

Pour les régimes qui vont du régime transitionnel au régime moléculaire libre l'hypothèse du milieu continu n'est plus pertinente. Dans le régime moléculaire libre (pour un nombre de Knudsen supérieur à 10 ou 15), les collisions entre molécules sont rares ou absentes rendant les collisions gaz/paroi prépondérentes: il est alors possible de considérer le mouvement de chaque molécule (ou de chaque famille de molécules, définie par une vitesse moléculaire) de façon indépendante. Ainsi pour définir les caractéristiques de l'écoulement il devient très important de prendre correctement en compte l'intéraction gaz/paroi, par exemple par des condition limites cinétiques traduites par l'opérateur Kernel (Cercignani [1972]).

D'autre par la modélisation de la théorie cinétique est évidemment également indispensable pour modéliser le "mouvement du gaz" (à travers la détermination de la fonction de distribution des molécules par l'équation cinétique).

En régime transitionnel (pour des nombres de Knudsen définis par ($0.3 < Kn < 10$ ou 15) le nombre de collisions intermoléculaires augmente et le nombre de collisions gaz/gaz devient à peu près de même ordre que le nombre de collisions gaz/paroi mais le fluide ne peut encore être considéré comme un milieu continu. C'est pourquoi le modèle cinétique est toujours nécéssaire. Comme pour le cas du régime moléculaire libre, ce modèle cinétique est requis tant au niveau de l'évolution des familles de molécules au sein du gaz (équation cinétique, équation de Bolzmann, par exemple) qu'au niveau des conditions limites cinétique gaz/paroi (par exemple loi de réflexion diffusive-spéculaire formulée au moyen de l'opérateur kernel Maxwellien). Il faut encore noter que l'approche cinétique est valable sur tout le spectre de la raréfaction sans limitation aucune.

Les modèles cinétiques classiquement utilisés pour l'étude des écoulements raréfiés en régimes transitionnel où moléculaire libre sont basés sur léquation de Boltzmann qui décrit statistiquement le fluide à travers la fonction de distribution des familles de molécules. On obtient ensuite les paramètres macroscopiques qui correspondent à divers moments de la fonction de distribution. Sans entrer dans les détails du bilan conduisant à l'équation de Boltzmann, on peut noter que, du point de vue de sa structure mathématique, cette équation est une équation intégro-différentielle où la fonction de distribution recherchée dépend a priori de sept variables: le vecteur d'espace, le vecteur de vitesse moléculaire, et le temps. La résolution de l'équation de Boltzmann permet de décrire l'évolution de la fonction de distribution dans l'espace et le temps et ceci quelque soit l'état de raréfaction du système dès lors que le milieu est un milieu dilué.

La structure de l'équation précédemment décrite permet de pressentir la difficulté d'une résolution de l'équation de Boltzmann sous sa forme complète. Aussi on a souvent recours à des formes plus simples (et moins rigoureuses) de l'èquation cinétique. Outre la résolution de l'équation de Boltzmann linéarisée, on recourt aujourd'hui à deux principales approches pour résoudre numériquement l'équation de Boltzmann.

Il s'agit d'abord de l'approche de simulation directe de Monte-Carlo qui traite statistiquement l'évolution des molécules en deux étapes; celle du mouvement sans collision (ou entre collisions) et celle de l'interaction intermoléculaire; sans s'attaquer à la résolution de l'équation de Boltzmann, le traitement reproduit ici l'analyse qui conduit à l'équation de Boltzmann. Il sagit ensuite des approches cinétiques d'ecrites par des équation cinétiques dites "équations modéles": justifiées souvent d'abord phénoménologiquement, mais parfois aussi théoriquement au moins en partie, elles constituent des approximations de l'équation de Boltzmann dont elles reproduisent certains résultats essentiels. On peut citer l'equation BGK (Bhatnagar, Gross et Krook), puis l'équation modèle de Shakhov (S-modèle) et le modèle statistique ellipso¨dal (ES modèle). Ces deux derniers modèles sont parfois préférés à l'équation BGK parce qu'ils fonctionnent avec un nombre de Prandtl plus réaliste. La résolution de ces différentes approximations de l'équation de Boltzmann font généralement appel à la méthode de discrétisation des vitesses (DVM).

En pratique on introduit souvent une autre forme du nombre caractérisant l'état de raréfaction du gaz. Cette forme, est inversement proportionnelle au nombre de Knudsen

$$\delta \sim 1/Kn. \tag{5}$$

Ce nombre appelé paramètre de raréfaction est directement proportionnel à la densité du fluide. Il a ainsi semblé plus pratique à certains auteurs. C'est pourquoi nous adopterons ce nombre (et non le nombre de Knudsen) pour présenter nos résultat à travers les differents états de raréfaction.

Les écoulements de gaz raréfiés sont étudiés classiquement dans les applications de la recherche spatiale ou dans les systèmes qui travaillent dans des conditions de vide poussé. Dans ces dernières décennies la taille courante des microsystèmes est passée au dessous du micron; ainsi le libre parcours moyen du fluide est souvent du même ordre que la dimension caractéristique du système et le gaz peut-être considéré comme raréfié même pour des pressions relativement élevées. A cet égard, l'éclosion des systèmes micro-electro-mécaniques (MEMS) a élargi considérablement le domaine oú les écoulements de gaz raréfiés présentaient de

l'interêt: elle a ainsi ouvert de nouvelles perspectives à l'étude de ces écoulements et notamment à l'étude de la transpiration thermique. Des applications de ces écoulements peuvent être trouvées dans de nombreux microsystèmes récemment créés: dans la chromatographie en phase gazeuse, dans les systèmes de contrôle de précision des écoulements, dans les compresseurs, dans les systèmes de refroidissement, dans les évaporateurs; et cette liste n'est pas exhaustive.

Structure du manuscript

Ce manuscrit se divise en huit chapitres et sa structure est construite en accord avec le déroulement de notre investigation sur la transpiration thermique.

Dans un premier chapitre d'introduction on présente le phénomène de transpiration thermique et les raisons qui nous ont conduits à nous intresser à cette étude. Nous définissons le cadre dans lequel la recherche a été développée et nous introduisons les conditions requises pour obtenir le phénomène de transpiration thermique comme la raréfaction du gaz.

Le Chapitre 2 nous permet de préciser les concepts essentiels de la théorie cinétique qui est le socle théorique permettant l'étude du phénomène considéré ici. Nous avons exposé les notions fondamentales qui nous ont paru nécessaires pour comprendre et interpréter les résultats expérimentaux et les résultats numériques obtenus dans ce travail. C'est pourquoi nous avons introduit la fonction de distribution de la vitesse, la distribution Maxwellienne, l'équation de Boltzmann, ainsi que l'opérateur kernel relatif aux conditions limites cinétiques qui sont nécessaires pour clore le système de l'équation de Boltzmann. De plus nous avons donné une description des équations cinétiques "modéles" telles que l'équation BGK et l'équation S-modèle et nous avons introduit la méthode de simulation directe de Monte-Carlo.

Ensuite, le Chapitre 3 est consacré au développement d'une revue bibliographique des travaux portant sur le phénomène: les principales recherches entreprises sur le sujet de Reynolds à nos jours y sont analysées en détail. Dans cette revue lon sefforce de distinguer les approches expérimentales et les approches théoriques tout en essayant de rapprocher les résultats provisoires respectifs. Une attention

particulière a été portée à la découverte du phénomène où les principaux concepts reliés aux effets de la transpiration thermique son traités et les mécanismes pouvant expliquer le déplacement du gaz par une inégalité de température à la surface du conduit sont largement discutés. Ainsi les discussions de Maxwell soulignant l'attention qu'il faut porter aux conditions de surface apparaissent d'un interêt tout particulier, de même que la nécessité qu'il souligne de trouver un chemin pour modéliser le mécanisme de l'interaction gaz/paroi. La discussion sur ce thème est toujours d'actualité. Nous avons aussi concentré notre attention sur les recherches de plusieurs auteurs portant sur le développement de formules semi-empiriques encore utilisées aujourd'hui, pour caractériser notamment "leffet de pompage" de la transpiration thermique. De plus nous avons remarqué que si la dépendance du phénomène à l'égard du temps avait déjà été observée expérimentalement aucun des auteurs concernés dans ces observations n'avait donné un aperçu détaillé sur les causes d'un tel phénomène; en outre aucun de ces auteurs n'avait fait de recherche sur la manière dont la variation de pression dans le temps pouvait dépendre de la nature du gaz, de son degré de raréfaction ou encore de la différence de température appliquée aux extremitées de la paroi du micro-tube.

Finalement nous avons essayé de regrouper les derniers résultats sur le sujet en analysant les études numériques et expŕimentales relatives aux caractéristiques d'un écoulement stationnaire d'un gaz , actionné par un gradient thermique dans un micro-tube. Nous avons conclu que l'écoulement de gaz induit par transpiration thermique n'avait jamais été expérimentalement quantifié avec précision et rigueur.

Le Chapitre 4 a été consacré à l'appareillage expérimental. Nous y avons décrit en détail, l'articulation de l'ensemble des composants qui nous ont permis de créer le micro système fluidique, les caractéristiques essentielles des instruments de mesure utilisés ainsi que la technique employée pour déterminer les dimensions des réservoirs. Nous avons consacré aussi une partie importante de ce chapitre à lanalyse du gradient thermique sur la température externe de la surface, à la précision des mesures de température ainsi qu'à l'étalonnage des sondes de pression compte tenu de l'effet parasite de transpiration thermique auquel ces sondes sont soumises. Finalement nous avons proposé une analyse des problèmes rencontrés avec le premier dispositif expérimental. Cette analyse nous a permis d'obtenir ensuite de bien meilleurs résultats expérimentaux: c'est pourquoi il nous a semblé indispensable

de présenter une brève discussion sur ce point.

Dans le Chapitre 5 nous avons expliqué en détail la méthodologie de notre investigation expérimentale. Nous avons décrit la manipulation de l'appareillage qui permet de créer un écoulement de transpiration thermique globalement dépendant du temps, le long de l'axe du micro tube de verre. Dans ce chapitre deux concepts fondamentaux sont introduits pour désigner deux phénomènes se produisant dans le microsystème. Le premier concept est celui de l'écoulement stationnaire de transpiration thermique, complétement établi et non perturbé et qui constitue la phase initiale d'un phénomène globalement évolutif. Le second concept est celui du brutal changement, imposé de l'extérieur, dans la configuration du système expérimental: concrètement ce concept est matérialisé par la fermeture d'une vanne qui perturbe la stationnarité de l'écoulement, en limitant la capacité des réservoirs. Des lors les pressions vont évoluer dans le temps et l'écoulement se voit contraint à l'évolution temporelle. On montre ainsi comment la stationnarité puis l'instationnarité ont pu s'illustrer tour à tour à travers le contrôle de la variation de pression, à l'entrée et à la sortie du capillaire, juste aprés le brutal changement originel. Dans la suite du chapitre nous avons montré plus précisèment comment le débit de transpiration thermique stationnaire pouvait être déduit de la variation de pression dans le temps juste à lorigine (i.e., juste après la fermeture de la vanne). Nous avons montré aussi que la variation de pression dans le temps pouvait être traduite par une fonction exponentielle et nous avons enfin décrit comment chaque résultat expérimental pouvait être caractérisé comme fonction du paramètre de raréfaction du gaz.

Dans le Chapitre 6 nous avons présenté les résultats de nos expériences. Nous avons analysé l'évolution des pressions de réservoir, p(t) en fonction du temps, ainsi que l'évolution de la "vitesse" $dp(t)/dt$ de cette variation de pression. Nous avons étudié aussi le temps caractéristique du système Nous avons déduit d'abord de ces différents paramètres, le débit stationnaire de transpiration thermique qui perdure pendant la phase initiale de l'évolution du système. Enfin, à partir des valeurs asymptotiques des paramètres de pression nous avons obtenu aussi les paramètres caractérisant l'état d'équilibre final de débit nul, cést à dire la différence des pressions thermiques d'équilibre final (TPD), le rap- port des pressions thermiques d'équilibre final (TPR) et l'exposant de ce rapport de pressions ther-

miques d'équilibre. Tous ces résultats ont étés obtenus pour diverses différences de températures appliquées le long du tube et pour trois gaz différents (Argon, Azote, Hélium) sur un large domaine de conditions de raréfaction (du proche régime moléculaire libre jusqu'au régime de glissement).

Dans le Chapitre 7 nous avons présenté les résultats numériques obtenus sur la base de la théorie cinétique ou de la méthode de simulation directe. Ces résultats ont été comparés aux résultats expérimentaux obtenus dans un but de validation. La première partie du chapitre a été consacrée à la description des méthodes numériques utilisées: d'une part l'utilisation du S-modèle de Shakhov. Cette équation, voisine de l'equation de BGK présente l'avantage de correspondre à un nombre de Prandtl réaliste, au moins pour les molécules monoatomiques (ce qui comme on le sait n'est pas le cas de l'équation BGK). On a utilisé ici la version linéarisée de l'équation S-modèle, ce qui semble permis par la relative faiblesse des gradients. D'autre part on a utilisée aussi la méthode de simulation directe de Monte-Carlo (DSMC). Ensuite une comparaison a été faite entre résultats expérimentaux et résultats numériques en ce qui concerne les paramètres de l'état d'équilibre de débit nul, c'est à dire pour le rapport des pressions thermiques d'équilibre (TPR), la difference de pressions thermiques d'équilibre (TPD) et lexposant γ du rapport des pressions thermiques d'équilibre. Par ailleurs les résultats numériques relatifs à la distribution des paramètres thermodynamiques et de la vitesse macroscopique le long du tube, ont été donnés.

Nous avons également donné une comparaison entre résultats expérimentaux et résultats numériques, respectivement obtenus pour le débit massique stationnaire de transpiration thermique. Finalement nous avons développé une étude que linteraction gaz/surface pourrait avoir sur l'exposant γ et sur le débit massique de transpiration thermique. Enfin nous avons décidé de consacrer un chapitre destiné aux perspectives possibles de ce travail (chapitre 8). Cette dernière partie est considérée par l'auteur comme un effort pour mieux définir ce travail dans sa totalité en explorant les pistes qu'il permet d'ouvrir. Dans cette partie nous avons notamment essayé de donner des éléments de preuves de l'existence d'un contre écoulement de Poiseuille qui à l'équilibre final contrebalancerait le débit stationnaire de transpiration thermique à partir duquel le processus transitoire a demarré. Pour cela nous avons tenté de montrer que pour un débit stationnaire de transpiration

thermique donné (et mesuré) le contre écoulement de Poiseuille équivallent était engendré par une différence de pression égale ou voisine à la TPD expérimentale obtenue pour le dèbit de transpiration thermique considéré.

De plus nous avons également développé une étude isotherme. L'un des buts de cette étude était de valider le montage expérimental (semblable à celui utilisé pour les expériences non-isothermes précédemment décrites) en utilisant ce montage pour retrouver des résultats (iso-thermes) obtenus précédemment. Ensuite l'idée fut de hiérarchiser l'importance de l'intéraction gaz/surface (i.e. aussi celle de l'accommoda- tion du gaz à la paroi) suivant les valeurs respectives des masses volumiques des différents gaz. Cette hiérarchie fut comparée avec celle obtenue pour l'accommodation dans l'écoulement (non-isotherme) de transpiration thermique. Quelques premiers commentaires furent développés pour expliquer les divergences.

Enfin, cette étude annexe a montré, que pour la mesure du débit stationnaire, le processus isotherme pouvait lui aussi être traité avantageusement comme la phase initiale d'un processus globalement dépendant du temps.

"24. No fear or shame in the dignity of
yr experience, language & knowledge"

Belief & Technique For Modern Prose: a list of 30 essentials
Jack Kerouac
1958

Chapter 1

Introduction

Thermal transpiration

Thermal transpiration refers to the macroscopic movement in a rarefied gas induced by a temperature gradient distributed along the solid surface bounding the fluid. The gas moves in the temperature gradient direction, from the lower to the higher temperature zone. In order to investigate a pure thermal transpiration flow, it is necessary to have a gas without any initial difference of pressure or any difference in chemical constitution. This phenomenon, which can allegedly appear simple from its definition, is of a very complex physical nature. Therefore, it is of interest to comprehend the whole complexity of the gas-surface interaction accompanying such gas displacement, which derives mainly from a momentum exchange between the fluid itself and the solid surfaces along which the inequalities of temperature are distributed.

Maxwell [1879] wrote on the subject that "[...the gas] velocity [at the surface] and the corresponding tangential stress are affected by inequalities of temperature at the surface of the solid (containing the gas), which give rise to a force tending to make the gas slide along the surface from colder to hotter places". More recently Sone [2007] regained possession of this concept and wrote that it is possible to show [mathematically] that the balance of momentum exchange between an elementary wall surface and the molecules of a fluid particle results in a force which is applied to the gas in the temperature gradient direction, thus a mass flow rate is engendered. Both Maxwell's and Sone's theoretical research, which were made

on the basis of a molecular approach, that is the kinetic theory, identified then a "force" which engenders the gas displacement. At the present state of the art the physics behind a gas displaced by a force engendered by thermal transpiration have been rarely investigated.

What has been mainly considered is the final zero-flow equilibrium stage, where the net mass flow rate along the system is zero and a final pressure equilibrium state is generated by the macroscopic movement of the gas. Reynolds [1879] experimentally discovered this phenomenon by imposing two different temperatures to two regions of finite dimensions which were separated by a porous plug. The porous plug assured the state of rarefaction of the gas whose importance we will discuss later. As a result of his experiment, Reynolds found that, in the final state, the pressure in the hotter region is higher in respect to the pressure in the colder region.

This final zero-flow equilibrium state was firstly understood and well explained by Knudsen [1909]. He had the intuition that it was a thermal transpiration flow which created a difference of pressure in the two regions. Meanwhile, this induced difference of pressure creates a counter directed Poseiulle flow which, in the final state of the experiment, fully compensated the initial thermal transpiration flow. Thus, the net mass flow rate in the system had to be zero. This final zero-flow equilibrium has been largely studied in the literature giving birth to several publications on the topic.

Motivation of this work

In the present work we introduced a different experimental approach to thermal transpiration by investigating the macroscopic gas displacement induced along a single micro-tube by a temperature gradient applied along its axis. Thus, we reported here the results for a stationary thermal-transpiration-induced mass flow rate. These experimental results were obtained with an original experimental methodology that was developed on the basis of the constant volume technique.

The innovation and originality of our experimental approach derives from us considering thermal transpiration as a time dependent phenomenon. This was done

by using Knudsen's intuition of a transient gas displacement stage in between two equilibrium stages. Thus, the experimental methodology consisted on the tracking of a pressure variation with time at the inlet and outlet of the micro-tube, which was triggered by an induced instantaneous configuration shift of the experimental apparatus.

The pressure variation with time was measured inside two reservoirs which were positioned at the inlet and outlet of the micro-tube. By taking this methodology as a pattern we were able to follow the flow engendered by thermal transpiration through a single glass micro-tube and thus we could deduce the mass flow rate at the initial instant of the pressure variation, where the thermal transpiration mass flow rate was stationary, fully-developed, uni-directed and not-perturbed.

During the investigation process we realized that, by studying the thermal transpiration flow by a technique that could follow the transient gas displacement, we were capable to obtain results that could be exploited in a broader way, and that led to important information on the time-dependency of the evolution of a flow which had a temperature field as unique driver.

Thus, we measured not only the stationary and fully developed thermal transpiration mass flow rate, but also the whole evolution with time of the phenomenon, that is from an initial state of equilibrium where a stationary mass flow rate was engendered, to a final state of equilibrium where the net mass flow rate that transits across any section of the tube is zero.

Consequently, in this work, we introduced a novel analysis of the physics governing the time dependency of a flow induced by thermal transpiration. Henceforth, we would like to present a wide analysis on the thermodynamic parameters that evolved with time during the transient gas displacement phase, that is the pressure variation with time, the pressure variation speed and the characteristic time of the micro-fluidic system.

In addition, we showed that, by using this experimental methodology, it was also possible to extract, with high experimental accuracy, the parameters characterizing the final zero-flow equilibrium stage of the process, such as the thermal molecu-

lar pressure exponent, the thermal molecular pressure difference and the thermal molecular ratio exponent. In order to put our experimental findings into context, we compared the zero-flow equilibrium experimental results with results obtained from the literature.

Finally, we compared our experimental results for the stationary mass flow rate and the final zero-flow stage parameters to results obtained by means of the direct simulation Monte Carlo (DSMC) method and the linearized solution of the Shakov (S) model kinetic equation.

Dilute gas

The present experimental and numerical investigation was conducted for gases in rarefied conditions, namely for near free molecular to slip regime.

Before defining the parameters which characterize the gas rarefaction it is essential to define the dilute gas, since the dilute conditions are the basis on which the classic kinetic theory is founded and therefore the concepts which will be subsequently introduced.

The main condition that a fluid has to respect in order to be considered as a dilute gas, is that the intermolecular distance, or mean molecular spacing l, which is the average distance between molecules in a gas, has to be large in respect to the molecular diameter d

$$\frac{d}{l} \ll 1, \tag{1.1}$$

where l is defined as $l = n^{-1/3}$ and n is the number of molecules per unit volume, that is the number density.

In a dilute gas the probability of binary molecular collisions is preponderant in respect to intermolecular collisions between more than two molecules.

Lets now introduce the conditions over which a gas can be considered as rarefied and hence lets introduce the Knudsen number, which correlates the molecular mean free path λ and the characteristic length of the system L. The Knudsen

number therefore responds to the following definition

$$Kn = \frac{\lambda}{L}. \tag{1.2}$$

The molecular mean free path is the average distance travelled by a gas molecule between collisions. It is defined for a fluid at rest and it is therefore equal to the mean thermal speed of the molecule $\overline{c}$, divided by the mean collision rate per molecule $\overline{\nu}$

$$\lambda = \frac{\overline{c}}{\overline{\nu}}. \tag{1.3}$$

It is obviously difficult to measure the mean thermal speed of the molecule and the mean collision rate per molecule, but the mean free path can also be relied to macroscopic physical parameters such as the pressure, the temperature, the viscosity and the specific constant of the gas, which are quantities that can be measured or can be found in the literature. This definition will be given in more details in Section 5.3 when we will use the rarefaction parameter in order to depict a single experiment.

The Knudsen number defines different states of rarefaction of the gas. The whole spectrum of rarefaction of a fluid can be divided in four regimes *i.e.* the free molecular regime, the transitional regime, the slip regime and the hydrodynamic regime (Figure 1.1). The limit cases of the free molecular regime, where the fluid is highly rarefied and it cannot be treated as a continuum medium, or the hydrodynamic regime, where the continuum medium assumptions are valid, are represented by Knudsen numbers tending respectively to infinite and zero.

In the case where the continuum assumptions are valid, the fluid flow can be described macroscopically and by using macroscopic models, such as the Navier-Stokes equations, which can give detailed information about the macroscopic physical parameters of the fluid flow. The continuum approximation is considered valid until the Knudsen number limit value of approximately 0.2 (Bird [1995]), that is from hydrodynamic to slip regime.

In the hydrodynamic regime ($Kn < 0.01$) the mean free path is very small in

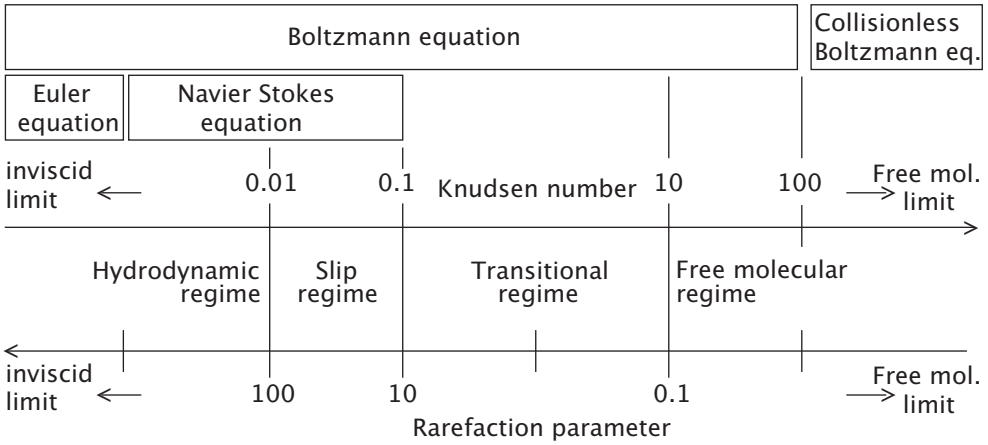

Figure 1.1: Scheme of the different rarefaction regimes as a function of the Knudsen number

comparison to the characteristic length of the system. Since the number of colliding molecules is extremely high, we can consider that locally the fluid tends to a thermodynamic equilibrium. Therefore, in this regime, it is possible to treat the fluid as a continuum medium and consider the fluid as composed by elementary fluid particles. From such a construction and by using the N-S equations, it is then possible to obtain information on the macroscopic physical parameters of the flow, i.e. velocity, pressure, density and temperature, by directly considering these variables as depending on physical space and time, which are the independent variables of the system.

In slip regime ($0.01 < Kn < 0.1$) the mean free path is ten times smaller in respect to the characteristic length of the system and therefore, in order to have a good description of the macroscopic parameters of the flow, the N-S equations have to be compensated by changing the classical boundary conditions at the wall, and therefore it is necessary to introduce a slip velocity condition at the wall and a temperature jump at the wall.

The continuum assumption is no longer valid from transitional to free molecular regime. In the free molecular regime limit case ($Kn > 10$), the collisions between molecules are absent, making collisions between gas molecules and surfaces preponderant: it is then possible to consider that each molecule moves independently

of one another. Thus, in order to define the characteristics of the flow it is necessary to closely take under consideration the interactions between surfaces and gas molecules. Therefore a molecular model and the kinetic theory has to be applied in order to solve the fluid flow.

In transitional regime ($0.1 \leq Kn \leq 10$), the collision number between molecules increase. Therefore gas/gas collisions are considered to be of the same order as the collisions between the gas and the walls, but at the same time we cannot still consider the fluid medium as a continuum. Therefore a microscopic model is still needed. Let us notice that anyhow, the molecular model approach has no limitations on the gas rarefaction regimes at which the fluid flow can be described: the entire spectrum of gas rarefaction could be treated.

The physical models that are classically used to solve rarefied flows in free molecular and transitional regime, are based on the Boltzmann equation which statistically describes the macroscopic physical parameters of the flow. Without entering in any details, from a mathematical point of view the Boltzmann equation is an integro-differential equation where the unknown distribution function depends on seven variables: a position vector, a molecular velocity vector and time. This equation describes the evolution in space and time of the distribution function and it is theoretically valid along the whole spectrum of gas rarefaction.

Nowadays, there are two different main approaches for the numerical solution of the BE: the direct simulation Monte Carlo method, that is a statistical approach where the motion of the molecules is simulated in two stages, that is the collisionless molecular motion and the intermolecular collisions; and the deterministic approaches which are approximations of the BE, such as the Bhatnagar-Gross-Krook (BGK) model, the Shakov model and the ellipsoidal-statistical (ES) model. The solution of the different approximations of the BE are usually based on the discrete velocity method (DVM).

Usually, a second parameter is used to characterize the rarefaction state of the gas: that is the rarefaction parameter. This parameter is inversely proportional

to the Knudsen number and it is

$$\delta \sim \frac{1}{Kn}. \tag{1.4}$$

The rarefaction parameter is directly proportional to the fluid density, therefore it is of more practical use when manipulating thermodynamic parameters such as pressure and temperature. Thus in this manuscript we adopted the rarefaction parameter notation instead of the Knudsen number in order to delineate our experimental results.

Typically rarefied gas flows are investigated in space applications or systems which operate under high vacuum conditions. In recent times, since current micro systems sizes have decreased to sub-micron dimensions, the gas mean free path is often of the same order as the characteristic length of the system, thus, in these micro-devices, the rarefaction parameter is relatively low and the gas may be considered to be rarefied even at relatively high pressures. In this way, the advent of micro-electro mechanical systems (MEMS) has extended the number of fields in which rarefied gas flows are of interest and therefore has opened up new perspectives on the study of rarefied gas flows and, hence, thermal transpiration. Applications for rarefied gas flows can be found in many recently created microsystems such as chromatographs, high precision flow control systems, compressors, cooling systems, evaporators and more.

Arrangement of the manuscript

This manuscript was divided into eight chapters and was structured accordingly to the manner in which this investigation was conducted.

The first introductory chapter (Chapter 1) was devoted to set the basis of the present work and enunciate the motivations which conducted us to put the thermal transpiration flow at the center of our research activities. We defined the framework around which the research was developed and finally we introduced the conditions which are necessary in order to obtain a thermal transpiration flow, such as the rarefaction of the gas.

Chapter 2 was devoted to give a basic explanation of what concerns the fundamentals of kinetic theory, which we believe are necessary in order to understand and properly interpret the experimental and numerical results obtained in this work. Therefore, we described the velocity distribution function, the Boltzmann equation, the Maxwellian form of the distribution function and the kernel or the boundary conditions that are necessary to close the BE system. Furthermore we gave a description of the model kinetic equations, such as the BGK and the S-model, and we introduced the direct simulation Monte Carlo method.

In Chapter 3 we effectuated a review of the literature concerning thermal transpiration. We discussed the experimental and numerical investigations conducted on the subject from the research of Osborne Reynolds to present times.

Particular attention was devoted to the discovery of the phenomenon, where the main concepts related to the effects of thermal transpiration and more generally the effects of a gas macroscopically displaced by temperature inequalities at the surface were treated and widely discussed. Of particular interest were the discussions of Maxwell on the fact that it was important to regard the conditions at the wall and therefore it was necessary to find a way to model the mechanisms of gas wall interaction. The discussion is still topical nowadays.

We focused our attention also on the investigations conducted by several authors on the development of semi-empirical formulas, which are still used at the present days, in order to characterize the pumping effects of thermal transpiration.

Subsequently, we noted that the time-dependency of the phenomenon had already been experimentally observed but none of the authors concerned in these investigations gave any detailed insight on the causes of such time-dependency or investigated in which form the pressure variation with time could vary if the rarefaction of the gas, different gases and different temperature differences were applied.

Finally, we tried to group the last findings on the subject by looking after experimental and numerical studies that could more clearly define the characteristics of a stationary gas displaced by a temperature gradient in a micro-device. We

concluded that the thermal transpiration flow was until now never properly experimentally quantified.

Chapter 4 described the experimental apparatus used. The chapter focuses mainly on the apparatus, the instrumentation, the problematics encountered during the experimental campaign and the measurement techniques implemented to determine the reservoir dimensions.

We dedicated a large part of this chapter to the analysis of the temperature inequalities induced on the external surface of the micro-tube and to the calibration of the pressure measurements which were affected by parasite thermal transpiration pumping effects.

Finally we offered an analysis of some of the problematics encountered in the first experimental setup. This analysis allowed us to obtain much better experimental results and therefore we considered necessary to perform a brief discussion on them.

In chapter 5 the methodology of the experimental investigation was explained in details. We described the manipulation of the experimental apparatus and how a thermal transpiration time-dependent flow was induced along the single glass micro-tube. In this section two fundamental concepts were introduced. The first was the stationary, fully developed, uni-directed and not-perturbed thermal transpiration flow. The second one was the instantaneous externally-generated configuration change in the experimental system that radically perturbs the stationarity of the thermal transpiration flow and forces it to be time-dependent.

We illustrated how the concepts of stationarity and time-dependency could be well captured by the monitoring of the pressure variation with time at the inlet and outlet of the capillary after the experimental configuration change. Finally, we explained how the thermal transpiration mass flow rate was deduced from the pressure variation with time at time t_0, how the pressure variation with time could be associated to an exponential function and how each experiment was characterized as a function of the rarefaction of the gas.

In chapter 6 the results of the experimental investigation were presented. We

analyzed the pressure variation with time, the pressure variation speed, the characteristic time of the system, the stationary thermal transpiration mass flow rate and the parameters characterizing the final equilibrium zero-flow state, such as the thermal molecular pressure difference, the thermal molecular pressure ratio and the thermal molecular pressure ratio exponent. All these results were obtained for different applied temperature differences along the micro-tube and for three gases, argon, helium and nitrogen, over a broad spectrum of rarefaction conditions, namely from near free molecular to slip regime.

Chapter 7 presented the results obtained by the kinetic theory based numerical methods. These results were compared to the experimental results. The first part of the chapter was dedicated to the definition of the numerical methodology adopted: both the linearized solution of the S-model and the direct simulation Monte Carlo were considered. Following a comparison with the zero-flow equilibrium stage parameters, such as the TPR, TPD and γ was performed and the numerical results obtained for the distribution of the thermodynamic parameters and the bulk velocity along the tube were shown. Subsequently, we presented a comparison of the results obtained for the stationary thermal transpiration mass flow rate and the associated thermodynamic parameters along the tube. Finally, we performed a study on the influences that the gas/surface interaction could have on both the zero-flow equilibrium thermal molecular pressure exponent and the thermal transpiration mass flow rate.

We decided to include a chapter dedicated to the perspectives of this work (Chapter 8). This final part was considered by the authors as a sort of brain storming that could better define the present work in its totality. We tried to give proof that the final pressure difference effectively generated a counter Poiseuille flow and we tried to associate this equivalent counter flow to a final pressure difference which would correspond to the TPD results which were experimentally found in the thermal transpiration experiments.

We performed isothermal mass flow rate measurements and we extracted the gas/surface interaction hierarchy as a function of the used gas, the glass micro-tube used was the same that the one used in the non-isothermal experiments. This was done in order to see if the hierarchy corresponded to the one found in

the non-isothermal experiments and therefore we tried to investigate an eventual divergence.

Finally we showed that, as in the thermal transpiration experiments, the isothermal experiments done in order to deduce the isothermal mass flow rate could be treated as a time-dependent phenomenon and therefore had to be studied differently than in respect to the works found in the literature.

Chapter 2

Molecular theory

In this chapter we introduced the basic concepts of rarefied gas dynamics. We gave a general introduction and description on some historical facts behind the first conceptions of the molecular theory, the mile-stones set by Maxwell, such as the equilibrium distribution function and the first construction of a molecular potential, the Boltzmann equation and its derivation, and the kernels which are the boundary conditions that close the BE system. Furthermore, we described the model kinetic equations, that are approximations of the BE, and the direct simulation Monte Carlo method, that permits the computation of the macroscopic flow parameters by following the molecular dynamisms inside a physical domain.

2.1 Kinetic theory of gases: basic elements

"Molecular theory supposes that all bodies, even when they appear to our senses homogeneous, consist in a multitude of particles, or small parts, the mechanical relations of which constitute the properties of the bodies. [...] Those (theories) which suppose the molecules to be in motion, even when the body is apparently at rest, may be called dynamical theories. In fluids the molecules are supposed to be constantly moving into new relative positions, so that the same molecule may travel from one part of the fluid to any other part. In liquids the molecules are supposed to be always under the action of the forces due to the neighboring molecules throughout their course, but in gases the greater part of the path of each molecule is supposed to be sensibly rectilinear and beyond the sphere of sensible action of the neighboring molecules". (Maxwell [1867])

2.1.1 Molecules

Knudsen [1935], during lectures delivered in the University of London in the autumn of 1933 at a time where this theory was considered to express well-established facts, presented the four fundamental assumptions of the kinetic theory of gases, which are:

1. Any gas consists of separate particles called molecules. In a pure gas these are all alike.

2. The molecules move about in all directions.

3. The pressure caused by the movement of the molecules is the only one existing in a gas, when it is in the ideal state.

4. The molecules are not infinitely small. Thus they collide with one another.

These assumptions, even if nowadays they can be considered apparently simple, hide a certain historical complexity by the way in which they have been established and proven during the years.

The earliest conceptions of kinetic theory were elaborated by Leucippus, Democritus and Epicurus (530a.c-270a.c), who hypothesized that there were two kinds of different realities composing the universe, that is void and atoms. They introduced sophisticated ideas such as the hypothesis that everything is composed by atoms, that between atoms lied empty space, that atoms have always been and always will be in motion, and that the atoms were of "infinite number, size and shapes". These theories, which were largely discredited in ancient Athens, would need more than two thousand years to be proven.

Leucippus and his disciples are considered by many today to be the fathers of modern science, even if some of their hypothesis were largely proven to be wrong, like the hypothesis of clusters of atoms which could come together by connections, which were attachments supplied by hooks and barbs on their surface.

On the basis of the Greek school, Lucretius (ca. 99 BC ca. 55 BC), a roman poet and philosopher, announced his theories on the principle of all things in his poem *De rerum natura*. Lucretius aim was to denounce the blinding of men's

cognition of reality by the inculcation of erroneous religious precepts. He wanted to prove in an appealing manner that nature could be explained in a logical way, and thus developed the atomism theory as modified by Epicurus. In his poem the main theory, that is the demonstration over the existence of atoms, was that any material is subjected to irreversible decay, but from the decay of a material, a new material, or the same material would be born again. The conclusion is that each material is composed by indestructible, eternal and invisible structures that would never decay and thus are to be used again by nature to form other materials. We now know that this last description is more suitable for molecules rather than atoms, anyhow, his hypothesis were more than revealing.

Bernoulli [1738] was the first modern investigator who re-proposed similar theories and re-applied them for the description of a fluid. Bernoulli, in a chapter of his book Hydrodynamica, defined the pressure inside a vessel containing air by considering it as a direct consequence of the sum of the forces exerted by the impact of a great number of gas molecules on the walls of the vessel. Bernoulli can be considered as the first modern promoter of the dynamical theory of gases: he defined a macroscopic property of the fluid by using a microscopic approach, which worked on the basis of describing the fluid as composed of gas molecules.

After Bernoulli, contributors to the dynamic theory of gases were Herapath [1847], who developed the causes of heat, gravitation and other natural phenomena by extending the dynamic theory, Joule [1848], who calculated the velocity of the molecules of hydrogen, Clausius [1857], who gave us first precise ideas about the motion of agitation of molecules and defined the free path in a gas, and Graham [1863], who studied experimentally the passage of gas through solid graphite set at the end of long narrow tubes. Graham's diffusiometer supported the hypothesis of gas composed by molecules against the at the time well accepted hypothesis of gas to be a continuum medium.

The scientist to whom we owe the largest extension of the dynamical theory of gases is Maxwell. His research, which was a pursuit of Clausius investigation, was elaborated at a time when the molecular theory of gases was controversial and the majority of the physical society did not considered it well-founded. One of the most remarkable results, whose confirmation by experimental proof helped to es-

tablish the dynamical theory of gases, was Maxwell's prediction in 1860 (Maxwell [1860-1890]) that the viscosity of a gas is independent of the density and should increase with temperature. The scientific outcome from Maxwell's investigation was certainly staggering: he developed a first formulation of what later would be known as the Boltzmann or Maxwell-Boltzmann equation (Maxwell [1867]), he introduced a molecular model that stated that the molecules interacted through a potential which was inversely proportional to the fifth power of the distance between them (Maxwell [1867]), and finally he defined the first conception of a gas-surface interaction model, which nowadays is known as the Maxwellian kernel (Maxwell [1879]).

From lectures delivered by Maxwell in the latest decades of the 19th century, it is possible to extract Maxwell's desire to understand and explain nature by starting the investigation from a microscopical point of view. From here came his interest in molecules and the molecular model, for what he called the dynamical theory. Now that we know the exactitude of many of Maxwell's theories, it is of extraordinary interest to observe in which manner his research evolved by putting it in relationship to common scientific knowledge of his time. In a lecture that he gave, which appeared in the September 1873 issue of Nature, it is possible to understand the value of the breaking through investigations that he was conducting. Maxwell's speeches reveal the impact that his studies were exerting on the scientific community of his time: "[...] we must go on to molecules. Molecule is a modern word. It does not occur in Johnson's Dictionary" (Maxwell [1873]).

2.1.2 Velocity distribution function

In theory, the molecular model is able to provide information on the physical properties of each molecule by identifying its position, its velocity and its internal state at a particular instant. Obviously, the number of molecules in a fluid is so large that such approach is not realistic, hence it was necessary to develop a statistical molecular description in terms of probability functions.

Historical facts

The first to develop a statistical molecular description in terms of probability functions was Maxwell in 1860 (Maxwell [1860-1890]). From this point, he gave proof

that it could be possible to obtain the main macroscopic properties of the gas from the velocity distribution function, if the latter was known.

Maxwell explained the distribution function in the following way: "When the working members of Section F get hold of a document containing the numerical data of Economic and Social Science, they begin by distributing the whole population into groups, according to age, income-tax, education, religious belief, or criminal convictions. The number of individuals is far too great to allow of their tracing the history of each separately, so that, in order to reduce their labour within human limits, they concentrate their attention on a small number of artificial groups. The varying number of individuals in each group, and not the varying state of each individual, is the primary datum from which they work. [...] The equations of dynamics completely express the laws of the historical method[1] as applied to matter, but the application of these equations implies a perfect knowledge of all the data. But the smallest portion of matter which we can subject to experiment consists of millions of molecules, not one of which ever becomes individually sensible to us. We cannot, therefore, ascertain the actual motion of any one of these molecules, so that we are obliged to abandon the strict historical method, and to adopt the statistical method of dealing with large groups of molecules. The data of the statistical method as applied to molecular science are the sums of large numbers of molecular quantities."(Maxwell [1873])

Definition

Let us consider a sample of a dilute monoatomic gas that is homogenous in physical space and contains a finite number of identical molecules. A typical molecule has a velocity $\mathbf{c}$ with components c_1, c_2 and c_3. These components define a velocity space and each molecule can be represented in this space by the point defined by its velocity vector.

Since generally we have fluid flows depending also on space and time, it is necessary to relate the distribution function to the physical space at a given instant, thus we must define the single particle distribution function in a multi-dimensional space, which it is commonly called a phase space. In this case, the volume element

[1] deterministic method

over which we look for the number of molecules with the desired characteristics at a precise instant is a part of a multi-dimensional space formed by the combination of physical space and velocity space and is defined as $d\mathbf{r}\ d\mathbf{c}$, where $d\mathbf{r} = dx\ dy\ dz$ is the physical space volume element.

Therefore we may define the single particle distribution function in phase space at a precise instant as

$$dN = \ f(t, \mathbf{r}, \mathbf{c})\ d\mathbf{r}\ d\mathbf{c}, \tag{2.1}$$

where dN is the number of molecules with velocity components ranging from c_1 to $c_1 + dc_1$, c_2 to $c_2 + dc_2$, and c_3 to $c_3 + dc_3$ and spatial coordinates ranging from x to $x + dx$, y to $y + dy$, and z to $z + dz$, at a precise instant.
The distribution function gives the probability of encountering a well defined number of molecules in the physical space elementary volume $(\mathbf{r},\ \mathbf{r} + d\mathbf{r})$ having a velocity comprised between $\mathbf{c}$ and $\mathbf{c} + d\mathbf{c}$. As it can be clearly seen, the single particle distribution function in phase space for a non-stationary flow depends on seven independent variables.

The distribution function has to attain certain properties and therefore can never be negative and must have finite bounds in velocity space. Additionally, the single particle distribution function has to necessarily respond to the following condition

$$n(t, \mathbf{r}) = \int dn = \int \ f(t, \mathbf{r}, \mathbf{c})\ d\mathbf{c}, \tag{2.2}$$

where n is the molecular number density in the elementary volume $d\mathbf{r}$ and therefore is defined as $dn = dN/d\mathbf{r}$.

Any macroscopic quantity of the fluid in a portion of physical space at a given instant can be related to the the single particle distribution function in phase space in the following manner

$$\overline{Q}(t, \mathbf{r}) = \frac{1}{n} \int \ Q\ f(t, \mathbf{r}, \mathbf{c})\ d\mathbf{c}. \tag{2.3}$$

Thus, the macroscopic quantities of the flow can be calculated as:

the bulk or stream velocity

$$\mathbf{u}(t,\mathbf{r}) = \frac{1}{n}\int \mathbf{c}\; f(t,\mathbf{r},\mathbf{c})\; d\mathbf{c}, \tag{2.4}$$

the pressure

$$p(t,\mathbf{r}) = \frac{m}{3}\int C^2\; f(t,\mathbf{r},\mathbf{c})\; d\mathbf{c}, \tag{2.5}$$

the temperature

$$T(t,\mathbf{r}) = \frac{m}{3nk_B}\int C^2\; f(t,\mathbf{r},\mathbf{c})\; d\mathbf{c}, \tag{2.6}$$

the heat flow vector

$$\mathbf{q}(t,\mathbf{r}) = \frac{m}{2}\int C^2\; \mathbf{C}\; f(t,\mathbf{r},\mathbf{c})\; d\mathbf{c}, \tag{2.7}$$

and the stress tensor

$$P_{ij}(t,\mathbf{r}) = m\int C_i C_j\; f(t,\mathbf{r},\mathbf{c})\; d\mathbf{c}. \tag{2.8}$$

where m is the gas molecular mass, k_B is the Boltzmann constant, $\mathbf{C} = \mathbf{c} - \mathbf{u}$ is the thermal or peculiar velocity and $\mathbf{u}$ is the bulk velocity. Of course $\overline{\mathbf{C}}$ is equal to zero. This process is often referred to as establishing a moment of the distribution function and therefore the previously introduced macroscopic quantities are referred to as moments of the distribution function. The derivation of the moments of the distribution function are given in Chapman & Cowling [1939].

Therefore, once the distribution function is known, all the macroscopic parameters which describe the fluid flow can be consequently derived. It is necessary now to introduce the equation that governs the distribution function, that is the Boltzmann equation.

2.1.3 Boltzmann equation

The mathematical model that describes microscopically the fluid flow is the Boltzmann transport equation which was derived in 1872 (Boltzmann [1872-1905]). The quantity of interest of the BE is the distribution function.

The equation can be derived for a dilute gas, where the probability of binary

intermolecular collisions is higher in respect to collisions of more molecules at the same time, when the following main two assumptions are respected:

1. Instantaneous collisions, that is when the time interval of the intermolecular collision is considered to be zero.

2. Molecular chaos, that is when the physical space and the velocity space are considered to be independent one from the other.

Let us now define the equation. We can state that the variation of the number of molecules which have the velocities between $\mathbf{c}$ and $\mathbf{c} + d\mathbf{c}$ during a time interval dt inside a phase space elementary volume $d\mathbf{r}d\mathbf{c}$ is

$$dN(t + dt) - dN(t) = [f(t + dt, \mathbf{c} + d\mathbf{c}, \mathbf{r} + d\mathbf{r}) - f(t, \mathbf{c}, \mathbf{r})]d\mathbf{r}d\mathbf{c}. \tag{2.9}$$

For sake of brevity from now on we will refer to $f(t, \mathbf{r}, \mathbf{c})$ as f.

Using the differential formalism eq 2.9 becomes

$$dN(t + dt) - dN(t) = \left(\frac{\partial f}{\partial \mathbf{r}}d\mathbf{r} + \frac{\partial f}{\partial \mathbf{c}}d\mathbf{c} + \frac{\partial f}{\partial t}dt\right) d\mathbf{r}d\mathbf{c}. \tag{2.10}$$

Therefore, if $\mathbf{F}$ represents an external force exerted on the molecules per mass unit, since $\mathbf{c} = d\mathbf{r}/dt$ and $\mathbf{F} = d\mathbf{c}/dt$ it is then finally possible to write

$$\left(\frac{\partial f}{\partial \mathbf{r}}\mathbf{c} + \frac{\partial f}{\partial \mathbf{c}}\mathbf{F} + \frac{\partial f}{\partial t}\right) d\mathbf{r}d\mathbf{c}dt, \tag{2.11}$$

where $-\mathbf{c}\ \partial f/\partial \mathbf{r}$ and $-\mathbf{F}\ \partial f/\partial \mathbf{c}$ are two transport terms. The first transport term represents the balance of molecules of class $\mathbf{c}$ that transit across the physical space $\{\mathbf{r}\}$. The second transport term represents the balance of molecules that leave or enter in the velocity space $\{\mathbf{c}\}$, thus accelerate or decelerate by the influence of external forces, as gravity or electromagnetic fields, acting on them.

Let us note that the transport process, and therefore the transport terms, affect in the same way all the molecules of the phase space. Therefore, only the intermolecular collision processes can effectively engender a real variation of the number of molecules from $dN(t)$ to $dN(t + dt)$. This variation is expressed by

means of a collision integral $J(f, f_1)$.

This collision integral represents the scattering of molecules into and out of the phase space elementary volume $\{\mathbf{c}, \mathbf{r}\}$ as a result of intermolecular collisions. In this way, the BE may be written in the following manner

$$\frac{\partial f}{\partial t} + \mathbf{c}\,\frac{\partial f}{\partial \mathbf{r}} + \mathbf{F}\,\frac{\partial f}{\partial \mathbf{c}} = J(f, f_1). \tag{2.12}$$

This is an integro-differential equation which depends on seven variables, difficult to solve even in the case where we consider collisions as a completely elastic phenomenon. Nevertheless, the main difficulty when solving the BE derives from the correct modeling of the collision term.

Without entering in any details, let see how the collision integral $J(f, f_1)$ can be derived. Let us remember here the assumptions made in order to be able to deduce this collision term: the collisions are binary, one collision is considered to be an instantaneous event at a fixed location in physical space and time and the physical space is considered to be independent from the velocity space considered. Thus, the collision can be represented as affecting only the element $d\mathbf{c}$.

We can calculate the rate of molecules of class $\mathbf{c}$ that leave the phase space $d\mathbf{c}\; d\mathbf{r}$ due to a collision with another molecule, this time of class $\mathbf{c}_1$. This means that when the molecule traveling with velocity $\mathbf{c}$ collides against a second molecule in the physical space $d\mathbf{r}$, both molecules will change their velocity and trajectory. In order to be able to compute a meaningful expression of the collision integral, it is then necessary to consider the pre-collision and the post-collision velocities of both molecules, therefore, we define four velocities: the pre-collision velocities of class $\mathbf{c}$ and $\mathbf{c}_1$ and the post-collision velocities $\mathbf{c}^*$ and $\mathbf{c}_1^*$. This is called a class $\mathbf{c}, \mathbf{c}_1 \rightarrow \mathbf{c}^*, \mathbf{c}_1^*$ collision.

Therefore, if we consider a test molecule of class $\mathbf{c}$ traveling across a field of molecules of class $\mathbf{c}_1$ it is necessary to compute the number of collisions of the class $\mathbf{c}, \mathbf{c}_1 \rightarrow \mathbf{c}^*, \mathbf{c}_1^*$ suffered by the test molecule per unit time. The test molecule of class $\mathbf{c}$ travels with a relative velocity $\mathbf{c}_r = \mathbf{c} - \mathbf{c}_1$ in respect to the field of

molecules of class $\mathbf{c}_1$, thus the volume swept out by it in unit time is

$$\mathbf{c}_r \ \sigma d\Omega \tag{2.13}$$

where $\sigma d\Omega$ is the differential cross-section of the molecule and represents the sphere of influence that the test particle has over approaching molecules (Figure 2.1). It is important to remember that the cross-section of the gas strongly depends on the model used, such as the variable hard sphere (VHS) model, the hard sphere (HS) model, the variable soft sphere (VSS) model or the inverse power law model. In a realistic model, the interaction between molecules should correspond to a force field which depends on the distance at which the molecule stands from another molecule. The force field should follow a law that reproduces a strong repulsion at close distances and a slight attraction after passing an equilibrium distance in which the force field is zero.

Since the number of molecules of class $\mathbf{c}_1$ per unit volume in physical space is $f_1 d\mathbf{c}_1$, the number of collisions of this class, suffered by the test molecule per unit time is

$$f_1 \ \mathbf{c}_r \ \sigma d\Omega \ d\mathbf{c}_1. \tag{2.14}$$

Finally, if we consider the whole number of molecules of class $\mathbf{c}$ in the phase space $d\mathbf{c}d\mathbf{r}$, that is $f d\mathbf{c}d\mathbf{r}$, and if we invoke the concept of molecular chaos, the equation that denotes the number of class collisions becomes

$$f f_1 \ \mathbf{c}_r \ \sigma d\Omega \ d\mathbf{c}_1 d\mathbf{c}d\mathbf{r}. \tag{2.15}$$

Analogously, if we consider the existence of inverse collisions, we may write the same equation for the collision class $\mathbf{c}, \mathbf{c}_1 \leftarrow \mathbf{c}^*, \mathbf{c}_1^*$

$$f^* f_1^* \ \mathbf{c}_r^* \ (\sigma d\Omega)^* \ d\mathbf{c}_1^* d\mathbf{c}^* d\mathbf{r}. \tag{2.16}$$

If we consider that $\mathbf{c}_r^* = \mathbf{c}_r$ and that $|(\sigma d\Omega) \ d\mathbf{c}_1 d\mathbf{c}| = |(\sigma d\Omega)^* \ d\mathbf{c}_1^* d\mathbf{c}^*|$ (Bird [1995]), the balance between these two terms, which have the name of loss and gain terms,

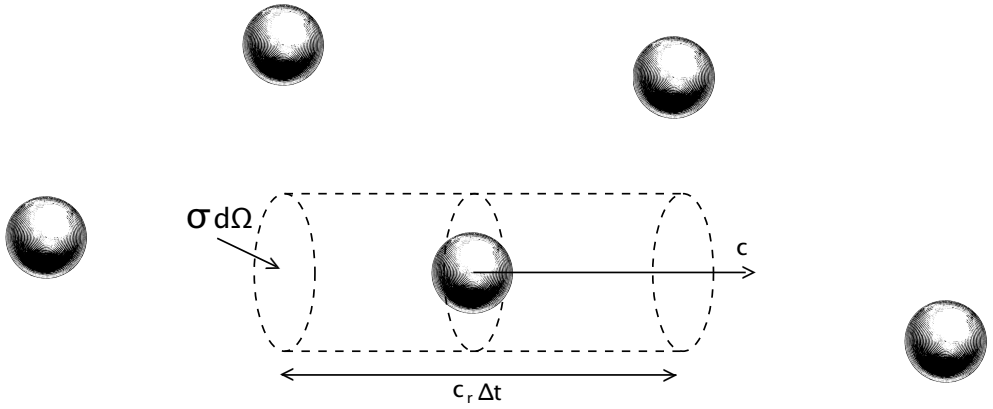

Figure 2.1: Volume swept out by moving test molecule among a molecule field

that is eq. (2.15) and eq. (2.16) respectively, gives us then the collision integral

$$J(f, f_1) = \int_{-\infty}^{\infty} \int_{0}^{4\pi} (f^* f_1^* - f f_1)\ \mathbf{c}_r\ \sigma d\Omega\ d\mathbf{c}_1, \tag{2.17}$$

where the integration is made over the complete cross-section for its collision with class $\mathbf{c}_1$ molecules followed by the integration of the class $\mathbf{c}_1$ over all velocity space.

The collision integral has two fundamental properties:

1. The Boltzmann inequality: if f is a non-negative function such that $logfJ(f, f_1)$ is integrable then
$$\int lnfJ(f, f_1)d\mathbf{c} \leq 0 \tag{2.18}$$

2. Conservation property: the conservation of mass, momentum and energy in every collision is represented by the identity
$$\int \psi(\mathbf{c})J(f, f_1)d\mathbf{c} = 0 \tag{2.19}$$
where the functions $\psi(\mathbf{c})$ are the collision invariants and they are equal to m, $m\mathbf{c}$ and $1/2mc^2$ for mass, momentum and energy respectively.

2.1.4 Maxwellian distribution function

The BE is a special case of Maxwell's general equation, however Boltzmann was able to deduce immediately a remarkable result from his formulation which was not evident from Maxwell's original equation. Boltzmann identified a quantity H defined as

$$H_D(t) = \int_D \int f ln f \mathrm{d}\mathbf{c}\mathrm{d}\mathbf{r}\,, \tag{2.20}$$

which is called the H function for the space D (integration domain). By analogy the function

$$H(t, \mathbf{r}) = \int f ln f \mathrm{d}\mathbf{c}\,, \tag{2.21}$$

is the H-function of the unite volume or Boltzmann H function and which is a measure for the negative of the logarithm of the probability for the distribution function $f(t, \mathbf{r}, \mathbf{c})$.

Multiplying the BE (2.12) by $(1 + \ln f)$ and integrating according to $\mathbf{c}$ one obtains

$$\int (1 + \ln f) \left(\frac{\partial f}{\partial t} + \mathbf{c} \frac{\partial f}{\partial \mathbf{r}} \right) \mathrm{d}\mathbf{c} = \int (1 + \ln f) J\,(f, f_1)\, \mathrm{d}\mathbf{c}. \tag{2.22}$$

Using notation (2.21) and some transformation one obtains

$$\frac{\partial H}{\partial t} + \frac{\partial H_i}{\partial r_i} = -\frac{1}{4} \int (\ln(f^* f_1^*) - \ln(f f_1))(f^* f_1^* - f f_1)\; \mathbf{c}_r\; \sigma d\Omega\; d\mathbf{c}_1 d\mathbf{c} \tag{2.23}$$

where

$$H_i = \int c_i f \ln f \mathrm{d}\mathbf{c}. \tag{2.24}$$

If we integrate eq. (2.24) in the domain D of physical space we can obtain

$$\begin{aligned} &\frac{\mathrm{d}H_D}{\mathrm{d}t} + \oint H_n dS = \\ &= -\frac{1}{4} \int (\ln(f^* f_1^*) - \ln(f f_1))(f^* f_1^* - f f_1)\; \mathbf{c}_r\; \sigma d\Omega\; d\mathbf{c}_1 d\mathbf{c} d\mathbf{r} = \\ &= G, \end{aligned} \tag{2.25}$$

here H_n is the projection on the external normal vector of the vector $H = (H_1, H_2, H_3)$. The integration for the second member in the left hand site is carried out according to boundary S of the domain D and the theorem of Ostrodradski is

implemented. If we suppose the specular reflection of the molecules of the surface S, then the second term in the left hand side is equal to zero and one obtains

$$\frac{\mathrm{d}H_D}{\mathrm{d}t} = G\,. \tag{2.26}$$

But the integral in the right hand side of (2.25) is always negative since the expression $(x-y)(\ln x - \ln y)$ is always positive, except if $f^* f_1^* = f f_1$, when it vanishes, therefore

$$\frac{\mathrm{d}H_D}{\mathrm{d}t} \leq 0\,. \tag{2.27}$$

This expression shows that the H-function is a non-increasing function of time. There is the Boltzmann H theorem, which shows that the time evolution of a solution of the Boltzmann equation has a direction. The Boltzmann H theorem is equivalent to the second law of thermodynamics which states that the entropy cannot decrease. It is in fact more general, as the quantity H is defined for all systems, whereas the entropy is defined only at equilibrium; however, the H theorem has been proven only for dilute gases, whereas the second law applies to any systems in equilibrium.

It is clear that $G = 0$ shows that an equilibrium of the system is obtained only if

$$f^* f_1^* = f f_1. \tag{2.28}$$

From relation (2.28) one can obtain the form of the equilibrium distribution function of the system. Equation (2.28) may be rewritten as follows

$$\ln f^* + \ln f_1^* = \ln f + \ln f_1. \tag{2.29}$$

Therefore if $\frac{\mathrm{d}H_D}{\mathrm{d}t} = 0$, then the state of the gas is such that $\ln f$ is a collisional invariant. If $\ln f$ is a collisional invariant, it must be a linear combination of the known collisional invariants, so that

$$\ln f = am + b_i m c_i + dmc^2, \tag{2.30}$$

where a, b_i, d are the functions of t and $\mathbf{r}$, which can be expressed via fife macroscopic variables n, $\mathbf{u}$, T. The velocity distribution function at local thermodynamic

equilibrium may be presented in the form

$$f^M(\mathbf{r},\mathbf{c},t) = n(\mathbf{r},t)\left(\frac{m}{2\pi kT(\mathbf{r},t)}\right)^{3/2}\exp\left(-\frac{m(\mathbf{c}-\mathbf{u}(\mathbf{r},t))^2}{2kT(\mathbf{r},t)}\right) \tag{2.31}$$

This function is called the local Maxwellian distribution function (or local Maxwellian).

In order to be in an equilibrium state a gas in a domain D must have the local Maxwellian distribution function. In other hand, an equilibrium state is described by the BE (2.12). It is evident that the collision integral is equal to zero because eq. (2.28) that the Maxwellian distribution satisfy also the right hand side of the BE only when the macroscopic parameters are constant n, $\mathbf{u}$, T. That means that a gas is in equilibrium only for the Maxwellian distribution with the constant macroscopic parameters. In the same time on the boundary the gas must have the same distribution. Therefore, the unique positive continuous solution of the BE (Sone [2002]) is

$$f_0^M = n_0\left(\frac{m}{2\pi kT_0}\right)^{3/2}\exp\left(-\frac{m(\mathbf{c}-\mathbf{u}_0)^2}{2kT_0}\right). \tag{2.32}$$

The function f_0^M is the equilibrium absolute Maxwellian distribution function, with the equilibrium constant parameters n_0, $\mathbf{u}_0$, T_0, describing an equilibrium state. This function is a solution of the Boltzmann equation for an equilibrium state ($\partial f/\partial t = \partial f/\partial \mathbf{r} = 0$).

The distribution (2.31) does not satisfy eq. (2.12) except for some special cases.

This is an approached solution of the BE for a state of local equilibrium. In this case we neglect the partial derivative in time $\partial f/\partial t$ and the transport terms $\mathbf{c}\,\partial f/\partial \mathbf{r}$ and $\mathbf{F}\,\partial f/\partial \mathbf{c}$, thus we find that $J(f,f_1) = 0$.

Therefore, it is also possible to consider this solution of the BE as a solution for a domain dominated by intermolecular collisions. Is to be noticed that the equilibrium state is completely independent from the physics involved in the intermolecular collisions.

The local Maxwellian distribution function has the following characteristics (Brun

[1986]):

1. It is a gaussian distribution which is centered on the bulk velocity or the most probable velocity.

2. It is the most probable distribution function for a system which is completely isolated or very far away from any external perturbations. The external conditions are only present through the geometry of the domain.

3. In a real configuration this solution would be valid only at a very far distance from an exterior domain, such as a wall or a high heat-flux or a highly dynamic influence. This means that very far from an exterior domain the information transmitted by a perturbation is completely lost.

2.1.5 Boundary conditions

In order to be a closed system, the Boltzmann equation has to refer to boundary conditions. In order to determine the distribution function in the case where the gas interacts with a surface element, wether this is a solid surface element or a liquid surface element, it is necessary to construct a kernel function which correlates the distribution function of incident molecules to the distribution function of reflected molecules.

As Cercignani [2006] enunciated, technically it would be possible to know in an exact manner the velocity and energy characteristics of a gas molecule after a strike against the wall if the trajectory within the wall could be computed exactly. By creating a gas-surface interactions kernel function it is possible to establish the nature of the heat transfer exchanged by the gas and the surface or the forces exerted by the gas over the surface.

To create a correct kernel is obviously a hard task: the interaction potential between gas and surface is very difficult to establish since the knowledge on the surface structure of liquids or solids has still to be improved. The difficulties to compute a correct interaction potential at the surface arise from the huge number of molecules that have to be taken into account in addition to other phenomena such as the adsorption phenomena, chemical reactions, the displacement of surface molecules, due to the impact of other molecules on them, dissociation, the

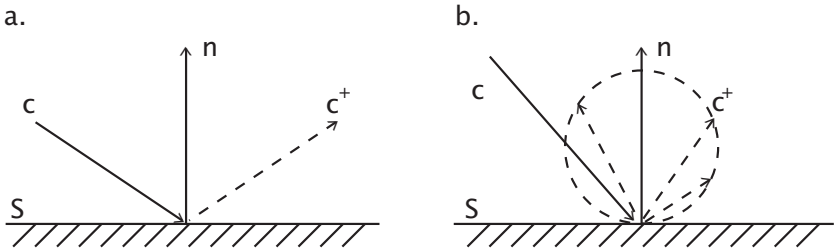

Figure 2.2: Incident and re-emerging velocities of a molecule after a gas-surface interaction. Box a. Specular reflection. Box b. Diffused reflection

characteristics of the surface, the temperature of the surface, outgassing and so on.

Let us now define the relationship that correlates the post-interaction distribution function f^+ to the pre-interaction distribution function f. The function that correlates both terms is named kernel and states that a particle of class $\mathbf{c}$, traveling with a velocity in between $\mathbf{c}$ and $\mathbf{c}+d\mathbf{c}$, that strikes the surface in $\mathbf{r}$ at an instant t, will bounce back from the surface with a velocity $\mathbf{c}^+$ at almost the same position, after a very small lapse of time τ_0 (Figure 2.2). In the case that we consider that the interaction is instantaneous, that is by considering that the sitting time τ_0 tends to zero and therefore the position $\mathbf{r}$ after the interaction is the same, the kernel function reads as follows

$$R\left[\mathbf{c} \rightarrow (t, \mathbf{r}, \mathbf{c}^+)\right]. \tag{2.33}$$

If R is known, we can write down the boundary conditions for the distribution function, by considering the surface at rest, as

$$f^+(t, \mathbf{r}, \mathbf{c}^+)|\mathbf{c}^+ \cdot \mathbf{n}| = \int_{\mathbf{c}\cdot\mathbf{n}<0} R\left[\mathbf{c} \rightarrow (t, \mathbf{r}, \mathbf{c}^+)\right] f(t, \mathbf{r}, \mathbf{c})|\mathbf{c} \cdot \mathbf{n}| d\mathbf{c}, \tag{2.34}$$

where $\mathbf{n}$ is the unit vector normal to the elementary surface dS at $\mathbf{r} \in S$. The condition of non permeability of the surface $\mathbf{c}^+ \cdot \mathbf{n} > 0$ has to be respected.

There are three fundamental properties that the kernel function has to respect (Cercignani [2006]):

1. Non-negativity: R cannot have negative values

$$R\left[\mathbf{c} \rightarrow (t, \mathbf{r}, \mathbf{c}^{+})\right] \geq 0. \tag{2.35}$$

2. Normalization: in the case where permanent adsorption is excluded, R must integrate to unity

$$\int_{\mathbf{c}\cdot\mathbf{n}\geq 0} R\left[\mathbf{c} \rightarrow (t, \mathbf{r}, \mathbf{c}^{+})\right] d\mathbf{c}^{+} = 1. \tag{2.36}$$

3. Reciprocity: in the case where the gas-surface interaction can be considered as reversible and the wall is not significantly disturbed by the gas shocks on it, and therefore is permanently in a local equilibrium state, R responds to the following identity,

$$\begin{aligned} f_w^M(\mathbf{c})|\mathbf{c}\cdot\mathbf{n}|\, R[\mathbf{c} \rightarrow (t, \mathbf{r}, \mathbf{c}^{+})] = \\ f_w^M(\mathbf{c}^{+})|\mathbf{c}^{+}\cdot\mathbf{n}|\, R[-\mathbf{c}^{+} \rightarrow (t, \mathbf{r}, -\mathbf{c})], \end{aligned} \tag{2.37}$$

where $f_w^M(\mathbf{c})$ is the local Maxwellian distribution at the wall with temperature $T_w(\mathbf{r})$ of the surface. There is a constraint on $f_w^M(\mathbf{c})$ and that is that it has to obviously preserve its state of local equilibrium after the gas-surface interaction.

Therefore, it is necessary to identify a kernel function R, that gives a correct physical description of the gas-surface interaction. A commonly used mathematical model, which was constructed by Maxwell [1879], reads as

$$R\left(\mathbf{c} \rightarrow \mathbf{c}^{+}\right) = \alpha f_w^M(\mathbf{c}^{+})|\mathbf{c}^{+}\cdot\mathbf{n}| + (1-\alpha)\delta(\mathbf{c} - \mathbf{c}^{+} + 2\mathbf{n}|\mathbf{c}^{+}\cdot\mathbf{n}|) \tag{2.38}$$

where α is the accommodation coefficient and it varies from 0 to 1 and $\delta(\mathbf{c})$ is the Dirac delta function. If the accommodation coefficient is 0, the gas-surface interaction is considered to be a specular reflection, if it is 1, the gas-surface interaction is considered to be a diffuse reflection or the gas to be completely accommodated to the surface. In the case where the accommodation coefficient lies in between 0 and 1, only a $(1-\alpha)$ fraction of molecules reflects specularly, while α fraction of molecules reflects diffusively.

In a completely specular reflection the molecule preserves its information and bounces back from the surface with same tangential velocity to the surface and same magnitude of the normal velocity to the surface but with opposite sign (Figure 2.2 box a). On the other hand in a completely diffused reflection the molecule, after the interaction with the surface, loses all precedent information and leaves the surface with the Maxwellian distribution with the parameters of the wall (Figure 2.2 box b).

Other kernel models exist, such as the Cercignani-Lampis model (Cercignani & Lampis [1971]), where two accommodation coefficients were defined, the tangential momentum accommodation coefficient and the energy accommodation coefficient associated to the kinetic energy of the normal components of the velocity; and the Meolans-Dadzie model (Dadzie & Meolans [2004]) which takes into account the anisotropic effects of the gas-surface interaction. This anisotropic characteristic of the surface derives basically from its physical properties and the manufacturing process. Consequently the real physical properties of the wall were embedded in three momentum accommodation coefficients.

2.2 Model kinetic equations

Theoretically, by associating the boundary conditions to the Boltzmann equation (2.12), it could be possible to solve analytically the closed system and thus obtain the values of the distribution function in phase space for steady and unsteady flows. From there in ahead, it would then be possible to compute the macroscopic parameters of the flow as the moments of the distribution function [eqs. (2.4-2.8)].

Due to the complexity of the problem, nowadays it is only possible to solve analytically the BE for some simple cases. However, in the case where the fluid flow is subjected to small perturbations, the velocity distribution function does not largely deviate from its equilibrium or Maxwellian form, therefore it is possible to linearize the BE and obtain good approximations to the solution of BE for a restricted set of problems.

On the other hand, in case of fluid flows that involve large perturbations, the solution becomes very hard to obtain, especially since the problem becomes non-linear.

The most complex term in the BE is the collision integral, therefore, different methods were developed in order to model and thus simplify this collision term by a collision model, which is a simpler expression of $J(f, f_1)$ [eq. (2.17)] that retains at least the qualitative and average properties of the collision term (Cercignani [2006]). Model kinetic equations, such as the one proposed by Bhatnagar, Gross and Krook (Bhatnagar *et al.* [1954]), and in parallel by Welander [1954], and the one proposed by Shakov [1968], are today widely used to solve fluid flow problems in a more practical way for an arbitrary rarefaction of the gas.

2.2.1 Bhatnagar-Gross-Krook model

The most widely known kinetic model equation is the BGK model. The structure of the model equation is that the variation of the distribution function is proportional to the deviation from equilibrium. The physical phenomena that bring back the fluidic system to its final equilibrium state are the intermolecular collisions. The general expression of the kinetic model equation, in the case where external forces are not acting on the fluidic domain, reads as follows

$$\frac{\partial f}{\partial t} + \mathbf{c}\,\frac{\partial f}{\partial \mathbf{r}} = J(f, f^{mod}), \tag{2.39}$$

where the collision integral was substituted by the collision model $J(f, f^{mod})$. This model collision term has the following relaxation form

$$J(f, f^{mod}) = \nu[f^{mod} - f(t, \mathbf{r}, \mathbf{c})], \tag{2.40}$$

where f^{mod} is the so called model distribution function and is an equilibrium distribution function which depends on the kinetic model used; and ν is the collision frequency. The collision frequency is inversely proportional to the relaxation time which is the time that the fluid system needs to come back to a local equilibrium state.

The collision frequency ν is independent from the velocity $\mathbf{c}$ and depends only on macroscopic parameters such as the pressure and the shear stress viscosity transport coefficient μ only for the pseudo Maxwell molecules, which are molecules with an inverse fifth power law potential. The collision frequency is then $\nu = p/\mu$.

For the BGK model the model distribution function is equal to the local Maxwellian or equilibrium distribution function

$$f^{mod} = f^{BGK} = f^{M}_{loc}[n(\mathbf{r}), T(\mathbf{r}), \mathbf{u}(\mathbf{r})], \tag{2.41}$$

where f^{M}_{loc} was previously defined in equation (2.31). By defintion, the Maxwellian distribution function has the same density, temperature and bulk velocity as $f(t, \mathbf{r}, \mathbf{c})$. Therefore, for any collision invariant the following law is always true,

$$\int \psi(\mathbf{c}) f^{mod}(\mathbf{c}) d\mathbf{c} = \int \psi(\mathbf{c}) f(\mathbf{c}) d\mathbf{c}. \tag{2.42}$$

Furthermore, it can be proven that the Boltzmann inequality [eq. (2.18)] and the collision invariant conservation property [eq. (2.19)] are always true for the BGK model collision integral. Therefore, the BGK model has the same basic properties as the Boltzmann collision integral Cercignani [2006].

The main drawback in the BGK model is that the collision frequency does not depend on the velocity $\mathbf{c}$. And also this model leads to an erroneous definition of the Prandtl number ($Pr = \mu/c_p\kappa$), which for the BGK model turns out to have a value of 1, while the correct Pr number was proven to be 2/3. Therefore the collision frequency in this model can be adjusted to give correct values either of the shear stress viscosity μ or the heat conductivity κ, but not for both parameters at the same time. Different models were proposed in order to overcome this main imperfection of the BGK model.

2.2.2 Shakhov model

Shakhov in 1968 proposed a second collision model. This collision model, which has a similar relaxation form as the BGK model, could prove the correct Prandtl number and at the same time satisfy the main properties of the collision integral.

The model collision term becomes

$$J(f, f^{mod}) = \nu[f^{S} - f(t, \mathbf{r}, \mathbf{c})], \tag{2.43}$$

where the only difference stays in the different definition of the model distribution function, which for this case is

$$f^S = f^M_{loc}\left[1 + \frac{2m}{15n(\mathbf{r})[kT(\mathbf{r})]^2}\mathbf{C}(\mathbf{r})\ \mathbf{q}(\mathbf{r})\left(\frac{mC^2}{2kT(\mathbf{r})} - \frac{5}{2}\right)\right]. \tag{2.44}$$

Through this model it is possible to obtain the correct shear stress viscosity μ and the heat conductivity κ at the same time. Therefore, the heat flux can be correctly determined. Anyhow, the main limitation of the model is that the expression for f^S contains the third-order polynomial of $\mathbf{c}$, thus, the distribution function may become negative in the region of large values of the velocities, where the distribution function itself is small. For this model the H-theorem was proven only for its linearized form.

2.3 Direct simulation Monte Carlo method

The direct simulation Monte Carlo method (Bird [1995]) is a numerical tool for scientists and engineers to analyze practical non-linear gas flows at the molecular level. The DSMC method is a probabilistic method that contains a physically realistic time parameter which can allow the computation of steady and unsteady dilute gas flows, by computing the trajectory and velocity of a population of model particles after a succession of intermolecular collisions and strikes with the boundaries of the physical domain. The trajectory and collision models used are derived from the kinetic theory of gases. The DSMC method was first applied to the homogeneous gas relaxation problem (Bird [1963]), and the first application to a flow was to the shock structure problem (Bird [1965]). It is to be remarked that this approach is of a completely different nature in respects to the approaches derived by using the model kinetic equations.

This method has been criticized over the years due to the fact that it has a physical, rather than a mathematical foundation. Graeme Bird, who introduced this method, answered to these criticisms by stating that DSMC was derived from a physical reasoning not far from the one used to establish the Boltzmann formulation: both the Boltzmann equation and the DSMC method require the assumption of molecular chaos and dilute gas. The major difference between the assumptions

that allowed Bird to establish the direct simulation Monte Carlo method and the ones that Maxwell proposed in his early kinetic theory formulation, is that the DSMC method does not depend on the assumption of inverse collisions.

Therefore the DSMC method could be considered as soundly based as the Boltzmann equation itself and since does not rely on inverse collisions, it can be applied to complex phenomena, such as chemical reactions. What makes this method to be verified by test cases are, rather than the simulation procedures, the numerical approximations that have been introduced, such as the number of simulated particles and the finite intervals in space and time. Hence, the assumptions introduced by the used physical models, such as the cross-section models and the gas-surface interaction kernels, are not to be considered as imprecisions induced by the DSMC method, but they have to be considered as limitations which are imported from the kinetic theory of gases.

Nevertheless, variations of the Bird's DSMC methods exist, such as the one created by Nanbu [1980], which was derived directly from the Boltzmann equation. This variation method was proof to converge to the Boltzmann solution by Babovsky & Illner [1989].

2.3.1 DSMC: main precepts

To summarize, the main concepts on which the direct simulation Monte Carlo method was established are:

1. It refers to the solution of the problem of molecular movement in a physical domain which contains a physically meaningful time parameter.

2. The main approximation is the uncoupling, over a small time interval, of the molecular motion and the intermolecular collisions. At every time step there is rectilinear and uniform displacement of the molecule with its designed velocity. At the end of the time step there is the modification, or not, of the velocity of the molecule.

3. Since it is impossible to represent the whole population of real molecules present in a physical domain, the test particle was introduced.

4. The test particle represents a group of real molecules at neighboring positions and with similar velocities. The test particles are of correct physical size, in respect to the species treated.

5. The laws of motion of the system of test particles are formulated according to the assumptions that were introduced in derivation of the Boltzmann equation.

6. All the test particles move over an appropriate distance to the designated time step, followed by the calculation of a representative set of intermolecular collisions that correspond to this time interval.

7. The test particles are indexed to cells and sub-sells. Intermolecular collisions therefore are to occur between near neighbors.

8. The cell or spatial element network is required only in physical space, with the velocity space information being contained in the positions and velocities of the simulated molecules.

9. The Monte Carlo procedure is applied twice: once in order to chose which test particle will intervene in the collision with a neighboring particle and secondly in the attribution of the velocity after an intermolecular collision and after a collision with the wall.

10. The macroscopic parameters of the flow are obtained per each cell from the averaging of the physical parameters that characterize the whole population of test molecules in the cell.

2.3.2 Statistical fluctuations

One fundamental problematic that is important to analyze when using the DSMC approach refers to the introduction in the numerical results of statistical scatter. This problem directly arises from the fact that one test particle represents many real gas molecules: the number of test particles in respect to real gas molecules is generally such that the scatter associated with an instantaneous sample would lead to simply unacceptable results. In the case where a test particle would represent a single real gas molecule, the scatter would then have real physical significance and therefore an instantaneous sample would lead to a real representation of the

fluid flow.

The statistical scatter is, in many applications and mainly in slow flows, many orders of magnitude greater in respect to the scatter that is present in a real gas. It should be possible to achieve any desired level of accuracy by continuing or repeating the simulation to build up the size of the sample to the required magnitude: the standard deviation is of the order of the inverse square root of the sample size. Let us remind that the results obtained are generally based on a time average for a steady flow or an ensemble average for an unsteady flow.

A second problematic that is necessary to take into account are random walks during the sampling of the macroscopic quantities obtained. The random walks are induced by erroneous simulation procedures: if a random walk is present, the statistical scatter will not be able to decrease beyond a certain level, or it could even increase with time.

As a given example, random walks were found when applying the weighting factor scheme to a gas flow containing different species. For this particular case, momentum and energy were not conserved at each collision, and each departure from exact conservation is effectively a random walk in that quantity.

In the past, the unavoidable statistical scatter, and the fact that it declines only as the square root of the sample size, has been a major problem for the DSMC method. The magnitude of the computational task meant that, for many years, the method was thought to be applicable only to problems that involved large perturbations. For example, the scatter applies to the molecular velocity components so that, in a problem that involves low subsonic stream velocities, as for the experimental case we will be treating, the statistical noise could be at least an order of magnitude greater than the required signal. The reduction in the cost of computing has meant that it is now possible to deal with time or ensemble averages in the millions, and the scatter is then reduced to less than one part in a thousand.

A weak disturbance can be completely lost in the scatter in an instantaneous sample or during the earlier stages of a simulation but, as long as the procedures are such that random walks are precluded, it emerges correctly as the average

builds up (Bird [1995]).

2.3.3 Technical tips

Since the DSMC method relies mainly on three physical approximations, such as the finite cell size in physical space, the time step over which the molecular motion and collisions are uncoupled and the ratio of number of simulated molecules to the number of real molecules, from a general point of view, some laws should be always kept in mind.

The DSMC simulation becomes more exact as the time step and cell size tend to zero. As guidelines it can be said that the linear dimensions of the cells should be small in comparison with the scale length of the macroscopic flow gradients in the direction in which the dimension is measured. In regions with large macroscopic gradients, this generally means that the cell dimension should be of the order of one third the local mean free path. The time step should be much less than the local mean collision time. To summarize it is possible to state that:

1. The largest of the two dimensions $CD = max(CW, CH)$, where CW is the cell width and CH is the cell height, has to be at least three times smaller than the local mean free path of the gas

$$CD < \frac{1}{3}\lambda. \tag{2.45}$$

2. The chosen time step (DTM) multiplied by the most probable speed $vmp = \sqrt{2RT}$ has to be lower than the smallest cell width or cell height

$$DTM < \frac{CD}{vmp}. \tag{2.46}$$

3. The number of simulated molecules in each cell has to be appropriate and its number depends on the flow speed. In the case of supersonic flows the number is in the order of 20 simulated molecules per cell, instead, in the case of slow flows, such as the experimental case treated, the number is in the order of the thousands simulated molecules per cell (Ewart *et al.* [2009]).

Chapter 3

Thermal transpiration

In this chapter we reviewed the existing knowledge on thermal transpiration. The primary objective was set in order to explain the investigative evolution on the subject of thermal transpiration, which initially was studied as a transpiration through porous plates and which nowadays is exploited in high-tech novel micro-fluidic applications.

The second objective of this wide review was set in order to give proof that at present times nobody has focused attention and experimental research on the gas displacement induced by a temperature difference applied to a micro-fluidic system and the associated intrinsic time-dependency of thermal transpiration. In the future thermal transpiration could therefore become an excellent test case for non-stationary rarefied gas problems.

3.1 Genesis

The phenomenon of a rarefied gas macroscopically displaced by a temperature inequality was entirely discovered by Reynolds [1879] and he named it *Thermal Transpiration*. The name references the early studies of Graham [1863] on the diffusion of gases through long narrow tubes.

Graham, by using a self-created "diffusiometer", studied the characteristic time of diffusion for different gases. In his investigations, he clearly differentiated the physics acting behind the passage of gas molecules through long narrow tubes in

respect to the passage of gas molecules through small apertures on a thin plate, which he respectively referred to as "Capillary Transpiration" and "Effusion".

Reynolds argued that the name transpiration was suitable for his findings since, as the aperture through which the gas should pass became narrow, according to the condition of the gas, the physical characteristics of transpiration were strictly the same as those of effusion. Therefore, since the passage of gas through porous plates was then in accordance with the passage of gas through tubes, as in the experiment of Graham, he suggested that the passage of gas induced by a temperature gradient through a porous plate should respond to the name of "Thermal Transpiration".

Based on the work of Crookes [1874], who discovered the radiometer, professor Reynolds had the intuition of fixed small apertures, where the gas could move past them, instead of using moving parts set in motion by the gas, as in the radiometer experience. In analogy with Graham's work, Reynolds called his self-created apparatus the "thermo diffusiometer".

He discovered then, that by applying a difference of temperature between two regions, 1 and 2, which were separated by a porous plate, gas might be caused to pass through it (Figure 3.1). The gas, which had no initial difference of pressure and no initial difference on chemical constitution, by transpirating through the plate created a pressure variation in both reservoirs. The porous plate configuration allowed Reynolds to obtain a high state of rarefaction of the gas even by imposing relatively high working pressure conditions in the two separated regions.

The final difference of pressure obtained between two regions by only applying a temperature inequality was largely analyzed by Reynolds for different rarefaction conditions of the gas. Therefore, by both experimental and theoretical observation, Reynolds could enunciate several laws, which were derived as a direct consequence of the kinetic theory of gases (Reynolds [1879]):

(i) *When gas exists at equal pressure on either side of a porous plate across which the temperature varies, the gas will transpire through the plate from the colder to the hotter side, with velocities depending on the absolute temperature and chemical nature of the gas, the relation between the density*

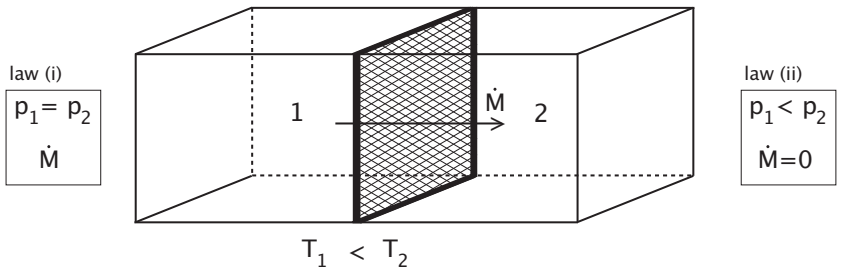

Figure 3.1: Thermal transpiration as studied by Reynolds. Inequalities of temperature applied to two regions separated by a porous plug: the pressure in the hotter region is higher in respect to the colder region.

of the gas and the fineness of the pores, the thinness of the plate and the difference of temperature on the two sides of the plate.

(ii) *In order to prevent transpiration through the plate, the pressure on the hotter side must be greater than the pressure on the colder side. This difference of pressure, at which the transpiration is zero, will depend on the same parameters as law(i) and the mean pressure of the gas, but not on the thickness of the plate.*

(iii) *The difference of pressure achieved in the case of law (ii), which depends on the rarefaction of the gas, touches a maximum value somewhere in between the free molecular and hydrodynamic regime.*

(iv) *In free molecular regime, the equilibrium state relation between pressure and temperature in the two regions is:*

$$\frac{p_2}{p_1} = \left(\frac{T_2}{T_1}\right)^{1/2}. \tag{3.1}$$

This equation correlates the equilibrium pressure ratio of both regions to the square root of the temperature ratio for the case of gas at very low densities.

Maxwell [1879], who was interested in the effects arising from inequalities of temperatures distributed along a gas, analyzed independently by theoretical investigation the phenomenon of motion of gas molecules induced by gradients of temperature and the stresses that the gas induced on objects to which a gradient of

temperature was applied. Nevertheless, it was only when he read Reynolds paper on the properties of matter that he conceived the methodology to physically represent the gas/surface interactions.

Maxwell theoretically treated the physics of the gas/surface interaction with the methodology he used in order to model the interior of a gas. In this manner he created the first kernel function of history. Maxwell therefore clearly improved Reynolds theoretical methodology and managed to describe realistically the motion of gas over surfaces to which inequalities of temperature were distributed.

It is to be noticed that Maxwell reconsidered Reynolds definition of *transpiration*: he pointed out that the passage of gas through porous plates is of an entirely different kind in respect to the passage of gas through capillary tubes, and is more nearly analogous to the flow of a gas through a small hole in a thin plate, as previously indicated by Graham. In the the latter case the gas molecules, during the passage through the hole, hardly encounter an other molecule or strike against the surfaces of the hole. On the contrary, in the case of long narrow tubes, a gas molecule has a greater probability of collisions.

Therefore Maxwell, always in analogy with Graham's terminology, proposed a different name for the case studied by Reynolds, avoiding the transpiration term in the case of apertures on thin plates, since it was more suitable for long narrow tubes, and redefined the specific case studied by Reynolds as "thermal effusion". The theory of *thermal effusion*, contrarily to the theory of *thermal transpiration*, is a very simple one, since it does not involve the theory of viscosity.

On the contrary, the theory of transpiration of gases through tubes had to necessarily depend altogether on viscosity, due to the higher amount of intermolecular collisions and the gas/surface interactions during the passage of one molecule along the tube. Hence Maxwell stated that the phenomenon of thermal transpiration through tubes could not be described by the simplistic theory of Reynolds. At least where the effects of the viscous forces were still relevant: in the case of gas in free molecular regime, it is anyhow possible to consider the passage through narrow tubes as conceived by the effusion theory.

In this manner, by applying the kinetic theory of gases, Maxwell developed a second theoretical methodology, in which he considered the intermolecular collisions and gas/surface interactions: the equations Maxwell arrived at, both express "the fact that the gas may slide over the surface with a finite velocity and the fact that this velocity and the corresponding tangential stress are affected by inequalities of temperature at the surface of the solid (containing the gas), which give rise to a force tending to make the gas slide along the surface from colder to hotter places" (Maxwell [1879]).

The differential equation that Maxwell arrived at, described the influences of inequalities of temperature on the velocity directed in the temperature gradient direction at the wall ($u|_{n=0}$) for a plane surface, was

$$u|_{n=0} = \frac{(2-\alpha)}{\alpha}\frac{\mu}{p}\left(\frac{\pi k_B T}{2m}\right)^{1/2}\left.\frac{du}{dn}\right|_{n=0} + \frac{3}{4}\frac{\mu}{p}\frac{k_B}{m}\frac{dT}{dx}, \tag{3.2}$$

where $\mathbf{n}$ is the normal to the surface and x is the coordinate along which the temperature gradient is applied.

While the equation that puts in relation the quantity of gas that transpires through any section of a tube, that is the mass flow rate $\dot{M}$, to the rate of variation of temperature and to the rate of variation of pressure along its axis x was

$$\frac{4\,\dot{M}}{\pi D^2 \rho} + \frac{(D^2 + 8G(\alpha)D)}{32\mu}\frac{dp}{dx} - \frac{3}{4}\frac{\mu}{\rho T}\frac{dT}{dx} = 0, \tag{3.3}$$

where $G(\alpha)$ was the slip coefficient function which depended on the gas surface interaction, or to the accommodation coefficient α (Section 2.1.5), and it was defined as $G(\alpha) = \frac{2}{3}(\frac{2}{\alpha} - 1)\lambda$. In the case that the gas surface interaction was considered as perfectly diffuse the value of G was $2/3\lambda$.

In this way Maxwell showed by means of a more precise theoretical approach how the rate of pressure variation along the axis of the capillary was closely interconnected to the gas mass flow rate along the tube and the rate of temperature variation along the axis of the capillary, but also that it was dependent on the rarefaction conditions of the gas and the gas itself.

It is possible to notice from eq. (3.3), in the case where the pressure is equal at the inlet and outlet and a temperature gradient is applied along the axis of the tube, that the gas will transpire from the colder to the hotter side of the tube, and in the case where the mass flow rate in each surface of the tube is zero, that the pressure along the axis of the tube will grow in the temperature gradient direction.

This equation was derived for the hydrodynamical pressure region and it was therefore not suitable for the free molecular regime, that is for $\lambda/D = \infty$, as might be readily realized from the fact that it does not satisfy the limiting condition of Reynolds law (*iv*) [eq. (3.1)].

3.2 Semi-empirical equations

Knudsen [1909], during experiments involving the passage of gases through small apertures, realized that the results were altered when imposing a difference of temperature across the apparatus. He decided then to investigate the phenomenon: he arrived at the conclusion that it was possible to obtain a pressure difference between two regions separated by a small aperture or a narrow tube by just imposing a temperature difference on them. He called this phenomenon the *thermal molecular pressure difference* (TPD). The results achieved by Knudsen were obtained in a totally independent frame work in respect to Reynolds' and Maxwell's results, as he wrote in 1935: "I must confess, however, that I could have spared part of this work because Osborne Reynolds, in 1879, described some experiments which demonstrated the phenomenon, and Maxwell treated the question theoretically in the same year" (Knudsen [1935]).

In his studies Knudsen proved the validity of Reynolds laws, this time in the case of a tube. However, Knudsen emphasized that Reynolds did not prove experimentally his law (*iv*) [eq. (3.1)], in the case of a porous body, achievement that is to be attributed entirely to Knudsen. Additional important hypothesis were given for what concerns the evolution of Reynolds experiments. Knudsen proclaimed that the law was valid only at a zero-flow final equilibrium stage which followed a transitional stage of gas displacement.

At the final zero-flow stage, when the net mass flow in every section of the tube

was zero, at sufficiently high pressures, that is when the number of mutual encounters of molecules cannot be disregarded in comparison with the number of impacts against the wall, then a counter flow of gas occurred along the axis of the tube. Knudsen hypothesis went even further, stating that it was this counter flow that would induce the final pressure difference to tend to zero, eventually, at very high pressures. Furthermore, Knudsen's considerations led as well to the idea that if the temperature difference on the tube was maintained constant, the gas would continuously flow through the tube in the case where the pressures at both ends of it, p_1 and p_2, were maintained equal.

By using an ingenious experimental apparatus Knudsen measured the thermal molecular pressure of hydrogen at different gas rarefaction conditions for the case of a tube. He proposed a semi-empirical formula which would allow the estimation of the TPD at any rarefaction condition for the case of hydrogen. The formula read as

$$\frac{dp}{dT} = \frac{p}{2T}\left[1 + 2.46\frac{D}{2\lambda}\left(\frac{1 + 3.15\frac{D}{2\lambda}}{1 + 24.6\frac{D}{2\lambda}}\right)\right]^{-2}, \tag{3.4}$$

where in this case the molecular mean free path of hydrogen could be obtained from $\lambda = 11.42\ p^{-1}(T/273)^{1.182}$, as proposed by Knudsen. Without entering in any details, the formula, in the case of $\lambda/D = \infty$, tend to the TPD limit value, namely $dp/dT = p/2T$: result that coincided with Reynolds law [eq. (3.1)]. On the contrary, if the mean free path was infinitely small in relationship to the characteristic length of the system, $\lambda/D = 0$, the reached limit value would be $dp/dT = 0$.

The evolution on the thermal transpiration theory evolved one step forward with the experimental findings of Weber & Schimdt [1936]. The authors defined a second semi-empirical formula which served well as a departure point on what concerned the final pressure ratio analysis, which we will call the *Thermal Molecular Pressure Ratio* (TPR), as a function of the gas rarefaction. Nevertheless, the Weber and Schmidt formulation, that was based on the formula of Maxwell [eq. (3.3)], was of a very complicated form, which made it difficult to use practically.

Accordingly to Liang [1953] it is to be noticed that, even if the starting point of Weber and Schmidt model was very rigorous, by considering a final zero-flow stationary state from the momentum balance of an axial flow and a tangential

flow, when they had to simplify some terms of the Maxwellian initial expression, the Weber and Schmidt formulation lost some of its accuracy. The semi-empirical formula was obtained for the case of helium. But it was proven by Van Itterbeek & De Grande [1947] that it was not suitable for other gases.

Los & Fergusson [1952] analyzed the thermal molecular difference behavior following closely Weber and Schmidt's research. Contrarily to the Weber and Schmidt assumptions, they considered the equation's constants to be dependent on the gas physical properties and depended on the applied temperature difference to the tube. By the integration of the Weber and Schmidt formula and their experimental results, Los and Fergusson redefined Weber and Schmidt semi-empirical constants and extended the semi-empirical formulation from helium to argon and nitrogen.

One remarkable result of their work was the conversion of the empirical formulation in order to describe rather than the TPR, the TPD and therefore they were able to clearly show the existence of a maximum in the thermal molecular pressure difference results as a function of the gas rarefaction, as enunciated by Reynolds law (*iii*).

Additionally, Los and Fergusson introduced a first rough estimation of the influence of the tube's surface roughness on the TPD results which can be relatively important for some cases, due to a possible wrong estimation of the local rarefaction conditions inside the tube.

Liang [1951], in the basis of the work made by Weber, extended the experimental research by analyzing the behavior of the TPR and the TPD using different gases and applying different temperature differences to his experimental system. Liang obtained a semi-empirical formula which was suitable for at least eight different gases. This was done by just changing the "pressure shifting factor" which was a fitting parameter that varied as a function of the used gas.

The initial aim of Liang's work was to obtain a correction factor to use for pressure measurements made at different temperatures in respect to the temperature at which the pressure gauges worked. The correction to be made was particularly relevant in cases where the gas mean free path was of the same order of

dimension in respect to the pressure gauge's connecting tube's diameter. The final result of his research was a much more easy-to-use equation in respect to Weber's semi-empirical formula. His empirical constants were functions of the gas physical properties and the applied temperature differences to the tube. Liang's formula is of a certain interest due to its simplicity and the accurateness in the prediction of the TPR in certain ranges of temperature differences used along a tube.

The formula reads as

$$\frac{p_1}{p_2} = \frac{A_L(p_2 D/F_L)^2 + B_L(p_2 D/F_L) + \sqrt{T_1/T_2}}{A_L(p_2 D/F_L)^2 + B_L(p_2 D/F_L) + 1}, \tag{3.5}$$

where A_L, B_L and F_L are Liang's fitting parameters. The pressure p_1 and the diameter D values were here measured in [torr] and [mm], respectively.

Furthermore, Liang [1953] questioned whether the rigorous starting mathematical treatment of Weber was a strong point on his favor or not. His suggestion was that a simpler formula could be more interesting from a practical point of view.

Liang brought the thermal molecular pressure difference analysis one step forward by giving a simple mathematical prove that the TPD has only one maximum as a function of $p_1 D$, that is a value directly proportional to the gas rarefaction, therefore, for a fixed tube diameter dimension, p_1^{max} could vary only together with the gas used. It is to be mentioned that his theory of a TPD maximum correlated to an unique pressure value was correct. However, his early attempts to define the pressure at which this maximum existed needed to be refined, since his formulation [eq. 3.5] did not include the viscosity of the gas, but depended only on his empirical constants.

The corrections that needed to be made on Liang's semi-empirical formula, were promptly pointed out by Bennett & Tompkins [1957]. Their paper was devoted to the analysis of Liang's formula: corrections were suggested to be made on the used empirical constants.

One final useful thought to be found in Bennett and Tompkins' paper was the proposition of considering possible parasite thermal transpiration effects inside

the connecting tubes of the gauges which could be considered erroneously infinite in relationship to the analyzed capillary: the error that this underestimation could induce is of 10% or more for particular cases.

Rosenberg & Martel Jr [1958] showed how Liang's equation could not predict the behavior of the TPR at extreme rarefaction conditions of the gas. Liang's formula gives an excessive estimation of this quantity.

Takaishi & Sensui [1963] improved Liang's law by creating a second version of it and recalculating its constants. Contrarily in respect to previous works, the authors made a wide analysis, using temperature differences with T_2 higher than the ambient temperature T_1. This equation seemed to be more suitable for a larger range of temperatures applied and gases used, for a large range of gas rarefaction conditions. Takaishi and Sensui's semi-empirical formula reads as

$$\frac{p_1}{p_2} = \frac{A_T(p_2 D/T_{av})^2 + B_T(p_2 D/T_{av}) + C_T(p_2 D/T_{av})^{1/2} + \sqrt{T_1/T_2}}{A_T(p_2 D/T_{av})^2 + B_T(p_2 D/T_{av}) + C_T(p_2 D/T_{av})^{1/2} + 1}, \tag{3.6}$$

where A_T, B_T and C_T are Takaishi and Sensui's fitting parameters. The average temperature along the tube is $T_{av} = (T_1 + T_2)/2$ while the pressure p_1 and the diameter D values are here measured in [torr] and [mm], respectively.

Takaishi and Sensui's formulation was also criticized. York *et al.* [2000] showed how some of the constants introduced by the authors could be changed in order to improve the fit to the experimental results presented by the authors.

Nevertheless, even if the Liang and the Takaishi and Sensuis semi-empirical equations were criticized by some authors, nowadays they are still used to correct or calibrate pressure measures done in cases where the gas has a different temperature in respect to the operating temperature of the pressure gauge. Therefore it is of interest to understand until which extent they actually reproduce the pumping effects of thermal transpiration.

3.3 Experimental campaigns during the 60s

Historically, the rarefied gas dynamics community was heavily stimulated by the important space race undertaken from the 1960s in ahead, therefore also the *thermal transpiration* phenomenon analysis attracted a large scientific interest. An extraordinary amount of experimental data on thermal transpiration was released during those years. Therefore, in addition to the experimental investigations conducted on thermal transpiration during the 1950s and those previously quoted (Bennett & Tompkins [1957]; Liang [1951, 1953]; Los & Fergusson [1952]; Rosenberg & Martel Jr [1958]), we estimate that it is of interest to introduce some of the experimental investigations that were conducted during the 1960s:

- Podgurski & Davis [1961] for the first gave time reliable data using the so called "absolute method" pressure measurements and showed how the TPR, for the case of a tube, depended not only on the gas rarefaction, the gas physical properties and the used temperature difference but also on the absolute temperatures T_1 and T_2. Their experimental results were made for free molecular regime gas rarefaction conditions.

- Takaishi & Sensui [1963] gave a more reliable semi-empirical formula in order to predict the *thermal molecular pressure ratio* (*Section* 3.2).

- Edmonds & Hobson [1965] tested different geometries using ultrahigh-vacuum techniques. They could prove indeed that the TPR tended to a certain constant value for gas rarefaction conditions in free molecular regime, namely $pD < 0.01$, where p was a reference pressure in *torr* and D was the tube's diameter in *mm*. Anyhow, they could not prove for the case of a tube that this limit value was the one proposed by Reynolds [eq. (3.1)]. To support their experimental findings, Edmonds and Hobson presented previous researcher's experimental results showing how this limit value was effectively never reached experimentally.

- Watkins *et al.* [1967] compared their results with the semi-empirical equation of Weber and Schmidt, finding data with a satisfying qualitative agreement. Nevertheless, Weber and Schmidt's equation was not suitable for a quantitative comparison, in the case of the temperature differences imposed by Watkins et al. to their system. As Los & Fergusson [1952], Watkins et al.

supported the conclusion that a new revision of Weber and Schmidt equation had to be done for their temperature differences applied.

3.4 Early comparisons to model equations

The great amount of experimental data released on rarefied gas flows provided excellent test cases for the numerical kinetic models developed during the 1950s. For example Cercignani & Sernagiotto [1966] and Ferziger [1967] studied accurately the Poiseuille flow case by solving numerically the previously introduced Bhatnagar-Gross-Krook model (*Section* 2.2.1). Therefore, after testing the kinetic model equation on isothermal cases, great interest grew around cases concerning non-isothermal cases, such as the thermal transpiration case.

Contemporarily Sone & Yamamoto [1968] studied the thermal transpiration and the Poiseuille flow through a cylindrical tube: by assuming that the temperature gradient and the pressure gradient along the axial direction of the cylindrical tube were sufficiently small, the authors could linearize the BGK model equation and the boundary conditions and solve the problem by using the small perturbation method. They could analytically solve the small perturbation scheme for small Knudsen numbers and they defined the Poiseuille coefficient G_p and the Thermal Transpiration coefficient G_T which were functions of the gas rarefaction parameter up to the second order. By integration along the longitudinal axis of the tube, these two coefficients finally allowed the authors to obtain the total mass flow rate along the cylindrical tube.

Loyalka [1969] promptly emphasized that the solution method of Sone and Yamamoto could lead to some errors due to the fact that they did not take into account that the studied problem of Poiseuille flow and thermal transpiration flow was to be considered both as a viscous and a thermal phenomenon. As already discussed in *Section* 2.2.1, the BGK model does not give correct values for the shear stress viscosity and the conductivity coefficient at the same time. Therefore Loyalka proposed that the collision frequency, which is the only free parameter, had to be properly adjusted. The author took this modification into account by defining the Poiseuille coefficient and the thermal coefficient as a function of a viscous mean free path and a thermal mean free path respectively, contrarily to

the single mean free path introduced by Sone and Yamamoto. Loyalka in this way arrived at the definition of a second function of G_T. The analytically obtained results were in better agreement in respect to the results obtained by Sone and Yamamoto when they were compared to the numerical solution of the BGK model for the case of thermal transpiration. Furthermore, even if the method employed was not new, Loyalka was the first to solve the thermal transpiration flow case by a direct numerical method.

It became clear from the experimental results of the thermal molecular pressure difference obtained by Annis [1972], that the complete diffuse reflection Maxwellian model and the thermodynamic approach proposed by Deryagin *et al.* [1967] were inappropriate to predict the thermal transpiration phenomenon at arbitrary Knudsen numbers. Annis extracted the accommodation coefficient from his experimental results by fitting Maxwell's formulation [eq. (3.3)] by means of the least square method: the author found that this value was different than 1. Through this method, Annis could fit the original theory of Maxwell in within 1.4% of divergence from his experimental results. Anyhow, the results showed that there was little or no dependence on the gas surface interaction in the thermal molecular pressure difference results: all the tested gases converged towards the same value. These results were in good agreement with the results of Loyalka & Cipolla Jr [1971], who treated the thermal transpiration problem numerically with arbitrary accommodation at the surface.

Porodnov *et al.* [1978] remarked that previous experimental works were accomplished only for cases where the temperature difference applied to the system was comparable to the average temperature of the system, that is $\Delta T/T_0 \sim 1$, making it then extremely difficult to compare experimental and numerical results since, at the time existing numerical solutions, were obtained for small perturbations of the velocity distribution function, namely $\Delta T/T_0 \ll 1$. Therefore, the experimental approach of Porodnov et al. consisted in applying a small temperature difference to a single glass capillary. By comparing the obtained results on a large number of monoatomic and polyatomic gases, Porodnov et al. realized that a maximum TPD value could be found in a precise range of the gas rarefaction conditions for all the studied gases, namely in between the transitional and the slip regime.

Porodnov et al., from their experimental research, extracted the thermal-molecular pressure ratio exponent (γ). This parameter varied with the gas rarefaction conditions and with the gas physical properties. The thermal molecular pressure ratio exponent substitutes the 1/2 value of Reynolds' initial law [eq. (3.1)]

$$p_2/p_1 = (T_2/T_1)^{\gamma}. \tag{3.7}$$

The thermal-molecular pressure ratio exponent limits tend to 1/2 for free molecular regime gas rarefaction conditions, as initially predicted by Reynolds, and to 0 for the hydrodynamic regime.

Theoretically, in the case of a perfect accommodation of the gas to the surface, γ should not variate as a function of the gas treated for a given gas rarefaction and for the same surface considered. Therefore, if γ for a given gas rarefaction varies as a function of the molecular weight or molecular dimension, this can be interpreted as a different gas/surface interaction. In other words, from the thermal molecular pressure difference it is possible to analyze in which manner the gas/surface interaction differed as a function of the gases used and the surface material used.

Porodnov et al. experimentally showed the influence of the gas/surface interaction by extrapolating the thermal molecular pressure ratio exponent for different gases. The authors compared their results with the numerical results obtained by means of the BGK model using the methodology defined by Loyalka [1969]. Their experimental and numerical results had a good agreement, even if their numerical results did not coincide with Loyalka's results for arbitrary accommodation coefficients. The authors attributed this divergence to an error made by Loyalka on one integration.

3.5 Micro-electro-mechanical systems

In recent times, the advent of micro-electro mechanical systems (MEMS) made way for new perspectives on thermal transpiration, since current microelectronic systems sizes have decreased to sub-micron dimensions, where the gas mean free path is often of the same order of the characteristic length of the system. Thus, the gas is found to be in advanced rarefied conditions also at even relatively high

working pressures. In this instance, thermal transpiration could be applied as a powerful micro-fluidic tool, since by just simply heating or cooling it is possible to create a gas flow or to create a pressure difference along a micro-system. On the other hand, thermal transpiration could also be regarded as a parasite phenomenon present in micro-fluidic systems that do not work under isothermal conditions and thus it is necessary to quantify it well.

Several authors looked into the thermal transpiration phenomenon in order to develop useful micro-fluidic devices for practical applications. For instance, the concept of using the pumping effect of thermal transpiration to create a pump without moving parts to be used for space exploration, led to ten years of intensive investigations on what today is known as the Knudsen micro-compressor, which assembles the important advantages of being a compact, low power-need and lubricating-fluid-free micro-fluidic system.

This device was developed by the investigations of Vargo *et al.* [1999a,b, 2000], Young *et al.* [2003], Alexeenko *et al.* [2006] and Han *et al.* [2007]. The final goal of these researchers was to obtain a functioning device, however, they opened up some interesting fluid-dynamics perspectives on the subject. Their investigations were conducted by means of experimental studies, direct simulation Monte-Carlo and BGK calculations. They tested their device at various temperature differences and with different operating gases in a wide range of gas rarefaction conditions. The researchers were mainly interested in the final difference of pressure they could achieve using their multi-stage device.

Ronney [2004], on this basis, developed a thermal transpiration pump which did not need an electrical power source, but used exhausted combustion gases in order to create a difference of temperature through the apparatus.

Passian *et al.* [2002, 2003] measured the forces exerted on a mechanical micro-cantilever induced by thermal transpiration. The motivations of their work derived from the need to quantify the calibration to be done on the imaging process of surfaces realized by means of the atomic force microscopy technique (AFM), which involved the use of a micro-cantilever. In the case where the surfaces to be pictured had a different temperature in respect to the micro-cantilever, the imag-

ing might have been slightly compromised by a thermal transpiration generated force between the surface and the micro-cantilever. The exerted force varied as a function of the gas rarefaction.

Sone *et al.* [2001], Sugimoto & Sone [2005] and Sugimoto *et al.* [2008] experimentally worked on the visualization of a thermal transpiration flow by means of a micro-windmill. The windmill, by rotating on its axis, showed how the flow was effectively directed in the temperature gradient direction and showed its qualitative dependence from the gas rarefaction.

McNamara & Gianchandani [2005] investigated the manner of producing a micromachined Knudsen compressor on-chip. The authors developed an efficient multistage vacuum pump that worked at ambient pressure. The characteristic length of the micro-system was reduced as much as possible in order to obtain the maximum possible compression, that was obtained for gas in free molecular regime.

Gupta & Gianchandani [2008] continued investigating on the Knudsen compressor and developed a second micro-system this time composed by different layers, one of which was a zeolite disks whose porosity guaranteed the rarefaction of the gas. By creating a difference of temperature in between the two regions separated by the zeolite disk, the micro-system obtained a gas compression.

3.6 Macroscopic gas movement

After more than a century of experimental research on thermal transpiration, it is still true that no real efforts have been made to measure the mass flow rate induced by the phenomenon along a capillary experimentally. The only advances in the subject known to us so far are the original experimental set-ups presented in Sone *et al.* [2001]. Their experimental apparatus, which consisted of a micro-windmill set at the end of a bent capillary, allowed qualitative but not quantitative analysis of the mass flow rate induced by thermal transpiration. It was difficult to overcome the evident difficulty on finding an accurate correlation between the rotation speed of the micro-windmill and the mass flow rate of the gas transiting along the tube. Nevertheless, through the windmill experience they visually demonstrated that the gas flowed from the unheated to the heated part of the tube.

Therefore, as the state of the art stands at present, most attention was paid to the final zero-flow equilibrium state induced by the phenomenon, where the net mass flow rate along the tube was zero and the final pressure equilibrium state was already engendered (Rojas Cardenas *et al.* [2012a]).

In the introductory chapter it was previously discussed that, in order to measure a stationary mass flow rate generated by applying only a temperature gradient to a tube, we used Knudsen intuition of a transient gas displacement stage between two equilibrium stages which could be monitored by following the variation of pressure with time at the two ends of a micro-fluidic system. The first to experimentally show this pressure variation with time was Huang *et al.* [1999].

Huang et al. presented a very complete analysis on the influence of thermal transpiration in binary gas mixtures. An effect that can be found in the growth of organic solid thin films by physical vapor transport in microgravity environments and in various chemical vapor deposition processes on Earth. By an ingenious experimental system the authors measured the pressure difference evolution in time due to thermal transpiration on a net of parallel capillaries. They predicted the establishment of an initial flow due to the imposed temperature gradient which would be fully compensated at the end of the experience by a contrarily directed Poiseuille flow created by the pressure difference evolution in time. In this way, the authors showed experimentally how thermal transpiration could be a time dependent process.

Later, York *et al.* [2000] and Han *et al.* [2007] also captured the pressure variation with time induced by thermal transpiration.

By using a similar experimental configuration based on the well known constant volume technique (Arkilic *et al.* [1997]; Colin *et al.* [2004]; Ewart *et al.* [2006]; Perrier *et al.* [2011]; Porodnov *et al.* [1974]) and by considering thermal transpiration as a time-dependent phenomenon, we found an original way to quantitatively determine the stationary mass flow rate by following the pressure variation with time at the inlet and outlet of a micro-tube (Rojas Cardenas *et al.* [2011, 2012b]).

For what concerns recent numerical work on thermal transpiration, authors as Sharipov [1996] and Graur & Sharipov [2009] have dedicated attention to the temperature driven flow. Contrarily to works presented in the past and those which we have already discussed, these authors used the S-model approximation of the BE and they presented numerical results of a reduced thermal transpiration flow rate and a reduced Poiseuille flow rate. These results were obtained for arbitrary pressure and temperature drops for a wide range of the gas rarefaction.

In particular, we will use the numerical results of Graur & Sharipov [2009], which were obtained for a cylindrical long tube, in order to effectuate a comparison between our experimental results and their numerical findings.

Chapter 4

Apparatus

The goal of the investigation was the measurement of a stationary thermal transpiration flow driven only by a temperature inequality. Therefore, to attain this objective it was necessary to construct an experimental apparatus that was able to follow the pressure variation with time at the ends of a micro-fluidic device, which in this case was a micro-tube subjected to a temperature gradient along its surface by being connected to two reservoirs at its inlet and outlet. In this chapter all the procedures that led to the obtention of a fully working experimental apparatus were presented in the following order.

First we described the micro-fluidic apparatus and the instrumentation used; secondly we introduced the methodology of application of the inequalities of temperature on the micro-fluidic test section and the temperature measurements realized; thirdly we quantified the parasite thermal transpiration phenomena inside the pressure gauges; lastly we illustrated the problems encountered during the experimental campaign and we explained the methodology used for the measurement of the dimensions of the reservoirs' internal volume.

4.1 General description

The experimental set-up was composed of a borosilicate (glass) micro-tube of circular cross-section, two reservoirs, a heater, three capacitance diaphragm pressure gauges, three thermocouples, a vacuum pump, an infrared camera, a solenoid micro-valve, three pressurized gas tanks and the acquisition system (Figure 4.1).

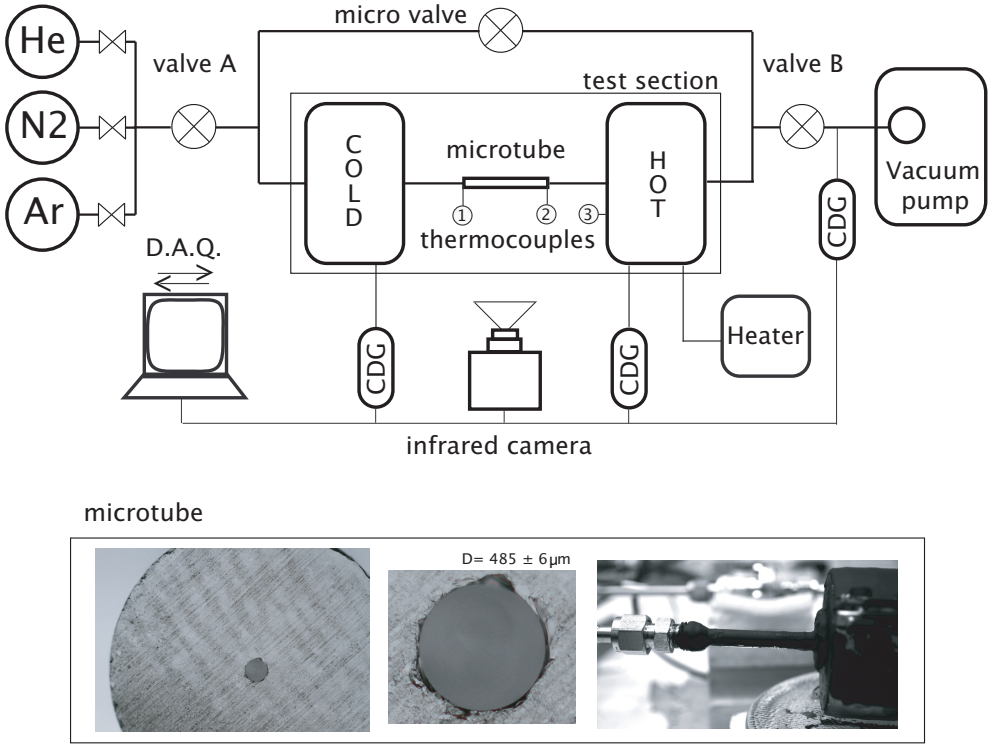

Figure 4.1: The experimental apparatus composed by the test section, the internal and external ring, the capacitance pressure diaphragm gauges (CDG), the heater, the infrared camera, the vacuum pump and the pressurized gas tanks. The test section is composed by the micro-tube, one thermocouple ($tp1$), two resistive thermal devices ($tp2$ and $tp3$) and the cold-side and hot-side reservoir. The circular cross-section micro-tube: internal and external diameter.

The two reservoirs, to which the micro-tube was connected, were considered as a part of the test section.

4.1.1 Test section

The test section was composed by a single glass micro-tube ($L_t = 52.7 \pm 0.1mm$, $D = 485 \pm 6\mu m$ and $D_{ext} = 6.5 \pm 0.1mm$) and two reservoirs which were positioned at the inlet and outlet of the capillary. The hot-side reservoir ($V_h = 16.4 \pm 0.5cm^3$) was heated, while the cold-side reservoir ($V_c = 20.5 \pm 0.5cm^3$) was cooled by natural convection of the ambient air.

The two reservoirs, where h and c stand for hot- and cold-side respectively, were manufactured appositely to host the single glass micro-tube used. Therefore the reservoirs were designed with special connections which were able to delicately host the fragile glass micro-tube ends. The notations h and c adopted here replace 2 and 1 respectively in the initially cited Reynolds law [eq. (3.1)].

The two reservoirs were connected through the borosilicate micro-tube. Therefore, due to the material properties of the tube ($\kappa = 1.14\ W/mK$) and since one reservoir was heated while the other one was cooled, a steep temperature gradient was set up along the axial surface of the tube. The temperature distribution along the tube was measured by means of an infrared camera positioned perpendicularly to the tube's axis. In order to obtain a better estimation of the temperature at the outlet and at the inlet of the micro-tube, two thermocouples were inserted inside the hot-side reservoir, additionally one thermocouple was positioned on the cold-side reservoir.

The temperature was maintained stable and did not vary during a given experimental sequence. The values applied to the hot-side reservoir and the corresponding temperatures engendered on the cold-side of the tube were $T_h = 372K$, $353.5K$ and $336K$ and $T_c = 301K$, $300K$, $299K$ respectively.

Inside the two reservoirs, the pressure variation with time was monitored at the inlet and outlet of the micro-tube by means of two fast response capacitance diaphragm pressure gauges (CDG). With an acquisition frequency of $333Hz$, these pressure sensors captured the pressure variation with time during the various stages of the thermal transpiration experiment. The pressure gauges had a full scale reading value of $1330Pa$.

4.1.2 Internal and external ring

The external and internal rings of the experimental system had different functions. The external ring was an open circuit, its inlet being connected to pressurized tanks, which contained three gases: helium, argon and nitrogen. At its outlet, the external ring was connected to the vacuum pump that created the rarefied gas

conditions in the test section.

The internal ring was a closed circuit and served, firstly, to damp and stabilize the pressure oscillations before the start of the initial stage of the experiment and, secondly, to connect the two reservoirs by means of a tube having a diameter 100 times the internal diameter of the micro-tube. The junction tube between the two reservoirs was equipped with a solenoid micro-valve, which was chosen since at its closure it displaced an infinitesimal volume of gas. Thus, the compression of the gas at valve closure was negligible. This internal ring could be isolated from the external ring by means of two valves, valve A and valve B. .

The vacuum inside the system was obtained by means of a vacuum pump. We were able to reach values in the order of $0.1Pa$ inside the test section.

In order to avoid leakage entering inside the test section, a powerful polyepoxide seal particularly effective at high temperatures was applied between the external surface of the micro-tube and the reservoirs junctions.

4.1.3 Instrumentation

The instrumentation systems mounted in the experimental setup were used to monitor the pressure and the temperature of the micro-fluidic system. For the pressure measurements three capacitance diaphragm pressure gauges (CDG) were used, while for the temperature measurements three resistive thermal devices and an infrared camera were used.

Capacitance diaphragm gauges

The pressure variation in the micro-fluidic apparatus was monitored by means of capacitance diaphragm gauges (Figure 4.2). The CDGs were integrated in the system by connecting them to the hot- and the cold-side reservoirs and at the inlet of the vacuum pump. The characteristics of the pressure gauges were specifically chosen in order to be conform to the temperature ranges at which the reservoirs were heated and conform to the pressure range at which we wanted to perform the experiments.

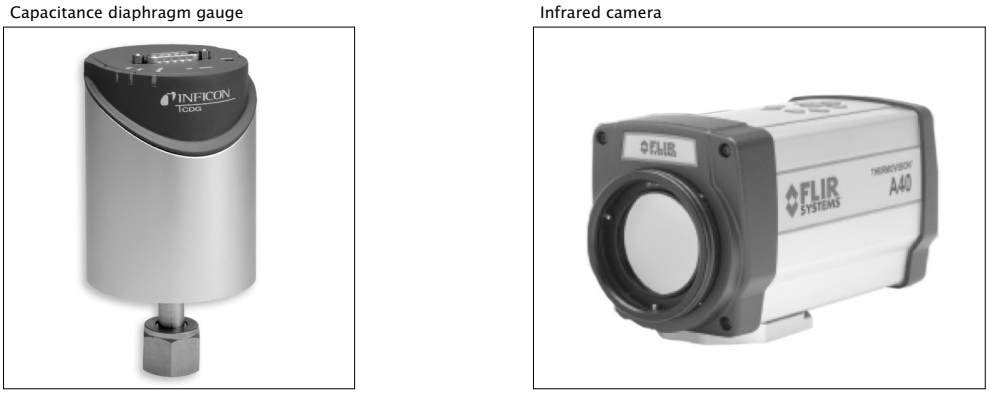

Figure 4.2: On the left the INFICON Capacitance Diaphragm Gauge used. On the right the FLIR systems A40 Thermovision infrared camera used.

The main idea was to make the CDGs work at ideal conditions, therefore we chose pressure sensors that worked at the same temperatures at which the gas inside the reservoirs was during the experiments. Hence, for the cold-side reservoir a CDG045 sensor was chosen, while for the hot-side reservoir a CDG160 was chosen. The peculiar characteristic of the sensors was the temperature at which they were internally heated, that is $45C$ and $160C$ for the cold- and hot-side respectively.

Since we needed to capture a pressure variation with time, the second necessary characteristic was the high acquisition frequency of the pressure gauges which had to be high enough in order to monitor the pressure variation without losing information in the surroundings of the initial phase of the experiment.

The acquisition frequency of the two pressure gauges positioned at the hot- and cold-side reservoirs was of $333Hz$ and the full scale reading value was of $1330Pa$. The accuracy in percentage of the reading value of the gauges was 0.15 and 0.4 for the CDG045 and CDG160 respectively. The resolution in percentage of the full scale value was 0.003 for the two gauges.

The third gauge was positioned at the external ring of the system next to the vacuum pump. This gauge did not have to be internally heated since the gas temperature at the inlet of the pump was not at high temperature as in the case of the hot-side reservoir. The function of this gauge was to control the vacuum quality

of the apparatus. A CDG025 pressure gauge was chosen with $13.3Pa$ of full scale reading.

Infrared camera

The temperature gradient applied to the external surface of the tube was monitored by means of a FLIR systems A40 Thermovision infrared camera. The peculiarity of this camera lies in the interchangeability of its lenses. The preferred option was its macro vision lens which offered the possibility of acquiring one temperature point every $50\mu m$. The camera was set up perpendicularly to the tube's longitudinal axis. The accuracy laid in within 2% of the reading temperature value in Celsius degrees and had a thermal sensitivity of 0.08 Celsius at 30 Celsius degrees.

The infrared camera was calibrated by the TCM[1] group of our laboratory. They provided us the correct emissivity coefficient ($\varepsilon = 0.94$) for a black paint with which we covered the external surface of the micro-tube. From here, it was possible to measure the correct heat flux at the external axial surface of the micro-tube. We tested the temperature measurements of the infrared camera by measuring the temperature at the inlet and outlet of the micro-tube by means of the thermocouples positioned in the hot- and cold-side reservoirs. These temperature measurements corresponded to the temperatures measured with the infrared camera.

The thermocouples used to measure the temperature at the inlet and outlet reservoir were of type K and they had an external diameter of $2mm$. The temperature measurements had an uncertainty of about 0.3% on the absolute measured value in Kelvin.

4.2 Non-isothermal survey

The physical properties of the borosilicate (glass) circular cross-section micro-tube ($\kappa = 1.14\, W/mK$), together with its dimensions, were sufficient to engender a steep temperature gradient along its axial surface by just heating the tube at its outlet. The cold-side reservoir was cooled by the ambient temperature natural convecting air. This configuration then allowed an axially directed temperature gradient along

[1] Transferts de Chaleur et de Masse, Ecole Polytechnique Universitaire de Marseille.

the micro-tube's external surface.

4.2.1 Inequalities of temperature applied

The hot-side reservoir was heated by covering its cylindrical surface with a second, concentric, stainless steel cylinder having heating resistances on its surface (Figure 4.3: right bottom image). The heating resistances were connected to a direct-current electrical power source. Due to the homogenous distribution of the heating resistances, a constant homogenous temperature was obtained on the surface of the hot-side reservoir once the final thermal equilibrium was reached. The cold-side cylindrical reservoir was cooled by natural convection of the ambient air. Since the two reservoirs were connected through the borosilicate micro-tube, a steep temperature gradient was set up along the micro-tube's axial direction.

This configuration thus allowed an exponential axially directed temperature distribution along the external surface of the micro-tube (Figure 4.3: left column). By changing the temperature of the hot-side reservoir, it was possible to engender different exponential distributions along the tube surface. The temperature was maintained stable and did not vary during a given experimental sequence. As previously mentioned, the values applied to the hot-side reservoir and the corresponding temperatures engendered on the cold-side of the tube were $T_h = 372K$, $353.5K$ and $336K$ and $T_c = 301K$, $300K$, $299K$ respectively.

As previously mentioned, the temperature distribution along the tube was measured by means of an infrared camera. In order to obtain a better estimation of the temperature at the outlet of the micro-tube, two thermocouples were inserted inside the hot-side reservoir (Figure 4.1): $tp2$ was a resistive thermal device in contact with the glass surface of the micro-tube. It measured the average temperature between the internal surface of the reservoirs internal surface and the hot-side extremity of the tube; while thermocouple $tp3$ measured the gas temperature inside the reservoir. $tp3$ was insulated from the metallic walls of the reservoir: the thermocouple's sheath was covered with a second, $0.5mm$-thick, polyvinylidene fluoride thermo-retractive sheath having a thermal conductivity of $\kappa = 0.12W/mK$. On the cold-side reservoir, the resistive thermal device $tp1$ was set-up in the same way as $tp2$.

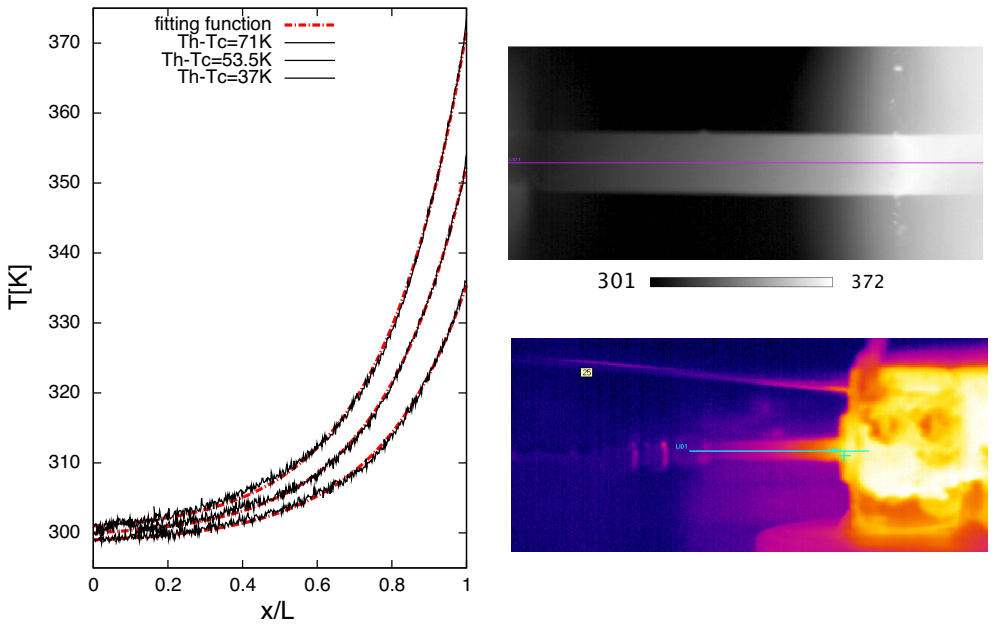

Figure 4.3: On the left: The temperature distributions along the external surface of the micro-tube. The imposed parameter was the heating power to the hot-side reservoir. The three temperature distributions have an exponential trend. The black full line is the temperature distribution monitored by means of the infrared camera [——], the red dashed line is the fitting exponential function [- - -]. On the top-right: temperature gradient along the external surface of the micro-tube infrared camera caption using the macro lens. On the top-right: infrared camera image of the test section ensemble, the micro-tube, the hot- and cold-side reservoir.

4.2.2 Infrared camera measurements

As previously introduced, the temperature gradient obtained along the capillary external surface was measured by means of an infrared camera positioned perpendicularly to the micro-tube's axis. The properties of the camera used allowed us to obtain one temperature data point every $50\mu m$. The temperature gradient along the tube's surface was then proven to be exponentially decreasing from the hot-side to the cold-side of the micro-tube (Figure 4.3).

Three different heating powers were applied to the hot-side reservoirs and three different exponential temperature distributions were thus engendered along the tube.

T_h[K]	T_c [K]	ΔT	a	b
372	301	71	0.822	4.47
353.5	300	53.5	0.655	4.40
336	299	37	0.541	4.22

Table 4.1: The hot-side temperatures T_h applied and the corresponding temperature obtained in the cold-side reservoir T_c. The temperature difference between both ends of the micro-tube ΔT. The fitting parameters a and b of the functions that reproduce the exponential trend of the temperature distribution along the external surface of the micro-tube [eq. (4.1)].

Hence, since the only variable parameter was the imposed temperature value on the hot-side reservoir T_h, the temperature value on the cold-side reservoir T_c and the temperature difference between inlet and outlet of the micro-tube ΔT were directly imposed by just adjusting the heating power applied to the hot-side reservoir.

In this study three different hot temperature values were imposed: $372, 353.5$ and $336K$ and due to the capillary's material and wall thickness, the final reached cold-side temperature was respectively $301, 300$ and $299K$ which were temperatures close to the ambient room temperature. Thus, the imposed temperature differences on the micro-tube were $\Delta T = T_h - T_c = 71K, 53.5K$ and 37 K.

Since the exponential axial variation of temperature was crearly visible, we could easily obtain the functions and the fitting parameters which reproduced the experimental temperature distributions along the external surface of the micro-tube. The equation that described the temperature axial variation was

$$T(xL^{-1}) = a\left(e^{\,xbL^{-1}} - 1\right) + T_c, \tag{4.1}$$

where a and b are the fitting parameters which vary as a function of the imposed temperature T_h on the hot side reservoir. The values of a and b are given in Table 4.1.

4.2.3 Temperature stability

The hot-side reservoir temperature was maintained constant during the whole duration of the experimental series and with it, then, the temperature distribution along the external surface of the micro-tube and the temperature in the cold-side reservoir.

In Figure 4.4 it is possible to appreciate that the temperature in the two reservoirs was stable during the whole duration of a single experiment. A single experiment lasts about 200 seconds. We can notice that the temperature oscillations measured by the thermocouples in the cold- and the hot-side reservoirs are of approximately $0.02K$ in the cold-side reservoir and of approximately $0.04K$ in the hot-side reservoir. This oscillations do not represent a physical oscillation of the thermodynamic system but are related to the resolution uncertainty of the instrument used for the temperature measurement.

Therefore we are able to state that the $\Delta T/T$ values in the two reservoirs can be considered as negligible and we estimate them in the order of 10^{-6} or lower for every single experiment.

4.2.4 Gas temperature measurements

We would like to add some comments on the difficulties encountered when measuring the temperature of the gas at the hot-side end of the tube. We introduced the thermocouple *tp3* inside the heated reservoir in order to monitor the temperature of the gas at different rarefaction conditions. To control this measurement, a second thermocouple *tp2* was inserted inside the metallic walls of the hot-side reservoir, half a millimeter from the external glass wall of the micro tube.

Unfortunately, due to the obvious high thermal inertia of the metallic walls in respect to the thermal inertia of the gas and due to the radiative exchange between the internal probe *tp3* and the metallic walls, the *tp3* thermocouple, even if in contact with the gas, measured something in between the gas and the temperature of the metallic walls. This value was nearly constant for fixed heating powers.

Let us add that since a gas flow is present along the tube, even if the flow speed

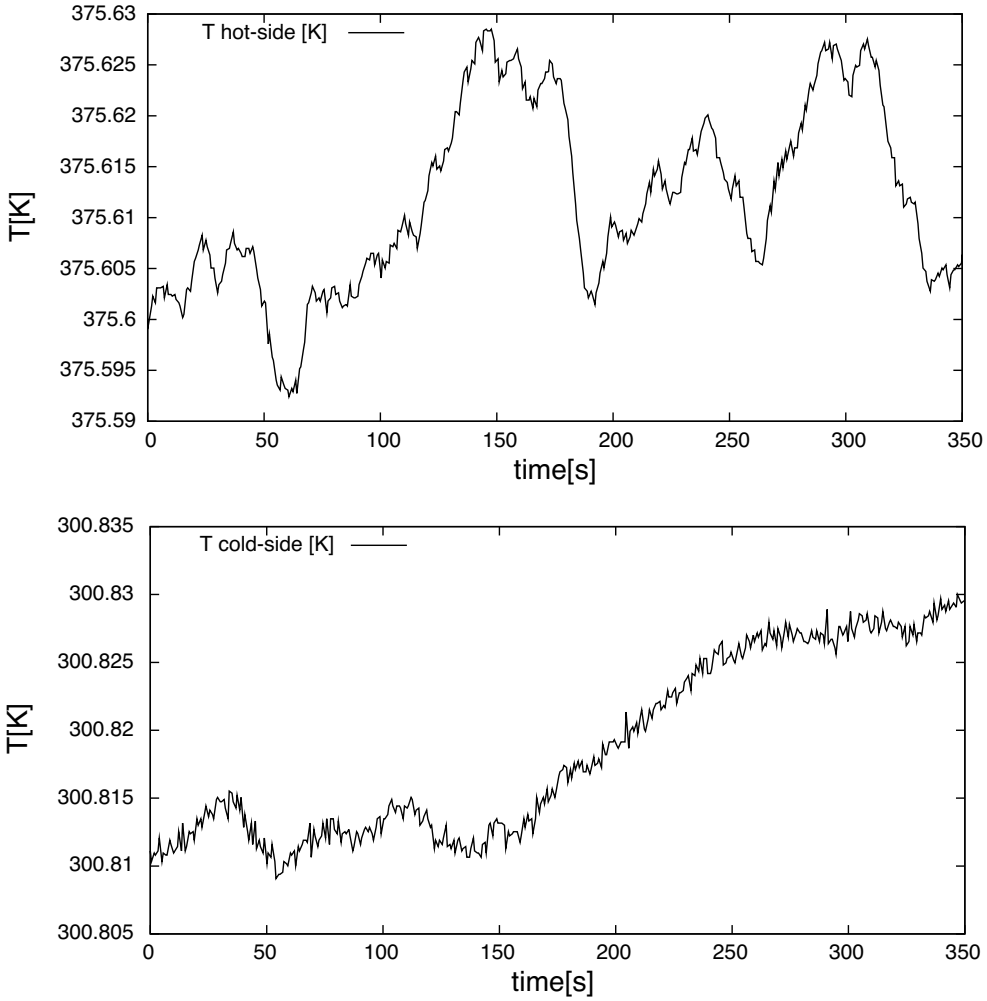

Figure 4.4: Temperature stability tests for the cold- and hot-side reservoir. The measurement was performed with the thermocouples *tp1* and *tp2*. Top: hot-side reservoir. Bottom: cold-side reservoir.

and flow mass are extremely low, there must be a temperature difference between the external tube surface temperature, measured by the camera, and the real temperature of the gas.

By computing a rough thermal calculation, it could be shown though that this temperature difference cannot exceed 3 degrees. Therefore, we chose to give as temperature reference values, in order to compare the different experimental se-

ries, the temperatures measured by the infrared camera on the cold and hot ends of the tube's external surface.

We estimated that satisfying gas temperature measurements at the hot end of the tube could be obtained by directly exploiting the measurements of the infrared camera on the external surface of the tube. The temperature values measured in the hot-side reservoir were slightly higher in respect to the temperature measurements values at the hot-end of the tube obtained with the infrared camera: this difference was in the order of $1K$.

4.3 Pressure measurements

Since we effectuated absolute pressure measurements, that is independent pressure measurements in the cold- and the hot-side reservoir by using two different pressure gauges, we needed to have the maximum precision as possible in the pressure measurement at the beginning of the experiment, when a first equilibrium was set. More details on the experimental methodology will be given in the next chapter.

Unfortunately, the calibration of the gauges as done by the constructor was not sufficient in order to ensure a precise pressure monitoring inside the reservoirs.

Therefore, it was necessary and of relative importance to take under account the inequalities of temperature arising from the utilization of heated gauges that could introduce a difference of pressure between the pressure inside the internal volume of the gauge and the pressure inside the reservoir, that is where the measurement had to be done.

Consequently a calibration had to be done in order to balance what we called a parasite thermal transpiration pumping effect introduced by the gauge inside the micro-fluidic system studied.

4.3.1 Parasite thermal transpiration

Let us now discuss the phenomenon of thermal transpiration from another perspective, that is in the case when it is not a desired phenomenon and thus might

alter the pressure measurements.

As previously introduced the pressure sensors were internally heated: we desired to have a CDG working temperature in the same range of the gas temperature where the measurement had to be made. We therefore chose to connect a pressure sensor heated at $45C$ to the cold-side reservoir and to connect a pressure sensor heated at $160C$ to the hot-side reservoir. Nevertheless, we did not want to heat the glass micro-tube until $160C$: the micro-tube was connected to two steel reservoirs, in the case where the glass and the steel are subjected to a same temperature jump, the two materials do not equally expand.

The micro-tube was positioned and installed in the reservoirs at a moment when the hot-side reservoir was not heated. If we would had heated the hot-side reservoir at $160C$, the jump of temperature, from the temperature at which the glass tube was at the installation moment, would had been of about $130C$. Therefore, when performing the experiments, we did not want to "push" the system to $160C$, which could have been a critical thermal point of collapse, also because the test section, as it was used during the experiments, was quite difficult to put into place.

Since we could not attain the expected heating temperature value of $160C$ in the hot-side reservoir, the temperature in the cold-side reservoir, too, did not reach the temperature at which the second gauge functioned, that is $45C$: the temperature jump between the gauge temperature and the gas temperature inside the cold-side reservoir was of about $18C$.

Hence, a parasite temperature gradient was present during the experiments and it was directed from the reservoirs towards the internal heated membrane of the pressure sensors, where the pressure measurement was effectuated. Thus, we had to deal with a typical example of parasite thermal transpiration, which had to be appropriately compensated. A calibration of the gauges was necessary.

4.3.2 Calibration of the gauge

Lets consider the case of two reservoirs connected by means of a large diameter tube and lets consider a gas pressure inside the thermodynamic system high

enough to be able to consider the gas as in the hydrodynamic regime.

Let us heat one reservoir, while the other one is left at ambient temperature, in this way we create a temperature difference between them. Under these circumstances, once the thermal equilibrium of the system has been reached, it is of common knowledge that the pressure inside both reservoirs will tend towards an equilibrium point and therefore be stable and equal everywhere inside the system. Ideally, we should obtain the same pressure measurement in both reservoirs.

Nevertheless, in every single experimental case analyzed, the pressure equality in the two reservoirs was never met. At the thermal equilibrium of the system, the pressure measurements diverged. This pressure divergence was due to the parasite thermal transpiration phenomenon present along the connections between the gauges and the reservoirs.

As can be seen on the left column of Figure 4.5 the pressure divergence $\Delta p'$ was significant. Nonetheless, neither the pressure measurement in the cold or in the hot- side reservoir was correct. Both gauges presented errors in the readings, overestimating the pressure inside the reservoirs of a quantity Δp_{45} for the case of the cold-side reservoir and a quantity Δp_{160} for the case of the hot-side reservoir. Therefore, these quantities needed to be quantified.

The pressure measurements were corrected by means of the Takaishi & Sensui [1963] formulation (*Section* 3.2). The semi-empirical formula was used to obtain pressure differences, therefore we used it under the following form

$$\Delta p_{CDG} = \frac{p_{CDG}(\sqrt{T_{gas}/T_{CDG}} - 1)}{A_T(\text{Ł})^2 + B_T(\text{Ł}) + C_T(\text{Ł})^{1/2} + 1}, \tag{4.2}$$

where $\Delta p_{CDG} = (p_{gas} - p_{CDG})$; p_{gas} was the pressure of the gas; p_{CDG} was the measured pressure; and $\text{Ł} = (pD)_{CDG}/T_{av}$, where D_{CDG} was the dimension of the internal diameter of the pressure gauge junction tube and it was equal to $2.35mm$. The D_{CDG} dimension was taken from Nishizawa & Hirata [2002] who conducted a study on a CDG45 gauge.

We show in Figure 4.6 the trend of the difference of pressure that had to be

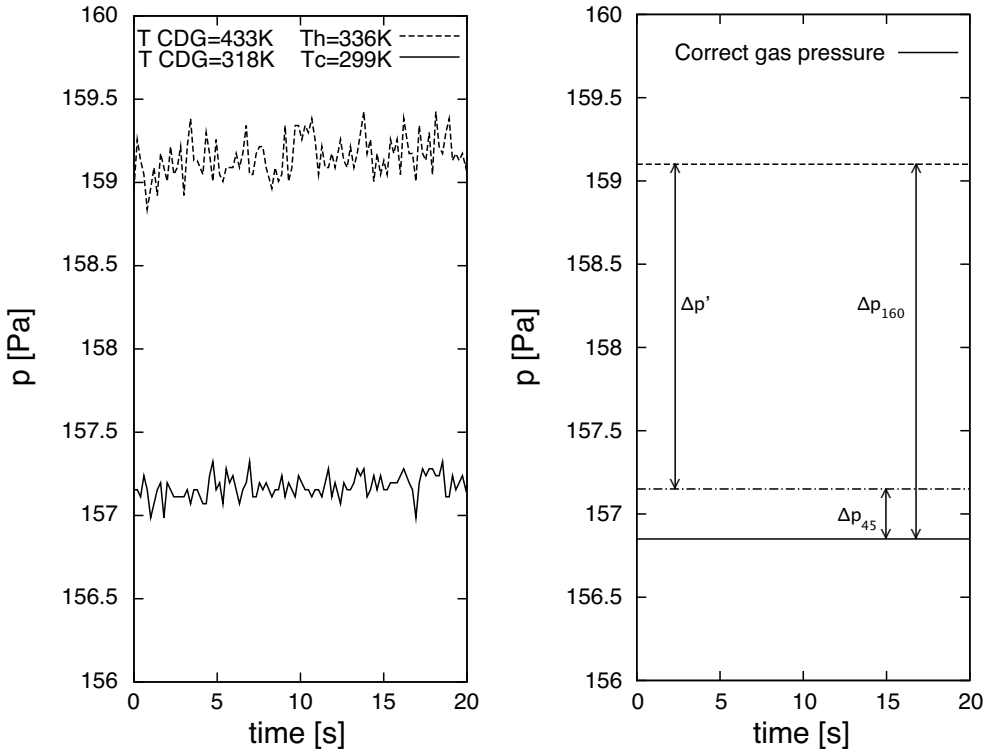

Figure 4.5: On the left: pressure measurements of Helium for $Th = 337K$ and $Tc = 299K$: not corrected values of pressure. The dashed line represents the hot-side pressure measurements done with the CDG160 ($433K$) sensor [- - -] ; while the full line represents the cold-side pressure measurements done with the CDG45 ($318K$) sensor [——]. On the right: Scheme of the corrections to be made. The lower full line represents the correct pressure of the gas [——].

subtracted from the pressure measurements. The difference of pressure varied as a function of the gas used, the rarefaction of the gas inside the junction tube and the ratio of the temperature of the gas to the temperature of the gauge. It is possible to see how the correction which had to be made increased with increasing differences of temperature between gas and gauge, and how the lighter gas was the one more affected by the parasite thermal transpiration pumping effect.

In the less favorable case, that is for Helium at a temperature difference applied between the ends of the tube of $\Delta T = 37K$ which corresponded to a temperature

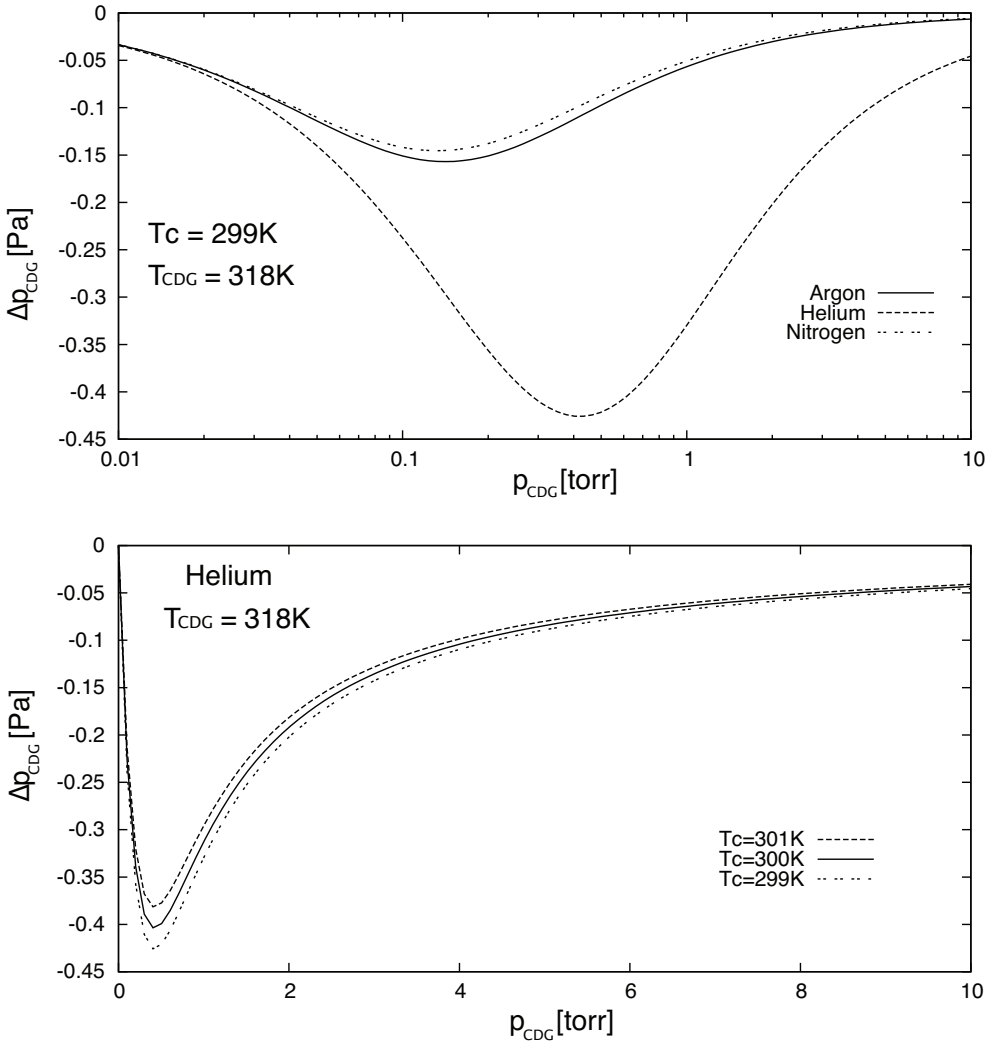

Figure 4.6: Takaishi and Sensui formulation pressure divergence correction. On the top: corrections to be made in the cold-side reservoir for the less favorable case, that is for a gas temperature of $299K$ in the cold-side reservoir, $T_{CDG} = 318K$. Comparison between argon full line [——], helium dashed line [**- - -**] and nitrogen dashed dotted line $[- \cdot -]$. On the bottom: corrections to be made in the case of helium for different temperature jumps between gauge temperature and gas temperature in the cold-side reservoir, $T_{CDG} = 318K$. Comparison between $T_c = 299K$ dashed dotted line $[- \cdot -]$, $T_c = 300K$ full line [——] and $T_c = 301K$ dashed line [**- - -**].

jump between gauge temperature and gas temperature in the cold-side reservoir of $\Delta T_{CDG} = 19K$, at the point of absolute minimum of the curve ($0.42[torr]$), the correction that had to be made to the pressure measurement of the CDG45 was of approximately $0.43[Pa]$ (Figure 4.6: helium).

The same procedure was applied to the pressure measurements performed with the CDG160 pressure sensor. As it can be seen from Figure 4.5, the correction to be made was higher. This is coherent since the temperature jump between gauge temperature and gas temperature in the hot-side reservoir was of $\Delta T_{CDG} = 97K$, $\Delta T_{CDG} = 79.5K$ and $\Delta T_{CDG} = 61K$ for the three different experimental series performed.

4.4 Troubleshooting

As in any investigative process, the more we tested the experimental apparatus, the more we gained awareness on the improvements we had to perform. To be consistent with the experimental procedures that led us to our final results, we would like to present the main problematics we encountered during the experimental campaigns realized and explain how we reacted to them.

4.4.1 Air leakage

In the first experimental apparatus conceived we encountered a major problem in maintaining a proper gas quality inside the micro-fluidic device. We experienced problems of leakage in the connecting junctions between micro-tube and hosting system inside the reservoirs. The adhesive we used did not attain to conserve its properties at high-temperatures.

Let us recall that the working pressure conditions inside the test section varied from $10^{-5}bar$ to $10^{-2}bar$: a great pressure difference was present between the interior of the test section and the external ambient pressure. As a consequence, air moved inside the internal ring of the apparatus, and therefore, instead of having a pure gas, the air leakage rapidly created a gas-mixture inside the test-section.

We could detect the air leakage by monitoring the pressure inside the two reser-

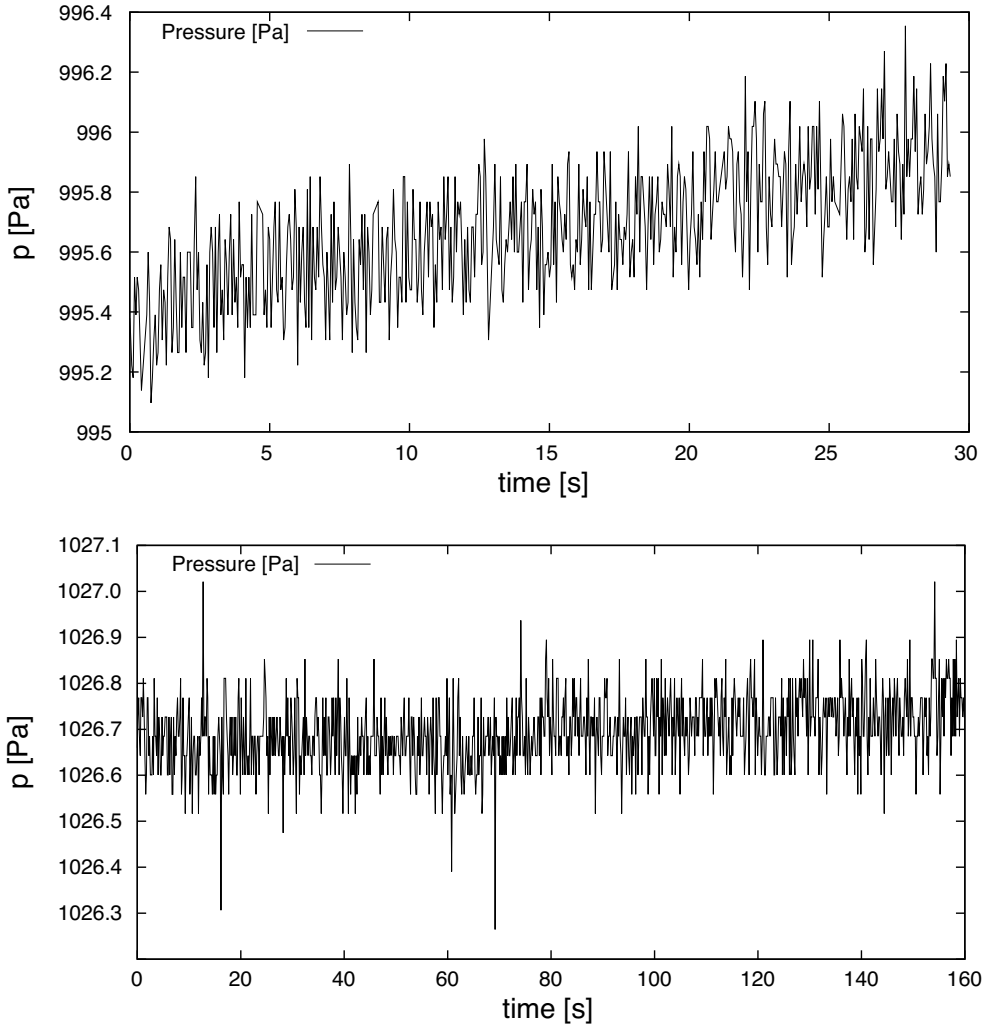

Figure 4.7: Top graph: first experimental apparatus. The pressure increase denounces air entering inside the system. Bottom graph: actual experimental apparatus. There is no pressure increase, the air leakage has been stopped.

voirs. The procedure was effectuated in isothermal conditions. As shown in Figure 4.7 (top graph), when the leakage was present, the pressure inside the reservoir increased. By a simple thermodynamic evaluation we were able to determine the volumetric flow rate of air entering inside the vessel. During a single experiment, the leakage was enough to corrupt the gas composition of at least 10% from its initial condition of purity.

By changing the adhesive used to seal the junctions between micro-tube and reservoirs and by slightly changing the structure of the hosting device, we could overcome the problem. The adhesive used was a powerful polyepoxide seal particularly effective at high temperatures.

In Figure 4.7 (bottom graph) it is possible to see that during the whole duration of an experiment, the pressure varied in within the pressure sensor resolution. Therefore we could be sure that the gas inside the test section met the desired standards of purity.

4.4.2 Compression at the valve closure

A major problem that we experienced in the first experimental setup was induced by the valve positioned in the big diameter junction tube in between the two reservoirs (Figure 4.1). Let us briefly introduce that this valve played a fundamental role during the experiments since it is at this valve's closure that the experiment began and therefore at this moment, the experimental system configuration changes and induces a pressure variation with time in the reservoirs. The details of the experimental methodology will be widely discussed in the next chapter.

Before the beginning of the experiment, the internal ring of the experiment, which comprehends the micro-tube, the two reservoirs, the big diameter junction and the valve, is at the same constant pressure. The internal ring can be considered a large volume which comprehends the sum of the totality of the internal volumes of the before mentioned components.

From here on, at the time of closure of the valve, if the volume occupied by the closed valve inside the volume of the internal ring is not considered as negligible, the valve at its closure inevitably compresses the gas.

As it can be seen from Figure 4.8, the compression inside the cold and hot-side reservoir could not be neglected due to the large perturbations induced at the beginning of the experiment, where an unperturbed pressure variation with time was needed.

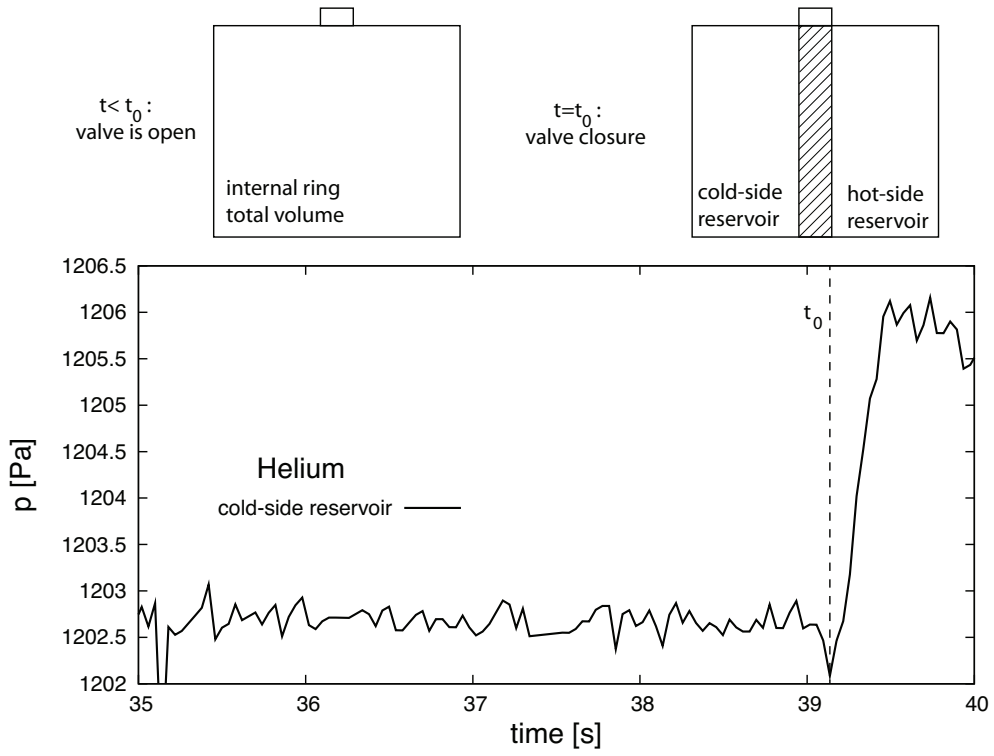

Figure 4.8: Top: scheme of the two system configurations, for $t < t_0$ the valve is open; for $t = t_0$ the valve is closed. Bottom: pressure data in the cold-side reservoir, it is possible to observe the pressure jump at the valve closure which corresponds to a gas compression.

This problem was avoided in the present experimental apparatus by placing in the big diameter junction tube a solenoid micro-valve instead of the previously used regular valve. The volume filled by the micro-valve at its closure can be neglected in respect to the volumes of the cold- or hot-side reservoirs.

4.5 Volume measurements

The dimension of the volumes was of crucial importance at the moment of calculating the mass flow rate induced by thermal transpiration. We determined these dimensions by simply performing an isothermal thermodynamic study. In order to do this we referred to two stages of thermodynamic equilibrium.

In the first stage we imposed a difference of pressure between the two reservoirs, obtaining then two separate volumes at a given pressure; in the second stage, by opening the micro-valve in the experimental apparatus, we connected the two reservoirs and waited until the thermodynamic system found its final state of pressure equilibrium (Figure 4.9). The methodology adopted to perform the volume measurements was chosen since it offered us the advantage of not introducing any modifications to the experimental apparatus.

The only drawback was that, since we wanted to perform an isothermal study in order to reduce as much as possible the measurement uncertainties derived from inequalities of temperature inside the system, it was necessary to use a different pressure gauge in the hot-side reservoirs in respect to the one used to perform the experiments, one that worked at $160C$. Therefore, in order to perform an isothermal study, we connected a gauge that was manufactured to work at ambient temperature to the hot-side reservoir. Since the internal volume of the gauge used was different in respect to the internal volume of the CDG160 used during the experiments, we might momentarily consider this hot-side reservoir volume as a test volume V_t.

The relationship that correlated the initial and the final thermodynamic equilibrium of the system was easily derived from the mass conservation law. Since we considered an isothermal system, the equation simply reads as

$$p'_1 V_c + p'_2 V_t = p'_f (V_c + V_t), \tag{4.3}$$

where p_1 and p_2 were the pressure at the initial thermodynamic equilibrium inside the cold- and hot-side reservoirs respectively; while p_f was the pressure at the final thermodynamic equilibrium inside the whole thermodynamic system.

Since the unknown variables were two, V_c and V_t, the problem could be solved only by introducing a second equation. The equation in matter responded to the same basic idea, only that this time the system was connected to a greater volume of known dimensions ($V_B = 209.02cm^3$). The volume of this latter reservoir was

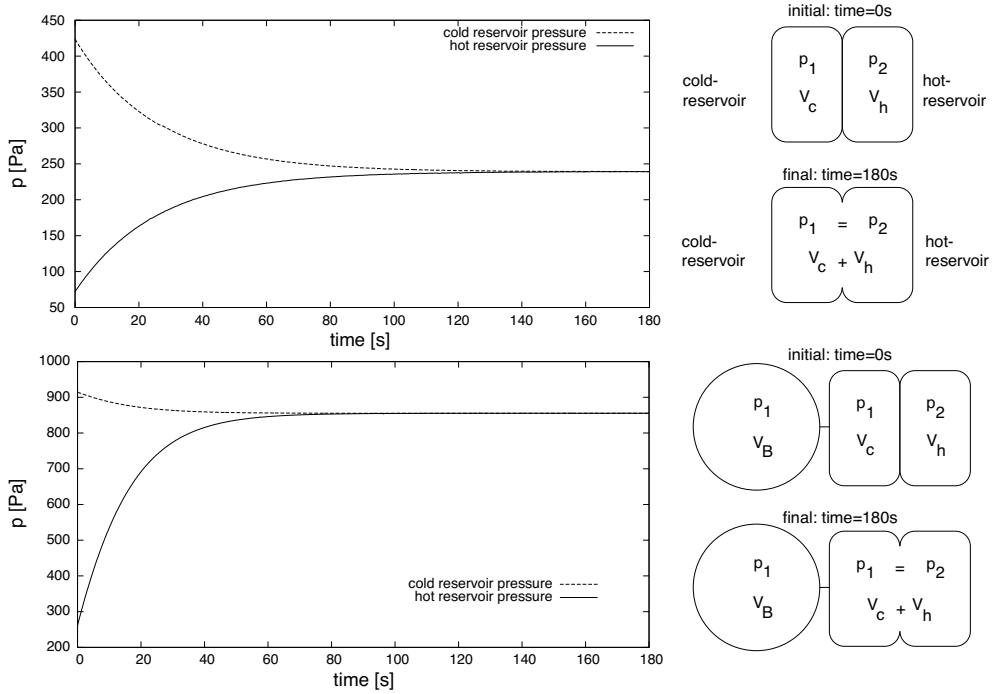

Figure 4.9: Top: the first configuration of reservoirs. On the right: the scheme of the two equilibrium stages, not connected reservoirs and connected reservoirs. On the left: the variation of pressure with time induced by the tendency of the system of reaching its point of equilibrium after that the reservoirs were connected. Bottom: the second configuration of reservoirs, a big reservoir was added at the cold-side reservoir side. On the right and on the left: as above.

measured in a conventional manner. Therefore, the second equation reads as

$$p''_1(V_c + V_B) + p''_2 V_t = p''_f(V_c + V_t + V_B). \tag{4.4}$$

Consequently, by solving the system of equations it was possible to calculate the internal volume of the cold-side reservoir

$$V_c = \frac{V_B}{(b/a - 1)}, \tag{4.5}$$

where $a = (p'_f - p'_2)/(p'_1 - p'_f)$ and $b = (p''_f - p''_2)/(p''_1 - p''_f)$.

The final step was the volume determination of the hot-side reservoir. As previously mentioned, the gauge represents a meaningful percentage of the volume of the reservoir, therefore, in order to perform the volume measurement of the hot-side reservoir we had to use the CDG160 pressure sensor.

Due to the inequalities of temperature introduced by the gauge itself, this procedure was not as precise as the one described before. The average temperature at which the gas was inside the reservoir was of impossible determination. Anyhow, by using the same methodology as for the determination of the cold-side reservoir volume, it turned out that the relationship that correlates both volumes is $V_h/V_c = 0.8$.

The cold-side reservoir volume was calculated to be $V_c = 20.5 \pm 0.5cm^3$ and the hot-side reservoir volume was calculated to be $V_h = 16.4 \pm 0.5cm^3$.

Chapter 5

Experimental methodology

In this chapter we presented the methodology used to obtain the experimental results: the constant volume technique implemented and the methodology used to perform the non-isothermal thermal transpiration experiments.

The constant volume technique is introduced in order to set the basis for the time-dependent methodology that was used in the present work notably in order to deduce the stationary, fully-developed, uni-directed and not-perturbed thermal transpiration flow.

Let us stress that the two methodologies are of a different nature: the constant volume technique was used in the past in order to deduce isothermal pressure driven mass flow rates, where the starting point was a pressure difference imposed, while in the present work the starting point is a temperature difference imposed with equal pressures at the inlet and outlet of the micro-tube. We will see in the next sections how the time-dependent methodology differs from the classical constant volume technique mass flow rate measurement. Therefore the experimental methodology used in this work can be considered of the same degree of interest as the experimental results themselves.

The thermal transpiration experimental methodology section, which was at the core of this chapter, compounded detailed explanations on the time-dependency of the experiment, on the specific method used to extract the thermal transpiration induced mass-flow rate and on the definition of the non-isothermal rarefaction

parameter used to characterize a single experiment.

5.1 Constant volume technique

Let us introduce a well known methodology used in order to deduce the stationary mass flow rate, that is the constant volume technique (Arkilic *et al.* [1997]; Colin *et al.* [2004]; Ewart *et al.* [2006]; Perrier *et al.* [2011]; Porodnov *et al.* [1974]).

In order to deduce the mass flow rate along the tube it is necessary to correlate the variation of the gas mass through the inlet or outlet section of the micro-tube to the pressure variation with time inside the cold- or hot-side reservoir during a specific time interval.

During the experiments, the experimental apparatus was conceived in order to work with two distinct finite reservoirs. The two reservoirs were connected only by means of the micro-tube. Therefore, the variation of mass inside each reservoir was attributed to the macroscopic movement of gas from the tube inside the reservoir, or from the reservoir inside the tube. Since we cannot directly monitor the gas mass variation inside a reservoir, it is necessary, as previously mentioned, to correlate the mass variation with time to the pressure variation with time inside each reservoir.

This can be done by performing a macroscopic thermodynamic study inside the reservoirs and by using the ideal gas law $pV = mRT$ as a starting point, where V is the volume of one of the two reservoirs connected to the micro-tube, R, p, T and m were respectively the specific gas constant, the pressure, the temperature and the mass of the gas.

In the case where the thermodynamic variations remain relatively small and the volume of the reservoirs are constant, the relationship is obtained from the derivation of the ideal gas law, and it is

$$\frac{dp}{p} = \frac{dm}{m} + \frac{dT}{T}. \tag{5.1}$$

Therefore, to extract the mass variation inside one of the volumes as a function of the other variating thermodynamic parameters, after some simple calculations, the equation becomes

$$dm = \frac{V}{RT} dp \left(1 - \frac{dT/T}{dp/p}\right). \tag{5.2}$$

In order to be able to use the constant volume measurement technique and to calculate the stationary mass flow rate in an isothermal constant volume reservoir in a simplified manner, it is desirable to experimentally work with the parameter ϵ small in comparison to unity

$$\epsilon = \frac{dT/T}{dp/p} \ll 1. \tag{5.3}$$

This implies that the case of an isothermal reservoir has to be effectively reproduced in order to obtain a temperature variation as close to zero as possible. At the same time the ratio dp/p should not tend to zero.

Finally, by the mass conservation law, the variation of mass inside the reservoirs corresponds to the mass flowing along the micro-tube. Therefore it is possible to state that the mass variation with time inside the reservoirs corresponds to the mass flow rate at the inlet or outlet of the tube. Furthermore, by choosing a sufficiently small specific time interval Δt where to effectuate the pressure measurement, it is then possible to measure the stationary mass flow rate at a precise instant. Thus, if the epsilon parameter is considered to be zero, eq. (5.2) becomes

$$\frac{dm}{\Delta t} = \frac{V}{RT} \frac{dp}{\Delta t}, \tag{5.4}$$

where $dm/\Delta t$ is the mass flow rate $\dot{M}$ that crosses the inlet or outlet of the micro-tube at a time t which stands in the range $(t - \Delta t/2) < t < (t + \Delta t/2)$.

It is to be noticed that the mass flow rate along a tube, in the case of a pure non-reacting gas, can be induced by a difference of pressure or a difference of temperature between its two ends. In both cases, if the temperature fluctuations could be neglected, the thermodynamic system, composed by the reservoir and the outlet or the inlet of the micro-tube, could be treated as isothermal. And therefore, eq. (5.4) can be applied.

Additionally, it is important to know that in order to be able to measure a stationary mass flow rate entering or leaving one of the reservoirs it is indispensable that the pressure variation with time varies in a linear way. Only in this case, the measured mass flow rate can be considered as being stationary and therefore independent from time.

Let us note that the measurement method adopted, that is the constant volume technique, is intrinsically correlated to a non-stationary evolution with time of the mass flow rate that enters or leaves the reservoirs. Therefore, this time-dependent mass variation engenders a non-stationary pressure variation with time inside both reservoirs. In simpler words, the mass flow rate, during the whole duration of one experiment, will vary and it will tend to a final stage of equilibrium where the net mass flow rate along the tube is zero.

Hence, in order to measure a stationary mass flow rate, it is necessary to choose a specific time interval in which the measurements are effectuated that is short enough in order to not loose the stationarity of the flow. At the same time, the specific time interval cannot be too short in order to not loose the physical consistency of the measurement. In the following sections this concept will be further developed.

5.2 Non-isothermal experiments

In order to understand the physical basic mechanism causing the movement of the gas, which is initially at rest when a temperature difference is still not imposed, it is necessary to regard the wall boundary conditions. It is possible to show, that the balance of momentum exchange between an elementary wall surface and the molecules of a fluid particle results in a force which is applied to the gas in the temperature gradient direction [Maxwell [1879]; Sone [2007]]. In other respects, the imposed gradient of temperature creates a gradient of density in direction of the tube's axis. The gas motion tends to reduce the density gradient: the gas flows from the higher to the lower density region *id est* from the cold-side to the hot-side reservoir. The main objective of this work was to measure this stationary mass flow rate generated by thermal transpiration along the tube. This was done by exploiting, in a pertinent way, the phenomenon's time dependance.

5.2.1 Time-dependent methodology

Let us remember that the micro-fluidic system was composed of a micro-tube, to which a distribution of temperature is applied along its axis, that is connected to two reservoirs: one was cooled by the natural air convection, while the other one was heated. The two reservoirs were connected through the micro-tube and through a big diameter tube connection. The big diameter connecting path between the two reservoirs could be closed at any time by a fast solenoid micro-valve (Section 4.1).

The key aspect of lecture of the non-isothermal experimental methodology relies on the fact that the experimental apparatus was specifically designed in order to allow the micro-fluidic system to instantaneously transit between two configurations and therefore create a strong thermodynamic disequilibrium along the micro-fluidic system. The thermodynamic system, after being set in strong disequilibrium, needs a certain relaxation time to tend to a new state of equilibrium.

We used this transient stadium of the thermodynamic system that tends to a final equilibrium, in order to measure the stationary, not-perturbed mass flow rate induced by thermal transpiration along a micro-tube subjected to a temperature gradient along its external surface. For this reason a time-dependent study was necessary.

Let us now introduce the two different configurations that were exploited during the experiments. The first one, which we will refer to as the open circuit configuration, offered the possibility to obtain a stationary, not-perturbed and fully developed macroscopic movement of gas molecules from the colder to the hotter region. In the case of a tube to which a distribution of temperature is applied along its axis and which is connected to two reservoirs of volume infinitely big in respect to the volume of the tube, or if the reservoirs are maintained at equal pressures, the rarefied gas in the tube continuously flows from the colder to the hotter side, therefore inducing a stationary and fully developed thermal transpiration flow.

On the contrary, if the micro-tube, to which a distribution of temperature is applied along its axis, its connected to reservoirs of finite dimensions, the effect induced

by thermal transpiration changes, and instead of creating a fully-developed and uni-oriented macroscopic gas displacement, it creates a difference of pressure between the two ends of the tube and a zero net mass flow rate along each transversal section of the capillary. We will refer to this second configuration as to the close circuit configuration, or the zero-flow configuration. Therefore, the zero-flow configuration offers the possibility to study the case investigated by Reynolds.

Subsequently, the instantaneous configuration change offers the possibility to monitor the transient thermodynamic variation of the parameters of the fluid flow inside the micro-fluidic system, that is from the initial stage of equilibrium to the zero-flow stage. In the studied case, for the experimental configuration proposed, this thermodynamic parameter was the pressure inside the cold- and the hot-side reservoir. This pressure variation with time is relatively fast and only in recent works it was possible to estimate its correct tendency and to measure it [Huang *et al.* [1999]; Han *et al.* [2007]].

Thus, by shifting from the initial idealistic infinite volume condition to a finite volume condition, the here used experimental methodology emphasizes the possibility of identifying four main stages for the entire duration of a single experiment. It is important to underline that the idealistic infinite volume condition is not experimentally achieved here. This condition is an assumption in order to introduce the methodology of the experiment. More to this aspect will be said in the following paragraphs.

5.2.1.1 Thermal transpiration flow

The first stage of the experiment (Figure 5.1: left column - top graph, stage 1) begins only when the desired initial gas pressure p_i is imposed inside the internal ring. This regulation process is achieved by means of the regulation valves A and B. Once the desired thermodynamic conditions are set inside the test section, the two regulation valves are closed, and they will remain shut for the whole duration of the experience.

As it has been already mentioned, after the test section has been isolated from the external ring, the internal ring of the system starts to operate as a stabilizing chamber. Therefore, once all the residual pressure oscillations inside the test sec-

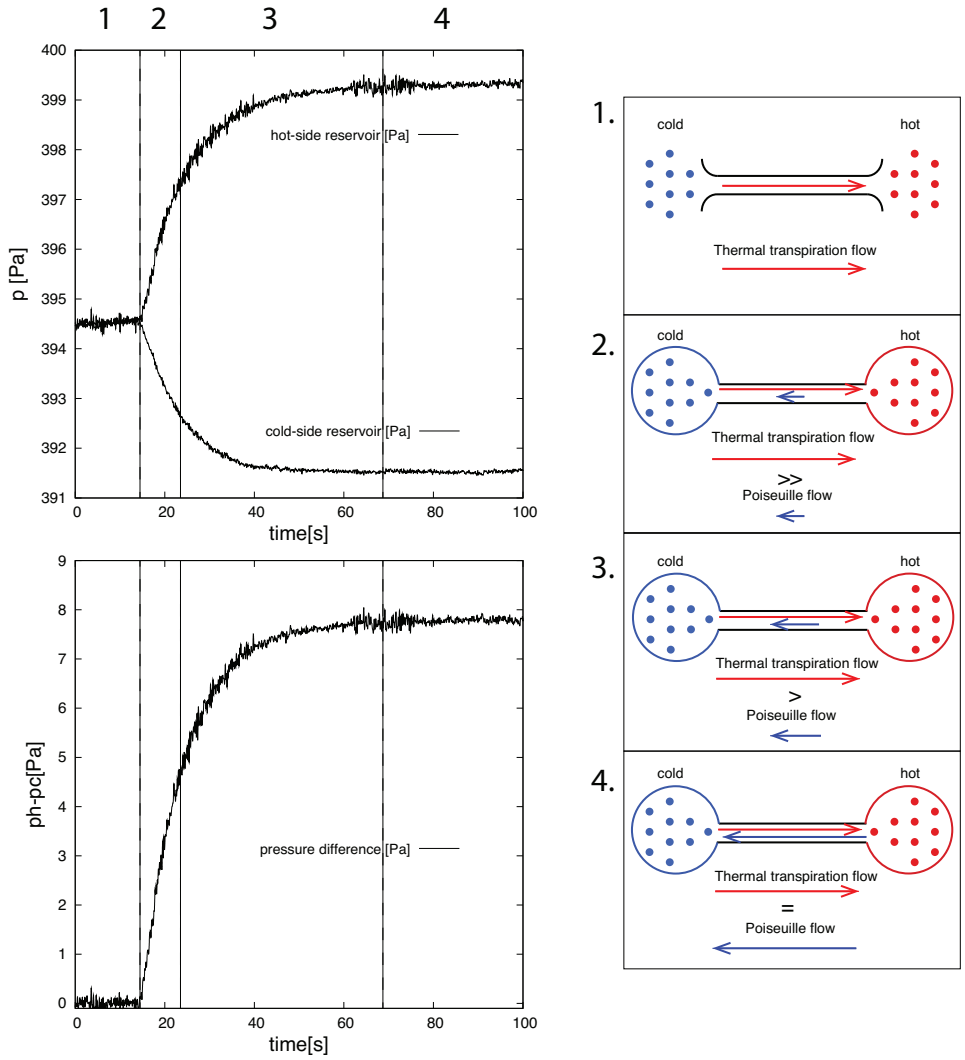

Figure 5.1: Helium for a temperature difference applied of $T_h - T_c = 71K$. Top left: pressure variation with time in the cold-side and in the hot-side reservoir. Bottom left: pressure variation with time of the difference between cold- and hot-side. The initial experimental conditions were the same as for the case in the top left graph. Right column: Explanatory scheme of the four main stages of the experiment: 1. Initial pressure equilibrium stage - the solenoid micro-valve is open; 2. Stationary transitional stage - the solenoid micro-valve is closed; 3. Non-stationary transitional stage - the solenoid micro-valve is closed; 4. Final pressure equilibrium stage - the solenoid micro-valve is closed.

tion have been dampen, the acquisition of our pressure data inside both reservoirs begins.

This is considered to be the starting point of the first stage of the non-isothermal experiment. One reservoir is already heated, while the other one is kept at ambient temperature, a stable temperature gradient is then obtained along the tube by means of the micro-tube's glass thermal conductance properties.

In the first stage of the experiment, due to the here used initial configuration of the experiment, the ideal case of a micro-tube connected to two infinite reservoirs is recreated, where the thermal transpiration mass flow rate is stationary, fully-developed, uni-directed and not-perturbed. In other words, a stable thermal transpiration flow is present along the tube.

In order to recreate the infinite volumes ideal case, the reservoirs are connected twice between each other: in the first case only through the micro-tube, in the second case also through a big diameter junction where its characteristic length, that is the junction tube's diameter, can be considered infinite in relationship to the capillary's characteristic length. This junction tube diameter's dimension has been chosen 100 folds larger in respect to the diameter of the micro-tube in order to avoid any parasite thermal transpiration effects between the two reservoirs for the case of the gas being in advanced rarefaction conditions.

This second large tube configuration, which was previously presented as the internal ring of the system, allows the pressure to continuously and equally distribute at the capillary's inlet and outlet. The pressure difference between the two reservoirs at the initial stage of the experiment is then zero (Figure 5.1: left column - bottom graph, stage 1).

The continuous pressure equilibration in both reservoirs can be considered infinitely faster in respect to the velocity of the thermal transpiration flow inside the micro-tube. Thus, the ideal case of two infinite volumes can be successfully recreated.

In conclusion, by avoiding a rise of pressure difference between the two reser-

voirs, a stationary flow is obtained along the micro-tube.

Let us note that in order to allow the reservoirs to be connected twice and thus to opportunely maintain a constant pressure equality equilibrium between them, the micro solenoid valve positioned in the big diameter junction tube has to remain necessarily open and it remains in this position during this first stage of the experiment.

5.2.1.2 Development of two flows

The solenoid micro-valve plays an important role: by shifting the valve's condition from fully closed to fully open it is possible to change the infinite volume configuration to the finite volume configuration.

Therefore, at time $t = t_0$ the solenoid micro-valve is shut. Its closure identifies the beginning of the pressure variation with time in both reservoirs (Figure 5.1: stages 2 and 3). Both stages 2 and 3 are considered to be part of the transitional phase of the experience, which shifts from its first point of equilibrium, that was the fully developed and unperturbed thermal transpiration flow, to its second point of equilibrium, that is the zero-flow stage. From now on we will consider t_0 to be the starting point of the experiment and we will attribute it to the value of 0 ($t_0 = 0$).

In the transitional stage the gas continues flowing from the colder to the hotter region of the micro-tube, this time, since the reservoirs have a finite volume, a gas concentration variance is registered inside both reservoirs. The flow increases the gas concentration in the hot-side reservoir, while it decreases the gas concentration in the cold-side reservoir. Thus, it is possible to measure and follow with time a pressure increase in the hot-side reservoir $p_h(t)$ and a pressure decrease in the cold-side reservoir $p_c(t)$.
The adopted notations h and c substitute the initially cited notations of Reynolds law 2 and 1 respectively, therefore $p_h(t)$ is the time dependent pressure variation in the hot-side reservoir, while $p_c(t)$ is the time dependent pressure variation in the cold-side reservoir.

This pressure variation with time can be then directly correlated to a macro-

scopical displacement of gas from one tank to the other. It is possible to consider the cold-side reservoir as a gas source volume, while the hot-side reservoir can be considered as a gas storage volume. Consequently, also the pressure difference $\Delta p(t)$ between the two reservoirs changes by monotonically increasing with time.

This pressure difference evolution generates a counter flow along the tube. Since the newly generated counter flow varies in the same manner as the $\Delta p(t)$, which is in continuous monotonic evolution, this flow variates in the same manner as the difference of pressure between the volumes. In conclusion, the pressure difference generated counter-flow is then due to the newly created and continuously increasing pressure difference which was originally induced by an initial stationary, fully-developed, uni-oriented and not-perturbed thermal transpiration flow.

Stationary transition

Let us stress the fact that it is fundamental to distinguish stage n.2 from stage n.3. The separation is made on the basis of considering one stationary and the other non-stationary in regards to the thermal transpiration mass flow rate.

At time t_{0^+}, in the first phase of the transitional stage of the experiment (stage n.2), the thermal transpiration flow is still considered to be stationary, fully developed, uni-oriented and not-perturbed.

This can be considered as a correct assumption only if a linear initial increase of the pressure in the hot-side reservoir $p_h(t)$ and a linear initial decrease of the pressure in the cold-side reservoir $p_c(t)$ is monitored. This is the case only until the newly created difference of pressure can still be considered as negligible.

This consideration is fundamental for measuring the thermal transpiration stationary mass flow rate: the measurement has to be done right after the closure of the solenoid valve, at time t_{0^+}, when the thermal transpiration flow has not been yet modified by the counter Poiseuille flow that, as previously introduced, is generated by the newly created pressure difference between the two reservoirs.

Non-stationary transition

In the second phase of the transitional stage of the experiment (stage 3), the pressure-variation with time speed (PVS) decreases considerably: stage n.3 is characterized by a non-linear pressure variation with time, thus the phenomenon is considered to be non-stationary.

The PVS decrease, which will tend finally to zero when the flow reaches its final equilibrium, directly depends on the continuous increase of the Poiseuille flow which is contrarily directed.

At time t_0^+ (stage 2) this counter-flow has not been created yet and is then negligible during the whole first phase of the transitional stage. In the non-stationary phase of the experiment (stage 3) the flow driven by the created pressure difference is not negligible and considerably modifies the thermal transpiration mean mass flow rate intensity.

5.2.1.3 Zero-flow at the final equilibrium

Finally, in the last stage of the experience (stage 4), the mean mass flow rate vanishes completely. This is the final equilibrium zero-flow state, where the Poiseuille counter flow completely balances the initial thermal transpiration flow: the pressure difference variation with time tends asymptotically to a final pressure difference value.

As previously introduced, when the pressure difference arrives to its maximum, the mean mass flow rate is zero.

In this stage, the final f on initial i pressure ratio for the hot-side reservoir h and the cold-side reservoir are respectively

$$\frac{p_{hf}}{p_i} > 1; \qquad \frac{p_{c_f}}{p_i} < 1. \tag{5.5}$$

Therefore, by defining the last stage of the experiment, it is possible to introduce the relationships through which we obtain the final equilibrium zero-flow parameters, such as the thermal molecular pressure difference (TPD), the ther-

mal molecular pressure ratio (TPR) and the thermal molecular pressure exponent (γ):

$$TPD = p_{h_f} - p_{c_f}; \quad TPR = \frac{p_{c_f}}{p_{h_f}}; \quad \gamma = \frac{ln\,(p_{h_f}/p_{c_f})}{ln\,(T_h/T_c)}. \tag{5.6}$$

5.2.2 Stationary mass flow rate measurement

As previously explained in Section 5.2.1.2, the measurement of the thermal transpiration induced mass flow rate ($\dot{M}_T$) has to be done at a moment when the mass flow rate satisfies the stationary conditions for the thermal transpiration flow, and therefore is still stationary, fully developed, uni-directed and not-perturbed. As we are using the constant volume technique to measure the mass flow rate (Section 5.1), the technique can be applied only if a pressure variation can be measured.

We now know that the thermal transpiration flow is perfectly developed only in the first stage of the experiment (stage n.1), when the pressure in both reservoirs are equal and constant. In this stage, as it can be easily realized, there is no pressure variation with time, thus it is not possible to effectuate a mass flow rate measurement.

Therefore, the measurement has to be effectuated at the time t_{0^+}, around the point of initial equilibrium, when the flow can be assumed to still fulfill the conditions of stationarity and there is already a pressure variation with time inside both reservoirs. Subsequently, it can be possible to effectuate a mass flow rate measurement by applying the constant volume technique.

One of the critical or crucial points in this study, is the determination of the time t^* that identifies the passage from the stationary transitional stage of the experiment (stage n.2), to the non-stationary transitional stage of the experiment (stage n.3). This time interval ($\Delta t = t^* - t_0$), as we know from eq. (5.4), will be used to effectuate the thermal transpiration mass flow rate measurement by using the pressure variation with time in the surroundings of t_0. The only difference from the general description of the technique is therefore the interval at which the measurement is done, which is not anymore $(t - \Delta t/2) < t < (t + \Delta t/2)$, but

instead is

$$t_0 < t < t_0 + t^*. \tag{5.7}$$

For this reason the transitional time t^* has to be chosen carefully: it cannot be chosen to far away from the moment of initial equilibrium, since the mass flow rate would not satisfy the stationary conditions, and it cannot be chosen to close from the moment of initial equilibrium, since the measurement would not have any physical consistence.

5.2.2.1 Pressure variation with time

In order to effectuate the thermal transpiration mass flow rate it was important to follow the pressure variation with time inside both reservoirs. By experimental observation we soon realized that the trend of this variation, which tend from an initial thermodynamic equilibrium to a final thermodynamic equilibrium, was of an exponential nature.

In the hereafter study we could fit the pressure variation with time for each individual experiment through an exponential analytical expression by using only one fitting parameter. The expressions which were used to effectuate the fitting for the hot-side and cold-side pressure variation with time were respectively

$$p_h(t) = p_{h_f} - (p_{h_f} - p_i)\, e^{-t/\tau_h}, \tag{5.8}$$

$$p_c(t) = p_{c_f} + (p_i - p_{c_f})\, e^{-t/\tau_c}, \tag{5.9}$$

where the fitting parameter was τ, that is the characteristic time constant of a single experiment. A single experiment behavior in its totality depends on the initial state of rarefaction of the gas, the temperature gradient applied and the gas nature. Therefore τ varies accordingly to the variation of these parameters.

Since the standard deviation of the fitting in respect to the raw data was estimated to be always less than 0.2%, we can consider the fitting function as a good representation of the pressure variation with time (Figure 5.2). Thus, from now on, when we will talk about $p_h(t)$ and $p_c(t)$ we will be considering the fitting exponential functions instead of the raw pressure variation with time data.

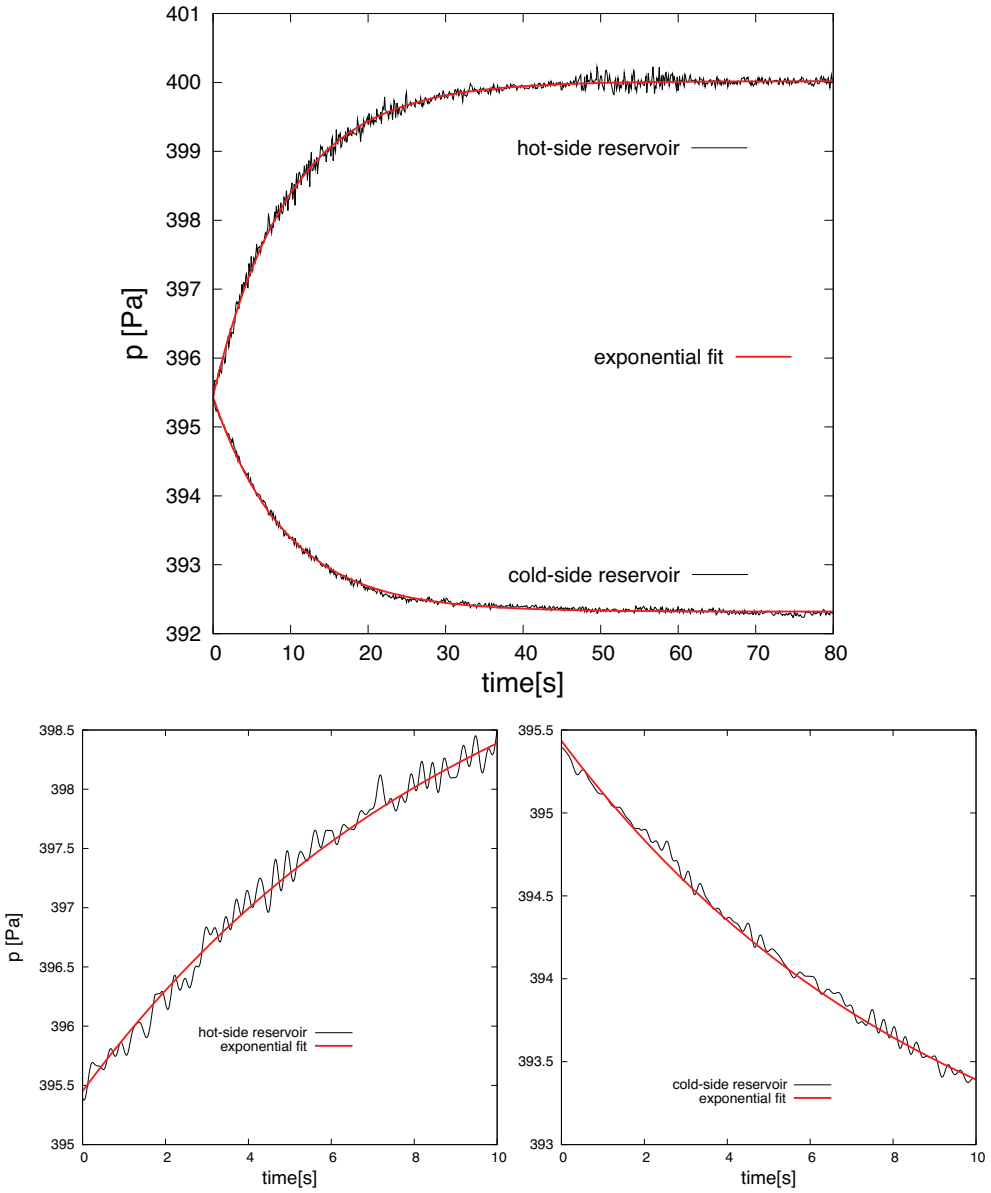

Figure 5.2: Helium for $\Delta T = 71K$. Top: pressure variation with time in the hot-side reservoir $p_h(t)$ and pressure variation with time in the cold-side reservoir $p_h(t)$ with their respective exponential analytical fittings for the full experimental time. Bottom left: $p_h(t)$ for the first $10s$ of the experiment. Bottom right: $p_c(t)$ for the first $10s$ of the experiment.

However, it is important to notice that we can experimentally observe that generally the pressure variation in the first instants of the experiment it is not as dynamic as it would be in the case for a pressure driven flow (Figure 5.2). Therefore, the measurement of a pressure variation with time in the immediate surroundings of t_0 could be misleading due to the fact that we enter in the pressure variation with time resolution limiting region of the pressure gauges which is in the order of $\pm 0.1 Pa$.

It is possible to observe that the two functions $p_h(t)$ and $p_c(t)$ are not perfectly mirror-symmetric in respect to the zero pressure axis since the volumes of the two reservoirs and the gas temperature inside both reservoirs differ ($V_h/V_c = 0.8$ and $T_h/T_c > 1$). More details will be given on this topic in the non-isothermal mass conservation section.

5.2.2.2 Pressure variation speed

Once the pressure-variation with time is defined it is possible to introduce the pressure variation speed $dp(t)/dt$ (PVS), that is an index of the dynamism of the thermodynamic system. It is possible to see, through the information extracted from the PVS of a single experiment, how the different parameters, such as the gas rarefaction, the temperature difference applied and the gas nature, affect the timing necessary to the thermodynamic system to pass from its initial equilibrium state to its final equilibrium state.

Therefore, once the parameter τ is extracted from every single experiment, it is possible to obtain the PVS for the cold- and the hot-side through the following equations

$$\frac{dp_h(t)}{dt} = + \frac{p_{h_f} - p_i}{\tau_h} \, e^{-t/\tau_h}, \tag{5.10}$$

$$\frac{dp_c(t)}{dt} = - \frac{p_i - p_{c_f}}{\tau_c} \, e^{-t/\tau_c}. \tag{5.11}$$

The pressure variation speed can also be used to monitor until which extent the thermal transpiration mass flow rate still fulfills the stationary conditions in the surroundings of t_0. Furthermore the PVS plays a fundamental role in the extrac-

tion of the mass flow rate at t_{0^+}.

5.2.2.3 Thermal transpiration mass flow rate

The measurement of a stationary, fully developed, uni-directed and not-perturbed thermal transpiration flow therefore has to be done necessarily in the surroundings of the initial time t_0 when the valve is shut and the pressure variation with time starts. We previously explained that it was necessary, in order to effectuate the thermal transpiration flow measurement by using the constant volume technique, to ensure that the time interval chosen corresponded to a linear variation of the pressure variation with time.

By fitting our pressure variation with time raw data with an exponential analytical expression and by assuming that this expression reproduces integrally the trend of the experimental data, we can make the consideration that the time interval that had to be chosen in order to meet the stationary conditions loses part of its meaning and it is partially not necessary anymore. This is due to the fact that in order to effectuate the thermal transpiration mass flow rate measurement, instead of using the pressure variation with time in a defined time interval, it is possible to directly use the pressure variation speed at the initial instant t_0 of the experiment.

Therefore it becomes possible to derive the thermal transpiration mass flow rate $\dot{M}_T$ from eq. (5.4), for ϵ values that tend to zero, in the following manner

$$\dot{M}_{T_h} = \frac{V_h}{RT_h} \left. \frac{dp_h(t)}{dt} \right|_{t_0}, \tag{5.12}$$

$$\dot{M}_{T_c} = \frac{V_c}{RT_c} \left. \frac{dp_c(t)}{dt} \right|_{t_0}, \tag{5.13}$$

where the pressure variation speed at time t_0 can be derived from eq. (5.10) or (5.11) and it is simply

$$\left. \frac{dp(t)}{dt} \right|_{t_0} = \frac{p_f - p_i}{\tau}. \tag{5.14}$$

To respect the conservation of the mass, the mass flow rate crossing the inlet section of the micro-tube has to necessarily be equal at the mass flow rate crossing

the outlet section of the micro-tube. Thus, the following expression has to be satisfied

$$\dot{M}_{T_h} = \dot{M}_{T_c}. \tag{5.15}$$

In order to obtain the condition on ϵ, the ratio of the temperature fluctuations to the pressure variation during the time of measurement has to be small.

As previously discussed in Section 4.2.3, the temperature fluctuations dT/T during the duration of a single experiment are in the order of 10^{-5} in the hot- and cold-side reservoirs. Instead, the values of dp/p are of a more difficult determination since the measurement is done through the derivative of the pressure variation with time at t_0.

If the timing needed for the thermodynamic system to reach the final state of equilibrium tended to zero, and therefore making the phenomenon extremely fast, the timing in which the pressure variation with time was stationary would be extremely small and correlative, in some cases, the dp/p parameter would tend to infinitesimal values. In these cases the measurement would not have any physical meaning.

For these reasons, it is necessary to determine until which extent the pressure variation with time remains linear and consequently find the timing t^* at which the transition from stationary to non-stationary transitional stage of the experiment takes place.

5.2.2.4 Stationarity of the measurement

According to eqs. (5.12) and (5.13), the mass flow rate is considered as stationary as long as the pressure variation speed is constant, given that its variation with time is almost negligible. This constant value of the pressure variation speed is essential to ensure that the phenomenon has not yet varied from its state of initial equilibrium and can still be considered as not perturbed and fully developed, thus stationary.

For the calculation of the mass flow rate, which is directly proportional to the

PVS, it is of no interest to determine the exact time at which the transition between stationary and non-stationary flow occurs. The stationarity of the flow is now considered as an assumption; the magnitude of the mass flow rate varies continuously after the valve is closed but, in the first period of its evolution, this variation can be assumed to be close to zero.

It is however of interest to characterize a transitional time t^* in order to better understand which parameters make the phenomenon faster and when the limits of the measuring system are reached.

As previously introduced in Section 5.2.2.3, the mass flow rate measurement can be largely affected by values of the dp/p parameter tending to zero. This pressure variation during the time of measurement has to be large enough in order to ensure that ϵ is way smaller than 1.

Let us now see how when this condition is effectively satisfied and when we arrive to the limits of the measurement in the here presented experiments. To do this it is necessary to extract the transitional time t^* of the experiment and consider the values of the dp/p parameter for the interval of time designated by the beginning of the experiment t_0 and t^*.

We chose to extract the characteristic transitional time t^* in the case where $dp(t)/dt$ varied by 5% from the original initial $dp(t)/dt|_{t_0}$ value right after the valve closure. Thus, the following identity has to be satisfied

$$\frac{dp(t^*)}{dt} = 0.95 \left.\frac{dp(t)}{dt}\right|_{t_0}, \tag{5.16}$$

Therefore, from eq. (5.10) or eq. (5.11) it is possible to easily define the transitional time as

$$t^* = \tau/19.5, \tag{5.17}$$

where τ is the characteristic time of either the hot-side or the cold-side PVS function.

Figure 5.3 shows how this was done and how the definition of a transitional time

can refer to a simple graphical explanation. Two transitional time values are to be found for each experiment: the cold-side t_c^* and the hot-side t_h^*. The pressure variation speed is different inside each reservoir and this behaviour can be attributed to the difference in the volumes of the reservoirs $V_h/V_c < 1$ and the difference of the gas temperature inside the reservoirs: $T_c/T_h < 1$.

From the example offered in Figure 5.3 it is possible to notice that the thermal transpiration mass flow rate remains stationary in the first 2 seconds of the experiment, which is a relatively high value if we consider that the difference of pressure obtained from the thermal transpiration flow is generating a contrarily directed Poiseuille flow that should modify the initial net value of the mass flow rate along the inlet and outlet cross-sections of the tube. This is mainly due to the fact that the thermal transpiration flow along the micro-tube is very slow and at the same time the macroscopically moved gas mass is very small.

Once the transitional time t^* is determined it is possible to make some considerations on the variation of pressure during the first stationary transition of the experiment. As can be seen in the example given in the bottom graphs of Figure 5.3, the dp/p parameter is in the order of 10^{-3}, which is a pretty fair value if we consider that the temperature fluctuations dT/T are in the order of 10^{-5}. Thus, the ϵ parameter is in the order of 10^{-2}, which allows us to use eq. (5.4) in order to obtain the measurement of a stationary, fully-developed, uni-directed and not-perturbed flow.

Nevertheless we must warn the reader that this parameter gives more annoyances when the experiments are fulfilled for rarefied conditions in slip regime or tending to hydrodynamic regime. In the case where the pressure varies faster and in the case when correlatively at the same time the initial pressure p_i becomes greater, the dp/p parameter becomes smaller and therefore it reaches the same order of values of the dT/T parameter, which would limit the assumption made on ϵ.

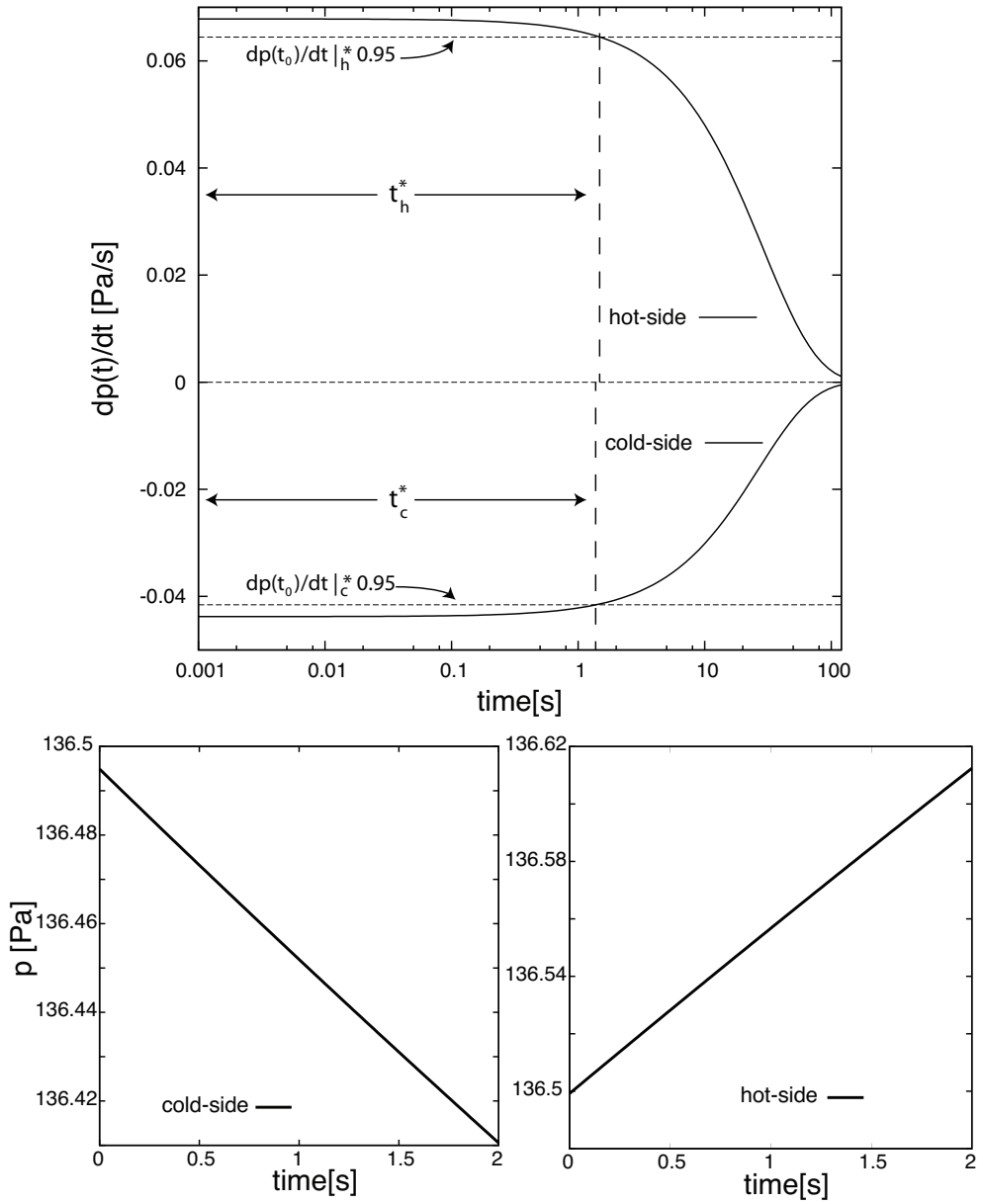

Figure 5.3: Top: pressure variation speed in the case of argon for $\Delta T = 71K$. The stationary limit is represented for the cold and hot-side by the dashed line. The intersection of this line with the PVS determines the transitional time t^* in the cold and the hot-side. The stationary limit is $dp(t_0)/dt \cdot 0.95$. Bottom: pressure variation with time for the cold- and hot-side in the first $2s$ of the experiment when the mass flow rate is still stationary.

5.3 Non-isothermal rarefaction parameter

In order to delineate a single experiment we must define the main parameters which are going to be used in order to compare one experiment to the other. As previously mentioned, these parameters are the nature of the gas, that in this study are argon, helium and nitrogen, the applied temperature difference along the capillary, which in this study are $\Delta T = 37K$, $53.5K$ and $71K$, and the initial pressure value inside the test section, which in this study ranges between $10Pa$ to $1300Pa$.

Once these parameters are fixed, it is possible to determine the gas rarefaction conditions along the micro-tube and therefore attribute to a single experiment a defined rarefaction parameter value.

However, in order to be precise, we must underline that the values of delta vary along the axis of the tube due to the imposed temperature difference. The rarefaction conditions also slightly vary during the whole experimental period due to the pressure variation with time. The pressure varies, from the initial equilibrium to the final equilibrium of less than 2% for all the experimental conditions, and therefore with it the rarefaction conditions vary, too.

We decided to define the rarefaction parameter for the non-isothermal experiments at the initial equilibrium stage of the thermodynamic system by using the macroscopic quantities measured in the cold-side reservoir

$$\delta_T = \frac{p_i \, D/2}{\mu(T_c)\sqrt{2RT_c}}, \tag{5.18}$$

where $\mu(T_c)$ is the gas viscosity and is computed by using the hard-sphere (HS) model.

This definition of the rarefaction parameter has the same physical meaning as the one introduced in Chapter 1, the only difference being the fact that the molecular mean free path of the gasλ is defined by macroscopic parameters rather than by the the mean thermal speed of the molecule and the mean collision rate per molecule.

Due to the tube's characteristic length and the applied pressure working conditions, the gas rarefaction conditions vary from near free molecular to slip regime: for helium from $\delta_T = 0.25$ to 12.6, for nitrogen from $\delta_T = 0.8$ to 37.4 and for argon from $\delta_T = 0.75$ to 33.6. The rarefaction spectrums for each gas are different since the imposed experimental initial working pressures were the same, while the gases have a different molecular weight.

Chapter 6

Experimental results

This chapter was dedicated to the analysis of the experimental results obtained by using the time-dependent methodology. Therefore we proposed the results by dividing them in stationary and non-stationary results.

We effectuated the non-isothermal experiments for argon, helium and nitrogen, by applying three temperature differences to the micro-tube, that is $\Delta T = 71K$, $53.5K$ and $37K$, for a wide spectrum of gas rarefaction conditions, namely from near free molecular to slip regime.

The stationary results comprehended the results obtained in the two states of equilibrium of the experiment: the zero-flow final equilibrium and the thermal transpiration flow initial equilibrium.

The non-stationary results comprehended the results obtained for the full transitional stage of the experiments, from the initial equilibrium stage to the zero-flow final equilibrium stage.

We decided to be coherent with the historical order in which the results of thermal transpiration were presented over the years, as shown in the thermal transpiration review chapter, in order to put into context and subsequently present the findings which are of more impact and interest.

Thus, first we analyzed the results obtained in the zero-flow final equilibrium and

then we compared these results to the results found in the literature. Hence, we presented the thermal molecular pressure difference, thermal molecular pressure ratio and thermal molecular pressure exponent.

After this due step, we presented the results concerning the stationary, fully-developed, uni-directed and not-perturbed thermal transpiration mass flow rate.

Finally, for what concerned the non-stationary results, we presented and analyzed the pressure variation with time, the pressure variation speed and the transitional time of each experiment.

6.1 Stationary zero-flow equilibrium

The results of the final zero flow stationary stage of the experiment correspond to what can be defined as a classical approach analysis to the thermal transpiration phenomenon. This approach was proposed in the literature in order to understand and characterize the final zero-flow dependence on the rarefaction conditions of the gas, the gas nature, the imposed temperature gradient and the geometry of the used system. This was done by means of the study of the thermal molecular pressure difference (TPD), the thermal molecular pressure ratio (TPR) and the thermal molecular pressure exponent (γ).

By analyzing the same parameters we proved that the here proposed original method for thermal transpiration flow measurements can not only capture the mean mass flow rate induced along the tube by just applying a temperature gradient along its axis, but it can also capture the final zero-flow stage. References to the literature were given in the thermal transpiration review chapter of this manuscript (Chapter 3). All the information hereafter studied referred to the pressure data acquired exclusively at the zero-flow final equilibrium stage of the experiment.

6.1.1 Thermal-molecular pressure difference

The thermal molecular pressure difference is the difference between the pressure in the hot-side reservoir and the final pressure in the cold-side reservoirs:

$TPD = p_{h_f} - p_{c_f}$.

First let us analyze the case where the difference of temperature applied to the tube was chosen as a fixed parameter.

If we refer to the results presented in Figure 6.1, it is possible to state that the pumping effect of thermal transpiration varies significantly as a function of the rarefaction and molecular weight of the gas. It is possible to clearly observe that the thermal molecular pressure difference has a parabolic trend: it monotonically increases from near free molecular to transitional regime and, after that it touches a maximum, it monotonically decreases from transitional to hydrodynamic regime. The values of TPD are expected to tend to zero in free molecular and in hydrodynamic regime.

As shown in Figure 6.1, the TPD maximum is always located in transitional regime. Let us remark that the TPD maximum for argon, helium and nitrogen, for whatever temperature difference applied to the tube, exists at a well defined value of the rarefaction parameter, that is approximately 3.5.

As expected, the TPD values increase with increasing values of the temperature difference applied to the tube. By comparing the maximal TPD values for the applied temperature differences, it is possible to notice that the TPD_{max}, in the case of argon at $\Delta T = 71K$, is somewhere around $3.2Pa$; while for the same gas at $\Delta T = 37K$ is somewhere around $1.7Pa$. We find the same trend for helium and nitrogen. If we would generalize, we could simply state that the increase of the TPD_{max} for each gas augments linearly with the difference of temperature applied.

Lets now make some remarks on the effects of the molecular weight of the gas in the TPD results. In Figure 6.2 it is possible to observe in which manner the thermal molecular pressure difference depends on the gas nature. The induced pumping effects of thermal transpiration on the different gases are evidently different and, if only the monoatomic gases are compared, it is clear that lighter gases are more influenced by thermal transpiration. In the case we considered, we can see that the maximum TPD of helium is 2.5 times larger than the maximum TPD of Argon.

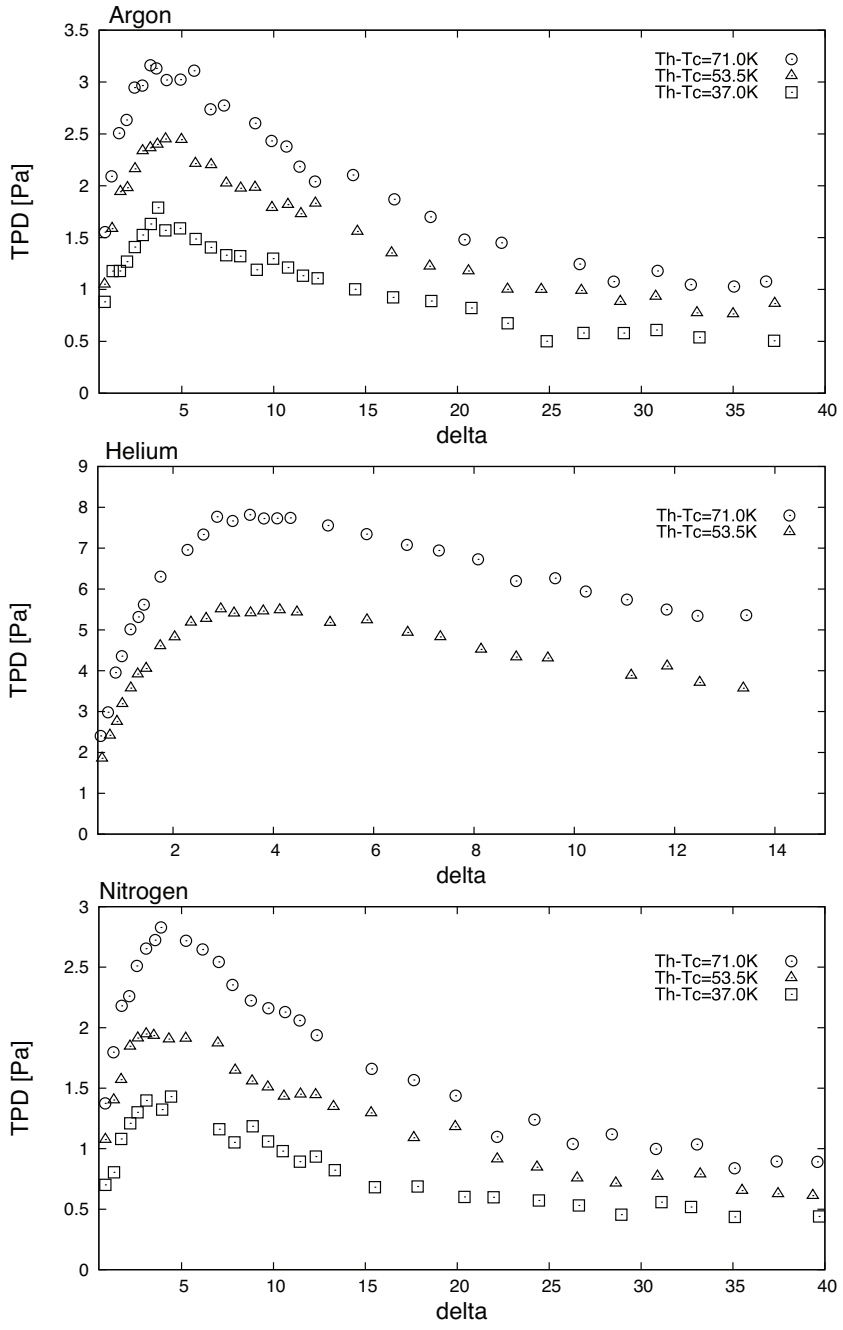

Figure 6.1: Thermal molecular pressure difference TPD of Argon, Helium and Nitrogen for three temperature differences applied. TPD as a function of the rarefaction parameter delta.

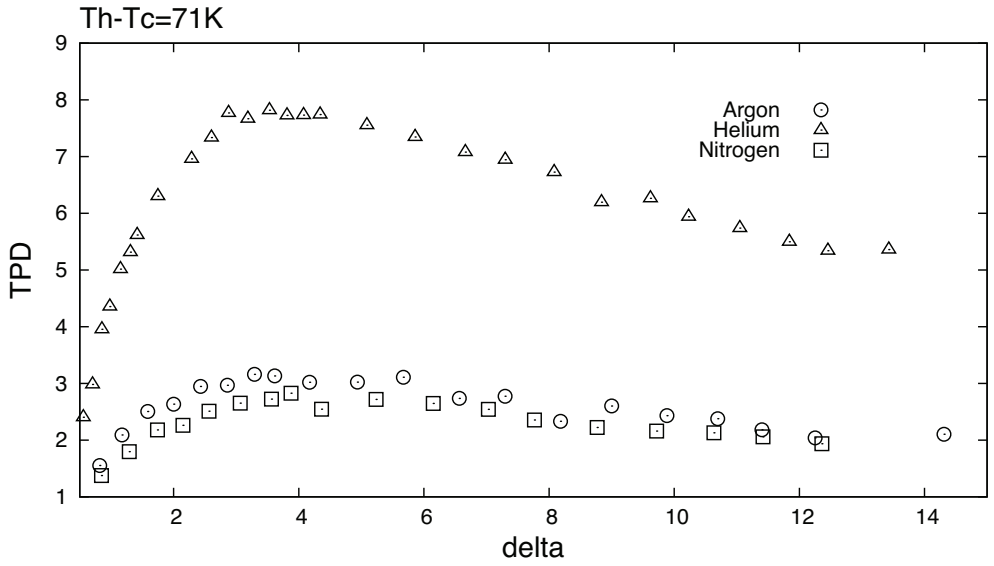

Figure 6.2: Thermal molecular pressure difference TPD for $\Delta T = 71K$: comparison between argon, helium and nitrogen. TPD as a function of the rarefaction parameter delta.

One interesting thing that can be noticed from these results is that for all the temperature differences considered in this study the TPD_{max} for helium is always governed by the same factor of difference in respect to argon and nitrogen.

We can state that the rough analysis made for the TPD_{max} results can be considered valid also for the thermal molecular pressure difference measured along the whole spectrum of the rarefaction parameter.

To summarize, it is then possible to state that the thermal molecular pressure difference is a function of the rarefaction conditions of the gas, the applied temperature distribution along the external surface of the tube, the temperature on both the hot-side and the cold-side reservoirs and the gas nature

$$TPD = f(p_i, D, T_h, T_c, Gas). \tag{6.1}$$

The uncertainty on the thermal molecular pressure difference measurements is around 1.5% of the reading values.

6.1.2 Thermal-molecular pressure ratio

The thermal molecular pressure ratio relates the final pressure in the hot-side reservoir and the final pressure in the cold-side reservoir: $TPR = p_{c_f}/p_{h_f}$.

Differently from the thermal molecular pressure difference tendency, the final pressure ratio does not show an evident shift in its behavior at any point of the rarefaction conditions of the gas. The TPR monotonically increases from molecular to hydrodynamic regime (Figure 6.3).

In the case of the thermal molecular pressure ratio an absolute minimum can be observed for rarefaction conditions tending to free molecular regime, namely when delta tends to zero. This is in good agreement with Reynolds law (iv) as expressed by eq. (3.1), that is a limiting value achieved by TPR in free molecular regime, which corresponds to $(T_c/T_h)^{1/2}$. Therefore, the free molecular thermal transpiration ratio changes as a function of the applied temperature difference to the tube.

As we did not measure in free molecular regime, we did not expect to reach this minimum TPR value. Anyhow, the limit value was used as a reference in order to check, in a first moment, the quality of the TPR measurements. Let us remind that Edmonds & Hobson [1965], as previously stressed in Chapter 3, showed that this limit value was very difficult to reach and had never been clearly reached by experiments made by using long capillaries.

The limit thermal molecular pressure ratio, in the case of $\Delta T = 71K$, where the temperatures of the surface of the tube's extremities are $T_h = 372K$ and $T_c = 301K$ is $TPR_{min} = 0.899$; in the case of $\Delta T = 53.5K$,where the temperatures of the surface of the tube's extremities are $T_h = 353.5K$ and $T_c = 300K$ is $TPR_{min} = 0.921$; and in the case of $\Delta T = 37K$, where the temperatures of the surface of the tube's extremities are $T_h = 336K$ and $T_c = 299K$ is $TPR_{min} = 0.943$.

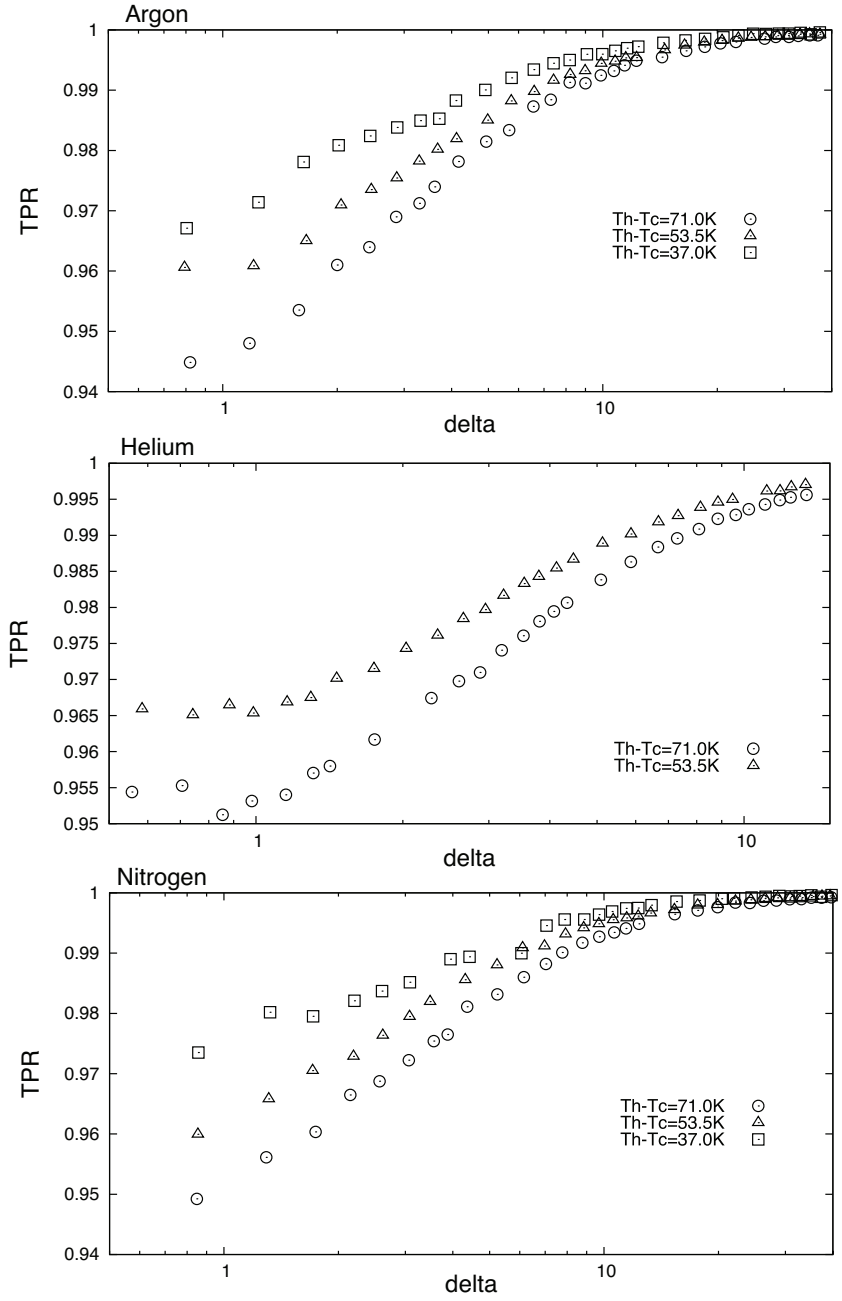

Figure 6.3: Thermal molecular pressure ratio TPR for argon, helium and nitrogen for three temperature differences applied. TPR is plotted as a function of the rarefaction parameter δ.

The values of the experimental data, in near free molecular regime, are obtained for gas rarefaction conditions of about $\delta_T \sim 0.8$ for argon and nitrogen, while for helium the value is around $\delta_T \sim 0.5$: these values correspond to gas rarefaction conditions in advanced transitional regime, relatively far away from the free molecular regime, which starts at about $\delta_T \sim 0.1$. However, it is possible to see that the tendency of the experimental data points tend to a minimum TPR value.

As expected, the thermal transpiration flow acts on the thermal molecular ratio more intensively for higher temperature differences applied (Figure 6.3). On the contrary, if we compare the influence of the thermal transpiration flow on the TPR values for argon, helium and nitrogen for a fixed temperature difference applied, it is possible to see that the gas nature hardly influences the behavior of the thermal molecular pressure ratio in slip and the first part of the transitional regime (Figure 6.4 top graph).

Approaching the free molecular regime, a slight divergence in the results is to be found that may correspond to a different interaction of the gas with the tube surface. As we know, in transitional and free molecular regime, the number of intermolecular collisions with the surface are preponderant in respect to the number of binary gas collisions. Therefore, a divergence in the TPR results could be directly attributed to a difference in the gas-surface interaction for different gases, if the surface considered is the same. Again, it is possible to see that the value of $\delta_T = 3.5$ can be determined as a shifting or divergent point in the results found, where the difference in the TPR results for the three gases starts to be more evident.

We would like to focus the attention of the reader on the fact that same gas rarefaction conditions do not correspond to same pressure working conditions for argon, helium and nitrogen. As it can be clearly realized from the bottom graph of Figure 6.4, the pumping effects of thermal transpiration differ greatly for light molecular weight and heavy molecular weight gases as a function of the pressure used in the micro-fluidic system. It is possible to see the same influence of the working pressure also in the case of argon and nitrogen, but this is less evident since the weights of the gases are more alike.

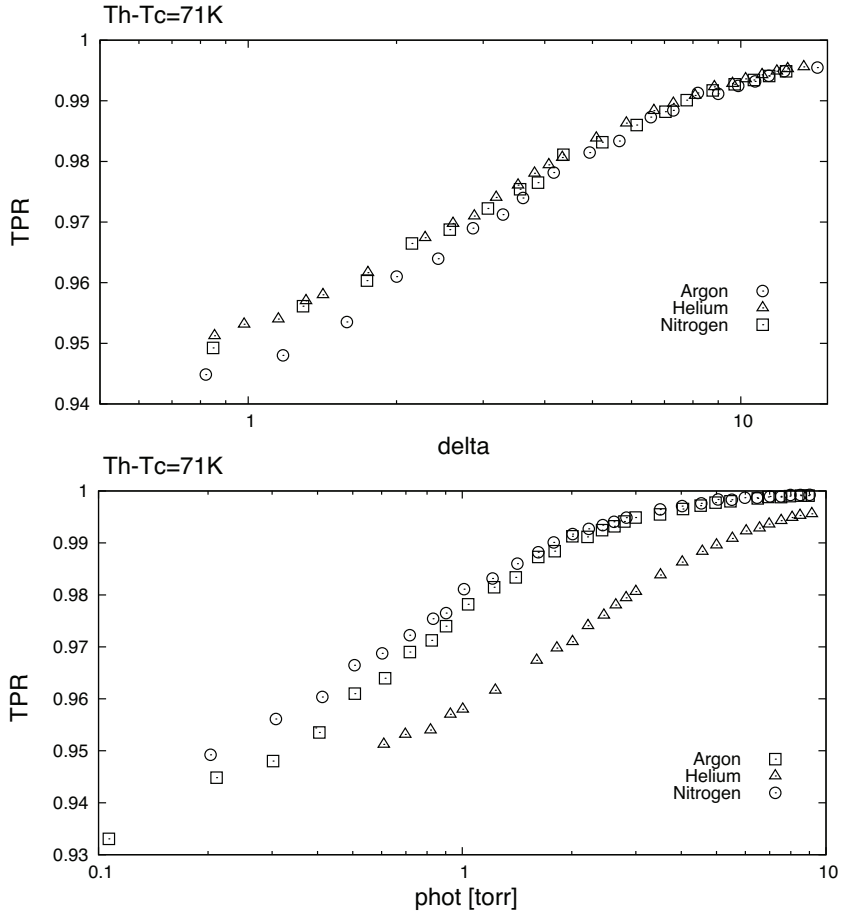

Figure 6.4: Thermal molecular pressure ratio TPR for $\Delta T = 71K$: comparison between argon, helium and nitrogen. Top: TPR as a function of the rarefaction parameter delta. Bottom: TPR as a function of the pressure in the hot-side reservoir in $[torr]$ ($1torr = 133Pa$).

To summarize, it is then possible to state that the thermal molecular pressure ratio is a function of the rarefaction conditions of the gas, the applied temperature distribution along the external surface of the tube, the temperature on both the hot-side and the cold-side reservoirs and the gas nature

$$TPR = f(p_i, D, T_h, T_c, Gas). \tag{6.2}$$

6.1.3 Thermal molecular pressure exponent

The thermal molecular pressure exponent is defined as

$$\gamma = ln(p_{cf}/p_{hf})/ln(T_c/T_h)$$

and is therefore governed by the ratio between the final pressure in the cold and hot-side reservoir and the ratio between the temperature in the cold- and in the hot-side reservoir.

The thermal molecular pressure exponent varies as a function of the rarefaction of the gas: it monotonically decreases from free molecular to hydrodynamic regime. It is 1/2 at its maximum, as defined by Reynolds, and it tends to zero at its minimum.

The thermal molecular pressure exponent is an extremely interesting parameter since it offers the possibility to check the data quality of the acquired points. For a single gas, by dividing the final pressure ratio by the temperature ratio, the gamma values are found to be the same for a fixed value of the rarefaction parameter for each temperature difference applied to the tube. Thus making the thermal molecular pressure exponent depend only on the gas rarefaction and the gas/surface interactions.

By observing the behavior of γ in Figure 6.5, it is possible to see that effectively the acquired data points are in agreement with the literature. If one gas is considered individually, for different applied temperature distributions to the tube, the gamma values are well superposed for a fixed value of the rarefaction parameter.

Nevertheless, some slight divergences can be observed for rarefaction conditions near free molecular regime in the case where the lowest temperature difference is studied. For this temperature and pressure difference and pressure range, the measuring instrumentation loses some of its accuracy.

Therefore, the thermal molecular pressure exponent can be considered as representative of the quality of the measurements, since, in order to have a perfect agreement of the γ results at a given rarefaction of the gas, for different gases and

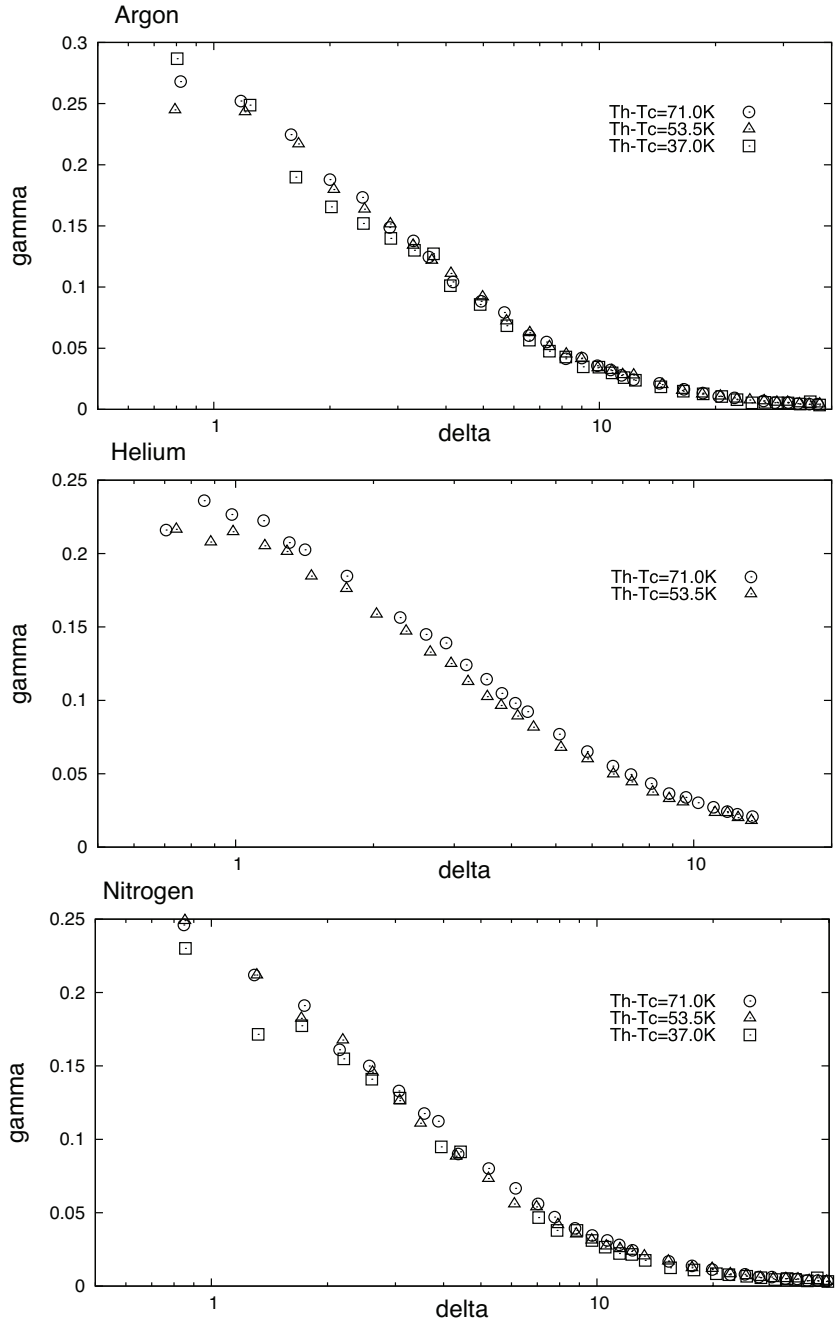

Figure 6.5: Thermal molecular pressure exponent γ for argon, helium and nitrogen. Comparison for three temperature differences applied. γ as a function of the rarefaction parameter delta.

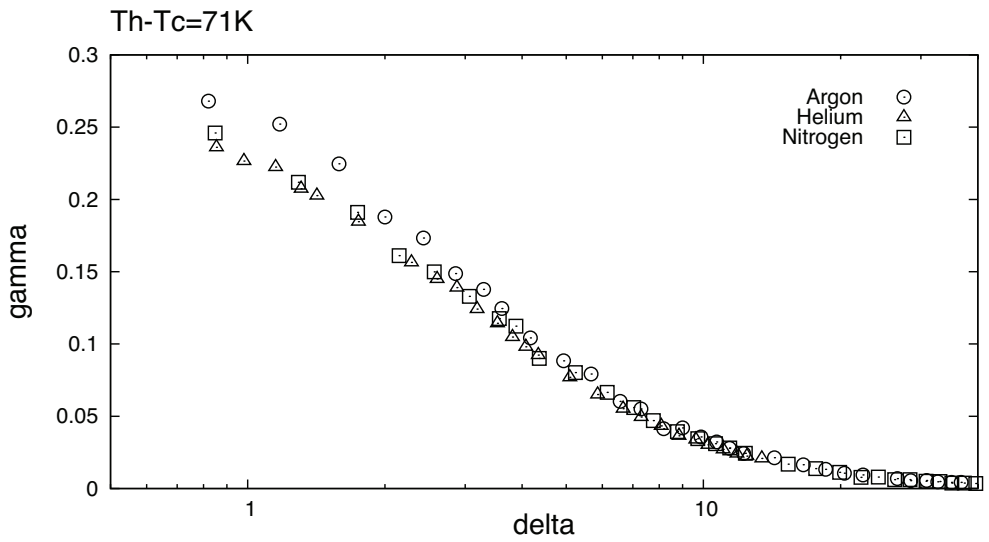

Figure 6.6: Thermal molecular pressure exponent γ: comparison between argon, helium and nitrogen for one temperature difference applied, $\Delta T = 71K$.

for different temperatures applied, the measurements of pressure and temperature inside the two reservoirs of the micro-fluidic system have to guarantee a relatively high accuracy.

From Figure 6.5 it is possible to notice that the experimental results of the thermal molecular exponent are around 0.25 in near free molecular regime and tend asymptotically to zero when arriving to almost hydrodynamical regime conditions. The tendency of the experimental points can be considered as a sign that in free molecular regime the experimental results may match the limit value, that is $\gamma = 1/2$. Anyhow, the comments on the limit value made in the previous section (Section 6.1.2) are valid also for what concerns the thermal molecular pressure exponent.

In the case where the different gases are compared for a fixed applied temperature distribution (Figure 6.6), it is possible to see that the values of gamma from slip to the first part of the transitional regime coincide at fixed values of delta; when the critical value of $\delta_T = 3.5$ is reached, that is from near free molecular to transitional regime, there is a divergence between the γ values of the different gases. This is considered to be related to a difference in what concerns the

gas/surface interaction for the gases analyzed. Let us recall that in free molecular regime the number of molecular collisions with the walls of the tube are preponderant in respect to the number of intermolecular collisions.

To summarize, in the case where different gases are analyzed in relationship to the same considered wall material and geometry, it is possible to state that the thermal molecular pressure exponent depends on the gas nature and the rarefaction conditions of the gas:

$$\gamma = f(\delta, Gas). \tag{6.3}$$

The relative uncertainty of the obtained results is in the order of 3%.

6.1.4 Literature comparison

Nowadays the semi-empirical formulas of Liang [1951] and Takaishi & Sensui [1963] are still used to calibrate pressure gauges that are internally heated. This is done in order to take into account the parasite thermal transpiration effects generated by the inequalities of temperature introduced by the gauges themselves.

In a first analysis we decided to compare the zero-flow experimental results obtained with the results that can be deduced from the semi-empirical formulas proposed by Liang and Takaishi and Sensui [eq. (3.5) and eq. (3.6)]. We wanted to test if these formulas could effectively reproduce the pumping effects of thermal transpiration for the temperatures that we applied in the experimental campaigns to the ends of the micro-tube.

Let us consider the general form of the Liang and the Takaishi and Sensui formulas for the thermal molecular pressure ratio

$$\frac{p_{c_f}}{p_{h_f}} = \frac{[...] + \sqrt{T_c/T_h}}{[...] + 1}, \tag{6.4}$$

and for the thermal molecular pressure difference

$$\Delta p = p_{h_f} \frac{[...] - \sqrt{T_c/T_h}}{[...] + 1}. \tag{6.5}$$

In its general form the term [...], that is valid for both the Liang and the Takaishi and Sensui formulas is

$$\left[...\right] = A\left(\frac{p_{h_f}D}{F}\right)^2 + B\,\frac{p_{h_f}D}{F} + C\sqrt{\frac{p_{h_f}D}{F}}\,, \tag{6.6}$$

where it is necessary to refer to the pressure p_{h_f} in $[torr]$ and to the dimension of the diameter of the tube D in $[mm]$, otherwise the semi-empirical constants A, B, C and F measured by the authors lose their meaning and are no longer able to fit the pumping effects of thermal transpiration.

The main difference in between the Takaishi and Sensui formula and the Liang formula lays in the fact that in the case of the Liang formula C is equal to 0 and for the case of the Takaishi and Sensui formula $F = (T_c + T_h)/2$. For the rest, the authors have measured, or fitted to their experimental results, the other semi-empirical constants, which are dependent on the gas used and the temperature range applied.

As shown in Figure 6.7, both formulas reproduce qualitatively the behavior of the thermal molecular pressure ratio in the full range of rarefaction measured. Anyhow, it is clear that the formula, or semi-empirical constants measured, by Takaishi and Sensui match the experimental results presented in this work better than the formula of Liang. That means that these constants, contrarily to the constants measured by Liang, are more suitable for the range of temperatures applied to the tube during the present experimental campaign.

If we consider only the Liang formula, we obtain the best fit for argon, the heavier gas, while the worst fit is for helium, which is the lighter gas. If we consider the Takaishi and Sensui formula, we obtain the best fit for helium, while the worst fit is for the heavier gases. Anyhow, we still think that the TS formula reproduces the TPR results within a reasonable accuracy.

Let us now consider the same cases considered for the TPR analysis, that is argon, helium and nitrogen at $\Delta T = 71K$, but this time by considering the thermal molecular pressure difference results (Figure 6.8). Also in these cases the TS formula describes our experimental results better than the L formula. Nevertheless it

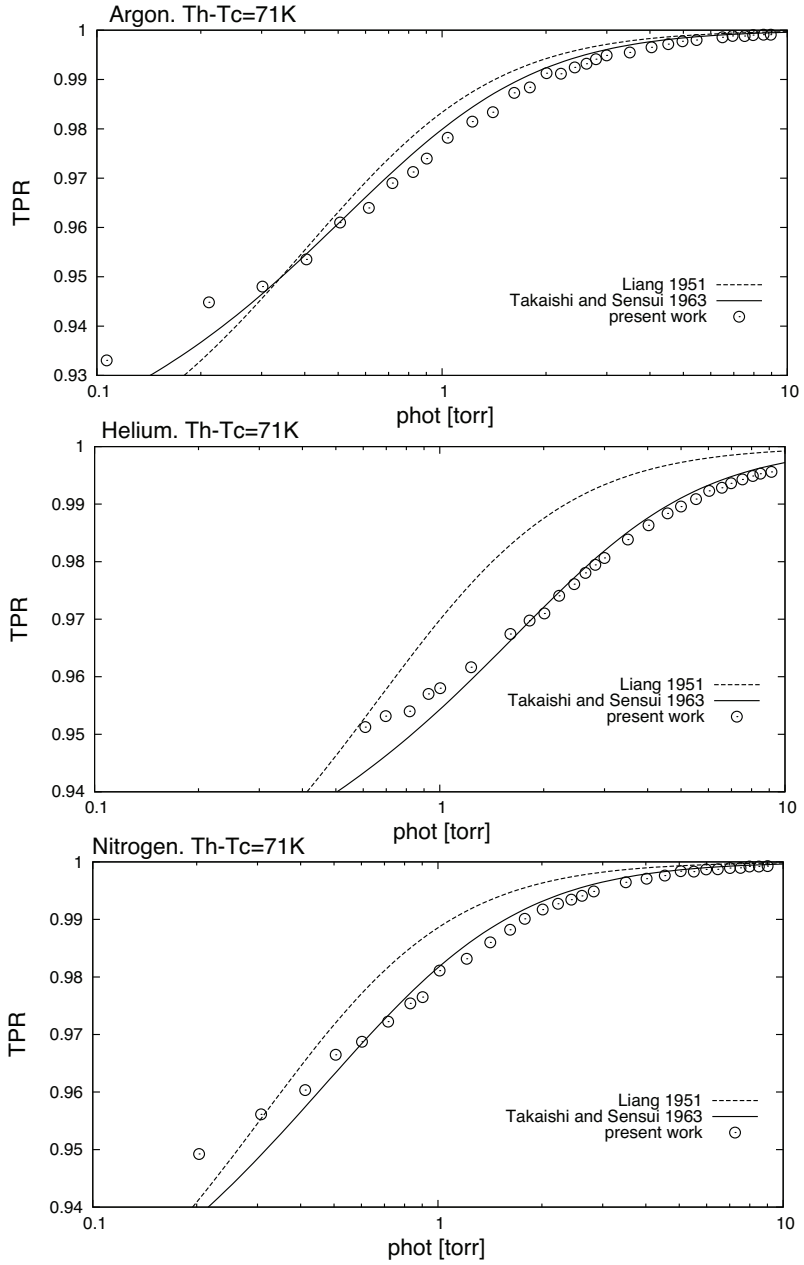

Figure 6.7: Thermal molecular pressure ratio TPR for argon, helium and nitrogen: comparison between the Takaishi and Sensui 1963 and the Liang 1951 formula and the present work; TPR is plotted as a function of p_{hf} in $[torr]$ $(1torr = 133Pa)$.

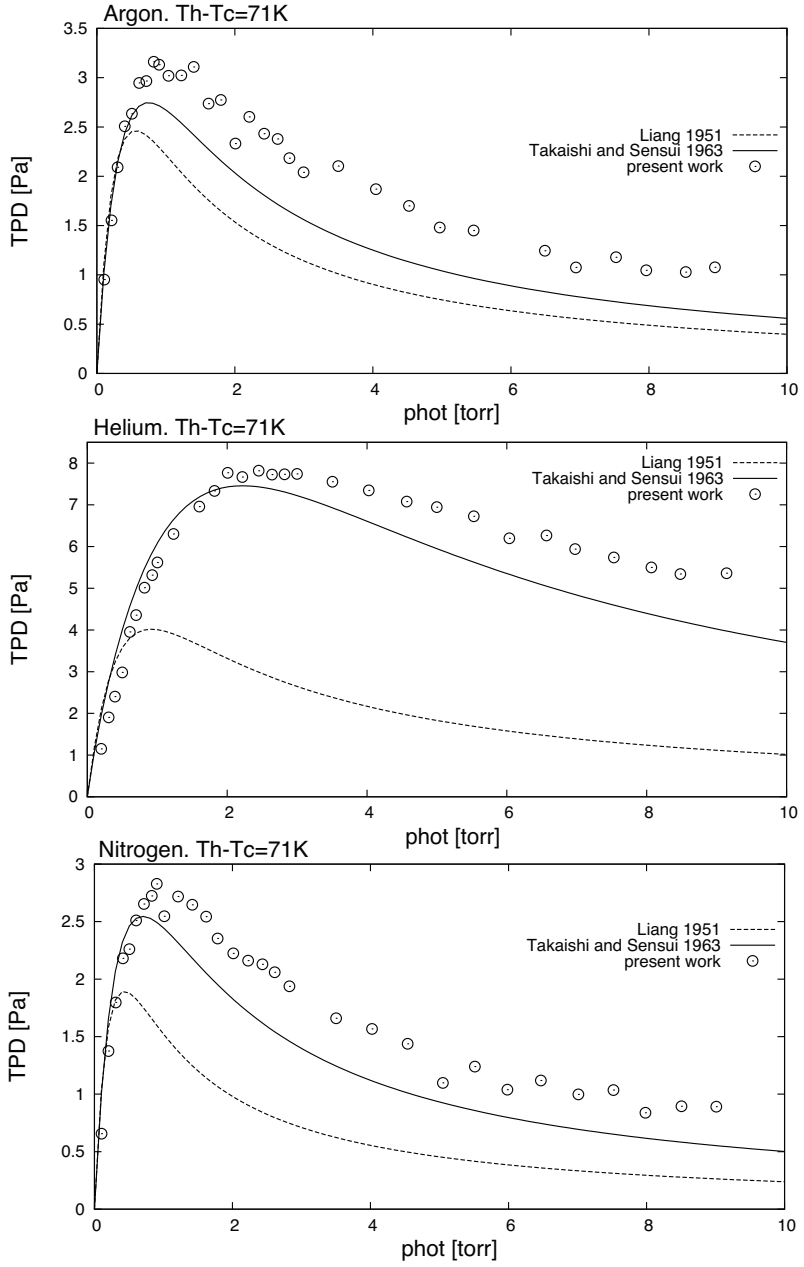

Figure 6.8: Thermal molecular pressure difference TPD for argon, helium and nitrogen: comparison between the Takaishi and Sensui 1963 and the Liang 1951 formula and the present work. TPD as a function of p_{hf} in $[torr]$ $(1torr = 133Pa)$.

is evident from this manner of representing the results that the TS formula largely underestimates the pumping effects of thermal transpiration.

Still the best fit corresponds to the case of helium, but in slip regime the TS formula underestimates the thermal transpiration pumping effect of approximately $1[Pa]$. Also in the cases of argon and nitrogen the TS formula underestimates the phenomenon of approximately $0.5Pa$, but this time in a more sensitive range of pressure measurements, that is already in transitional regime. Therefore, the uncertainty of the measurement that could be introduced in the calibration of pressure gauges by applying the TS formula would be relatively higher.

We would like now to introduce new coefficients for the TS formula by using our thermal molecular pressure difference experimental results. By doing so we would like to show how there is relatively no manner to introduce semi-empirical constants able to reproduce large ranges of temperature differences applied. The constants vary as a function of the used gas, but also as a function of the temperature difference.

It is possible to see from Figure 6.9 that the new constants fit perfectly the experimental data. But it is important to underline that the constants vary for each temperature difference applied, making it practically impossible to define a range under which the empirical constants would eventually reproduce exactly the experimental values (Table 6.1). The fit proposed was done by iterating around two rather than three constants, that is A and C. The constant B was kept as given by Takaishi and Sensui.

It is evident that new methods have to be introduced in order to quantify the thermal transpiration pumping effects, or parasite effects that are introduced in pressure sensors that work at different temperatures in respect to the temperature of the gas.

In Chapter 7 of this manuscript we offered a confrontation of the experimental results with numerical methods. By doing this we would like to focus the reader attention on the fact that effectively this empirical methods are not suitable for arbitrary ranges of rarefaction conditions and large ranges of applied temperature

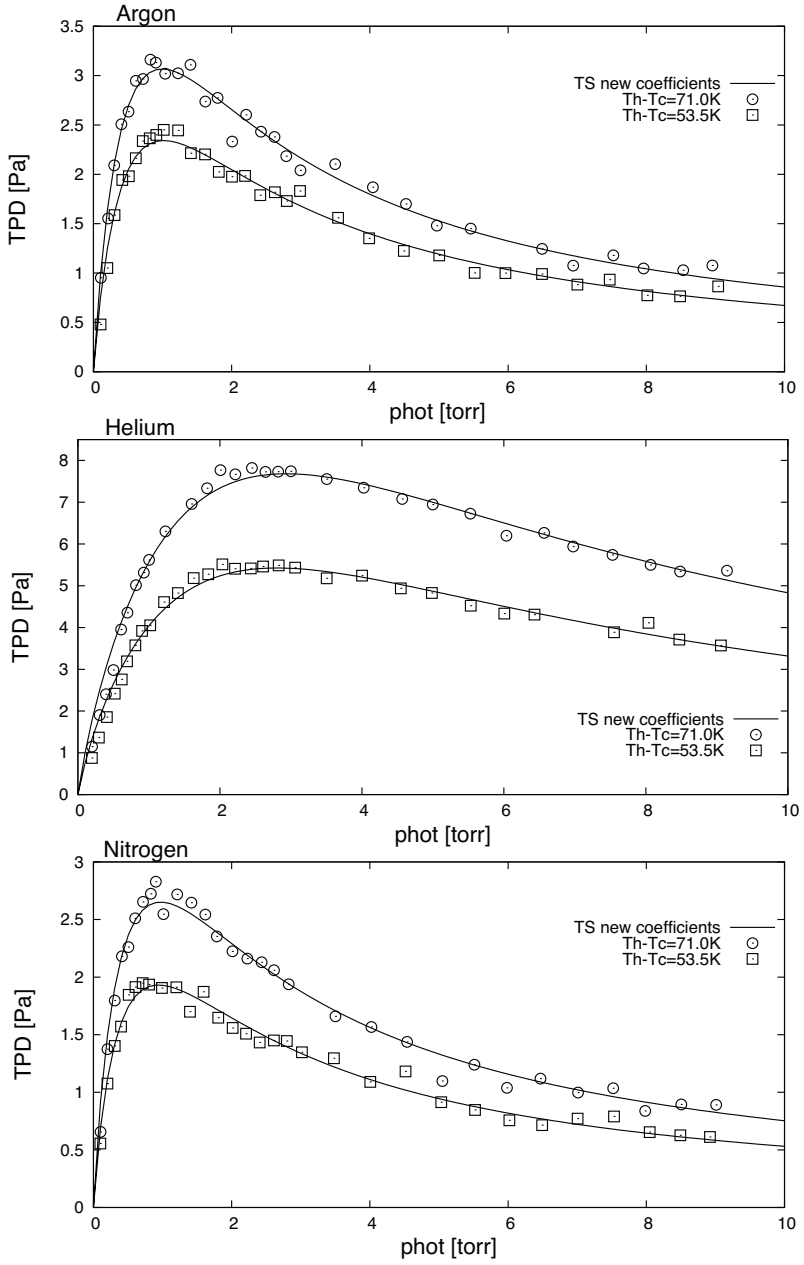

Figure 6.9: TPD for argon, helium and nitrogen: redefinition of the empirical constants of the TS formulation. comparison with the experimental results obtained in the present work. TPD as a function of p_{hf} in $[torr]$ ($1torr = 133Pa$).

	$A \cdot 10^{-5}$	$B \cdot 10^{-2}$	C
Argon			
TS: $77 \sim 673[K]$	10.8	8.08	15.6
PW: $71.0[K]$	6.77	8.08	20.7
PW: $53.5[K]$	6.36	8.08	22.6
Helium			
TS: $4.2 \sim 90[K]$	1.4∼1.6	1.2∼1.1	18∼20
PW: $71.0[K]$	1.01	1.15	26.8
PW: $53.5[K]$	1.14	1.15	30.3
Nitrogen			
TS: $77 \sim 195[K]$	12	10	10∼18
PW: $71.0[K]$	7.64	10	26.7
PW: $53.5[K]$	8.06	10	30.3

Table 6.1: Comparison between the old TS empirical constants and the new empirical constants obtained by fitting the current experimental results with the Takaishi and Sensui formulation. TS: Takaishi and Sensui; PW: present work $71[K]: \ T_h = 372K, \ T_c = 301K.$ $53.5[K]: \ T_h = 353.5K, \ T_c = 300K.$

differences.

On the other hand, the Takaishi and Sensui and the Liang formulations can give a first estimation of the intensity of these pumping or parasite thermal transpiration effects.

6.1.5 Conservation of the mass

It is possible to check the quality of the measurements by controlling the conservation of the mass during the whole duration of one single experiment. This study is done by coupling together two absolute pressure measurements effectuated independently one from the other, that is in the hot-side reservoir and the cold-side reservoir.

Let us consider the whole evolution of the thermodynamic system and write, from the equation of state $pV = mRT$, the balance between the mass that enters inside the hot-side reservoir and the mass that leaves the cold-side reservoir from t_0, that is the initial thermal transpiration flow stage, to t_f, that is the zero-flow final equilibrium stage.

Then it is possible to write that, at the final stage of the experiment, the mass of gas contained by each reservoir is

$$m_f = m_i + \Delta m, \tag{6.7}$$

where m_i is the gas mass in one of the reservoirs at the time $t = t_0$, when the solenoid micro-valve is still open, and m_f is the gas mass at the final zero flow equilibrium stage of the experiment.

Because of the law of mass conservation and since the reservoirs are connected from t_0 in ahead only by the micro-tube, which has an infinitesimal volume in respect to the volume of the reservoirs, any mass variation in one of the reservoirs can be considered as corresponding to an equal absolute mass variation in the other reservoir.

Therefore, if the hot-side reservoir is considered to be a gas storage volume and the cold-side reservoir is considered to be a gas source volume, the variation of mass during the the full duration of one experiment in the hot-side reservoir has to be equal to the the absolute variation of mass in the cold-side reservoir ($\Delta m_h = |\Delta m_c|$).

From eq. (5.2) and by considering the ϵ term equal to zero, the variation of mass during the the full duration of one experiment in the hot-side reservoir can

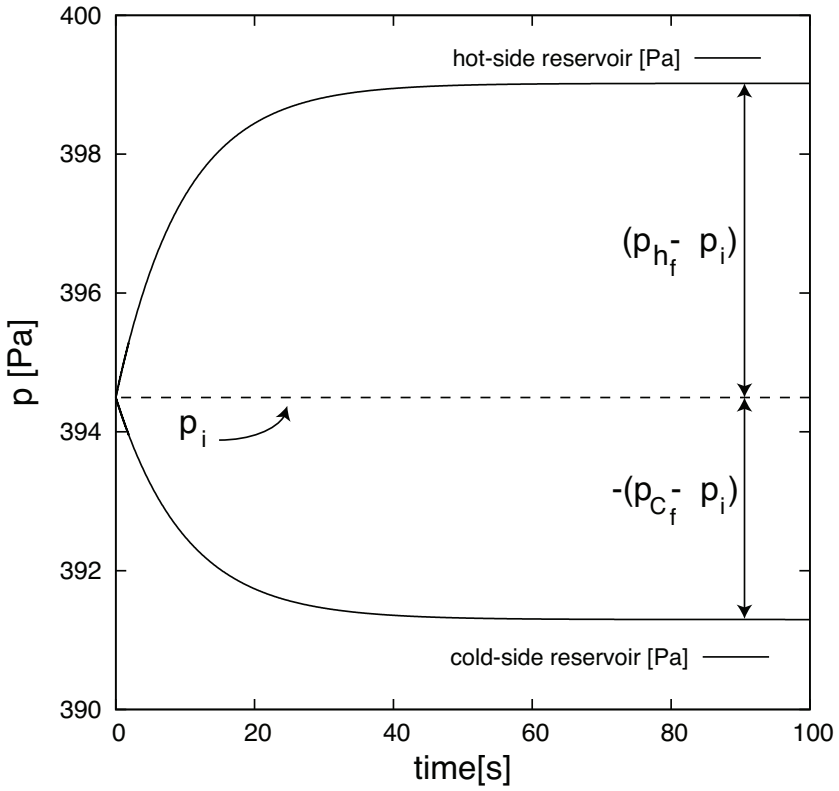

Figure 6.10: Pressure variation with time. Scheme of the final pressure difference achieved in the hot- and cold-side reservoir in respect to the initial pressure value at the beginning of the experiment at time t_0.

be written as

$$\Delta m_h = \frac{V_h}{RT_h}\,(p_{h_f} - p_i), \tag{6.8}$$

while the variation of mass in the cold-side reservoir can be written as

$$\Delta m_c = \frac{V_c}{RT_c}\,(p_{c_f} - p_i). \tag{6.9}$$

From Figure 6.10 it is possible to graphically see more in a more precise manner to what the terms $(p_{c_f} - p_i)$ and $(p_{h_f} - p_i)$ correspond to.

In order to have some information on the quality of the measurement it is possible

to therefore refer to the measurable quantities $(p_{h_f} - p_i)$ and $(p_{c_f} - p_i)$ and see under which extent they respect the relationship imposed by the mass conservation law.

Therefore, from equations (6.8) and (6.9) the mass conservation is respected only if the following identity is true

$$\frac{p_i - p_{c_f}}{p_{h_f} - p_i} = \frac{T_c}{T_h} \cdot \frac{V_h}{V_c}. \tag{6.10}$$

Considering that the volume ratio V_h/V_c is always constant for all the experiments and it is equal to 0.8, the only parameter that varies is the temperature ratio T_c/T_h. Therefore, for an imposed temperature difference the expected reference value is constant for the whole spectrum of rarefaction. The reference values for the temperature differences imposed in the experimental campaigns must then be 0.712 for $\Delta T = 37K$; 0.679 for $\Delta T = 53.5K$; and 0.647 for $\Delta T = 71K$.

In Figure 6.11 is shown that the conservation of mass along the tube is well captured by the here used technology in within a 10% from the theoretical reference value. We can state that the final ratio does not depend on the rarefaction conditions of the gas, but only on the volume ratio and the temperature difference applied.

It is necessary to analyze the greater fluctuations around the reference value for what concerns the argon experimental results. This is derived from the fact that the measured pressure differences are approximately 2.5 fold lower in respect to the helium pressure differences measured. We are therefore pushing the measuring system more to its limits in the case of a heavier gas, for what concerns the final pressure differences measurements.

These statements have been made considering the case of argon and helium for a temperature difference applied of $\Delta T = 53K$, the same considerations can be made for nitrogen and the other temperature differences applied.

Lets do some final considerations on the measurement quality. In order to match the reference value derived from the conservation of the mass law, it is necessary

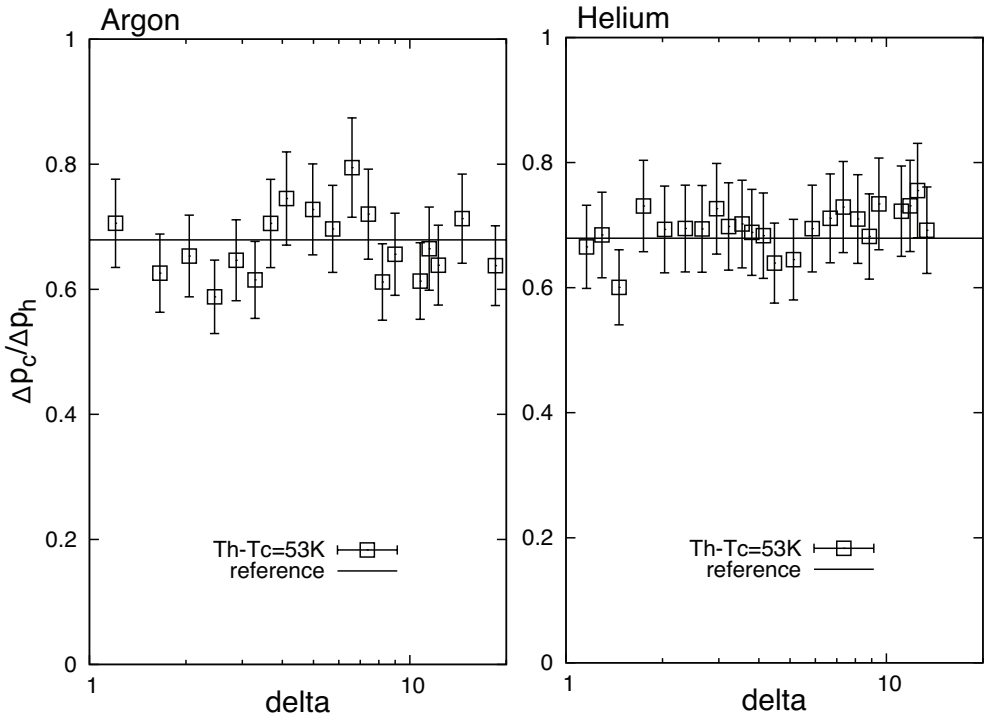

Figure 6.11: Mass conservation verification for $\Delta T = 53.5K$, the reference value is $\frac{T_c}{T_h} \cdot \frac{V_h}{V_c} = 0.679$. Left: helium. Right: argon.

to have measurements of the gas pressure and of the gas temperature with a relatively high level of accuracy in both the hot- and cold-side reservoirs.

The results presented for the mass conservation were performed by coupling two independent pressure measures done with two different CDG gauges at the inlet and outlet of the micro-tube and by coupling two independent temperature measures at the cold- and hot-side reservoir, which makes the quality of the measurement test by means of the mass conservation results a very complex task to achieve.

The divergence that we have between the measured values and the reference values derive from a slightly erroneous calibration of the gauges in reservoirs which are maintained at a relatively high difference of temperature: the parasite thermal transpiration effects inside the gauges themselves can be a sufficient reason in order to have a profound relative measurement error. As we saw in the previous

section, the Takaishi and Sensui semi-empirical formula that we used initially to calibrate the pressure measurements underestimates the pumping effects of thermal transpiration. Anyhow, we believe that in the present experimental work, these problematics have been analyzed and minimized as much as it was possible.

It is important to remember that the main objective of this work was to capture the pressure variation with time and the stationary thermal transpiration mass flow rate. The differential technique that here is shown to measure the final difference of pressure will not be used to compute the mean mass flow rate. When computing the mean mass flow rate, a different method is adopted which relies only on one capacitance diaphragm gauge in order to follow the pressure variation with time inside one reservoir. In addition, we are not interested in absolute values of pressure, but instead pressure variation speeds. More on this respect has been already said in Section 5.2.1.

6.2 Stationary mass flow rate

We now propose what is at the core of the experimental results obtained, that is the stationary, fully developed and not-perturbed thermal transpiration mass flow rate induced by subjecting a temperature gradient along the axis of a micro-tube. The gas flows in the temperature gradient direction, from the cold to the hot region.

As previously introduced in the non-isothermal methodology section (Section 5.2), the measurements of the thermal transpiration mass flow rate were effectuated immediately after the micro-valve closure t_0, that is when the macroscopic movement of gas could be still considered as stationary and not yet perturbed by the contrary directed Poiseuille flow generated by the increasing pressure difference between the two reservoirs attached to the tube.

By following the pressure variation with time for every single experiment and subsequently by finding the characteristic time τ of the time-dependent thermodynamic system that properly fits the experimental pressure variation with time raw data, it is possible to obtain the thermal transpiration mass flow rate by using eq. (5.12) or eq. (5.13). These equations correlate the pressure variation speed to the mass of gas moving across the outlet or the inlet section of the micro-tube at

time t_0^+.

Since the thermal transpiration mass flow rate entering the hot-side reservoir $\dot{M}_{T_h}$ has to be equal to the thermal transpiration mass flow rate leaving the cold-side reservoir $\dot{M}_{T_c}$, the equations may assume the following general form

$$\dot{M}_T = \frac{V}{RT}\frac{(p_f - p_i)}{\tau}, \tag{6.11}$$

where the macroscopic thermodynamic parameters can be measured inside a single reservoir.

By positioning one pressure sensor in the cold-side reservoir and one pressure sensor in the hot-side reservoir we could effectuate two thermal transpiration mass flow rates measurements. This was done in order to always have a reference value to which we could compare the mass flow rate results with and therefore this methodology allowed us to have a quality control over all the experimental results obtained.

We would like to stress that the thermal transpiration mass flow rate measurement was effectuated twice, once at the hot-side end of the tube and once at the cold-side end of the tube.

Let us identify the parameters that we used in order to define a single experiment, that is the monitoring of the pressure variation with time from the initial stationary thermal transpiration flow state of equilibrium to the zero-flow final state of equilibrium. In order to effectuate a single experiment we fixed: the pure gas inside the test-section, the temperature difference applied along the external surface of the micro-tube and the initial pressure inside the micro-fluidic system. By imposing these parameters at the beginning of one experiment it is then possible to define the rarefaction conditions present inside the micro-tube at t_0, that is δ_T.

6.2.1 Influence of the rarefaction

Lets now analyze the results obtained. The thermal transpiration mass flow rates measured in the spectrum of gas rarefaction considered are in the order of $10^{-12} \div 10^{-11}[kg/s]$, for argon, helium and nitrogen. As shown in Figures 6.12, the dimensional mass flow rates monotonically increase from near free molecular to slip regime.

Quantitatively speaking, for a temperature difference imposed of $\Delta T = 71K$, when passing from transitional to slip regime the mass flow rates approximately vary from $6 \cdot 10^{-12}$ to $20 \cdot 10^{-12}$ $[kg/s]$ for argon ; from $2 \cdot 10^{-12}$ to $13 \cdot 10^{-12}$ $[kg/s]$ for helium; and from $3 \cdot 10^{-12}$ to $14 \cdot 10^{-12}$ $[kg/s]$ for nitrogen. This tendency is respected also for the other temperature differences applied.

One important reflection to be made on the tendency of the mass flow rate is that the values of the thermal transpiration induced flow tend asymptotically to a plateau from the end of the transitional regime towards slip regime. It is better to refer to Figure 6.12 to see this trend, since it is not really visible when plotting the results in logarithmic scale. The trend is respected for argon, helium and nitrogen for all the applied temperature differences.

When going from transitional to slip regime and further, the increase of density is counterbalanced by the decrease of the speed of the flow. Therefore, if we consider the well known equation

$$\dot{M}_T = A\rho u, \tag{6.12}$$

where A is the section of the tube, ρ is the density of the fluid and u is the average velocity in the axial direction, for increasing densities, the mass flow rate at the inlet or at the outlet of the tube could tend to a constant value only if the density tends to increase inversely proportional to the flow velocity.

The explanation of this trend can be deduced from the fact that when passing from transitional to slip regime the viscous forces and the mass inertia start to become preponderant in the gas flow, therefore, if the the driver of the flow remained of the same magnitude, the thermal transpiration flow speed would start to drastically decrease. By observing the mass flow rate experimental results it

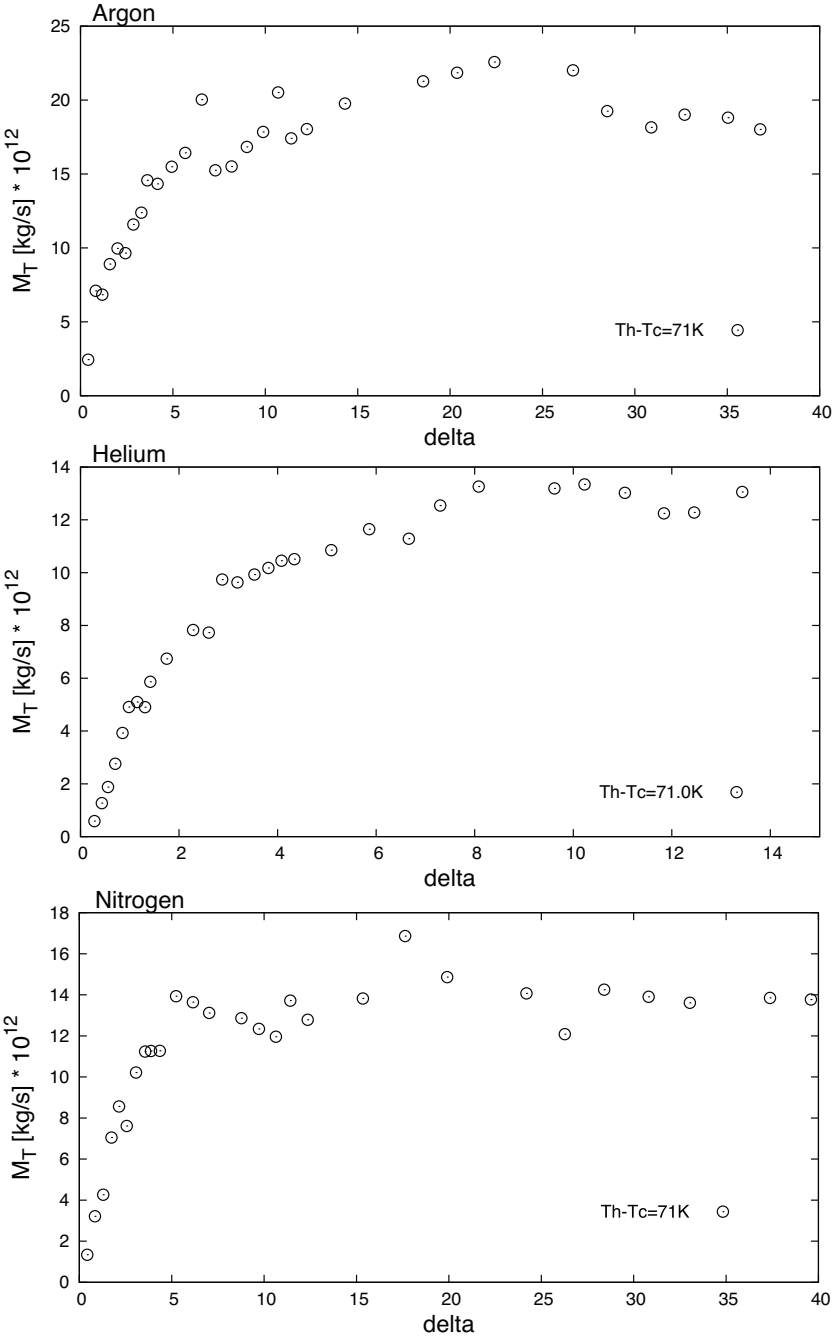

Figure 6.12: Thermal transpiration mass flow rate in [kg/s] for argon, helium and nitrogen as a function of the rarefaction δ_T. Temperature difference applied $\Delta T = 71K$.

could be possible to deduce that from a certain point of the gas rarefaction in ahead the flow speed may decrease as inversely proportional to the density.

It is possible to see that again, the value of rarefaction at which the transition from thermal transpiration mass flow linearly increasing to tending to a constant value becomes more evident at approximately $\delta_T = 3.5$, that is in transitional regime, for all of the three studied gases.

We would like to remind the reader that we found this rarefaction value to be a critical value also for what concerned the thermal molecular pressure difference experimental results. At this value of the rarefaction parameter we had a TPD_{max} for argon, helium and nitrogen.

6.2.2 Influence of the molecular weight

Lets now analyze the influence of the gas used on the thermal transpiration mass flow rate at a fixed temperature difference applied (Figure 6.13).

It is possible to notice that effectively the mass flow rates are influenced by the molecular weight of the gas. The mass flow rates of argon are superior in respect of those of helium in the whole spectrum of rarefaction studied. The gas with the higher molecular weight seems more influenced by the inequalities of temperatures applied on the surface. The same can be said if confronting argon, which is a monoatomic gas that has a molecular weight of 39.948 ± 0.001 u, and nitrogen, which is a diatomic gas that has a total molecular weight of $2 \cdot (14.0067 \pm 0.0002$ $u)$.

The surprising result is the behavior of helium, which is a monoatomic gas that has a molecular weigh of $4.002602 \pm 0.000002u$, in respect to nitrogen: the mass flow rates of the two gases seem to coincide for the whole spectrum of rarefaction studied, even if the gases molecular characteristics are very different.

In Figure 6.14 it is possible to observe the hierarchy of the mass flow rates when plotted in respect to the initial pressure of the experiment. We can see that for a same working pressure applied, the mass flow rates are higher for argon, then nitrogen and finally lower in the case of helium. This trend corresponds to the

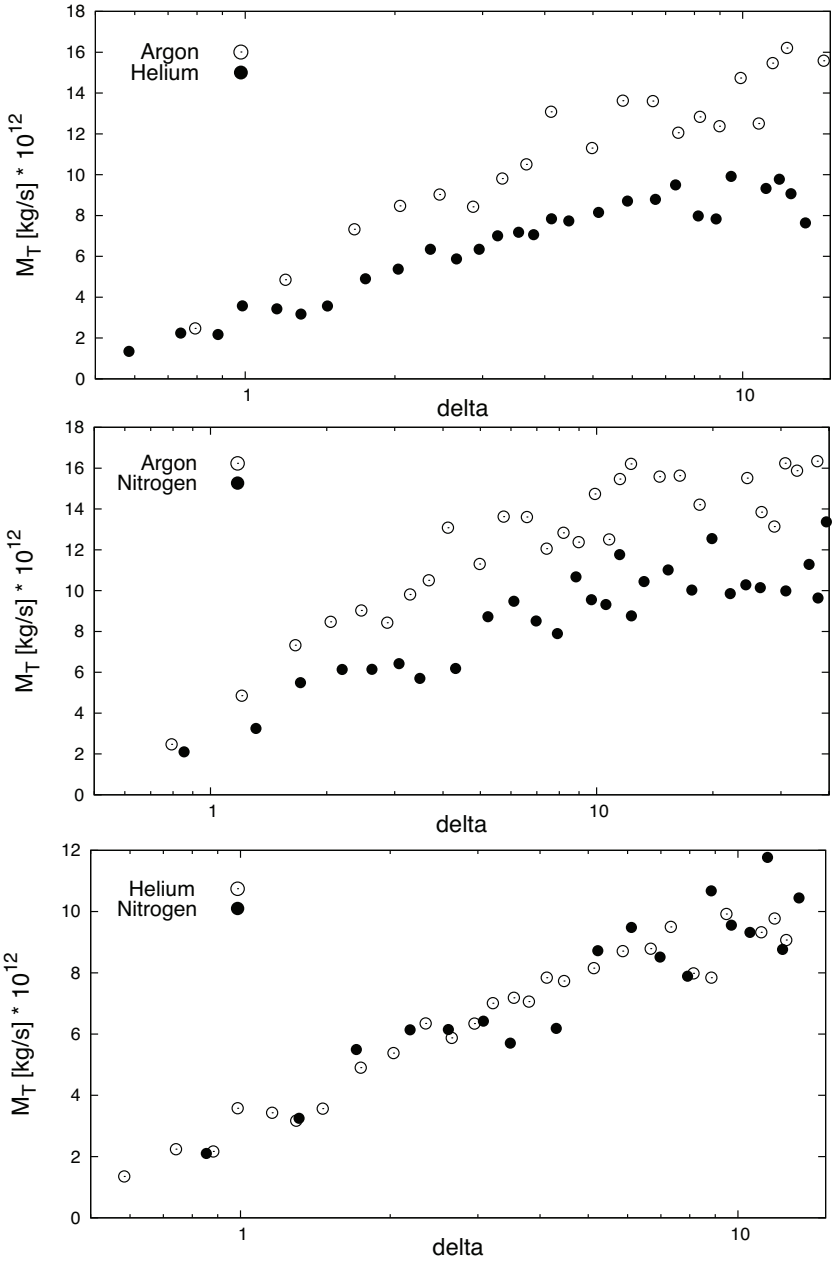

Figure 6.13: Comparison of the molecular weight influence on the thermal transpiration mass flow rate as a function of the rarefaction δ_T in logarithmic scale. Top: argon and helium. Middle: argon and nitrogen. Bottom: helium and nitrogen. Temperature difference applied $\Delta T = 53.5K$.

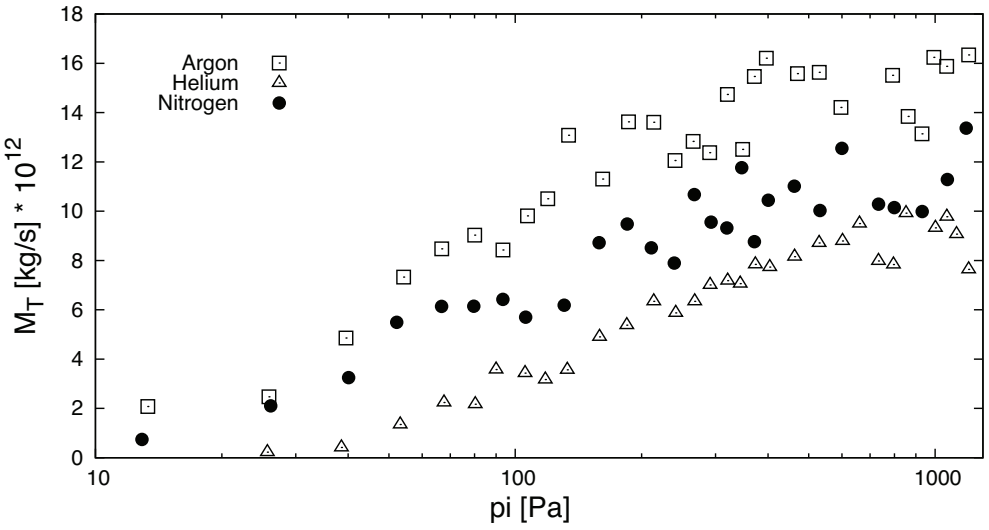

Figure 6.14: Thermal transpiration mass flow rate in [kg/s] for argon, helium and nitrogen as a function of the initial pressure p_i in logarithmic scale. Temperature difference applied $\Delta T = 53.5K$

molecular weight hierarchy.

The uncertainty of the measuring system for the thermal transpiration mass flow rate is in the order of $\pm 8\%$ of the measured value. We would like to remember to the reader that the dimensions of the measured quantities are extremely low. We arrive very close to the measuring limits of the instrumentation used in order to measure the pressure variation speed at time t_0, which is directly proportional to the thermal transpiration mass flow rate.

We will analyze this issue in the section dedicated to the non-stationary results (Section 6.3), where the pressure variation with time and pressure variation speed will be analyzed as a function of the rarefaction. Therefore, we will evaluate how the passage from the initial thermal transpiration flow equilibrium stage to the zero-flow final equilibrium stage becomes faster when passing from transitional to slip regime, and therefore it gets more difficult to effectuate a stationary thermal transpiration mass flow rate measurement due to the fact that the thermodynamic system more rapidly "loses" its stationarity.

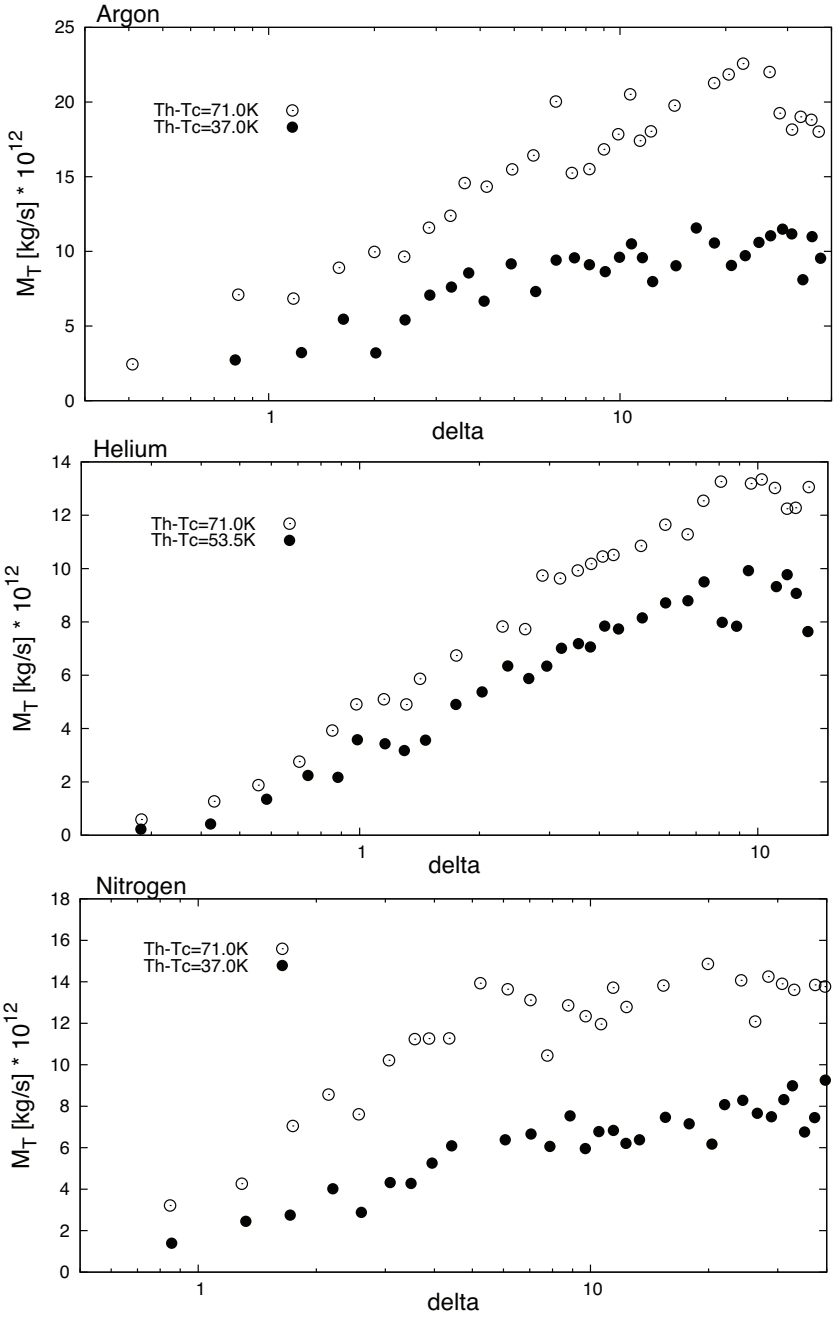

Figure 6.15: Thermal transpiration mass flow rate in [kg/s] for argon, helium and nitrogen as a function of the rarefaction δ_T in logarithmic scale. Comparison between two temperature differences applied: $\Delta T = 71K$ and $\Delta T = 37K$ for argon and nitrogen. $\Delta T = 71K$ and $\Delta T = 53.5K$ for helium.

6.2.3 Influence of the temperature

If we look at the influence of the temperature difference applied on the thermal transpiration mass flow rate, we find that the higher the energy applied in order to heat the hot-side reservoir is, the higher the temperature difference subjected to the micro-tube is, and therefore the mass of gas displaced along the tube is higher (Figure 6.15). The trend is analogous for argon, nitrogen and helium: the mass flow rate increases linearly with the temperature difference applied.

Due to the uncertainty of the measurements, it is possible to make only a rough estimation on the effects of the temperature difference applied on the micro-tube. Nevertheless, we can state that the intensity of the mass flow rate at $\Delta T = 71K$ is approximately two times higher in respect to the intensities of the mass flow rates at $\Delta T = 37K$, which is the same order of ratio in respect of the two temperature differences applied. The same trend is approximately respected for the case of helium at $\Delta T = 71K$ and $\Delta T = 53.5K$ where the ratio between the mass flow rate intensities becomes approximately 1.3.

6.2.4 Conservation of the mass

Let us now make a similar analysis to the one made in Section 6.1.5. This time lets analyze the measurements made for what concerns the thermal transpiration mass flow rate.

As previously introduced, in order to respect the conservation of the mass at time t_0, the mass flow rate measured in the hot-side reservoir has to be equal to the mass flow rate measured in the cold-side reservoir $\dot{M}_{T_c} = \dot{M}_{T_h}$ [eq. (5.15)]. This test can be then considered as a reference of the quality of the measurements. We therefore offer in Figure 6.16 the comparison between the thermal transpiration mass flow rate measured in the hot- and the cold-side reservoirs, for argon, helium and nitrogen for a fixed temperature difference applied.

As it may be readily seen from the graphs, the mass conservation is well captured in within the experimental uncertainty which is of approximately 8%. Again it is possible to identify the helium thermal transpiration mass flow rates, in respect to argon and nitrogen, as being the less fluctuating results. This is specially due to

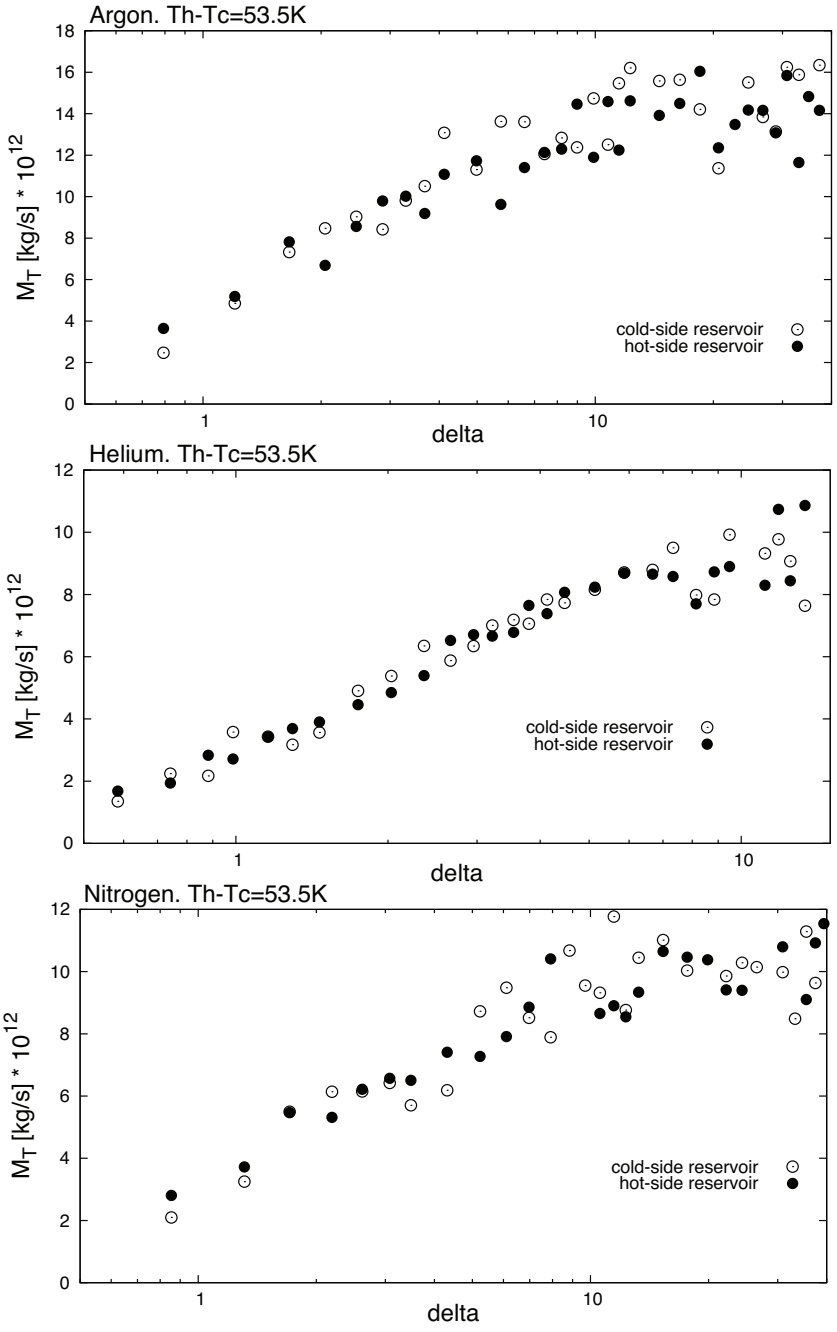

Figure 6.16: Thermal transpiration mass flow rate in [kg/s] for argon, helium and nitrogen as a function of the rarefaction δ_T in the hot- and cold-side reservoirs. Temperature difference applied $\Delta T = 53.5K$

the speed of the macroscopic movement of the gas that, for an equal temperature difference imposed, is higher for a lighter gas. Therefore, the pressure varies with time faster after the micro-valve closure and it is easier for the pressure gauges to capture its trend.

A second reason of the better quality of the helium measurements can be considered to be the fact that the final pressure difference at which the helium pressure variation with time tends is greater for a lighter gas in respect to a heavier gas. In the heavier gas case the final pressure difference obtained in some cases could reach the order of magnitude of the instrument resolution and therefore the measurement quality could be seriously affected.

6.3 Non-Stationary results

The thermal transpiration phenomenon as presented in this experimental work, can be considered as the driver of a strong time-dependent thermodynamic change inside the micro-fluidic system considered. More specifically in this study, the time-dependent pressure variation was obtained by means of a configuration shift in the system, in order to obtain a pressure variation with time inside the two reservoirs.

While exploiting the experimental results in order to obtain the thermal transpiration mass flow rate results, we observed and considered that it was of extreme interest to analyze the time-dependent phenomenon that had thermal transpiration as a drive also from a non-stationary point of view.

As the results that we presented in this section show, the pressure variation with time depends on three distinct parameters, such as the temperature difference imposed, the gas nature and the pressure working conditions of the micro-fluidic system. Thus, these results could constitute a first step towards what could constitute future novel micro-fluidic devices that may work on the basis of the time-dependency of thermal transpiration.

We could imagine, for example, in gas chromatography systems that it could be possible to detect different gas compositions by looking at the time needed for the

thermodynamic system to pass from the first stationary thermal transpiration flow equilibrium stage to the final zero-flow final equilibrium stage.

Other possible applications for the hereafter presented results could be to refer to them as test cases for computational modeling in non-stationary conditions.

6.3.1 Characteristic time and transitional time

Let us start the non-stationary analysis by considering the time that the thermal transpiration mass flow rate needs to pass from its stationary, fully-developed, uni-directed and not-perturbed state at the initial stage of the experiment to zero at the zero-flow final equilibrium stage of the experiment. This timing needed to reach the final equilibrium is well represented by the characteristic time length of the system τ, that was introduced in eq. (5.8) in Section 5.2.2.1.

We will see by which parameters this characteristic time is influenced, the parameters considered were the temperature applied, the gas nature and the initial pressure in the system.

Before looking at the experimental results lets make an initial consideration on one property of the characteristic time of the pressure variation with time which can be derived directly from the law of the conservation of the mass.

If we take into account that the thermal transpiration mass flow rate at t_0 has to be equal in any section of the micro-tube it is possible to state that the mass flow rates measured at the inlet and outlet of the tube have to follow the same law ($\dot{M}_{T_c} = \dot{M}_{T_h}$), as expressed by eq. (5.15). Therefore, from this initial consideration we can arrive at the following balance by just inserting equation (6.8) and equation (6.9) in equation (5.15)

$$\frac{V_h}{RT_h}\frac{p_{h_f} - p_i}{\tau_h} = \frac{V_c}{RT_c}\frac{p_i - p_{c_f}}{\tau_c}. \tag{6.13}$$

From here, by simply using the mass conservation equation derived in the section regarding the analysis of the conservation of the mass in the zero-flow final equilibrium stage (Section 6.1.5), that is equation 6.10, it is possible to write that

$$\frac{V_h}{RT_h}\frac{p_i - p_{c_f}}{\tau_h}\frac{T_h}{T_c}\frac{V_c}{V_h} = \frac{V_c}{RT_c}\frac{p_i - p_{c_f}}{\tau_c}, \tag{6.14}$$

from which is evident that the characteristic time of the pressure variation with time in the cold-side reservoir has to be equal to the characteristic time of the pressure variation with time in the hot-side reservoir. In other words, we can write that

$$\tau_c = \tau_h. \tag{6.15}$$

It is then possible to say that the pressure variation with time in the cold- and in the hot-side reservoir has to tend from its initial state to its final state in the same absolute timing. Therefore, even if we fitted the exponential variation with time inside the two reservoirs by using two distinct fitting parameters, that is τ_h and τ_c, the characteristic time of the system is one and it depends on the dimensions of the reservoirs and the conductance of the micro-tube used.

Thus, from the definition given for the transitional time, that is the time of passage between stationary to non-stationary pressure variation with time in the two reservoirs, we can state that also the transitional time of the cold-side reservoir must be equal to the transitional time of the hot-side reservoir

$$t_c^* = t_h^*. \tag{6.16}$$

The experimental transitional time results which are shown in Figure 6.17 give proof of the condition obtained from the conservation of the mass. The transitional time of the pressure variation with time in the cold- and hot-side reservoirs are equal in within the experimental uncertainty. The results are shown for the case of argon, helium and nitrogen at $\Delta T = 71K$.

We present the experimental results of the transitional time rather than the characteristic time of the system since by presenting the transitional time results we are able to also make some considerations on the stationarity of the mass flow rate measurements. Anyhow, the tendencies of the transitional and characteristic time parameters are the same in respect to the rarefaction: the transitional time is directly proportional to the characteristic time ($t^* = \tau/19.5$).

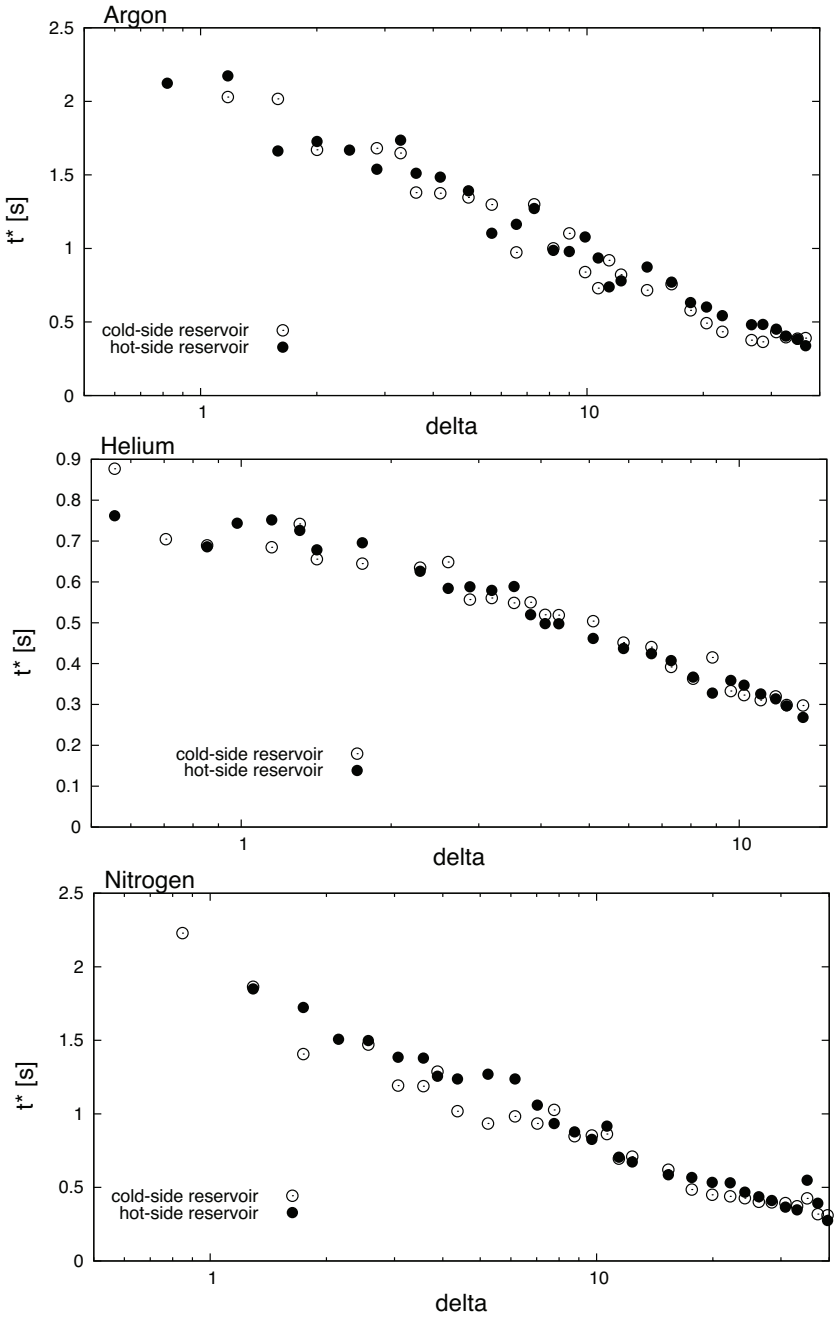

Figure 6.17: Transitional time t^* as a function of the rarefaction δ_T at $\Delta T = 71K$ for argon, helium and nitrogen. Confrontation between cold- and hot-side reservoir transitional time.

Influence of the rarefaction

From Figure 6.17 it is possible to see that the transitional time decreases when passing from near free molecular to slip regime, that means that for increasing densities the phenomenon becomes faster.

It is evident how the transitional time becomes indubitably small for rarefaction conditions tending to hydrodynamic regime, where the density becomes higher. The zero-flow final equilibrium stage is reached much faster for the experimental results obtained in slip regime in respect to the results obtained in near free molecular regime. Therefore, the measurement of the thermal transpiration mass flow rate becomes increasingly difficult in slip regime due to the fact that the thermodynamic system loses its stationarity more rapidly.

For the case of a gas at high densities, additionally to the quick loss of stationarity, we can consider that the limits of the measurement are attained also since the resolution of the pressure sensor becomes of a similar order in respect to the final attained pressure difference.

This problematic becomes evident when looking at the thermal transpiration mass flow rate results in Section 6.2: the measurements are fluctuating more for slip regime rarefaction conditions.

The transitional time decreases approximately of 7 folds from near free molecular to slip regime for argon and nitrogen, being approximately $t^* = 2[s]$ at the beginning of the transitional regime and being $t^* = 0.25[s]$ at the heart of the slip regime. For what concerns helium the transitional time decreases of approximately 2.5 folds from near free molecular regime, that is $t^* = 0.8[s]$ to the beginning of the slip regime $t^* = 0.3[s]$.

Influence of the molecular weight

The molecular weight of the gas plays a fundamental role in the timing needed for the pressure variation with time to pass from the initial stage to the final stage. It is possible to see in Figure 6.18 that the lighter gas, for the whole spectrum of rarefaction, is approximately 2.5 folds lower than the heaviest gas, that is argon.

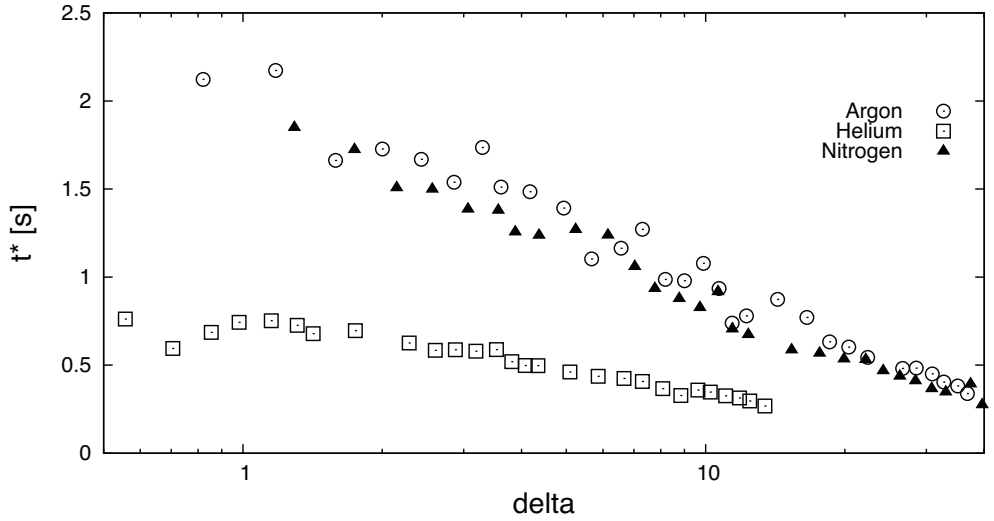

Figure 6.18: Transitional time t^* as a function of the rarefaction δ_T at $\Delta T = 71K$. Comparison between argon, helium and nitrogen.

Nitrogen instead tends to its final equilibrium slightly faster in respect to argon. Therefore it seems that the molecular weight hierarchy of the different gases goes in the same direction as the timing needed for the transition: the lighter the gas is, the more rapidly the final zero-flow equilibrium stage is reached.

Therefore, it is possible to notice that the thermal transpiration mass flow rate for helium loses its stationarity much faster in respect to the heavier gases making the mass flow rate measurement more difficult in the case of a lighter gas. It is not clear under which extent the mass flow measured can be still considered stationary when such a rapid transition takes place.

The problem can be avoided if we consider that the exponential fitting describes well the pressure variation with time at any rarefaction condition of the gas and therefore the measurement should be independent from the time during which the thermal transpiration mass flow rate preserves its stationarity.

Anyhow, the only open question still is if the pressure gauges describe well the pressure variation with time in the surroundings of t_0. The resolution of the pressure sensor is the limiting factor in the case where the linearity of the pressure

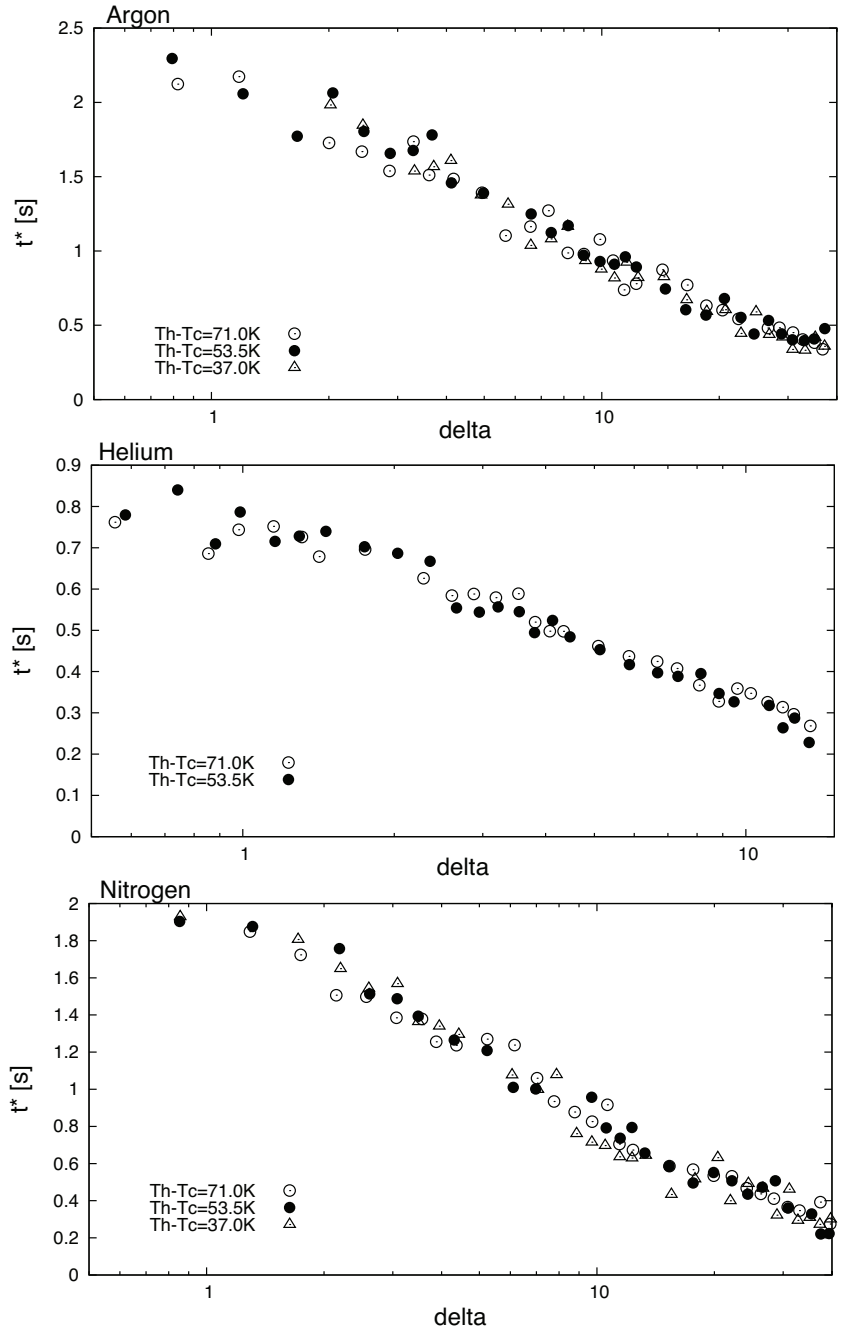

Figure 6.19: Thermal transpiration mass flow rate in [kg/s] for argon, helium and nitrogen as a function of the rarefaction δ_T. Comparison between three temperature differences applied $\Delta T = 71K$, $53.5K$ and $\Delta T = 37K$.

variation with time is lost too quickly. This can induce increasing uncertainties in the fitting expression in the surroundings of the beginning of the pressure variation with time.

Therefore, for the methodology here adopted for measuring the thermal transpiration mass flow rate, the transitional time has to be a parameter which has to be seriously taken under account before performing this kind of measurements, the best case would be to have the largest lapse of time as possible in which the mass flow rate can still be considered as stationary.

Influence of the temperature

In Figure 6.19 it is possible to see that the temperature does not influence the transitional time or characteristic time of the experiment. In the plotted graphs we show the values for argon, helium and nitrogen for three temperature differences applied. For a single gas, the transitional time is the same, in within the measurement uncertainty, for any temperature difference applied at a fixed rarefaction of the gas.

6.3.2 Pressure variation with time

Let us now enter in the core of the non-stationary experimental results. In this section the pressure variation with time (PV) inside both the cold-side $p_h(t)$ and the hot-side reservoirs $p_c(t)$ is analyzed. Let us remind the reader that the pressure variation begins when the solenoid micro-valve is closed at time t_0. At this time, the two reservoirs remain connected only by the micro-tube and the absolute pressure inside them varies. The pressure variation with time is induced by the macroscopic movement of gas which is directed in the same way as the temperature gradient. The pressure increases in the hot-side reservoir and the pressure decreases in the cold-side reservoir. Therefore we obtain a time-dependent phenomenon and from an initial stationary thermal transpiration flow stage the system tends asymptotically to a final zero-flow equilibrium stage.

During the exploitation of the pressure variation with time in order to obtain the thermal transpiration mass flow rate, we understood that it could be of interest to analyze the transitional stages in between the initial thermal transpiration

flow equilibrium stage and the final zero-flow equilibrium stage. We therefore saw that the pressure variation with time was largely influenced by the rarefaction of the gas, the gas nature and the temperature difference applied. At the same time, in addition to this it depended also from the internal volume of the reservoirs and the dimensions of the capillary itself which determined the conductivity of the system and therefore the speed of the variation. Thus we can write that $p(t)$ is a function of

$$p(t) = f[Gas, dT/dx, T_h, T_c, p_i, V_h, V_c, L, D]. \tag{6.17}$$

Unfortunately the influence of the last parameter will not be taken into account in this analysis since the test section was prepared to accept just one specific geometry of a single capillary.

Influence of the rarefaction

The gas rarefaction plays a fundamental role in the behavior of the variation of pressure with time inside the reservoirs (Figure 6.20-6.22). By considering the state of rarefaction of the gas δ_T as a fixed parameter, it is possible to observe, when we move from near free molecular to transitional regime, that the PV magnitude is higher for higher density flows in respect to lower density flows, at any time of the experiment. This trend stops when we move from transitional to slip regime: after touching a maximum in transitional regime, the pressure variation with time magnitude decreases drastically, for any time of the experiment, if the density continues to increase, that is when tending to slip regime conditions.

It is possible to observe that the behavior of the magnitude of the pressure variation with time shifts from rising to descending at a very precise gas rarefaction value, that is for approximately $\delta_T = 3.5$. This is a common trend for argon, helium and nitrogen, as previously seen in the thermal molecular pressure difference study.

Another observation that can be made by looking at $p_h(t)$ and $p_c(t)$ in Figures 6.20-6.22 for the case of the same fixed rarefaction conditions δ_T, for a given gas and by applying the same temperature gradient to the tube, is that the pressure variation with time in both tanks is not perfectly mirror symmetric. In other words, when $p_h(t)$ is compared to $p_c(t)$ at the same fixed time between $t = 0^+$ and $t = t_f$, the relation $p_h(t) > |p_c(t)|$ is always true if the condition on eq 6.10 is

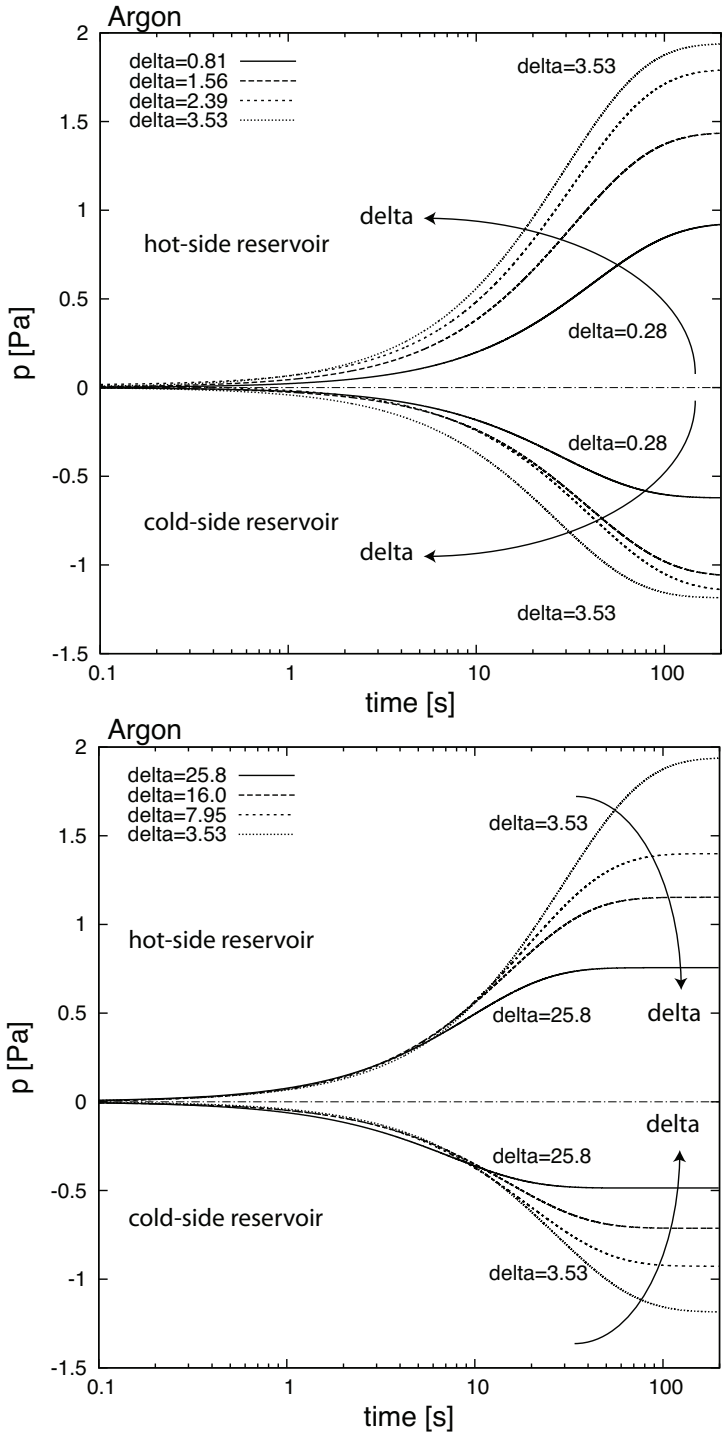

Figure 6.20: Pressure variation with time inside the two reservoirs $p_h(t)$ and $p_c(t)$ for argon at $\Delta T = 71K$. Top: from free molecular to transitional regime. Bottom: from transitional to slip regime.

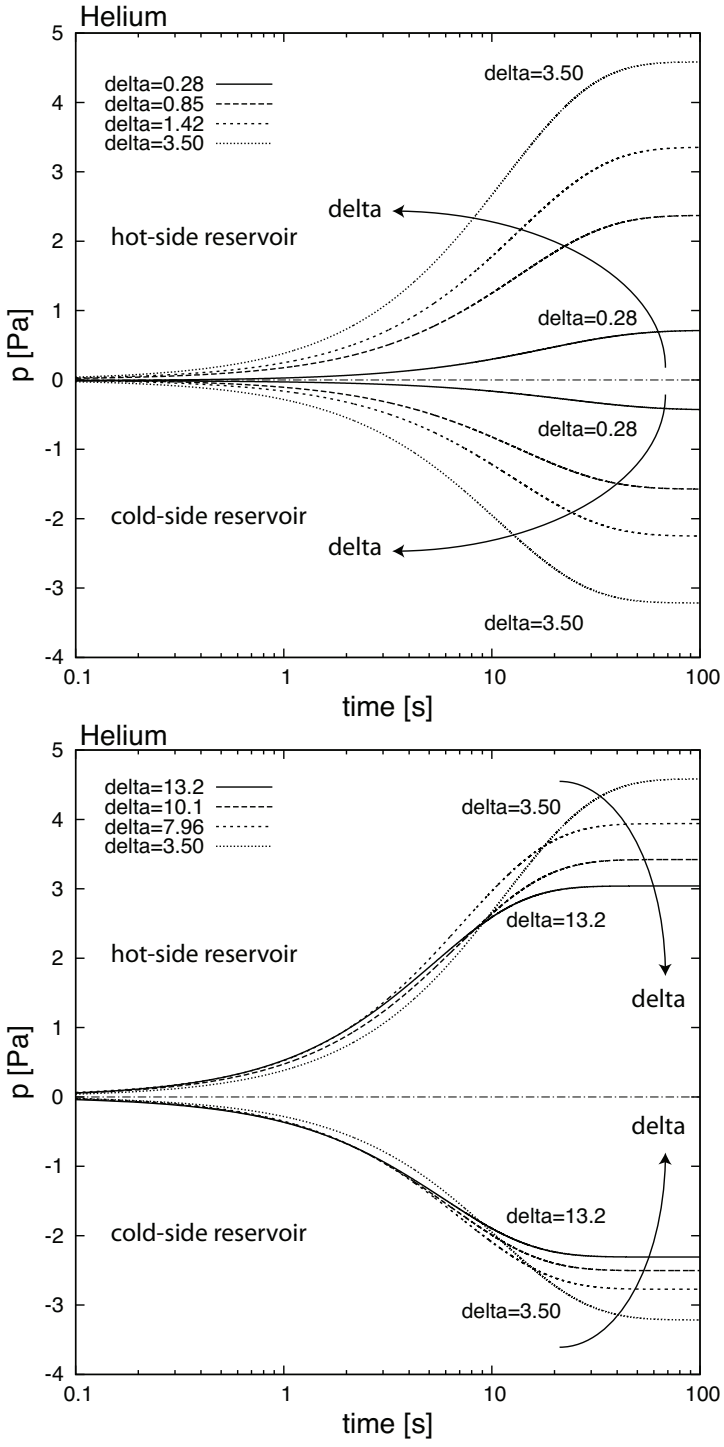

Figure 6.21: Pressure variation with time inside the two reservoirs $p_h(t)$ and $p_c(t)$ for helium at $\Delta T = 71K$. Top: from free molecular to transitional regime. Bottom: from transitional to slip regime.

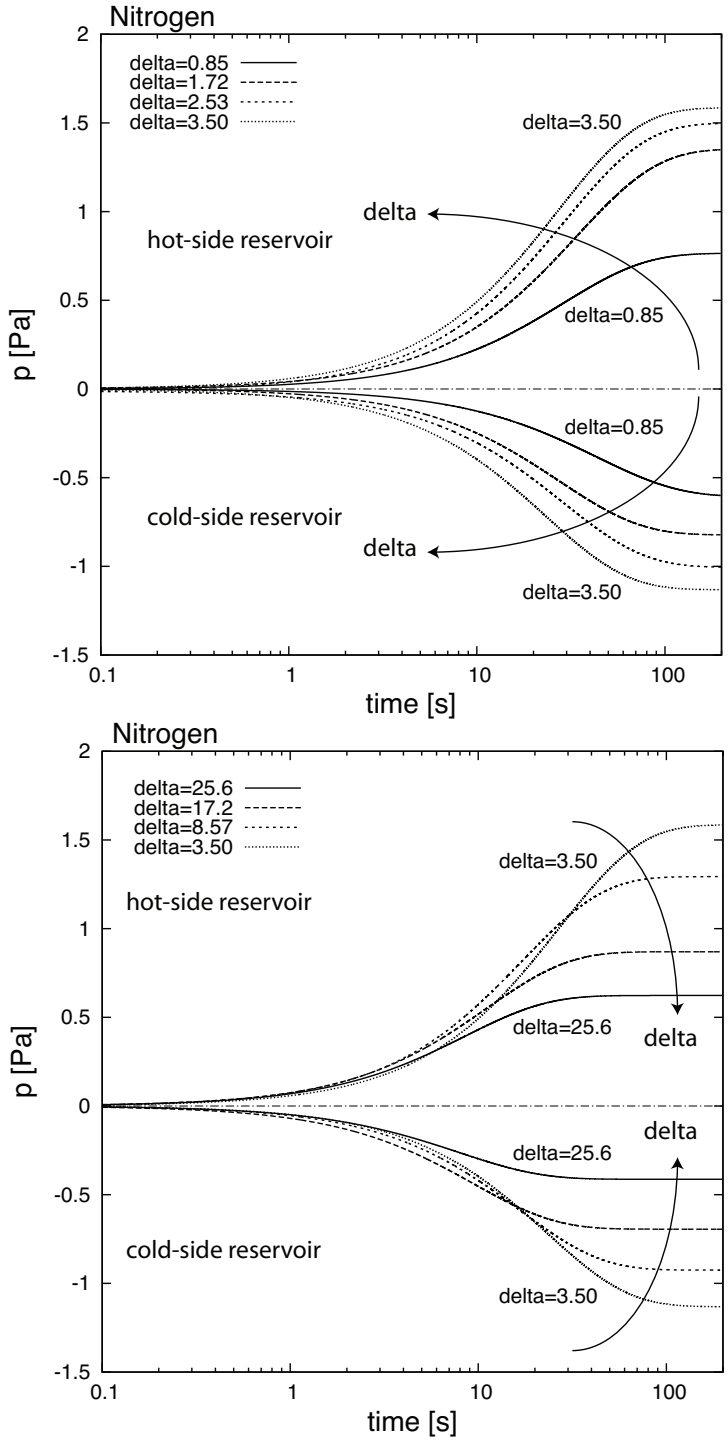

Figure 6.22: Pressure variation with time inside the two reservoirs $p_h(t)$ and $p_c(t)$ for nitrogen at $\Delta T = 71K$. Top: from free molecular to transitional regime. Bottom: from transitional to slip regime.

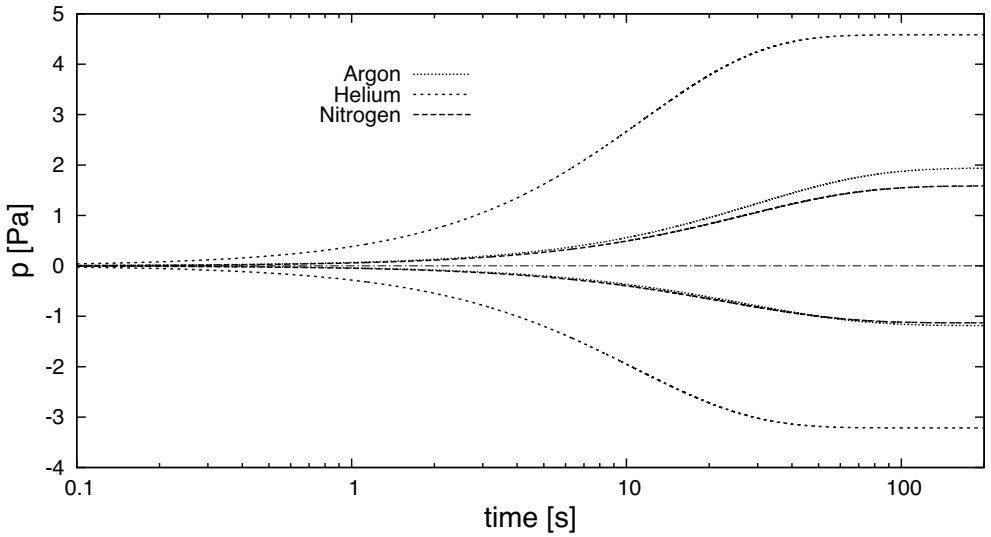

Figure 6.23: Pressure variation with time inside the two reservoirs $p_h(t)$ and $p_c(t)$ for $\Delta T = 71K$ at $\delta_T = 3.5$. Comparison between argon, helium and nitrogen.

respected, that is $\frac{T_c}{T_h}\frac{V_h}{V_c} < 1$. It can be easily proven from the conservation of mass law that this inequality arises from the temperature difference in between the two reservoirs and the volume difference of the two reservoirs.

Influence of the molecular weight

Let us now consider the influence of the working gas on the magnitude of the pressure variation with time in both tanks. As shown in Figure 6.23, different gases have different behaviors for the same rarefaction conditions of the gas and the same applied temperature distribution along the tube.

If just the monoatomic gases are considered, such as helium and argon, it is clear that helium, which is the lighter gas, is more influenced by the thermal transpiration phenomenon than argon, which is approximately 10 times heavier.

In the case of nitrogen, which is a polyatomic gas, the tendency is inverted with respect to argon. Although the standard atomic weight of nitrogen is lower in respect to argon's, the time dependent pressure variation of nitrogen achieved at

every time of the experiment is slightly lower than the pressure variation with time of argon.

It is possible to clearly see here that the difference in the pressure variation with time magnitudes in the case of argon in respect to the case of nitrogen is more accented in the hot-side reservoir. As previously said, this is due to the fact that the volume ratio and the temperature ratio in between the two reservoirs is different than unity. Therefore we always obtain greater magnitudes of the pressure variation with time in the hot-side reservoir.

Thus, it is easier to eventually see differences in the behavior of the pressure variation with time if considering two gases. We can notice the same property if helium and argon are compared. The difference in between the pressure variation with time of the two gases is higher for the measurement made in the hot-side reservoir in respect to the measurement made in the cold side-reservoir.

These considerations are valid for the three different temperature distributions applied and for the whole range of gas rarefaction studied.

Let us note that these results are consistent with those pointed out in previous works [Ewart *et al.* [2007]], on the tangential momentum accommodation coefficient hierarchy in gas-wall exchanges. In these works, in the case where monoatomic gases are considered, the increase of the momentum accommodation at the wall clearly appears when the molecular mass of the working gas decreases. That would also mean [Sone [2007]] an increase of the wall action per unit mass on the gas movement for a decreasing molecular mass. The magnitudes of the pressure variations with time, which are induced here by the tangential momentum exchange at the wall, follow the same trend with respect to the molecular masses of the gases.

Influence of the temperature

In Figure 6.24, the differences in the magnitudes of pressure variation with time are shown, for argon, helium and nitrogen as a function of the temperature gradient applied. It can be noted, as expected, that by increasing ΔT in the case of fixed rarefaction conditions of the gas, greater values of $p_h(t)$ and $p_c(t)$ are obtained at every time t of the experiment.

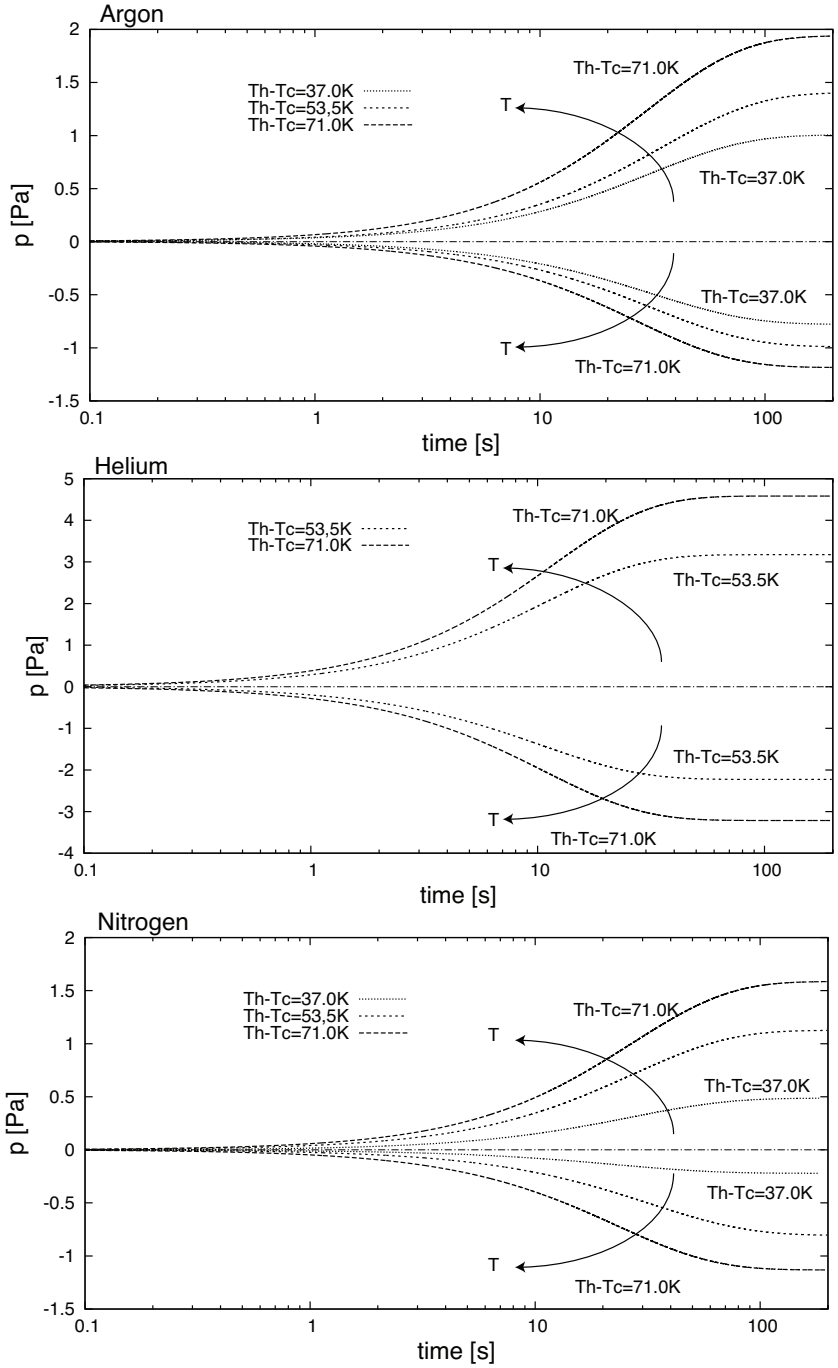

Figure 6.24: Pressure variation with time inside the two reservoirs $p_h(t)$ and $p_c(t)$ for argon, helium and nitrogen at $\delta_T = 3.5$. Comparison between three temperature differences applied: $\Delta T = 71K$, $53.5K$ and $37K$.

In other words, as previously seen in the other results analysis, the thermal transpiration phenomenon is stronger when we increase the strength of its driver, which is the temperature difference between the inlet and the outlet of the tube.

6.3.3 Pressure variation speed

The pressure-variation speed (PVS) is obtained by deriving the pressure variation with time in respect to time. As previously mentioned (Section 5.2.2.2), the PVS is described by equations 5.10 and 5.11, in the hot- and cold-side reservoirs.

The first information that can be extracted from the pressure variation speed is the value of the thermal transpiration mass flow rate transiting along the tube before the valve closure, by assuming that the gas macroscopic displacement is stationary in the surroundings of t_0. Subsequently the stationary thermal transpiration mass flow rate is directly proportional to $dp(t)/dt|_{t_0}$.

In this respect, the pressure variation speed is then a reference for the number of gas molecules transiting per second from the cold-side to the hot-side of the micro-tube, or vice-versa. In the stationary transitional stage (stage 2) the flow is fully developed and uni-directed: the gas flows without being perturbed.

On the other hand, during the non-stationary transitional stage (stage 3), $dp(t)/dt$ involves not only the gas molecules entering the hot-side reservoir (or leaving the cold-side reservoir) moved by the applied temperature distribution, but also the gas molecules leaving the hot-side reservoir (or entering the cold-side reservoir). The newly created difference of pressure between the tanks is the driver that deviates the gas molecules from their original path. It engenders a motion of molecules in the opposite direction to the motion of molecules induced by thermal transpiration. Thus, in the non-stationary transitional stage, the pressure variation speed information obtained is an average value for the displacement of gas molecules leaving or entering the reservoirs.

At the final pressure equilibrium stage of the experiment, when the pressure variation speed is zero, the same number of gas molecules are displaced by thermal

transpiration as by the counter-directed Poiseuille flow.

No information on the velocity profiles along the sections perpendicular to the tube axis can be obtained by looking at the pressure variation speed evolution inside the two reservoirs, but it can be expected that two flows, one directed from the cold-side to the hot-side induced by thermal transpiration, and the other in the opposite direction induced by the difference of pressure, are present along the tube at the final stage of the experiment (Han *et al.* [2007]; Knudsen [1909]).

Influence of the rarefaction

Analogously to the pressure variation with time, the pressure variation speed (PVS) is strongly affected by the rarefaction. From Figures 6.25-6.27 it can be seen that the dependence of the pressure variation speed on the gas rarefaction influences both the stationary and non-stationary transitional stages of the experiment.

Because of a visible difference in the phenomenon behaviour, two different gas rarefaction ranges are considered for analysis: from $\delta_T > 0$ to $\delta \approx 3.5$ and from $\delta_T > 3.5$ to $\delta_T \approx 30$, in other words, from near free molecular to transitional regime and from transitional to slip regime conditions. Again, the value $\delta \approx 3.5$ can be considered as our point of change.

First, let us consider the stationary transitional stage of the experiment ($t < t^*$). For rarefaction parameter values lower than 3.5, a fairly linear rise of the PVS at t_0 is recorded.

After this value of rarefaction is reached, the trend changes, and $dp(t)/dt|_{t_0}$ seems to tend asymptotically to a maximum value when approaching the gas rarefaction conditions of the slip regime. A fair explanation of the asymptotic trend of the initial pressure variation speed towards a constant value is that, ideally, the flow speed tends to zero in the hydrodynamic regime. While the density increases, its increase is inversely proportional to the flow speed. Thus, the two effects are balanced and $dp(t)/dt|_{t_0}$ tends to an asymptotic value.

In contrast, for δ values below 3.5, the density increase does not yet seem to be perfectly balanced by a decreasing gas flow speed and thus the PVS at the ini-

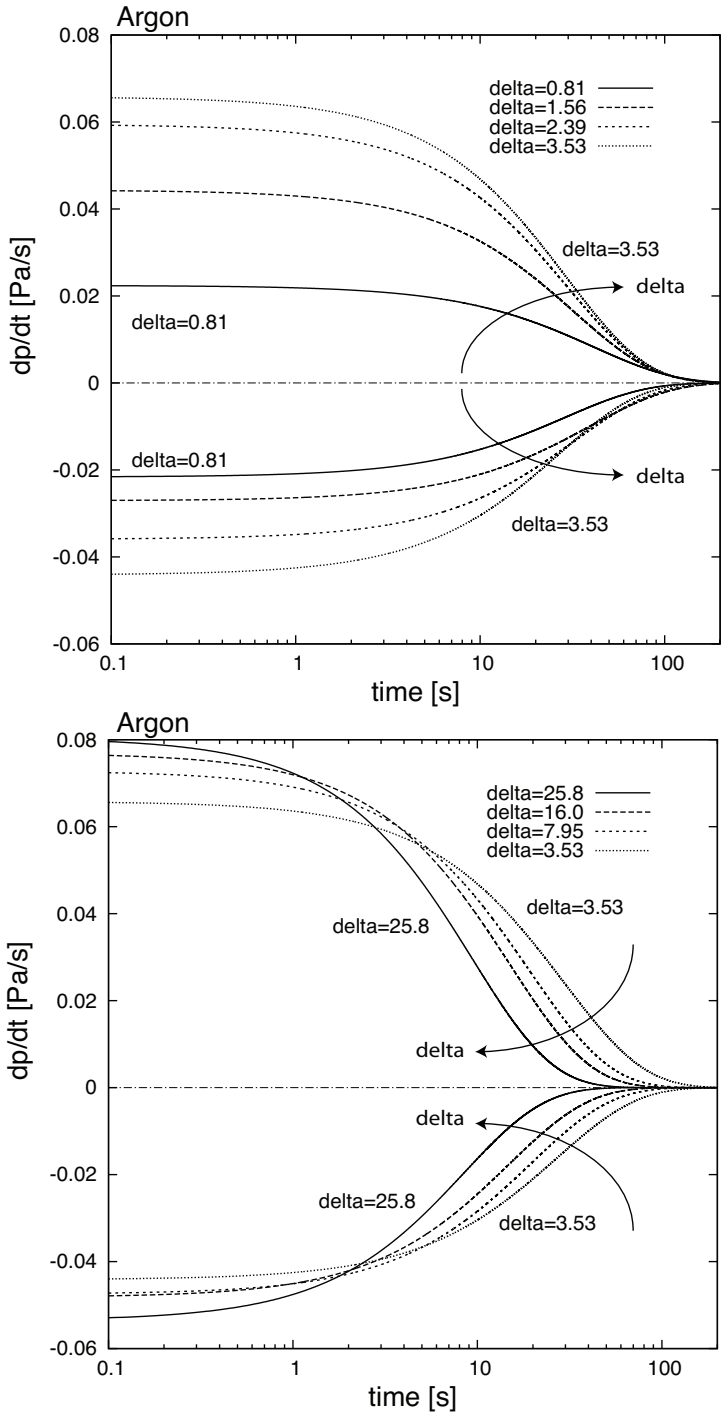

Figure 6.25: Pressure variation speed inside the two reservoirs $dp_h(t)/dt$ and $dp_c(t)/dt$ for argon at $\Delta T = 71K$. Top: from free molecular to transitional regime. Bottom: from transitional to slip regime.

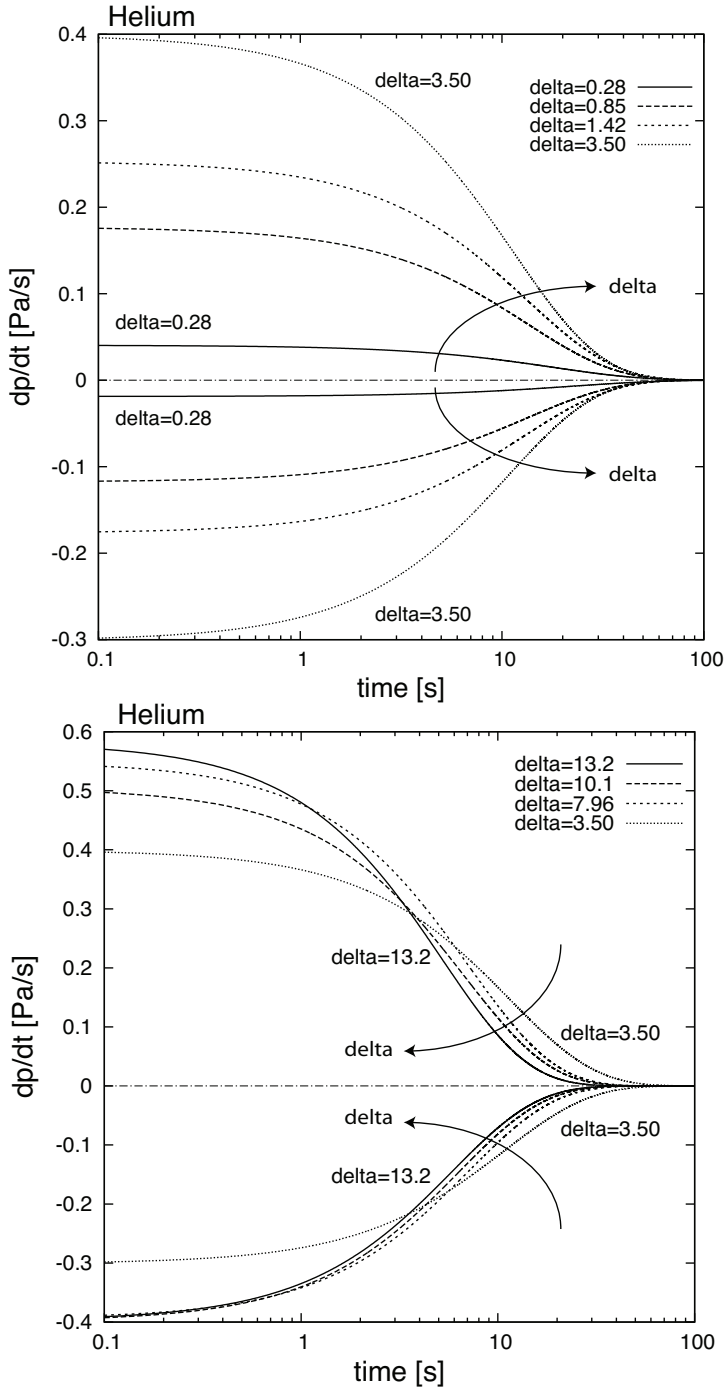

Figure 6.26: Pressure variation speed inside the two reservoirs $dp_h(t)/dt$ and $dp_c(t)/dt$ for helium at $\Delta T = 71K$. Top: from free molecular to transitional regime. Bottom: from transitional to slip regime.

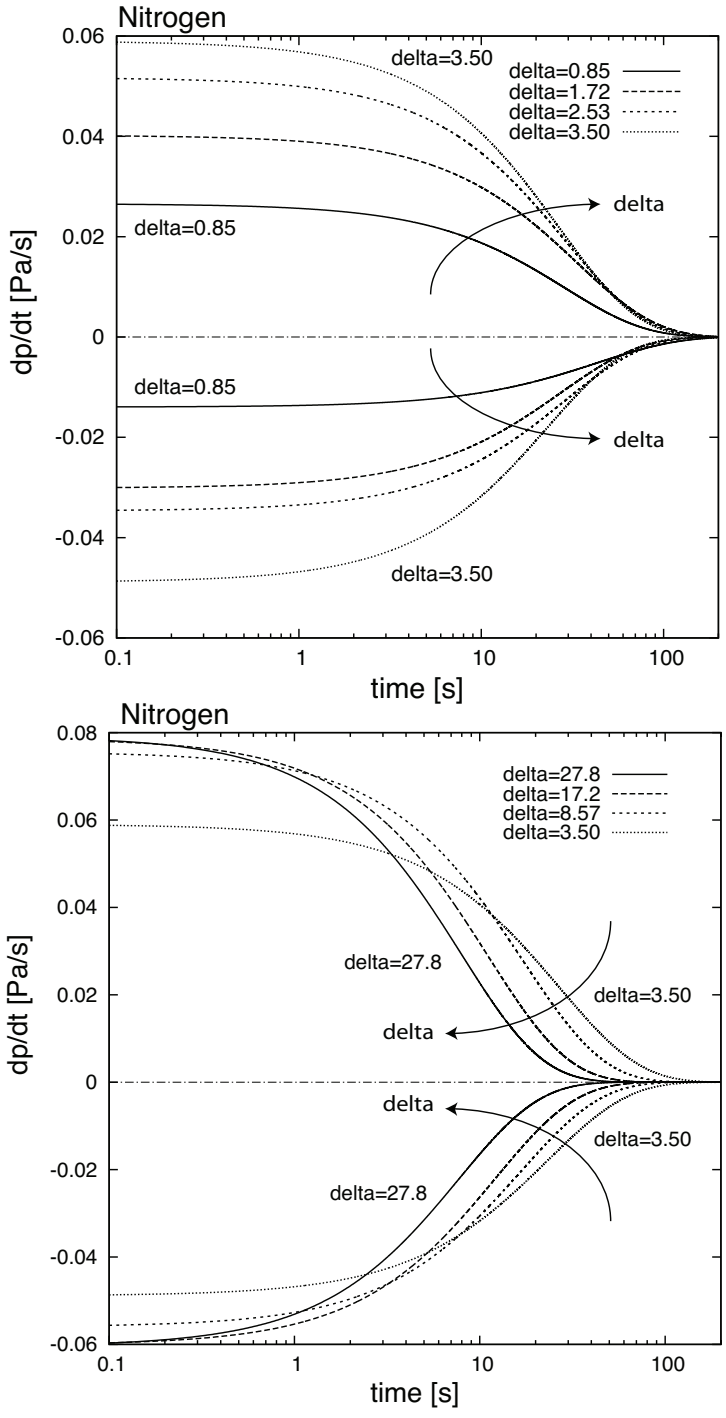

Figure 6.27: Pressure variation speed inside the two reservoirs $dp_h(t)/dt$ and $dp_c(t)/dt$ for nitrogen at $\Delta T = 71K$. Top: from free molecular to transitional regime. Bottom: from transitional to slip regime.

tial time $t = 0^+$ increases from the near free molecular to the transitional regime.

Analogous information can also be extracted from the non-stationary transitional stage ($t > t^*$). It can be seen from Figures 6.25-6.27 how the transitional stage experimental timing ($t_f - t_0$) speeds up for rarefaction values that go from near free molecular to slip regime. Again, $\delta_T \approx 3.5$ seems to be the transitional value.

In the case of experiments performed at transitional regime gas conditions, the absolute timing ($t_f - t_0$) for the pressure variation speed to become zero, for $\delta < 3.5$, is always higher than in experiments done at near free molecular regime gas conditions.

For $\delta > 3.5$ the PVS speeds up, drastically decreasing the absolute time that $dp(t)/dt$ needs to reach the zero-flow stage. The results obtained for nitrogen coincide with the results for helium and argon. In addition, this analysis is valid for the three temperature distributions applied to the tube.

Influence of the molecular weight

In Figure 6.28, the results illustrate the influence on the pressure variation speed according to the nature of the gas.

The influence of the gas molecular weight is again evident: in the case of helium, the $dp(t)/dt|_{t_0}$ is approximately six times higher than for argon. Argon and nitrogen seem to behave similarly, although the thermal transpiration effects on the initial PVS magnitude for nitrogen are slightly smaller than for argon.

In fact, the lighter gas configuration tends to reach its new position of equilibrium, i.e. it moves from the first thermal transpiration mass flow rate equilibrium stage to the zero-flow final equilibrium stage, faster than a heavier gas. The absolute time to reach the final equilibrium stage is of the same order as for a heavier gas, but the initial state of equilibrium $dp(t)/dt|_{t_0}$ is up to six times higher, as previously mentioned.

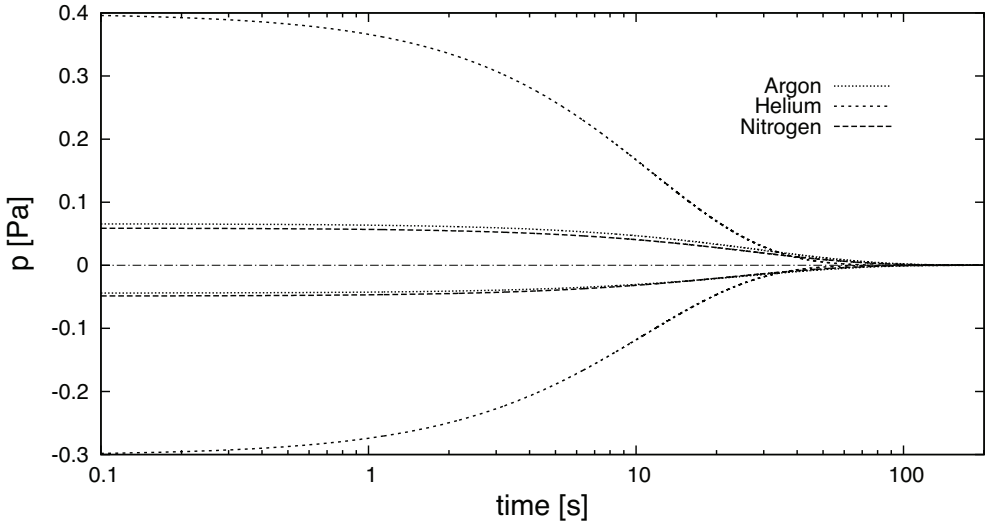

Figure 6.28: Pressure variation speed inside the two reservoirs $dp_h(t)/dt$ and $dp_c(t)/dt$ for $\Delta T = 71K$ at $\delta_T = 3.5$. Comparison between argon, helium and nitrogen.

Influence of the temperature

Moreover, the pressure variation speed is also strongly affected by the temperature distribution applied to the tube (Figure 6.29). As expected, the pressure variation speed magnitude in the stationary and non-stationary transitional stages of the experiment increases with higher temperature differences applied.

It can be noted that the behaviours of the PVS throughout the time spectrum of one experiment are qualitatively identical to one another if the applied temperature difference is shifted. Thus it is again possible to state that the characteristic time of the system τ is not affected by the temperature difference applied. We give the results of helium as a case in point. The same characteristics were found for argon and nitrogen. The rarefaction parameter was fixed.

Finally let us analyze the PVS values at time t_0 ($dp(t)/dt|_{t_0}$) as a function of the temperature difference applied. For argon, helium and nitrogen, the intensity of the PVS at $t = 0+$ increases for higher differences of temperatures. The trend is the same for every rarefaction parameter considered.

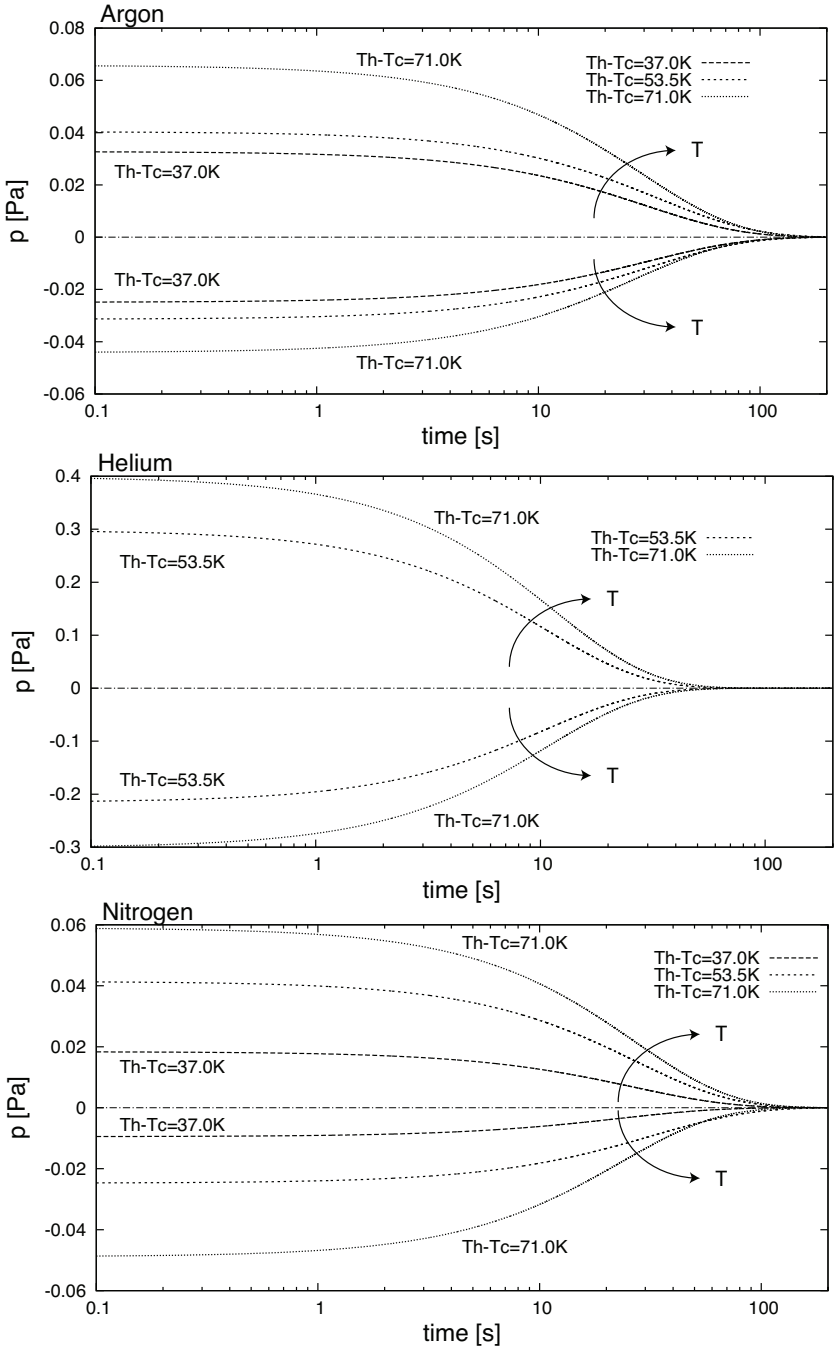

Figure 6.29: Pressure variation speed inside the two reservoirs $dp_h(t)/dt$ and $dp_c(t)/dt$ for argon, helium and nitrogen at $\delta_T = 3.5$. Comparison between three temperature differences applied: $\Delta T = 71K$, $53.5K$ and $37K$.

6.3.4 On the shifting tendency at a precise rarefaction

The shift in the behaviour of the pressure variation with time at the final equilibrium stage and the pressure variation speed at t_0, when the gas density increases, can be attributed to a change in the ratio of the number of gas/gas collisions to the number of gas/wall collisions.

In free molecular regime, since the mean free path of the gas is extremely long in comparison to the characteristic length of the system, there are no collisions between gas molecules. On the other hand, gas-wall collisions are present, statistically giving some of the gas molecules the necessary momentum to travel from the cold to the hot region and in this way they contribute to create a pressure difference at the final zero-flow stage of the experiment.

When the rarefaction conditions of the gas change from free molecular to transitional regime the ratio of the number of gas/gas collisions to the number of gas/wall collisions increases. Thus, through the increased number of collisions between gas molecules, the momentum exchanged by the walls with a certain population of gas molecules is transmitted to the whole population of gas molecules present in the tube. Thus, with more gas molecules being stimulated, a higher mass of gas is displaced in the temperature gradient direction. An increased mass of gas displacement directly affects the magnitude of the pressure variation with time, as does the pressure variation speed at t_0 (Figures 6.20-6.22 and Figures 6.25-6.27).

Let us consider the PV at the final equilibrium stage and the PVS at t_0. From near free molecular to transitional regime ($\delta_T < 3.5$) the magnitude of PV at the zero-flow stage increases monotonically. At the beginning of the transitional regime, near to delta values of 3.5, the PV at the final equilibrium stage reaches a maximum. From δ_T approximately 3.5 onwards, namely from the transitional to the hydrodynamic regime, the magnitude of PV at the zero-flow stage starts to decrease, eventually tending to zero in the case of a high density flow. Also the tendency of PVS at $t = 0+$ shifts drastically near to delta values of 3.5. The trend of PVS at t_0 is linearly increasing from near free molecular to transitional regime but, after passing the limit value of $\delta_T \approx 3.5$, when moving from the transitional to the hydrodynamic regime, the PVS at t_0 tends to a constant value. These two

tendency shifts are connected.

Since the magnitude of PVS at t_0 is directly proportional to the thermal transpiration stationary mass flow rate [eqs. (5.12) and (5.13)], it is possible to deduce that, for higher densities, the thermal transpiration mass flow rate tends asymptotically to a constant value. A reason for this tendency is the rapid growth of viscous and inertial forces which are engendered by the greater density of the gas. Thus, while the gas density increases, the flow speed decreases and it tends ideally to near zero values. In this way, the stationary mass flow rate engendered by thermal transpiration tends to a plateau.

The shift in the tendency of the PV magnitude is directly related to the fact that the system tends to an equilibrium between two oppositely directed flows: when the rarefaction varies from free molecular to transitional regime, the thermal transpiration flow increases rapidly with the gas density, hence ever higher final equilibrium zero-flow pressure differences must be reached by the PV in order to engender a sufficiently large oppositely directed Poiseuille flow.

On the other hand, from transitional to hydrodynamic regime ($\delta > 3.5$), when the mass flow engendered by thermal transpiration tends to a plateau (Figure 6.12), in order to engender an oppositely directed Poiseuille mass flow rate of the same value, lower pressure differences of the PV at the final equilibrium zero-flow stage of the experiment are necessary. In other words, the PV at the final equilibrium zero-flow stage reaches a maximum at a precise gas rarefaction since the oppositely directed flow induced by pressure difference for higher densities can equilibrate the thermal-transpiration-induced flow in a faster and easier way. The density of the flow plays a fundamental role in this mechanism.

Chapter 7

Numerical comparison

In this chapter we presented the results obtained by the numerical solution of the Shakov model kinetic equation introduced in Section 2.2 and by using the direct simulation Monte Carlo method introduced in Section 2.3. The numerical solution of the S-model kinetic equation that we used was developed by Graur & Sharipov [2009], while the DSMC code used was developed by Bird [1995].

The numerical results were obtained for the stationary thermal transpiration flow initial stage and for the stationary zero-flow final stage.

7.1 Shakov model

The authors Graur & Sharipov [2009] have developed a numerical technique based on the solution of the linearized S-model kinetic equation in order to simulate a gas flow trough a long tube due to a pressure and a temperature gradient. The general case of an elliptical tube cross section was considered and the numerical simulations were carried out for a large spectrum of the rarefaction parameter.

In the present analysis we use the numerical results found in Graur & Sharipov [2009] in order to compare them to the experimental results obtained in the initial stage of the experiment, when the thermal transpiration flow is stationary, fully-developed, uni-directed and not-perturbed, and in the zero-flow final stage, when the net mass flow rate along every section of a tube is zero.

7.1.1 Statement of the problem

According to Graur and Sharipov, we consider a long circular cross section tube connected to two reservoirs (Fig. 7.1). The pressure and the temperature in the left and right reservoirs are respectively p_c, T_c and p_h, T_h. In order to apply the numerical approach explained below we need to make two main assumptions. The first one is that the tube length has to be significantly larger in respect to its radius $D/2 \ll L$. This assumption allows us to neglect the end effects and to consider only the longitudinal component of the bulk velocity and heat flux vector, which depend only on z and y coordinates. The second one, which allows us to linearize the model kinetic equation, is that the temperature and the pressure depend only on the longitudinal component x and that their normalized gradients along x are small

$$\epsilon_p = \frac{D/2}{p}\frac{dp}{dx}, \qquad \epsilon_T = \frac{D/2}{T}\frac{dT}{dx}, \tag{7.1}$$

where the terms ϵ_p and ϵ_T have to be

$$|\epsilon_P| \ll 1, \qquad |\epsilon_T| \ll 1. \tag{7.2}$$

Since the reduced pressure and temperature gradients are small the reduced flow rate G^* can be defined as

$$G^* = \frac{1}{\pi\,(D/2)^2\,p}\sqrt{\frac{2kT}{m}}\dot{M}, \tag{7.3}$$

and it can be decomposed in the following form

$$G^* = -\epsilon_p G_p(\delta) + \epsilon_T G_T(\delta), \tag{7.4}$$

where $\dot{M}$ is the mass flow rate.

Here the terms G_p and G_T are usually supposed to be independent from the gradients ϵ_p and ϵ_T: they only depend on the local rarefaction parameter δ.

G_p is the Poiseuille coefficient, while G_T is the thermal transpiration coefficient. They are introduced in order to be always positive.

In Graur & Sharipov [2009] the linearized S-model kinetic equation, which gives

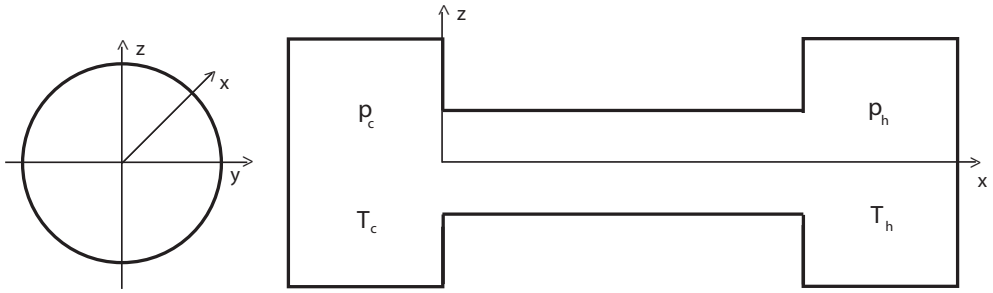

Figure 7.1: Scheme of the domain used in the Shakov numerical modeling. Tube cross section and tube longitudinal axis with the respective spatial coordinates.

results very close to those obtained by the linearized Boltzmann equation, but with lower computational efforts, has been solved by the discrete velocity method. Furthermore, the flow rates G_p and G_T were calculated. The flow rates G_p and G_T were calculated with a numerical error which is lower than 0.1% for a large range of the rarefaction parameter.

7.1.2 Arbitrary pressure and temperature drop

Since in practice the temperature or the pressure drops between the ends of a tube do not fulfill this condition, an extension of the theory is necessary.

When the tube length is significantly larger in respect to its diameter, the pressure and temperature gradients can be estimated as

$$\epsilon_p \sim \frac{D(p_h - p_c)}{2Lp_{av}}, \qquad \epsilon_T \sim \frac{D(T_h - T_c)}{2LT_{av}}, \tag{7.5}$$

and since $(D/2 \ll L)$ the ϵ_p and ϵ_T terms are small in comparison to unity. The average pressure and the average temperature are $p_{av} = (p_c + p_h)/2$ and $T_{av} = (T_c + T_h)/2$.

Therefore, by considering that the two ϵ terms are small, it is still possible to use the computed G_p and G_T values. Anyhow, it is necessary to take in consideration that in the case of a long channel with arbitrary temperature or pressure drop, the rarefaction parameter changes considerably along it. We can define a

rarefaction parameter that varies along the axis of the micro-tube and therefore depends on the axially directed coordinate

$$\delta(x) = \frac{p(x)D/2}{\mu(x)\sqrt{2RT(x)}}. \tag{7.6}$$

Usually the pressure or the temperature distribution along the tube is not known, thus, it is useful to introduce a reduced mass flow rate G that does not depend on the local rarefaction parameter $\delta(x)$

$$G = \frac{L}{\pi(D/2)^3 p_c}\sqrt{\frac{2kT_c}{m}}\dot{M}. \tag{7.7}$$

From the conservation of the mass along the channel, if the mass flow rate along the tube is stationary, every section of the tube is crossed by the same mass flow rate $\dot{M}$. Therefore it is possible to state that the reduce mass flow rate G^* can be associated to the thermodynamic parameters at the inlet of the tube in the following manner

$$G^* = G\frac{p_c}{p}\sqrt{\frac{T}{T_c}}\frac{D^2}{4L}. \tag{7.8}$$

From here, once the results of the flow rates G_p and G_T have been obtained it is possible to write the following differential equation which is computed by substituting eqs. (7.1), (7.3) and (7.8) in eq. (7.4) and that reads as

$$G\frac{p_c}{p}\sqrt{\frac{T}{T_c}}\frac{D/2}{L} = -\frac{1}{p}\frac{dp}{dx}G_P(\delta) + \frac{1}{T}\frac{dT}{dx}G_T(\delta), \tag{7.9}$$

where G^* has been substituted by the reduced mass flow rate G.

Therefore, when the temperature distribution is known and when the pressure boundary conditions in the two reservoirs are known, by applying an iterative method called the shooting method, it is possible to numerically obtain the pressure distribution along the tube and the reduced mass flow rate G.

Temperature driven mass flow rate

In the specific case of a mass flow rate driven only by a temperature difference applied in between the ends of a the tube, that is by imposing a pressure equality in between the two reservoirs ($p_c = p_h$), the flow will still create a pressure gradient along the tube. Therefore it is necessary to again use eq. (7.9) in order to obtain information about the thermodynamic parameters along the tube.

Pressure driven mass flow rate

In the specific case of a mass flow rate driven only by a pressure difference applied in between the ends of a the tube, that is by imposing a temperature equality in between the two reservoirs ($T_c = T_h$), the flow will not create a temperature gradient along the tube.

It is assumed that the heat capacity of the tube surface is essentially higher in respect of the one of the gas, therefore the temperature distribution of the gas along the channel is determined by the wall temperature distribution, which in this case is a constant value. Eq. (7.9) then becomes

$$G_{iso}\frac{p_c}{p}\frac{D/2}{L} = -\frac{1}{p}\frac{dp}{dx}G_P(\delta), \tag{7.10}$$

7.1.3 Zero-flow

In order to study the precise case of the zero-flow final equilibrium stage of the experiment, where the net mass flow rate in every cross section of the channel has to be zero $\dot{M} = 0$, equation (7.9) has to be reduced to

$$\frac{1}{p}\frac{dp}{dx}G_p(\delta) = \frac{1}{T}\frac{dT}{dx}G_T(\delta). \tag{7.11}$$

Equation (7.11) may be solved from the known temperature boundary conditions in both reservoirs and from the known pressure in the cold-side reservoir. The thermal molecular pressure ratio (TPR) p_c/p_h and the pressure distribution along the tube is found by solving this equation.

From here, the pressure in the hot-side reservoir, the thermal molecular pressure difference (TPD) and the thermal molecular pressure exponent (γ) can be

calculated.

7.2 Direct simulation Monte Carlo method

The experimental results were compared to the results obtained by using the numerical method introduced by Bird [1995]. The DSMC numerical code was used as originally given by Bird for an axially symmetric case. This is an open source code (dsmc2a.for) and it can be downloaded from Bird's website.

Nevertheless, in order to be able to model the thermal transpiration phenomenon and the specific experimental case studied, Bird's code had to be slightly modified. In order to be able to do this, we could not use the visual version given by the author, but we had to work with the code as it was originally written in FORTRAN.

7.2.1 Modifications introduced to the original version

Slight modifications to the original code were made in order to model the specific thermal transpiration problem studied. Therefore after the modifications introduced it was possible to:

1. Set as many horizontal or vertical walls as desired in the computational domain, in this way almost any geometry can be reproduced.

2. Set a temperature gradient along the walls, instead of just a constant temperature for each wall.

3. Initialize the domain with the desired thermodynamic parameters (density and temperature) in every cell of the domain, this leads at less computational time consumption if the nearby solution to the problem can be estimated.

4. Control at each boundary of the domain the flux of inlet modeled particles. In this way the thermodynamic parameters at the boundaries can be controlled and maintained stable.

7.2.2 Temperature driven mass flow rate

In order to recreate the conditions necessary to reproduce a thermal transpiration flow a numerical domain composed by a micro-tube and two reservoirs was used. The two reservoirs are maintained at equal pressure and at constant temperature. As in the experimental case, there is a cold-side reservoir and a hot-side reservoir (Figure 7.2).

Let us remind the reader that the code used was axial-symmetric and therefore the explanations refer to a two dimensional numerical domain $y - x$, where x is the coordinate that follows the axis of the micro-tube and y is the coordinate that follows the radius of the micro-tube. When we talk about an horizontal wall we are defining a cylindrical surface which extends in the axial direction, when we talk about a vertical wall we are defining a circular surface which is the reservoir boundary.

Conditions on the reservoirs

The boundaries of the reservoirs were set to be of two different kinds. We set two open boundaries at the top and at the side of the reservoirs, and one closed boundary at the inlet or outlet of the tube. We imposed to have a constant and equal pressure in both reservoirs.

In each reservoir a flow of model particles which have a zero bulk velocity was injected from the top and from the side. The injected model particles in each reservoir have the most probable velocity defined by the temperature of the reservoir.

In order to maintain the same pressure in the two reservoirs, the number of particles introduced in the hot-side reservoir at each time step balanced the pressure inequality introduced by the temperature difference in between the two reservoirs. Therefore, the number of injected model particles in the hot-side reservoir in respect to the number of injected model particles in the cold-side reservoir was imposed to satisfy the following identity

$$n_h = n_c \frac{T_c}{T_h}. \tag{7.12}$$

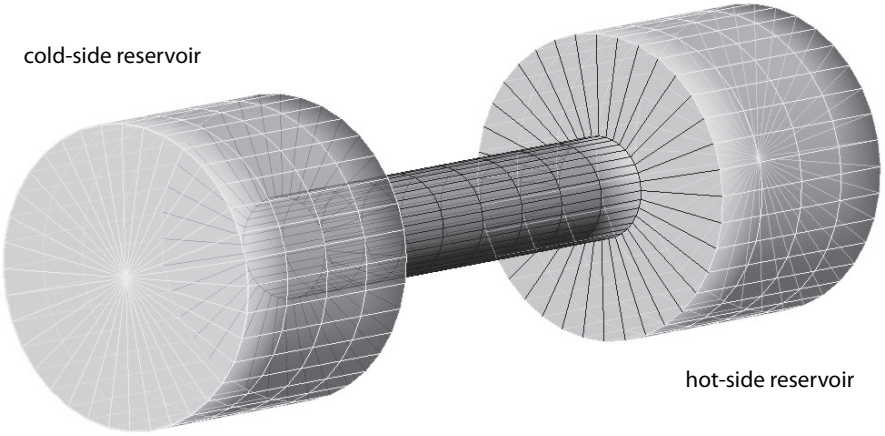

Figure 7.2: Scheme of the numerical domain used for the direct simulation Monte Carlo modeling for the temperature difference driven flow case. The micro-tube to which a temperature gradient is applied and the two reservoirs that are kept at constant temperature and equal pressure. The two reservoirs have open boundaries.

In the cold- and hot-side reservoirs two vertical walls were introduced at the inlet and outlet of the micro-tube, respectively. The cold-side vertical wall was set to have a constant temperature T_c and the hot-side vertical wall was set to have a constant temperature T_h.

Conditions on the micro-tube

Along the external surface of the micro-tube an exponential temperature distribution was imposed by using equation (4.1) and the respective fitting constants that correspond to the experimental case. The temperature limit values, if we consider the inlet of the tube to be the origin of the cartesian coordinates, at $x = 0$ and $x = L$, were $T(0) = T_c$ and $T(L) = T_h$.

Physical dimensions of the domain

The domain was chosen to be much smaller in respect to the experimental case. Instead of having a ratio of the length of the tube to the diameter of the tube of

approximately $L \sim 100D$, the ratio was chosen to be $L = 5D$. This choice was due to the fact that the computational efforts, in the case where the experimental dimensions were used, would have been excessively high. It is evident also that for this L to D ratio the end effects will have an impact on the flow structure.

The diameter of the micro-tube was $D = 0.2mm$ and the length of the tube was $L = 1mm$. The diameter of the reservoirs was set to be three folds, according to (Ewart *et al.* [2009]) the diameter of the micro-tube and their length was set to be one-half in respect to the length of the tube. No special study of the influence of the reservoirs dimensions on the flow was carried out.

Gas/surface interaction

The gas/surface interaction was set to correspond to a complete accommodation of model particles on the walls.

Cell structure

An uniform mesh was set along the x and y coordinates. The width, or the height of the cells were set in order to respect the already introduced condition $CD < \lambda/3$ (Section 2.3.3), therefore, for a fixed physical domain, their number changed as a function of the rarefaction of the gas studied. CD is the maximum quantity in between the width or the height of the cell.

Time step and convergency

The time step was set in order to satisfy the condition $DTM < CD/vmp$, where DTM is the time step and vmp is the most probable velocity (Section 2.3.3). The time step, for all the computational cases was set to be $10^{-8}[s]$.

For the presented case the number of time-steps was in the order of 10^8, but no special study on the number of iterations to reach convergence was realized.

Model particles

By using the experience of the DSMC simulation of slow flows by other authors (Ewart *et al.* [2009]), the number of model particles was set in order to satisfy the

condition on the number of model particles per cell, that is around 1000 model particles per cell. No special study of the influence of the number of particles per cell was carried out in this work.

Molecular model

The molecular model used was the variable hard-sphere (VHS) model.

7.2.3 Zero-flow

In order to recreate the conditions necessary to reproduce the zero-flow final equilibrium a numerical domain composed by a micro-tube and two reservoirs of the same characteristic dimension of the micro-tube was used. The two reservoirs are maintained at constant temperature. As in the experimental case, there is a cold-side reservoir and a hot-side reservoir (Figure 7.3).

As for the previous case of the thermal transpiration flow, the code used was axial-symmetric and therefore the explanations refer to a two dimensional numerical domain $y - x$ (see Section 7.2.2).

Conditions on the reservoirs

The cold-side reservoir was set to have one open boundary on its side, from where a flow of model particles having zero bulk velocity was injected at each time step, and an horizontal wall on its top. The model particles were introduced in this reservoir with a most probable velocity defined by the temperature of the reservoir. The cold-side vertical wall was set to have a constant temperature T_c and the hot-side vertical wall was set to have a constant temperature T_h.

The hot-side reservoir was set to have only closed boundaries, that means that the reservoir was a closed cylinder modeled by an horizontal wall on its top and by a vertical wall at the final end of the domain. Only one condition on the pressure was set and it was defined to be a constant pressure in the cold-side reservoir. The hot-side reservoir pressure and the pressure gradient along the micro-tube were the investigated parameters and therefore were left free to converge to the solution.

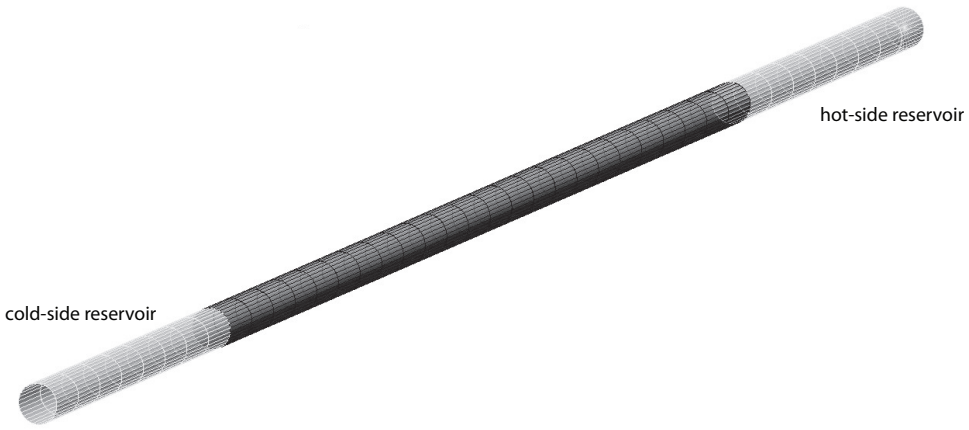

Figure 7.3: Scheme of the numerical domain used for the direct simulation Monte Carlo modeling for the zero-flow case. The micro-tube to which a temperature gradient is applied and the two reservoirs that are kept at constant temperature. The cold-side reservoir is an open boundary kept at constant temperature and pressure while the hot-side reservoir is a closed boundary kept at constant temperature.

Physical dimensions of the domain

The domain was chosen to be smaller in respect to the experimental case. Instead of having a ratio of the length of the tube to the diameter of the tube of approximately $L \sim 100D$, the ratio was chosen to be $L = 30D$. This choice was due to the fact that the computational efforts, in the case where the experimental dimensions were used, would have been excessively high.

The diameter of the micro-tube was $D = 0.5mm$ and the length of the tube was $L = 15mm$. The diameter of the reservoirs was set to be equal to the diameter of the micro-tube and their length was set to be one-third in respect to the length of the tube.

This was done since from the thermal transpiration theory and experimental results it was possible to deduce that the final pressure difference in between the inlet and outlet of the tube, or the pressure distribution along the tube, created by a temperature distribution applied, was independent from the dimensions of

the reservoirs. By choosing this way of modeling it is possible to greatly decrease the computational efforts.

Other conditions

It is possible to refer to Section 7.2.2 for what concerns the conditions on the micro-tube, the gas/surface interaction, the cell structure, the time-step and the model particles.

7.3 Results and comparisons

Let us now introduce the results obtained with the S-model and the DSMC method approaches. The following section is organized in two parts, the zero-flow final equilibrium results and the stationary thermal transpiration results. We compared in each of this parts the S-model, the DSMC and the experimental results.

The first part and the second part of this section are organized in the same way, that is by presenting and comparing initially the results obtained with the S-model and the DSMC method of the thermodynamic parameters and of the averaged velocity along the tube and by afterwards comparing the S-model and DSMC results with the experimental results obtained at the inlet and outlet of the tube.

7.3.1 Zero-flow

Lets now comment on the results found on what concerns the stationary zero-flow. The thermal transpiration pumping effect is engendered by subjecting a temperature distribution along the micro-tube. The gas macroscopically moves from the cold- to the hot-side. This movement engenders a pressure difference in between the inlet and outlet of the tube.

We were not able to numerically process the experimental geometry by the DSMC method. The length of the numerically computed micro-tube is $15mm$ against the length of $52.7mm$ of the micro-tube used in the experimental campaign.

Nevertheless, it was still possible to compare the DSMC results in the cold-side and hot-side reservoirs with the experimental results since, for the zero-flow case,

the geometry of the tube does not alter the cold- and hot-side reservoir pressure results. However, the S-model results were computed by considering the right length of the experimental micro-tube.

7.3.1.1 Along the tube

From Figure 7.4 it is possible to observe the distribution of temperature, pressure and density along the axial coordinate of the micro-tube, in the case of a zero net mass flow rate across each section of the tube. As previously said, the temperature distribution was chosen to be exponential, as in the experimental case [Section 4.2.2 eq. (4.1)]. This was the only parameter imposed and therefore the only driver of the variation of pressure and consequently the variation of density along the axis of the micro-tube.

As shown in the middle graph of Figure 7.4, the pressure monotonically increases from the cold- to the hot-side of the tube following the exponential tendency of the temperature distribution. The pressure starts from a constant value in the cold-side reservoir and reaches a higher pressure which is constant in the hot-side reservoir. On the contrary, the density monotonically decreases from the cold- to the hot-side of the tube.

It is possible to notice that both the S-model and the DSMC results are in perfect agreement. The stationarity of the zero-flow final equilibrium can be readily seen in the DSMC results by the equality of the thermodynamic parameters in each transversal cell of the tube, in other words, for a fixed axial coordinate the thermodynamic parameter are equal and in equilibrium in each cell of the section. The chosen example case was argon for a temperature difference of $\Delta T = 71K$ at a rarefaction of $\delta_T = 0.03$.

From Figure 7.5, it is possible to see that the bulk velocity is zero at each cell of the tube in within the statistical scatter of the results. Therefore, it is clear that the net mass flow rate across each section of the tube is zero, which validates the assumptions made previously in the experimental methodology section for the case of the zero-flow final equilibrium stage. We are showing the DSMC results for the bulk velocity since for the S-model case the mass flow rate was imposed to be zero in order to solve eq. (7.11).

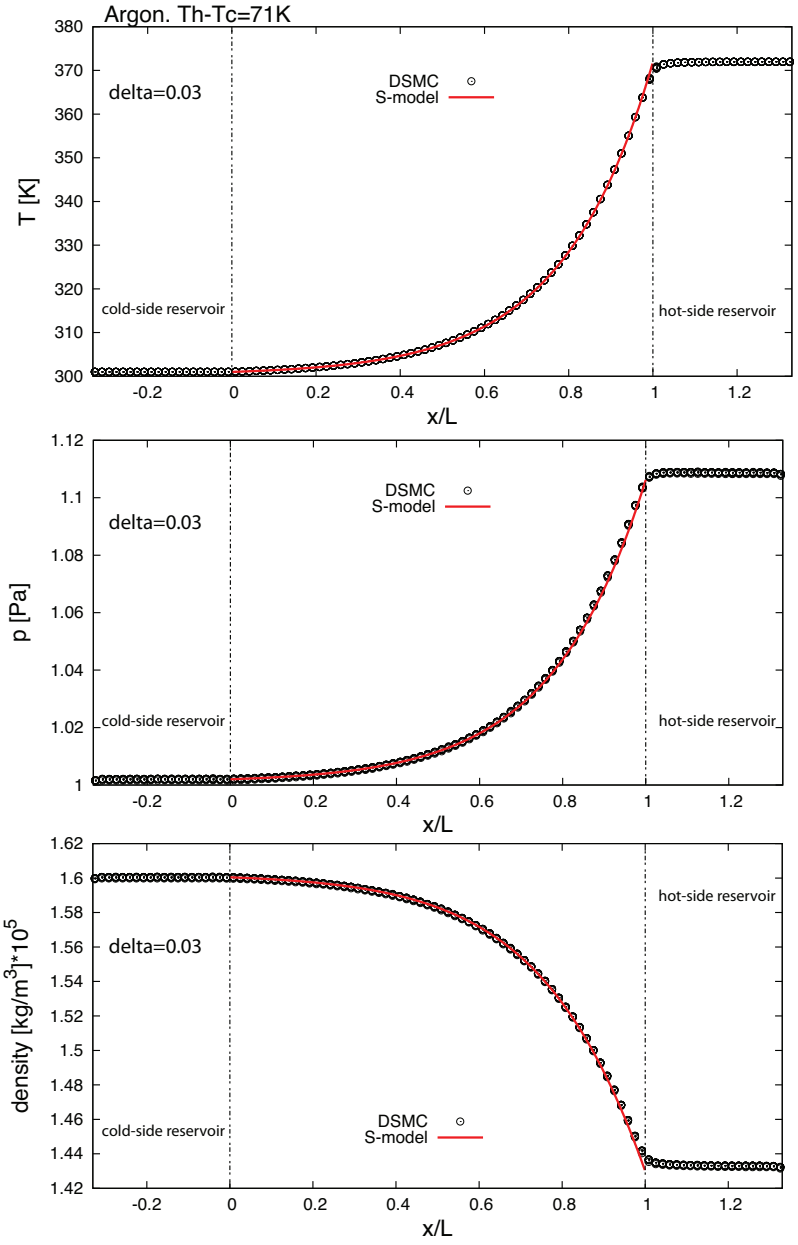

Figure 7.4: Thermodynamic parameters along the axial direction of the micro-tube for argon in the zero-flow case at $\Delta T = 71K$ for rarefaction $\delta_T = 0.03$. Red full line [——]: S-model; black circles [○]: DSMC method. Top: temperature distribution. Middle: pressure distribution. Bottom: density distribution.

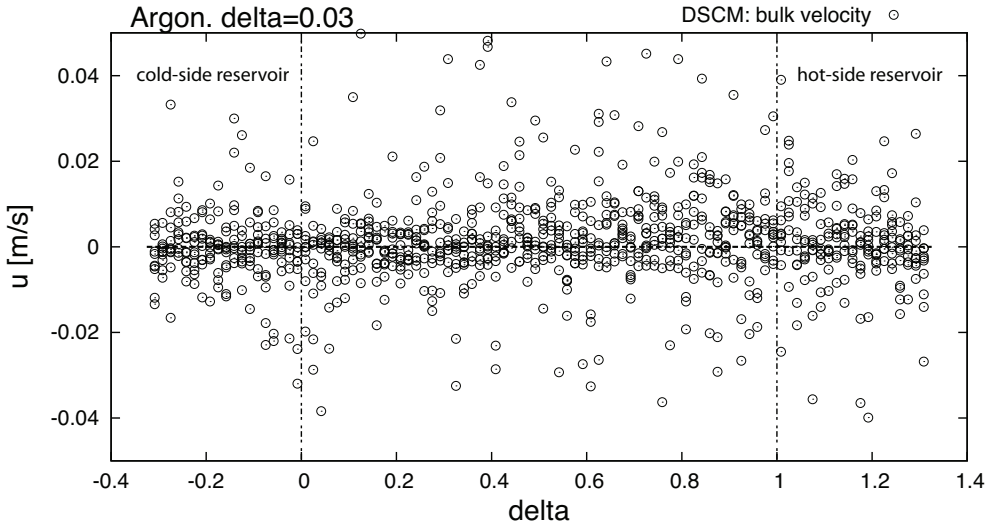

Figure 7.5: The bulk velocity along the axial axis of the tube. Black circles [○]: DSMC method.

7.3.1.2 Thermal molecular pressure ratio

Let us now compare the experimental results to the numerical results obtained at the inlet and outlet of the tube at the zero-flow stage. From Figure 7.6 and Figure 7.7 it is possible to see how the numerical results of the thermal molecular ratio (TPR) for the DSMC method and the S-model method are in good agreement with the experimental results. We have modeled the case of argon and nitrogen at $\Delta T = 71K$ and $\Delta T = 53.5K$.

In the case of argon (Figure 7.6), the S-model results and the experimental results are in perfect agreement in within the experimental uncertainty. The only divergence is to be found at gas near free molecular regime where we are very close to the measurement resolution limit.

Nevertheless, this difference between experimental and numerical results could be induced by the gas surface interaction, which effects become preponderant for very small rarefaction parameter values. The S-model results here shown have been computed with an accommodation coefficient equal to unity.

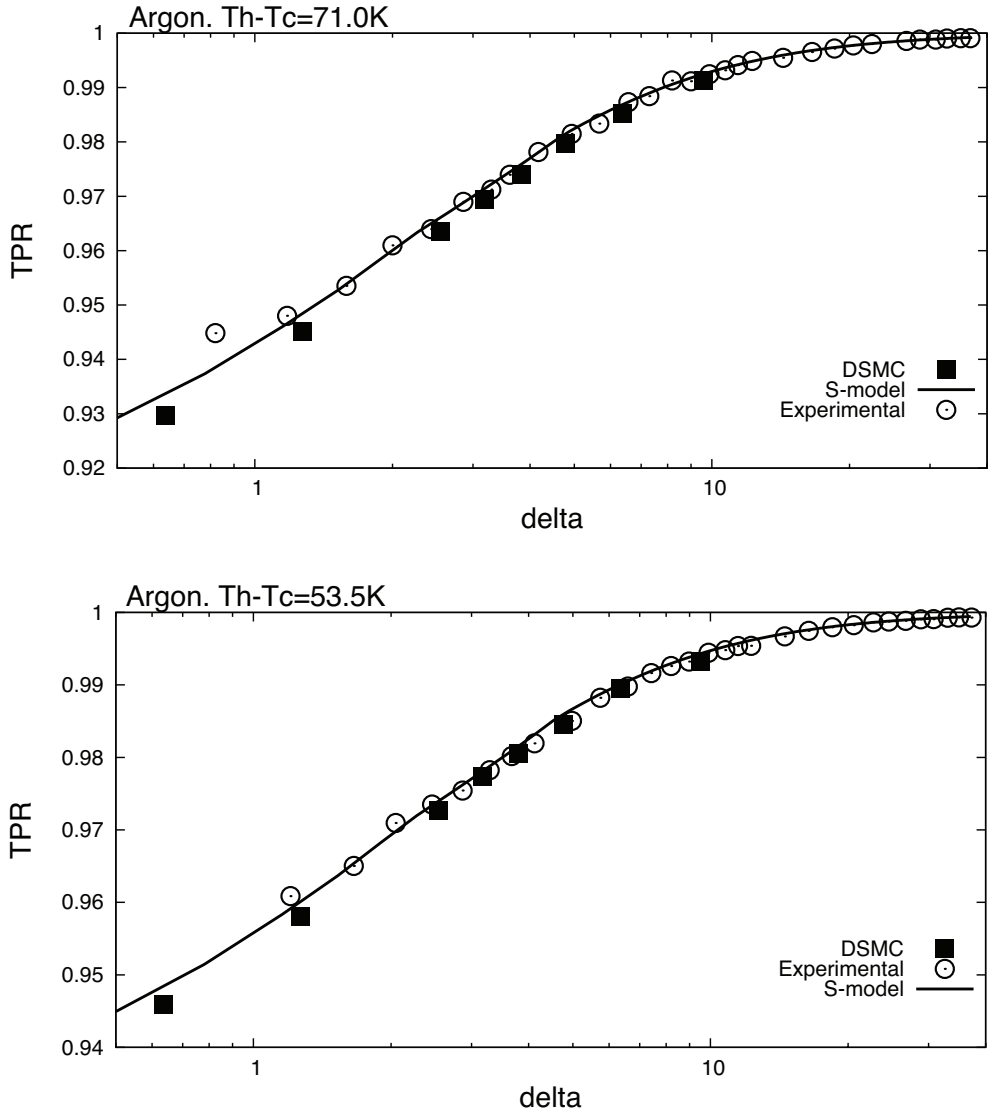

Figure 7.6: Thermal molecular pressure ratio TPR for the case of argon. Black empty circles [○]: experimental results. Black filled squares [■]: DSMC ($\alpha = 1$). Black full line [——]: S-model ($\alpha = 1$). Top: $T_h - T_c = 71K$. Bottom: $T_h - T_c = 53.5K$

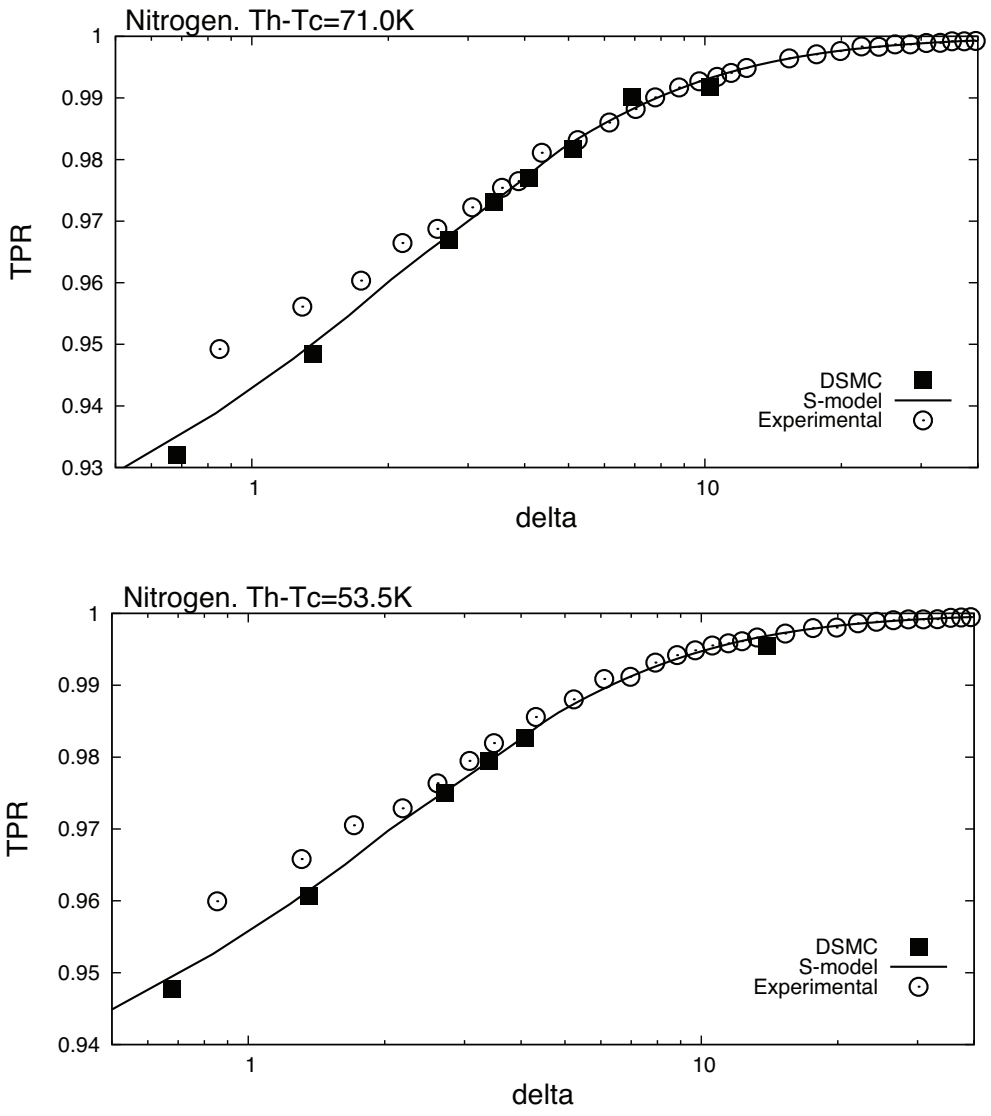

Figure 7.7: Thermal molecular pressure ratio TPR for the case of nitrogen. Black empty circles [○]: experimental results. Black filled squares [■]: DSMC ($\alpha = 1$). Black full line [——]: S-model ($\alpha = 1$). Top: $T_h - T_c = 71K$. Bottom: $T_h - T_c = 53.5K$

On the other hand, the DSMC results slightly overestimate the intensity of the pumping effects of thermal transpiration. The divergence between DSMC and S-model results could be due to the molecular model used, which in the S-model case was the hard sphere (HS) model and in the DSMC method case was the variable hard sphere (VHS) model. Let us remind the reader that as in the S-model case, the DSMC results have been obtained by imposing a complete diffuse reflection at the wall, and therefore by imposing an accommodation coefficient equal to unity.

We decided to study the nitrogen case instead of the helium case since DSMC offers the possibility to model a polyatomic gas by taking into account the different degrees of freedom of the diatomic molecule. In the case of a diatomic molecule the degrees of freedom are six: 3 degrees of freedom induced by the translational motion, 2 degrees of freedom induced by two rotational degrees of motion and 1 degree of freedom induced by the vibrational mode of the molecule.

In the DSMC model we take into account 5 degrees of freedom, since we do not consider the vibrational mode of the molecule. Therefore, we desired to see if there was any difference from the S-model case where we could not introduce the rotational degrees of freedom. In the S-model case we had to model nitrogen as a monoatomic gas.

As it can be seen from Figure 7.7, the S-model and the DSMC results match fairly well. The differences introduced by the two models do not change significantly the TPR results. On the other hand, the experimental results do not match as well as in the case of argon the numerical results in advanced transitional regime and near free molecular regime conditions. Again, this divergence could be induced by the gas/surface interaction.

7.3.1.3 Thermal molecular pressure difference

As we saw in the literature comparison section (Section 6.1.4), the comparison of the results of the thermal pressure ratio results with the semi-empirical formulas could give rise to an erroneous lecture on the amount of the divergence between the formula and the experimental results.

In the comparison with the Takaishi & Sensui [1963] and Liang [1951] semi-

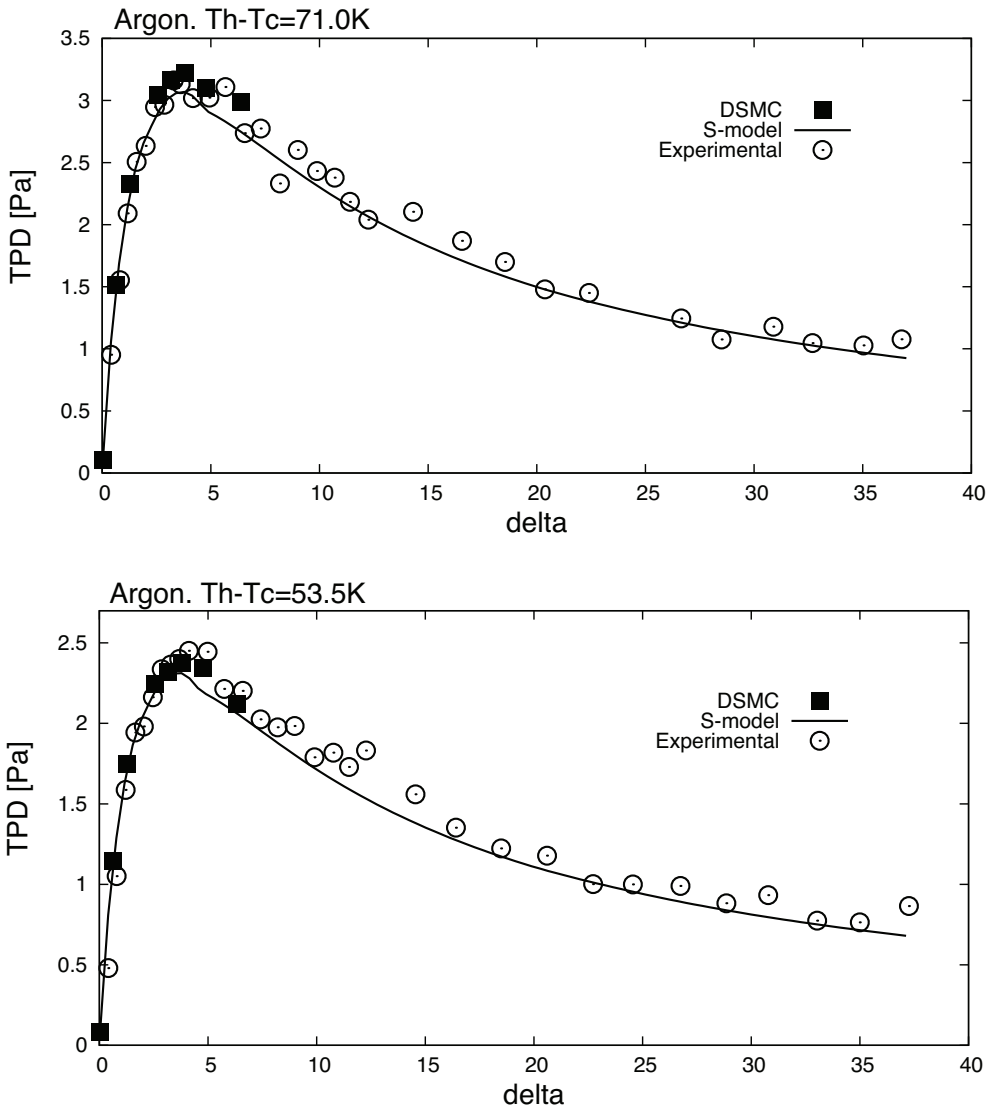

Figure 7.8: Thermal molecular pressure difference TPD for the case of argon. Black empty circles [○]: experimental results. Black filled squares [■]: DSMC ($\alpha = 1$). Black full line [——]: S-model ($\alpha = 1$). Top: $T_h - T_c = 71K$. Bottom: $T_h - T_c = 53.5K$

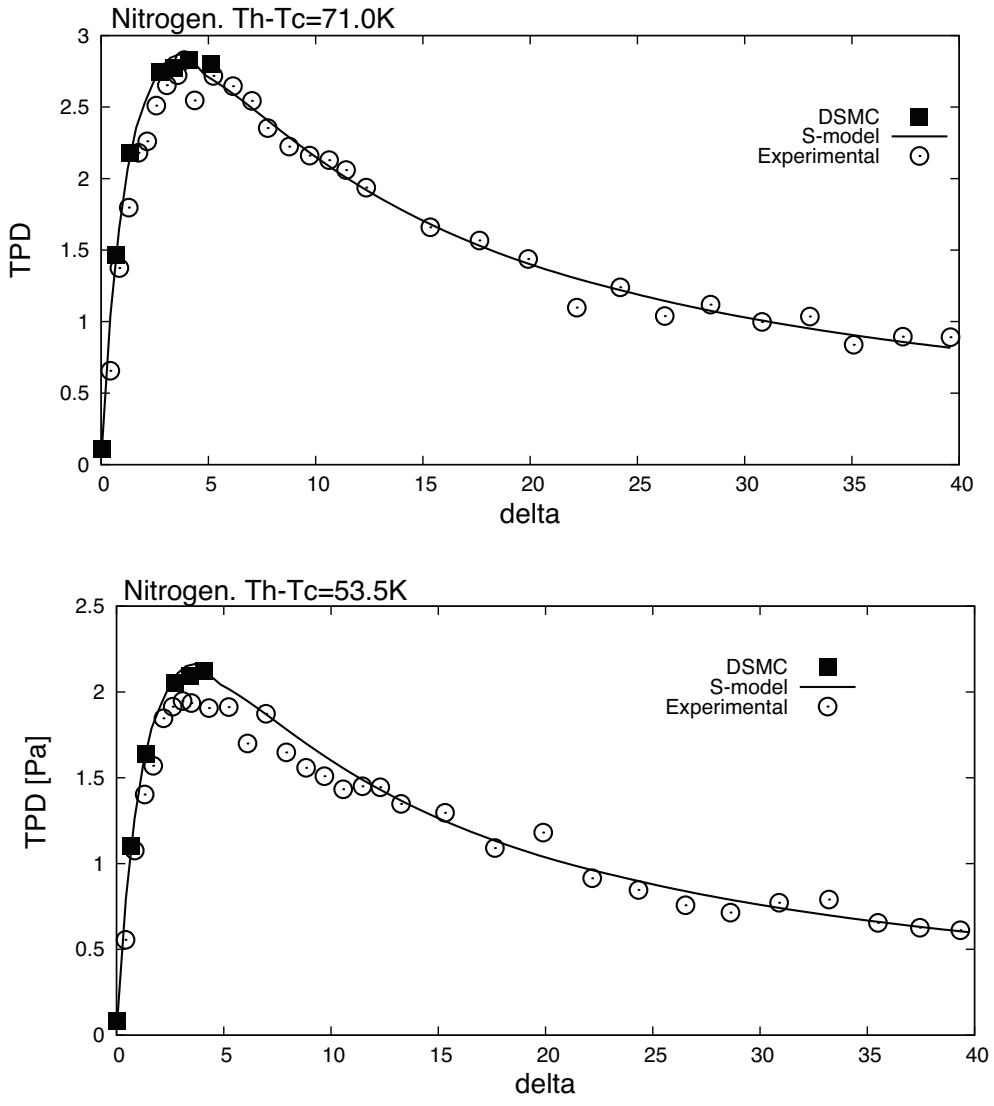

Figure 7.9: Thermal molecular pressure difference TPD for the case of nitrogen. Black empty circles [○]: experimental results. Black filled squares [■]: DSMC ($\alpha = 1$). Black full line [——]: S-model ($\alpha = 1$). Top: $T_h - T_c = 71K$. Bottom: $T_h - T_c = 53.5K$

empirical formulas, a not attentive observer could have the impression of a perfect match where the real absolute pressure measurement could be quite different in respect to the absolute pressure values related by the semi-empirical formulas. Therefore we give the comparison also for the thermal molecular pressure difference (TPD).

In Figures 7.8 and 7.9 we wanted to rise again this kind of question by showing the values of the thermal molecular pressure difference for the case of argon and nitrogen and therefore check if effectively the numerical solution matches the experimental results.

It is possible to see that both the S-model and the DSMC results are in good agreement with the experimental results of the TPD for the whole range of the studied rarefaction parameter. Possibly there is a slight better agreement for the DSMC method in respect to the experiments, specially for argon, where the experimental values that are slightly higher in respect to the S-model values for transitional regime, namely at the maximum of the curve ($\delta_T = 3.5$).

For what concerns nitrogen, the DSMC, the S-model and the experimental results practically coincide along the whole spectrum of the studied rarefaction. Anyhow, it is possible to see a slight divergence at the maximum of the curve ($\delta_T = 3.5$) where the experimental results values are slightly lower in respect to the numerical values.

7.3.1.4 Thermal molecular pressure exponent

Finally we wanted to conclude the section on the zero-flow final equilibrium stage by showing the influence of the gas/surface interaction on the thermal molecular pressure exponent. This parameter varies consistently when tending to free molecular regime if different accommodations at the surface of the micro-tube are considered.

We would like to remind the reader that this is due mainly to the fact that in free molecular regime the number of gas/surface collisions are preponderant in respect to the intermolecular collisions. Therefore, it is possible to extract information on how the molecular weight and the molecular dimensions of different

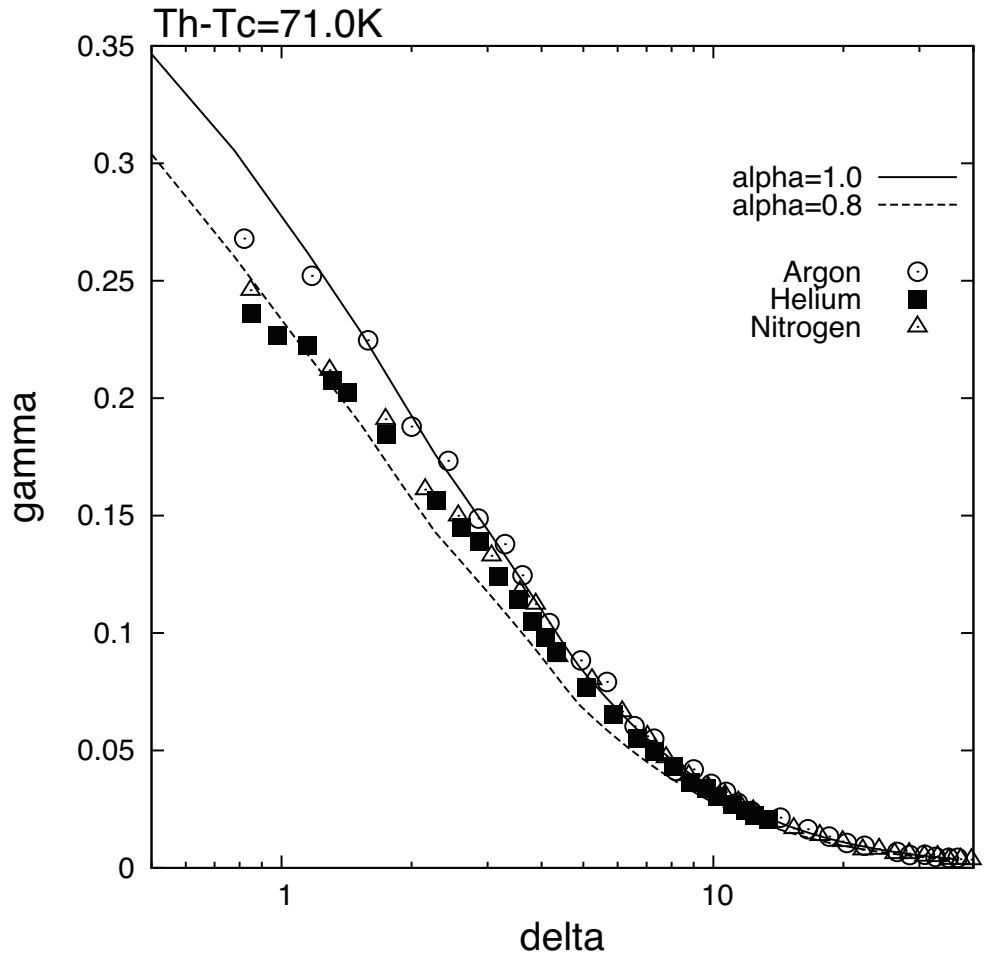

Figure 7.10: Thermal molecular pressure exponent γ for the case of $\Delta T = 71K$. Comparison between experimental results and S-model. Experimental results: black empty circles [○], argon; black filled squares [■], helium; black empty triangles [△]: nitrogen. S-model: black full line [——], $\alpha = 1$; black dashed line [- - -], $\alpha = 0.8$.

gases affect the gas/surface interaction.

This analysis was made by confronting the experimental results to the results obtained with the S-model. The numerical curves were obtained by changing the accommodation coefficient α. In addition we would like to underline that the S-model results show that γ does not depend on the gas nature but only on the

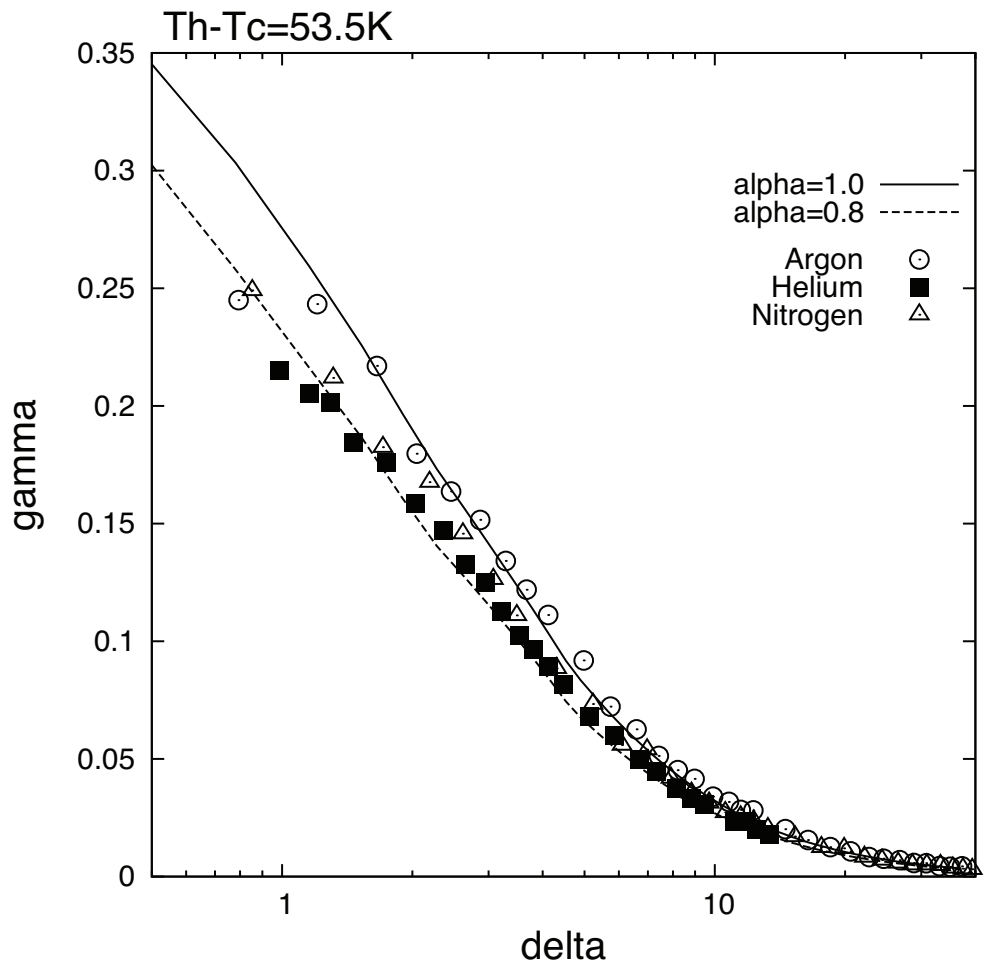

Figure 7.11: Thermal molecular pressure exponent γ for the case of $\Delta T = 53.5K$. Comparison between experimental results and S-model. Experimental results: black empty circles [○], argon; black filled squares [■], helium; black empty triangles [△]: nitrogen. S-model: black full line [——], $\alpha = 1$; black dashed line [- - -], $\alpha = 0.8$.

accommodation coefficient. The kernel model that was used in the S-model linear solution, in order to extract the different values of the thermal molecular pressure exponent γ as a function of the accommodation coefficient, was the diffuse specular kernel developed by Maxwell.

Let us remind the reader that in Section 6.1.3 we saw that the thermal molec-

ular pressure exponent did not vary for a single gas for whatever temperature difference applied at a fixed rarefaction. We could observe that this measured quantity varied only as a function of the gas used.

Then, from Figures 7.10 and 7.11 we can see that this tendency could be explained by a different interaction of the molecules against the walls of the micro-tube, which for the whole experimental campaign was the same.

The tendency is clear, argon seems to be completely accommodated to the walls, while, in order, nitrogen and helium are less accommodated. That means that for lighter gases, the reflection would be in some percentage also of a specular nature. The tendency is respected for two temperature differences applied to the tube.

It is necessary to add a remark: it could appear that the present results are in contradiction with the comments given in Section 6.3.2 about the accommodation process. But the reader must keep in mind that in the Maxwellian kernel a single constant α appears. Thus, depending on the context and on the parameter under consideration α can be interpreted in different manners: as a tangential momentum accommodation coefficient, an energy accommodation coefficient or an accommodation coefficient that considers both. As it is well known the respective values are different for each gas.

7.3.2 Thermal transpiration flow

Lets now comment on the results found on what concerns the stationary thermal transpiration flow. The thermal transpiration flow is engendered by subjecting a temperature distribution along the micro-tube. The reservoirs are left at equal and constant pressure, there is therefore no difference of pressure between the two ends of the micro-tube. The gas macroscopically moves from the cold- to the hot-side.

We were not able to numerically process the experimental geometry by the DSMC method. Contrarily in respect to the zero-flow final equilibrium, we could not compare directly the results obtained with DSMC with the experiments. On the one hand, for the zero-flow case, the geometry of the tube does not alter the cold- and hot-side reservoir pressure results, on the other hand, for the case of the thermal

transpiration mass flow rate, the geometry of the tube is essential in order to be able to compare numerical and experimental results.

It is still true that it could be possible to compare mass flow rate results obtained with different geometries by considering a reduced mass flow rate, that is a non-dimensional mass flow rate, but the DSMC method cases that have converged to its final result, at the present moment do not match the region of rarefaction which was experimentally investigated. The DSMC computations are extremely heavy and time-consuming in the case of slow flows crossing a numerical domain with relatively large dimensions.

Nevertheless, we think that these results could offer a good insight in what concerns the distribution of the thermodynamic parameters and bulk velocity along the tube for the thermal transpiration flow case and therefore we are still offering them.

Finally, the thermal transpiration mass flow rate experimental results were compared with the S-model results, which is a model that is more suitable for the geometry of the experimental micro-tube used. However in order to compare the S-model results with the DSMC results, we carried out numerical simulations with the same tube length and tube diameter dimensions ($D = 0.2mm$ and $L = 1mm$). In this case $D/L = 0.2$ and $\Delta T/L = 0.21$. Hence we are in the limits of the applicability of the linearization of the S-model [eq. (7.1)]. In addition to the used L/D ratio the end effects can influence the flow structure.

7.3.2.1 Along the tube

The temperature distribution imposed along the tube was exponential as in the experimental case. There is a flow along the micro-tube, from the cold- to the hot-side and this gas displacement engenders a pressure gradient along the micro-tube (Figure 7.12). The pressure distribution has a sort of parabolic form which is asymmetric in respect of the middle of the capillary. The parabolic curve has a concave behavior and has a minimum on the hotter side region of the tube.

The concave parabola traced by the pressure distribution long the tube was a result which diverged from the results found by Graur & Sharipov [2009]. The

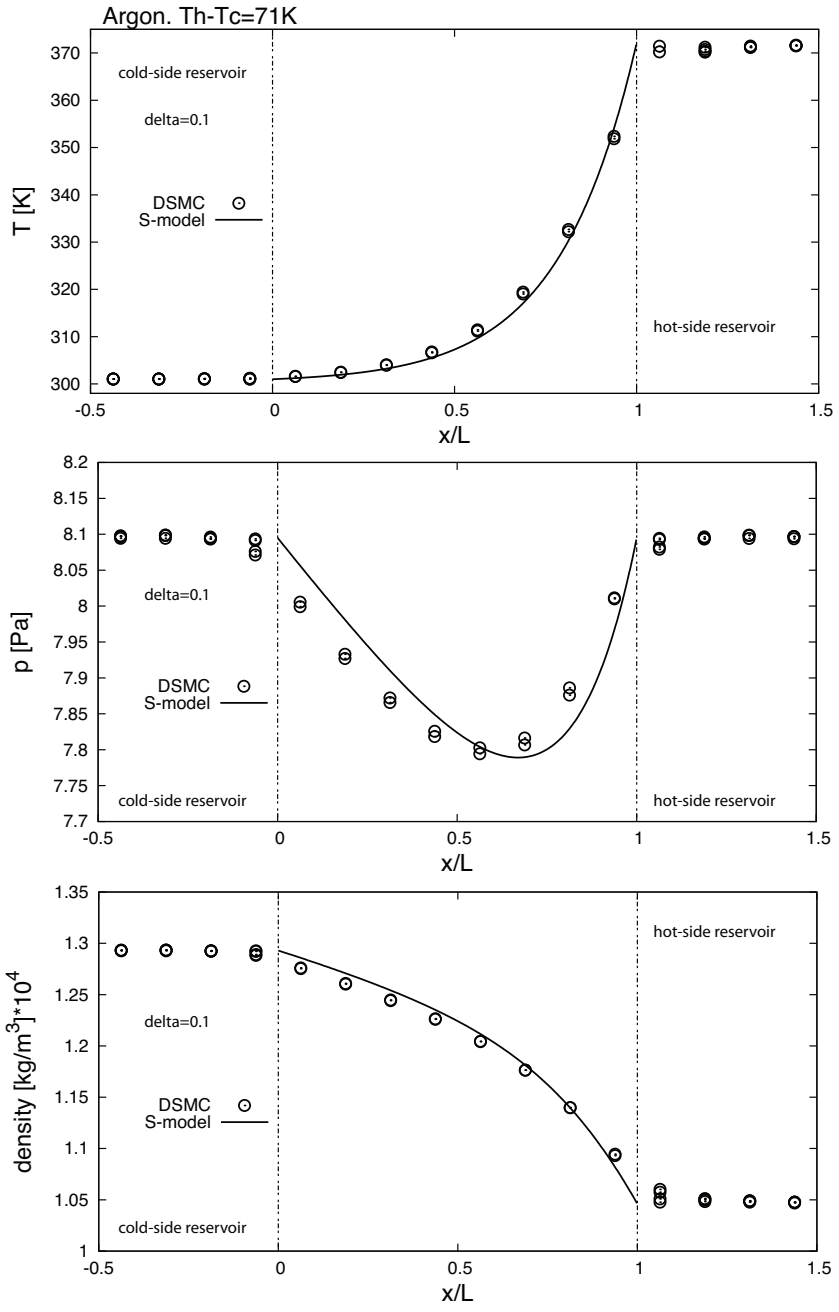

Figure 7.12: Thermodynamic parameters along the axial direction of the micro-tube for argon at $\Delta T = 71K$ for rarefaction $\delta_T = 0.1$. Black full line [——]: S-model; black circles [○]: DSMC method. Top: temperature distribution. Middle: pressure distribution. Bottom: density distribution.

authors found a convex parabolic shape of the pressure along the tube, but the temperature they imposed along the tube was linearly increasing. Therefore it is possible to imagine that the shape of the pressure distribution along the channel can severely change as a function of the imposed temperature distribution.

As in the zero-flow case, the density distribution along the tube is monotonically decreasing.

As it can be seen in Figure 7.12, for rarefaction conditions of $\delta = 0.1$ the S-model and DSMC method results match well for the case of the density and they have a good agreement for the pressure distribution. The S-model results are slightly more asymmetric in respect to the DSMC results.

We compared the S-model and the DSMC results for a second case of rarefaction, that is $\delta = 1$ (Figure 7.13). Unfortunately, the time of convergence required was quite expensive and therefore, at the present moment, the results of the DSMC method are not yet sufficiently sampled.

Nevertheless the results give a good agreement with the S-model results and they show the tendency of the pressure gradient magnitude as a function of the rarefaction. It can be noticed that the results of the pressure distribution along the tube match better for lower rarefaction parameter values, where the DSMC results have converged better to its final solution.

Let us now comment on the results of the average velocity in a section along the tube (Figure 7.14). The DSMC velocity results are offered as an average of the velocity along the section of the tube. The S-model velocity results were obtained from the mass flow rate and the information of the pressure and temperature distribution along the tube.

The results of the S-model again match the results of the DSMC method. It is possible to identify the positive velocity of the gas across all the sections of the tube. In other words, there is a clear macroscopic gas displacement from the cold- to the hot-side of the tube.

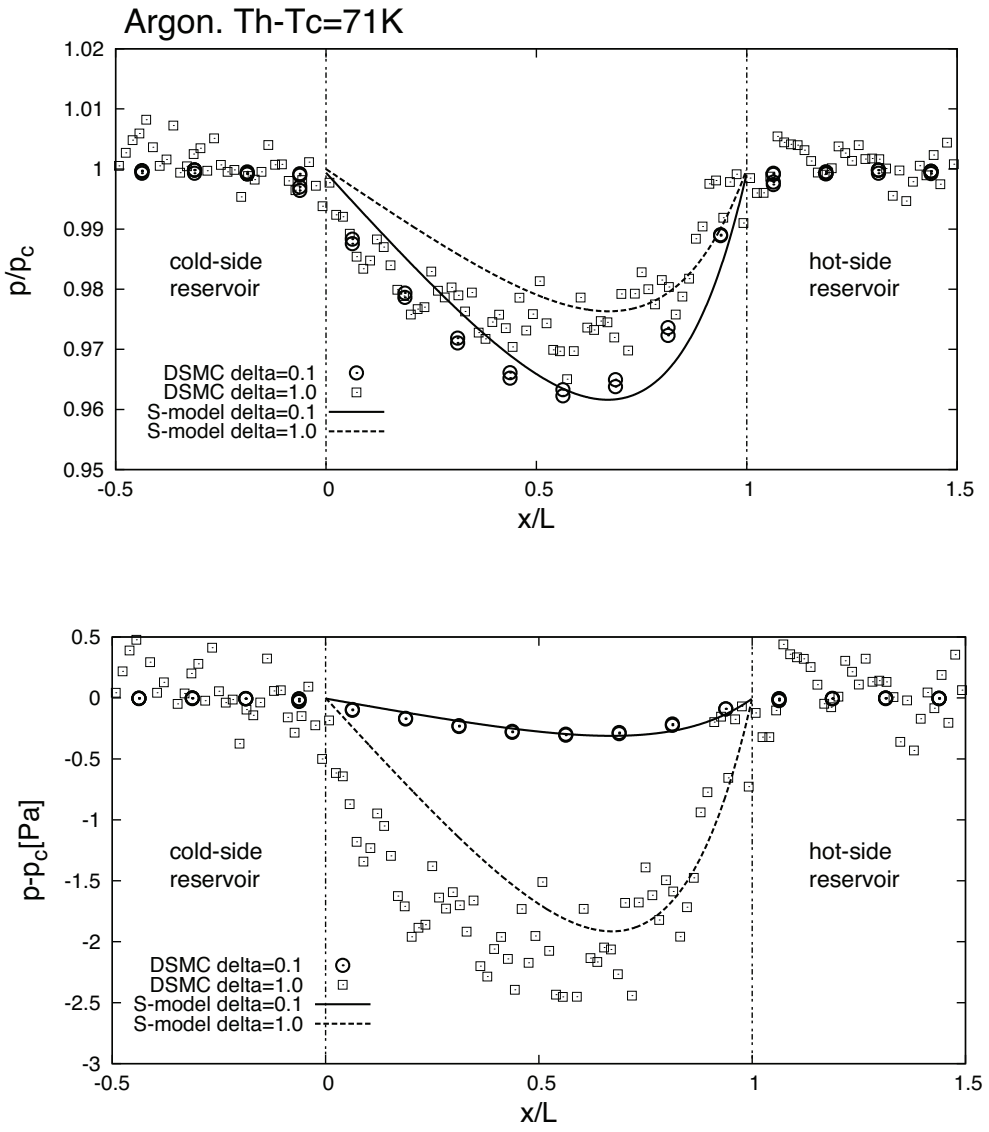

Figure 7.13: Pressure distribution along the axial direction of the tube for argon at $\Delta T = 71K$. Comparison between two rarefaction values. DSMC: black empty circles [○], $\delta_T = 0.1$; black empty squares [□], δ_T=1. S-model: black full line [——], $\delta_T = 0.1$; black dashed line [- - -], $\delta_T = 1$. Top: ratio between pressure and pressure in the cold-side reservoir. Bottom: difference between pressure and pressure in the cold-side reservoir.

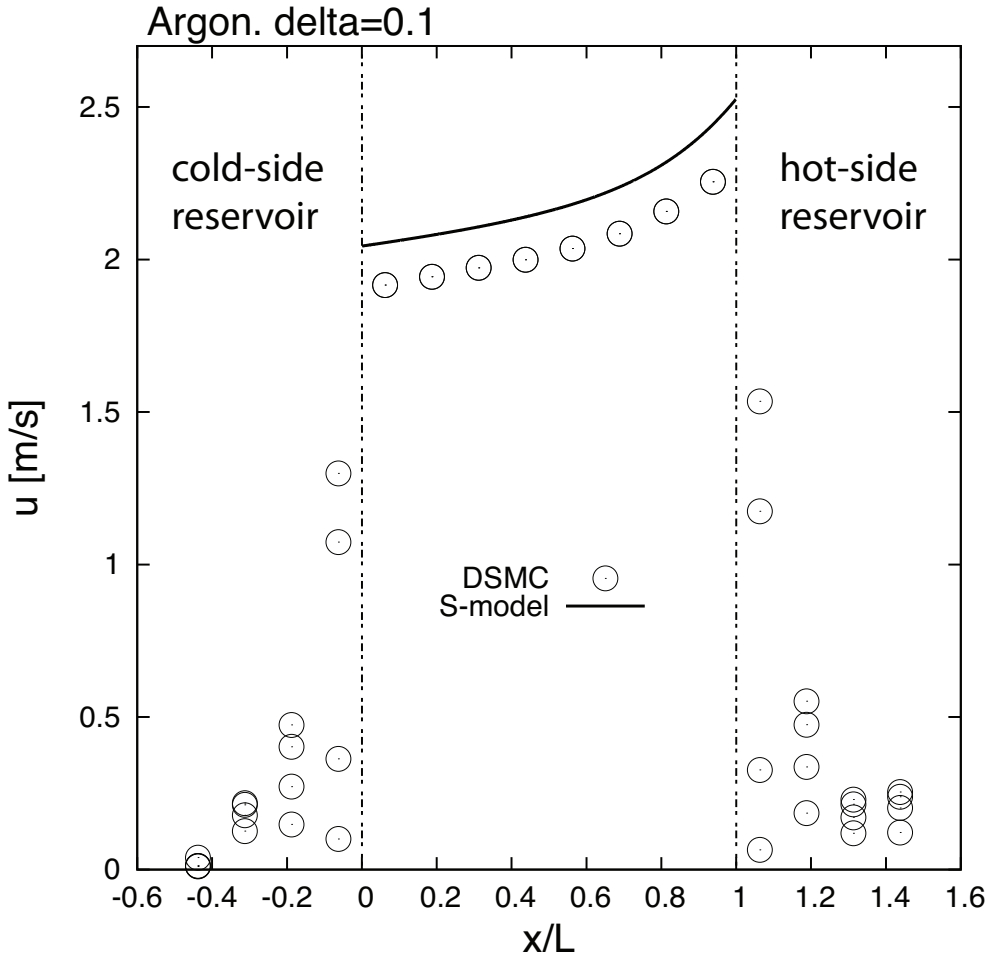

Figure 7.14: Average velocity at each section of the tube for argon at $\Delta T = 71K$ in the case of $\delta_T = 0.1$. Black empty circles [○]: DSMC. Black full line [——]: S-model.

There is a slight discrepancy, the S-model gives higher results, but the tendency is respected by both the numerical approaches and an acceleration of the fluid is to be found going from the inlet section to the outlet section of the tube. In the two reservoirs, the gas bulk velocity tends quickly to zero.

7.3.2.2 Stationary mass flow rate

The last parameter that is presented is the stationary thermal transpiration mass flow rate. The experimental results are compared to the S-model results which were

obtained for the same spectrum of rarefaction that was considered experimentally and for the real dimensions of the tube ($D = 0.485mm$ and $L = 52.7mm$). In this case the $L/D \sim 100$ ratio well respects eq. (7.1) and therefore we can neglect the end effects of the tube.

Lets make an initial remark for what concerns the comparison of the experimental thermal transpiration mass flow rate with the model. The parameters that have to be injected in the numerical model, such as the diameter, the length of the tube and the temperature difference in between both ends of the micro-tube were never explicitly used in order to deduce experimentally the mass-flow rate. The global uncertainty of these parameters (L, D^3, T_c) can be estimated to be in the order of 4%. Lets remind the reader that the parameters used in order to deduce the thermal transpiration mass flow rate were the dimension of one reservoir, the temperature in one reservoir and the pressure variation speed. Therefore, we have to consider that the parameters injected in the numerical model introduce a new source of uncertainty when comparing the experimental results to the numerical results. The uncertainty estimated for the experimental mass flow rate was in the order of 8%, hence, when comparing the experimental results with the model, the uncertainty has to be considered higher.

As it can be seen from Figures 7.15-7.17, the numerical results match the experimental results. Better results can be found for the heavier gases, while the results for the lighter gas, that is helium are slightly different: the experimental thermal transpiration mass flow rates for helium are lower in respect to the ones given by the S-model.

There are some considerations that can be made on these results. The first one is in respect to the fluctuations of the experimental points found for the heavier gases. This is specially due to the fact that the intensity of the pressure variation with time for a heavier gas is much lower in respect to the intensity of the pressure variation with time of a lighter gas (Section 6.3.2). Therefore, the pressure measurement has a better quality in the second case, since the resolution limit of the instrument does not disturb the measurement. In other words, the higher the magnitude of the final pressure difference (TPD) is, the better the pressure measurements are.

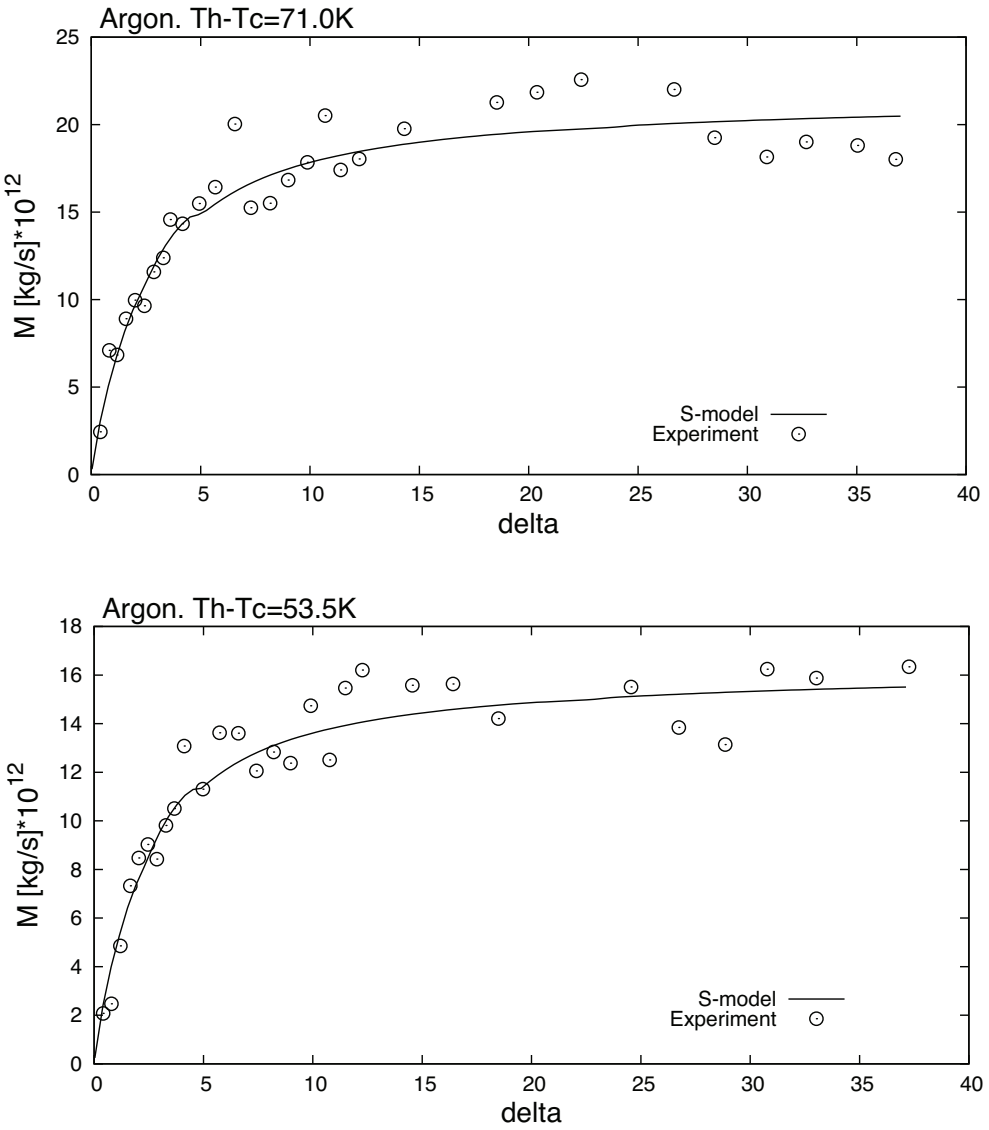

Figure 7.15: Thermal transpiration mass flow rate for argon. Black empty circles [○]: experimental results. Black full line [——]: S-model. Top: $\Delta T = 71K$. Bottom: $\Delta T = 53.5K$.

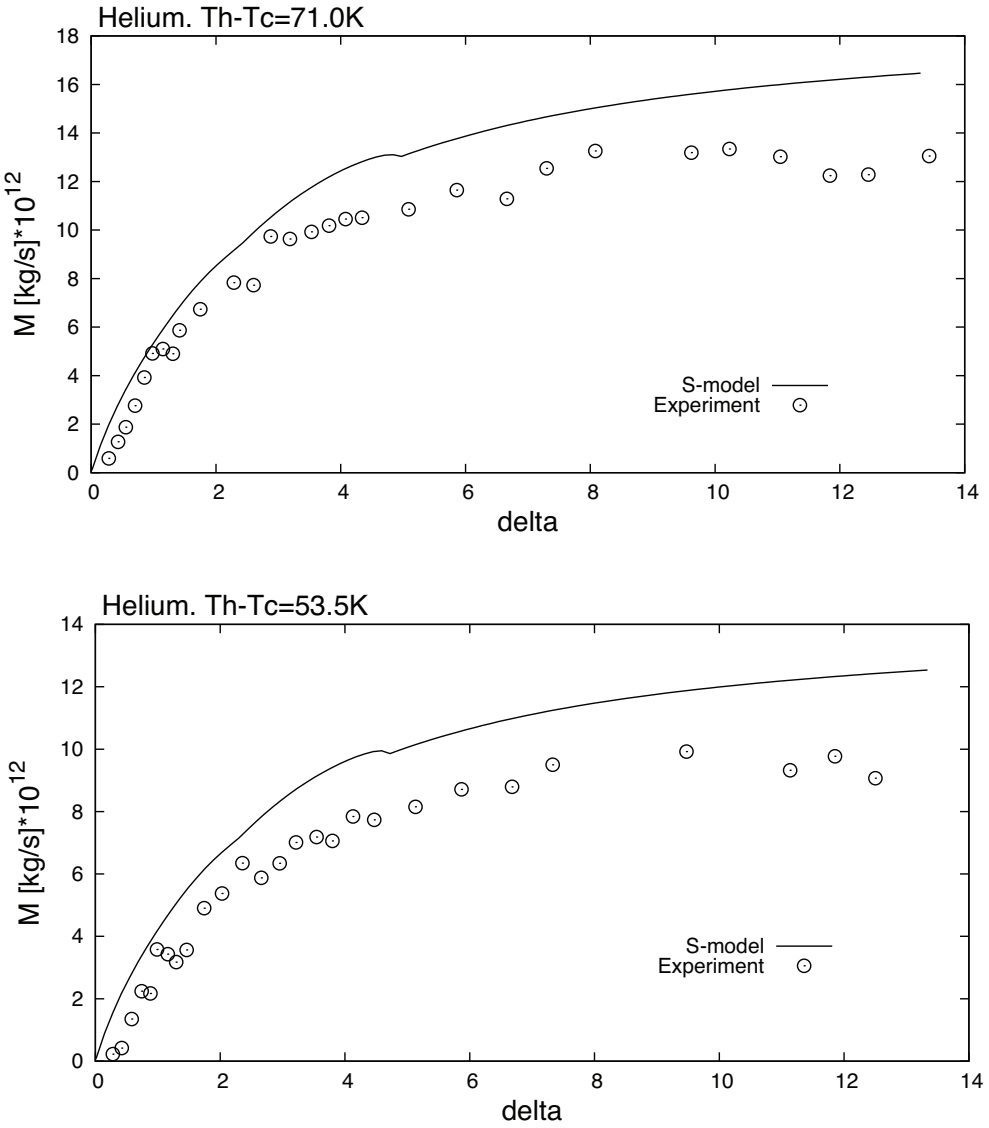

Figure 7.16: Thermal transpiration mass flow rate for helium. Black empty circles [○]: experimental results. Black full line [——]: S-model. Top: $\Delta T = 71K$. Bottom: $\Delta T = 53.5K$.

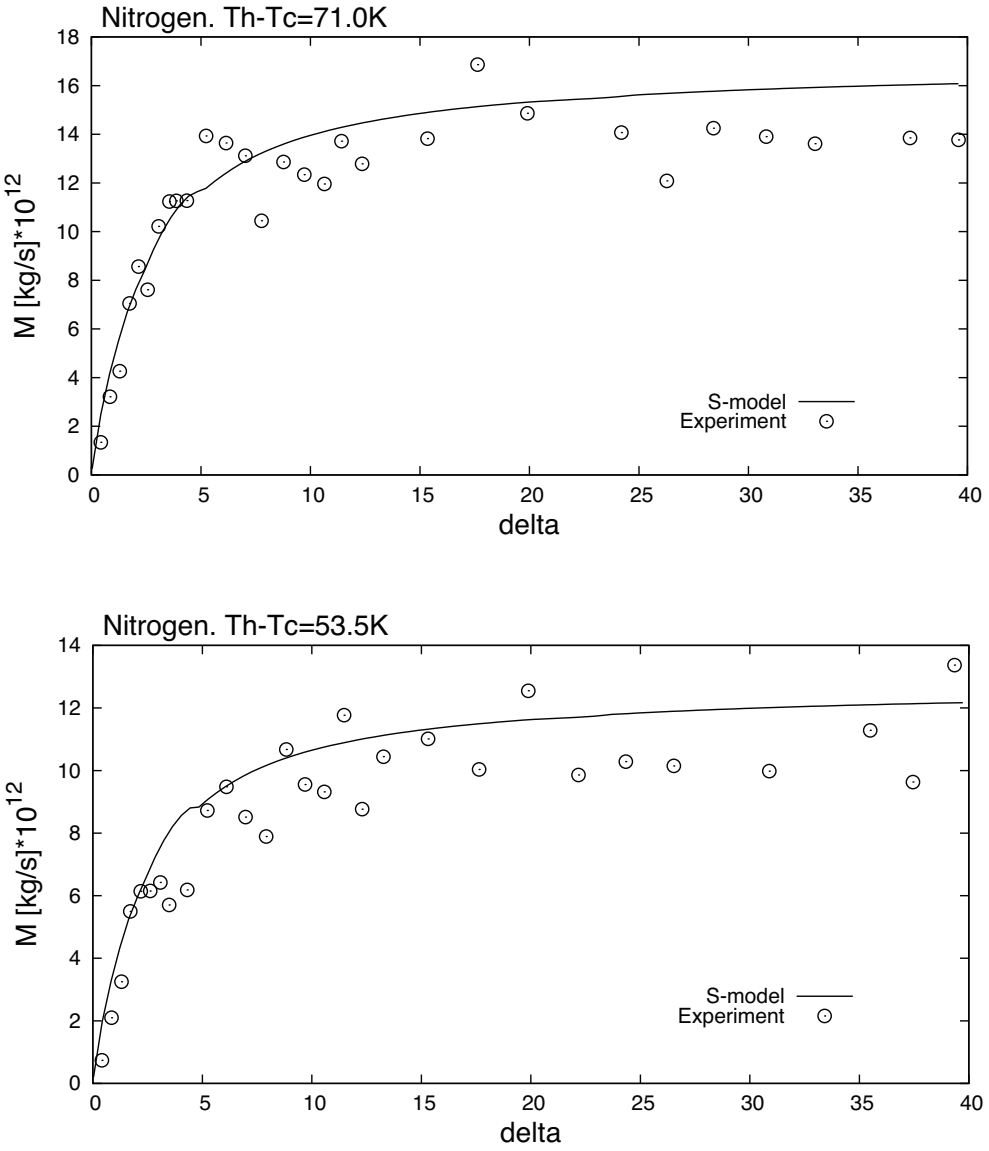

Figure 7.17: Thermal transpiration mass flow rate for nitrogen. Black empty circles [○]: experimental results. Black full line [——]: S-model. Top: $\Delta T = 71K$. Bottom: $\Delta T = 53.5K$.

The second consideration that can be extracted is in respect to the stationarity of the measurements. In the case of a lighter gas, as seen in Section 6.3.1, the transitional time t^* is much lower in respect to the transitional time of the heavier gases. In some cases, when the transitional time is in the same order of the acquisition frequency of the pressure sensors, the mass flow measurements may be corrupted since the pressure sensors are not able to perfectly follow the pressure variation with time in the first moments of the experiment.

A solution in this respect would be to increase the dimensions of the reservoirs, in order to make the pressure variation with time of a lighter gas slower, and therefore have a longer time of stationary pressure variation with time.

The second consideration to be made is in respect to what concerns the temperature reference value chosen in the numerical modeling. It is possible to observe from Figures 7.15-7.17 in respect the slight divergence in between the experimental and numerical results for the three gases. Moreover it is possible to see that this difference is greater for the lighter gas, that is helium. By closely regarding the thermal molecular pressure exponent experimental results and the comparison made in Section 7.3.1.4 with the numerical results obtained by varying the accommodation coefficient α, it is possible to see that the lighter gas it could be less accommodated to the wall in respect to the heavier gases.

Therefore, we interpreted this divergence by assuming that the temperature of the lighter gas in the hot-side reservoir could be different in respect to the temperature at the wall which was measured with the infrared camera. In order to use the numerical model we need to inject a temperature difference reference value which in this case was chosen to be the temperature measured at the wall. Instead for the case of a heavier gas, this temperature jump would also be present but in a less markable manner, thus the experimental results for argon and nitrogen are better reproduced by the numerical results obtained with the S-model.

The third consideration to be done is in respect to the asymptotic behavior of the thermal transpiration mass flow rate when passing from transitional to slip regime conditions. We can effectively see from the figures that also the S-model

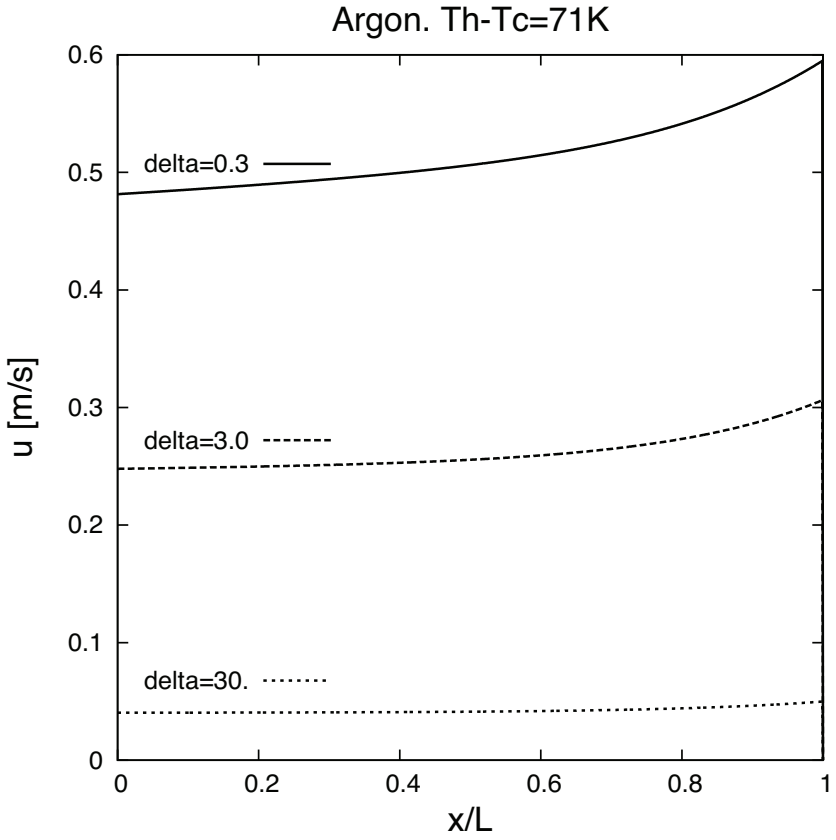

Figure 7.18: Velocity distribution along the tube for argon at $\Delta T = 71K$: S-model results. Black full line [——]: $\delta_T = 0.3$. Black dashed line [- - -]: $\delta_T = 3$. Black dotted line [· · ·].

result tends to a constant value as the experimental results. We have previously given a rough explanation on the subject (Section 6.2.1) stating that this was probably due to the fact that, while the density of the fluid increased, the velocity of the macroscopic gas displacement had to consequently decrease in the same manner.

We decided to look closely at this aspect through the aid of the S-model and therefore we have computed the averaged velocities along the tube for the case of the experimental dimensions. From Figure 7.18 it is possible to see that the numerical results coincide with the hypothesis of a lower flow average velocity for higher values of the rarefaction parameter.

7.3.2.3 Non-dimensional mass-flow rate

We wanted to see the influence of the gas surface/interaction on the stationary thermal transpiration mass flow rate as a function of the used gas. To do so we computed the non-dimensional mass flow rate G_0 which reads as

$$G_0 = \frac{L\sqrt{2RT_c}}{\pi p_i (D/2)^3} \dot{M}_T. \tag{7.13}$$

If we consider the results of the non-dimensional mass flow rate obtained with the S-model, this quantity, for a fixed rarefaction, remains the same for any dimensions of the tube used and for any gas used.

We computed the non-dimensional mass flow rate through the S-model by using two different accommodation coefficients, that is $\alpha = 1.0$ and $\alpha = 0.8$. This was done since it gave us the possibility, by regarding closely the divergence of the two numerical curves, to obtain information for what concerns the gas/surface interaction. Consequently we compared the obtained numerical results to the experimental results.

As it can be seen from Figures 7.19 and 7.20 the numerical results with different accommodation coefficients do not defer excessively for the rarefaction spectrum considered. Higher divergences are to be expected for rarefaction conditions tending to free molecular regime, where a stationary thermal transpiration mass flow measurement becomes really difficult to perform.

Furthermore, the experimental results for the heavier gases match the numerical results, while the results for helium slightly differ. We solicit the reader to refer to Section 7.3.2.2 in order to obtain more information about this divergence. Anyhow, the experimental results of helium respect the trend of the numerical results and the experimental results obtained for the heavier gases cases.

As a conclusion we can state that it is quite difficult to obtain information on the gas/surface interaction from the thermal transpiration mass flow rate results. The non-dimensional mass flow rate measurements resolution is not enough in order to be able to extract such a fine information. The experimental apparatus should be re-designed in order to be able to measure mass flow rates with a higher

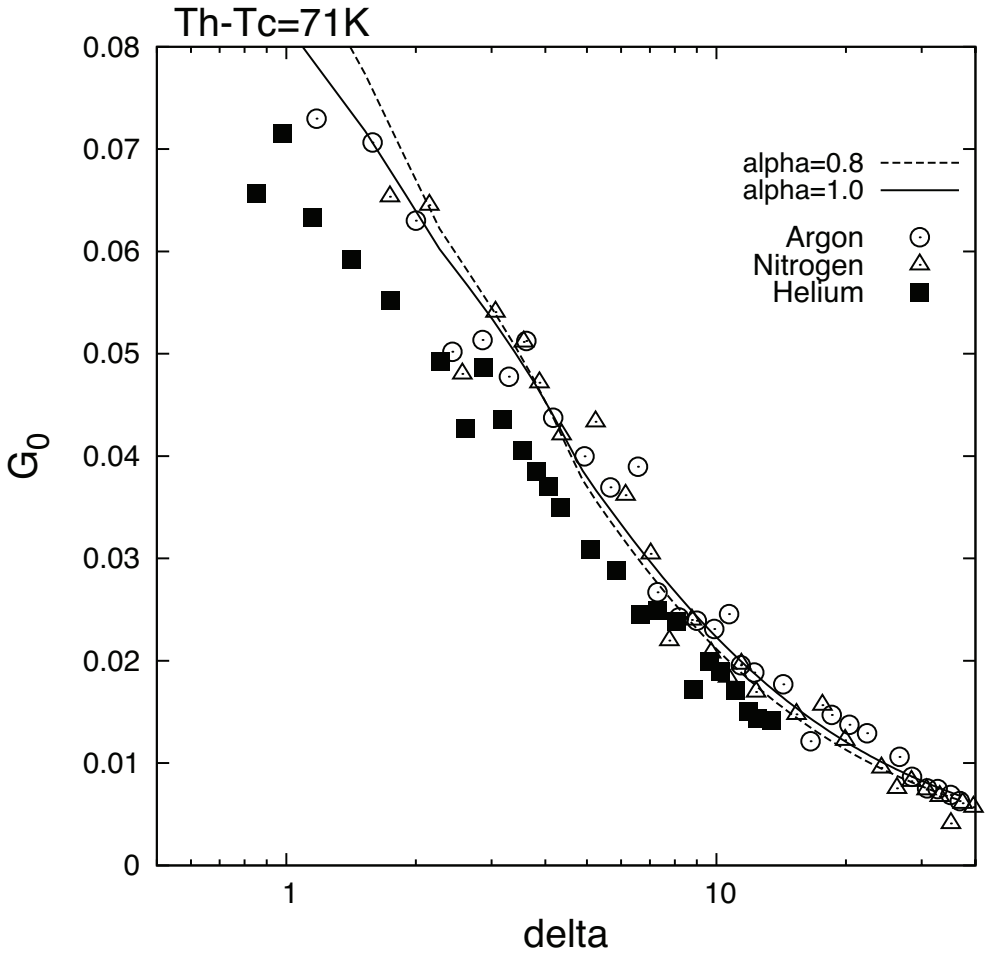

Figure 7.19: Thermal transpiration non-dimensional mass flow rate for $\Delta T = 71.0K$. Comparison between experimental results and S-model. Experimental results: black empty circles [○], argon; black filled squares [■], helium; black empty triangles [△]: nitrogen. S-model: black full line [——], $\alpha = 1$; black dashed line [- - -], $\alpha = 0.8$.

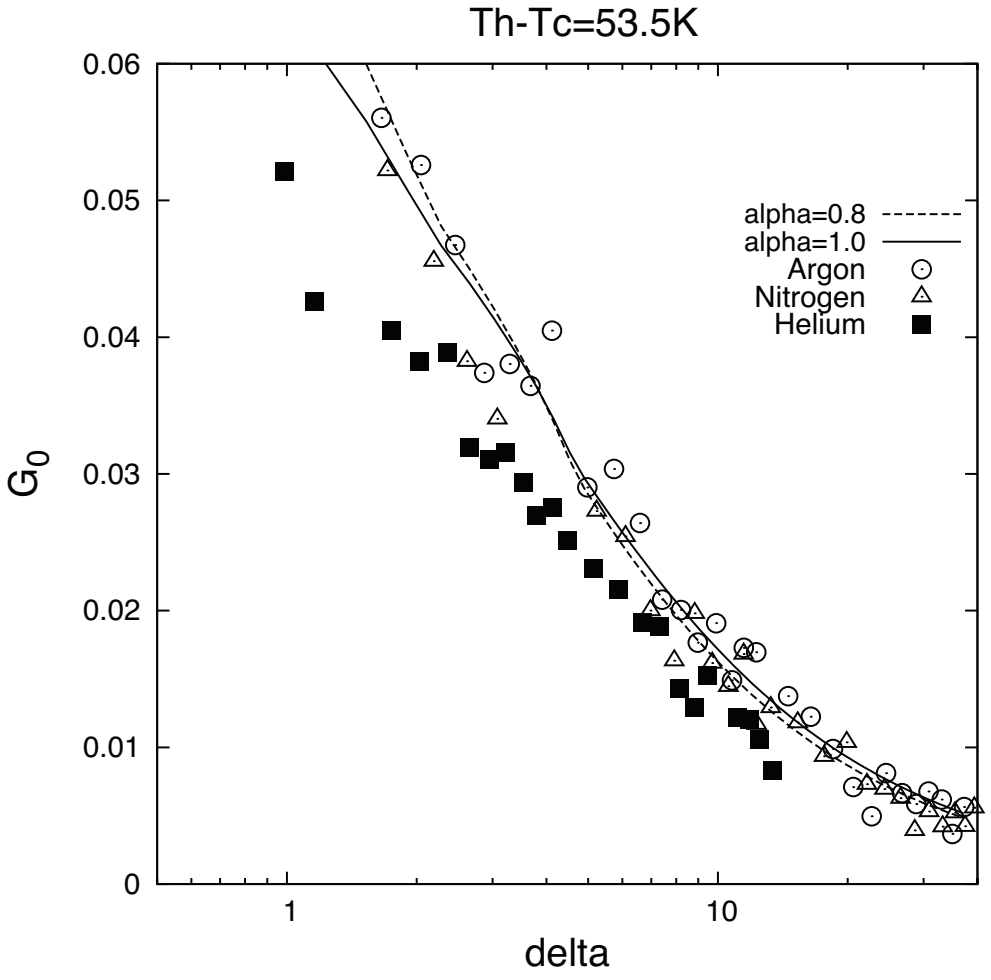

Figure 7.20: Thermal transpiration mass flow rate for $\Delta T = 53.5K$. Comparison between experimental results and S-model. Experimental results: black empty circles [○], argon; black filled squares [■], helium; black empty triangles [△]: nitrogen. S-model: black full line [——], $\alpha = 1$; black dashed line [- - -], $\alpha = 0.8$.

accuracy for rarefaction conditions tending to free molecular regime.

A possible solution for future experiments would be to work with light gases, larger volume dimensions and higher temperature differences imposed.

We would like to remind the reader that information on the gas/surface interaction can still be obtained from the thermal pressure exponent parameter, as previously discussed in Section 7.3.1.4.

Chapter 8

Perspectives: isothermal measurements

The information and results that we presented in this chapter are to be considered as on going research. They are the direct consequence of the research that we already presented in the previous chapters. Even if the ideas are not fully developed we would like to introduce them to the reader, in order to depict in which way the investigations made by this working group are developing.

When we studied the gas/surface interaction for a non-isothermal case, that is for the thermal transpiration thermal molecular pressure exponent zero-flow parameter (Section 7.3.1.4), we realized that the accommodation at the wall of different gases did not respect the results which can be found in the literature for gas/surface interactions in isothermal cases, that is when the pressure driven mass flow rate is studied [Perrier *et al.* [2011]]. Therefore we decided to check ourselves if effectively the hierarchy of the gas accommodation at the surfaces changed, in respect to the hierarchy found for the thermal transpiration case and if a pressure difference was imposed in between the inlet and outlet of the micro-tube.

In order to do this we performed isothermal experiments by using exactly the same experimental apparatus than in the thermal transpiration experiments. By testing argon, helium and nitrogen, we therefore checked the differences exerted by the gas/surface interaction on the non-dimensional isothermal mass flow rate.

Since we had already developed a time-dependent methodology in order to obtain the thermal transpiration mass flow rate, we decided to adopt a similar methodology for the case of a pressure driven flow, and see if a slightly modified methodology could be applied to the isothermal case.

We realized that the time-dependent methodology as applied to a isothermal case could work even better than in respect to a non-isothermal case since the perturbations introduced in the reservoirs are larger. Therefore, from this point on we decided to start investigating the pressure driven flow as a time-dependent phenomenon by following the transitory evolution of the pressure inside the two reservoirs positioned at the inlet and outlet of the micro-tube.

Finally, once we were in possession of all these elements and once we had checked the influence of hierarchy of the gas/surface interaction for the isothermal case, we started studying the thermal transpiration zero-flow stage from another perspective. The questions that we wanted to answer were: is it possible to prove that effectively two flows are present along the tube at the final stage of the thermal transpiration experiment? And, can we better clarify the reasons of the shifting tendency of the TPD, PV and PVS in transitional regime $\delta = 3.5$ (Section 6.3.4)?

8.1 Isothermal methodology

The experiments performed in this section were obtained by using exactly the same micro-tube that was used in the thermal transpiration experiments ($D = 485 \pm 6 \mu m$ and $L_t = 52.7 \pm 0.1 mm$).

After imposing a difference of pressure in between two regions, the gas tends to re-equilibrate this non-equilibrium state by macroscopically moving from the higher to the lower pressure zone. In the studied experimental cases we imposed a difference of pressure in between the two reservoirs connected by a micro-tube. Since in this case the whole system worked under isothermal conditions, we defined the reservoirs as 1 and 2, at the place of cold- and hot-side reservoirs, respectively.

The pressure imposed was higher in 1 and lower in 2, that is $p_1 > p_2$. Once the difference of pressure was imposed, the gas moved from the former to the

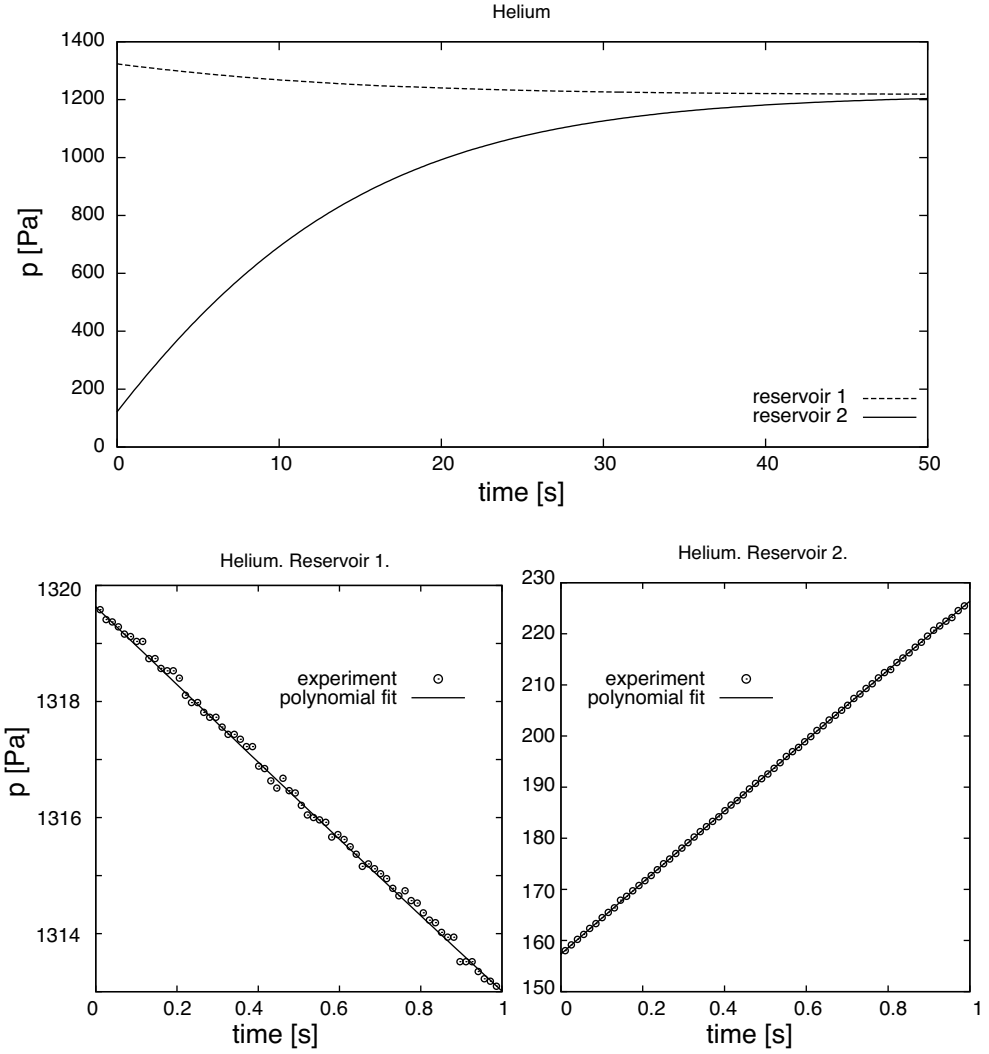

Figure 8.1: Top: Isothermal experiment for helium. At the initial conditions a pressure difference is imposed between the two reservoirs. Therefore the pressure variates with time inside reservoirs 1 and 2. The different variation speeds depend on the volume ratio of the two reservoirs that is $V_1/V_2 = 10.2$. Dashed line [**- - -**] reservoir 1. Full line [——] reservoir 2. Bottom: the pressure variation with time in the first second of the experiment. Bottom left: reservoir 1, circles [○] experimental points, full line [——] polynomial fitting function. Bottom right: reservoir 2. Same as before.

latter through the micro-tube re-equilibrating the initial pressure disequilibrium. The macroscopic gas displacement process ended once a final pressure equilibrium was reached. The final equilibrium was reached when the two reservoirs attained a pressure equality, that is at $p_1 = p_2$ (Figure 8.1: top graph).

As explained in *Section* 5.1, it is necessary to follow the pressure variation with time inside one of the reservoirs in order to measure the stationary mass flow rate induced by a pressure difference imposed between the ends of the tube. Therefore, once the pressure variation is monitored and recorded inside one reservoir, it is necessary to chose the specific time interval in which the measurement will be effectively done. This specific time interval has to be short and physically consistent.

8.1.1 Stationarity of the measurement

Let us test the stationarity of the pressure variation with time inside the two reservoirs for the experiment proposed in Figure 8.1 (top graph). We decided to perform the specific measurement of pressure variation with time at the moment when the experiment starts, therefore at time $t = 0$. It is possible to directly visualize from the bottom left and bottom right graph of Figure 8.1, that by choosing a time interval of 1 second the pressure decrease in reservoir $n.1$ and the pressure increase in reservoir $n.2$ is always linear during the whole duration of the experiment. The speed of pressure variation with time inside the two reservoirs largely differs. The pressure varies more rapidly in the second reservoir. This is due to the ratio of volume $n.1$ to volume $n.2$: volume $n.1$ is approximately 10 times larger in respect to volume $n.2$ ($V_1/V_2 = 10.2$).

We decided to fit the pressure variation with time inside both reservoirs by means of a polynomial function of the third order (Figure 8.1 bottom graphs) identified by the following form

$$p_{iso}(t) = a\,t^3 + b\,t^2 + c\,t + p_0, \tag{8.1}$$

where a, b and c are the fitting parameters while p_0 is the starting pressure point of the experiment. The first and the second order term effects vanish when t tends to 0 and then the pressure variation with time is linear. Consequently the form of

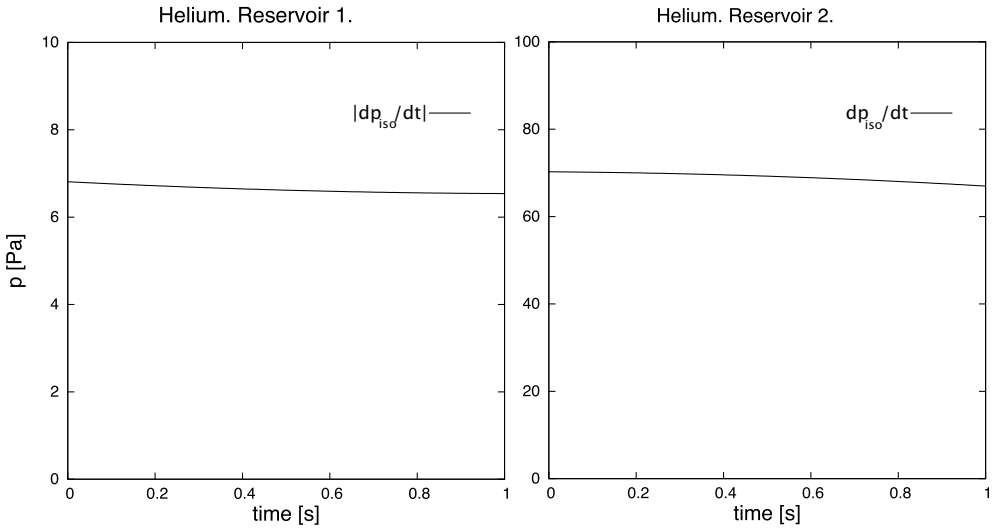

Figure 8.2: Stationarity of the pressure variation with time monitoring by means of dp_{iso}/dt. Left: absolute value of dp_{iso}/dt in reservoir n.1. Right: dp_{iso}/dt in reservoir n.2.

eq. (8.1) may be used only in the vicinity of $t = 0$. The standard deviation of the fitting was estimated to be always less than 0.1%.

We consider firstly the pressure evolution starting from p_0 given in eq. (8.1). We can check the stationarity of the experiment by analyzing the derivative of the fitting function that describes the pressure variation with time. If we plot its evolution with time we may promptly realize that the pressure variation with time is linear if dp_{iso}/dt stays constant and equal to c, which is its initial value at $t = 0$. In Figure 8.2 it is possible to see that the latter condition is met: for both reservoirs the derivative of the pressure variation with time remains constant in within 3% from the initial value c, for the 1 second of duration of the measurement. Therefore it is possible to state that the measurement is indeed stationary in this time lapse.

It is well understood that the relaxation time of the pressure in order to tend to its natural equilibrium depends on the gas used, the difference of pressure imposed and the rarefaction of the fluid inside the system. Here, we are offering a limit example: the pressure difference imposed is quite large $(p_1 - p_2) \sim 1200[Pa]$ and the used gas is helium, which has an extremely light molecular weight, which

makes the process quite fast. The corresponding gas rarefaction conditions are in the transitional regime.

8.1.2 Points of measurement

It is clear then that during one experiment the pressure variation with time could be considered as linear in the vicinities of any instant t_{0_j} of the measurement. But, by following the previous comments about eq. (8.1), we have to write a local version of eq. (8.1) written near t_{0_j}

$$p_{iso}(t) - p(t_{0_j}) = a_j\,\theta^3 + b_j\,\theta^2 + c_j\,\theta, \tag{8.2}$$

where $\theta = t - t_{0_j}$. The only requirement is that $dp_{iso}/d\theta|_0 = dp_{iso}/dt|_{t_{0_j}} \sim c_j$ in within acceptable limits. In this study the limits were arbitrarily chosen to be at 5% of variation from the original value of derivative of the pressure variation with time at the beginning of the experiment for time $t = t_{0_j}$, that is c_j if the local polynomial fitting notation is taken into account. The specific time interval which was used to fit the experimental data was chosen accordingly in order to satisfy the condition of stationarity.

We saw from the example shown in Figure 8.1 that this condition is easily met. Therefore, if the stationarity condition was always true, it could eventually be possible to obtain one mass flow rate measurement at each instant t_{0_j} of the experiment and not only at the instant $t = t_0$ which was previously regarded in Section 8.1.1, that is from when the first initial pressure difference is imposed to near the final equilibrium stage. Obviously, when the mass flow rates along the tube become too small and approach negligible values, that is near the final equilibrium stage, the measurement technique loses its accuracy radically.

It is fascinating to see the quantity of information that is possible to acquire from one single experiment. Parameters such as the pressure difference or the pressure ratio imposed continuously vary (Figure 8.3 right column top) and therefore it is up to us to choose the right, or the desired, moment to effectuate a mass flow rate measurement. Thus, in order to obtain a given stationary mass flow rate it is possible to chose, along the whole duration of one time-dependent experiment, different pressure ratios or different pressure differences. As an example we propose

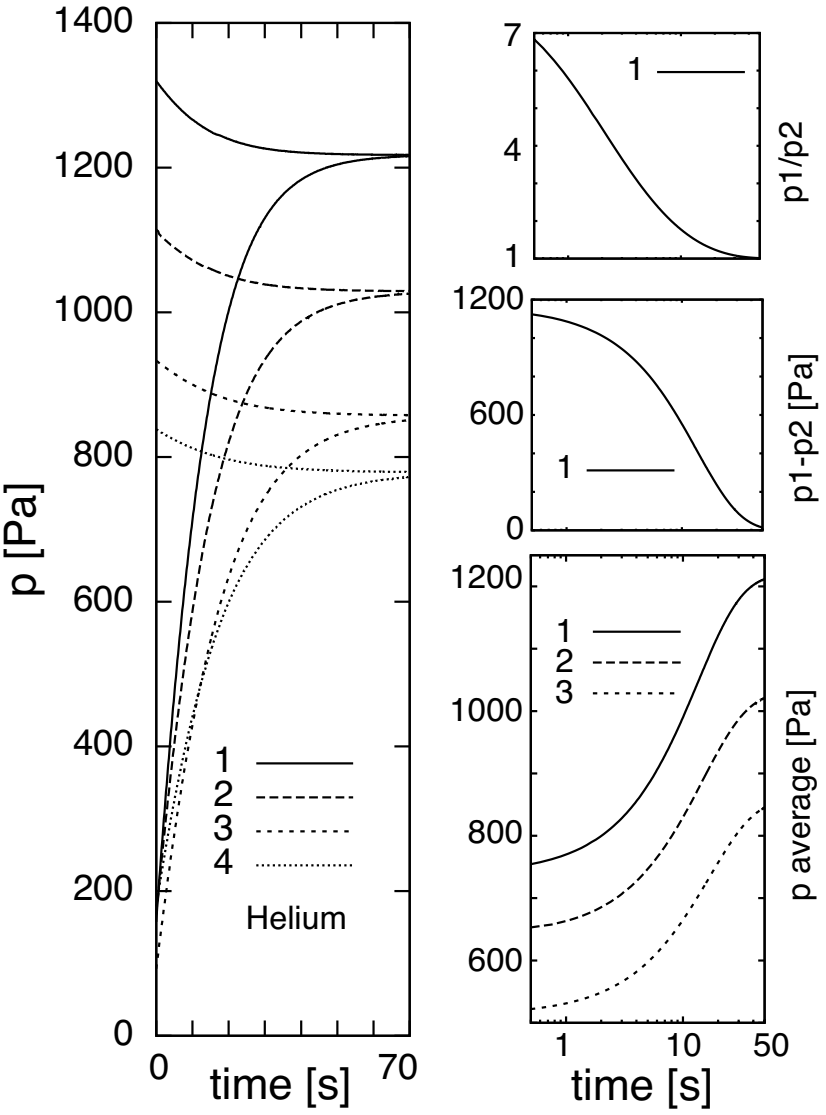

Figure 8.3: Left column: four different isothermal experiments. The initial difference of pressure was arbitrarily chosen. The initial average of pressure along the tube was set to be different at each experiment. We plotted for each experiment the pressure variation with time in reservoir n.1 and reservoir $n.2$. Right column from top to bottom: the pressure ratio variation with time for experiment n.1; difference of pressure variation with time for experiment n.1; the average of pressure variation with time for three different experiments.

experiment n.1 in Figure 8.3 where it is possible to see the spectrum of pressure ratios or pressure differences at which it could be possible to measure a mass flow rate, that is from ~ 7 to 1 for p_1/p_2 and from ~ 1200 to 0 for $p_1 - p_2$.

Furthermore, it is possible to chose the desired rarefaction of the gas at which the measurement has to be effectuated. The gas rarefaction conditions along the tube are directly proportional to the average pressure of the micro-fluidic system, which is $p_{av} = \frac{1}{2}(p_2 + p_1)$.

Lets introduce the isothermal rarefaction parameter as

$$\delta_p = \frac{p_{av}\, D/2}{\mu(T)\sqrt{2RT}}. \tag{8.3}$$

Therefore, if we choose *experiment n.1* as a reference, the gas rarefaction in one single experiment can variate from the beginning to the end of the process approximately 1.5 times (Figure 8.3 right column bottom).

8.2 Isothermal mass flow rate

Therefore, if we hypothesize that at every instant of the experiment it can be possible to obtain a mass flow rate measurement, we are able to obtain a great quantity of data by correctly post-processing the acquired pressure variation with time information.

To effectuate the measurement, it is necessary to decide the instant at which the measurement has to be done, this can be carried out by choosing a fixed parameter like the pressure ratio or the pressure difference in between the two ends of the tube which will give us a precise and unique instant at which the condition is met. Once this instant is chosen, it is possible to obtain a function $p_{iso}(t)$ that from the corresponding p_{0_j} follows the pressure variation with time around the considered instant t_{0_j} at which the measurement has to be done (Section 8.1).

In the case where the stationary condition is met, it is then possible to substitute the $dp/\Delta t$ term of eq. (5.4) by the derivative of the function that described the pressure variation with time $p_{iso}(t)$ at the initial instant of the measurement,

that is at $t = t_{0_j}$ where the derivative of the function was $dp_{iso}/dt|_{t_{0_j}} = c_j$ (eq. 8.1). Therefore, the mass flow rate $\dot{M}_p$ entering reservoir n.2 or leaving reservoir n.1 can be calculated as

$$\dot{M}_p = \frac{V}{RT}\, c_j. \tag{8.4}$$

As commonly found in the literature, the mass flow rate results were proposed after in a dimensionless form which is

$$G_{iso} = \frac{8L\sqrt{2RT}}{\pi D^3 (p_1 - p_2)}\, \dot{M}_p, \tag{8.5}$$

where G_{iso} is the non-dimensional mass flow rate for the case of a pressure difference induced flow [eq. (7.10)].

8.2.1 Arbitrary pressure ratio imposed

In order to proceed to the comparison with the S-model numerical results for the case of a pressure driven flow, we proposed the non-dimensional mass flow rate results. We compared the results obtained by choosing the pressure ratio in between the two reservoirs as a fixed parameter: we showed three series of experiments, that is the non-dimensional mass flow rate results for $p_1/p_2 = 5$, $p_1/p_2 = 4$ and $p_1/p_2 = 3$ for the transitional regime gas rarefaction conditions. The gas used was helium.

It is possible to see from Figure 8.4 the excellent agreement of the results for different pressure ratios applied. The non-dimensional mass flow rate, as shown by the kinetic theory S-model numerical results, does not vary as a function of the pressure difference imposed, but varies just as a function of the rarefaction of the gas. It is possible to see as well that the results found for helium coincide with the S-model numerical results when the accommodation coefficient imposed is equal to unity, that is for a complete diffuse reflection at the wall.

We estimated the experimental uncertainty of this results to be in the order of 4%, but this uncertainty would be mainly introduce by the dimension of the volume and the dimension of the diameter which are difficult to perfectly estimate. Therefore a great percentage of the uncertainty is introduced by a systematic uncertainty which plays a role in the absolute values of the measurements but not

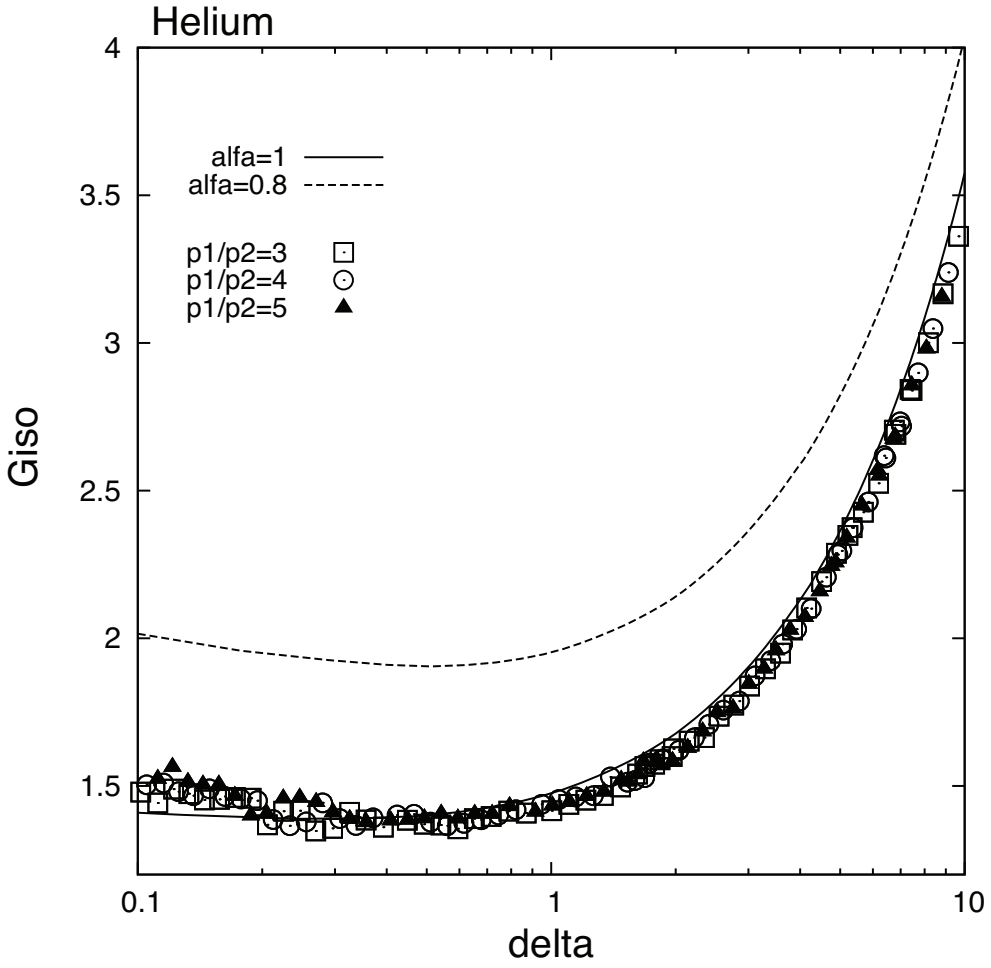

Figure 8.4: Non-dimensional mass flow rate in transitional regime for helium. Experimental results: filled triangle [▲], $p_2/p_1 = 5$; empty circles [○], $p_2/p_1 = 4$; empty square [□], $p_2/p_1 = 3$. S-model numerical solution for a pressure driven flow: black full line [——], $\alpha = 1$; black dashed line [- - -], $\alpha = 0.8$.

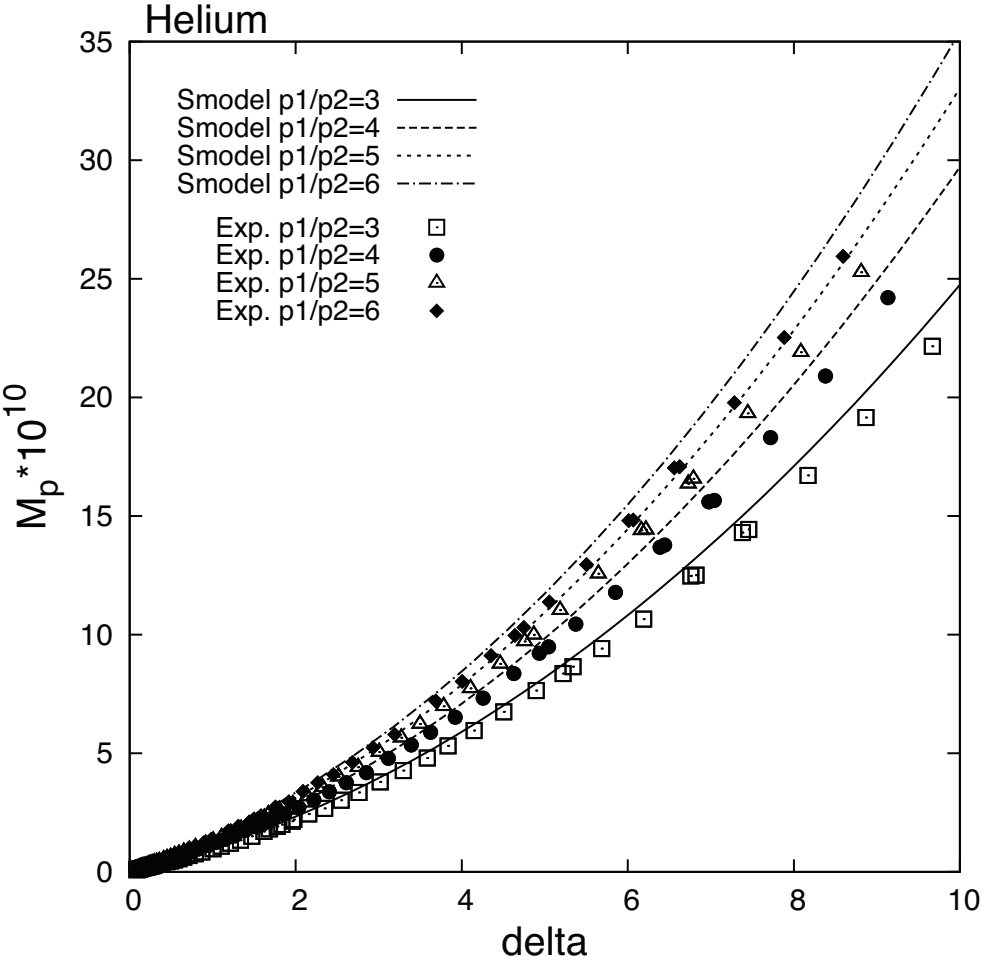

Figure 8.5: Dimensional mass flow rate in transitional regime for helium. Experimental results: filled diamond [◇], $p_2/p_1 = 6$; empty triangle [△], $p_1/p_2 = 5$; filled circle [●], $p_1/p_2 = 4$; empty square [□], $p_1/p_2 = 3$. S-model numerical solution for a pressure driven flow for $\alpha = 1$: from $p_1/p_2 = 3$ black full line [——]; to $p_1/p_2 = 6$ black dash-pointed line [$- \cdot -$]

on their trend.

It is possible to better see this from Figure 8.5 where the trend of the dimensional experimental mass flow rates follows the trend of the S-model numerical solution, but slightly diverges from its absolute value. In the future, it will be necessary to check if this divergence is effectively introduced by the tools and methodology used when measuring the tube diameter and the volume of the reservoir, or if it is due to the model used or due to a physical reason.

It could be possible to introduce a correcting factor that takes into account a dimensional measuring uncertainty, both of the tube diameter and of the reservoir volume by confronting the mass flow rate experimental results to the analytical solution of a Poiseuille flow in hydrodynamic regime. This procedure has not been done at the moment because the mass flow rates have not been measured in hydrodynamic regime since that would require to change the pressure sensors used in order to have a higher full scale reading of the sensor. Nevertheless the considerations already introduced in Section 7.3.2.2, for what concerned the comparison between the experimental mass flow rate results and the S-model numerical results, are still valid here.

For the studied cases the dimensional mass flow rates are in the order of $10^{-10} kg/s$. As it was expected the values of the mass flow rate increase with the density of the gas. The intensity of the mass flow rate increases with increasing ratios of pressure applied between the ends of the micro-tube.

It is still clear that the measurements are very stable, and it is possible to obtain from this kind of experimental methodology a great amount of information which can be deduced from a reduced number of experimental series.

8.2.2 Small pressure difference imposed

It is also possible to impose small pressure differences between the inlet and outlet of the micro-tube. In this case, since the dynamism or the speed of the pressure variation with time is not as high as in the case of high pressure ratios, the quality of the measurement is reduced and the results are more fluctuating.

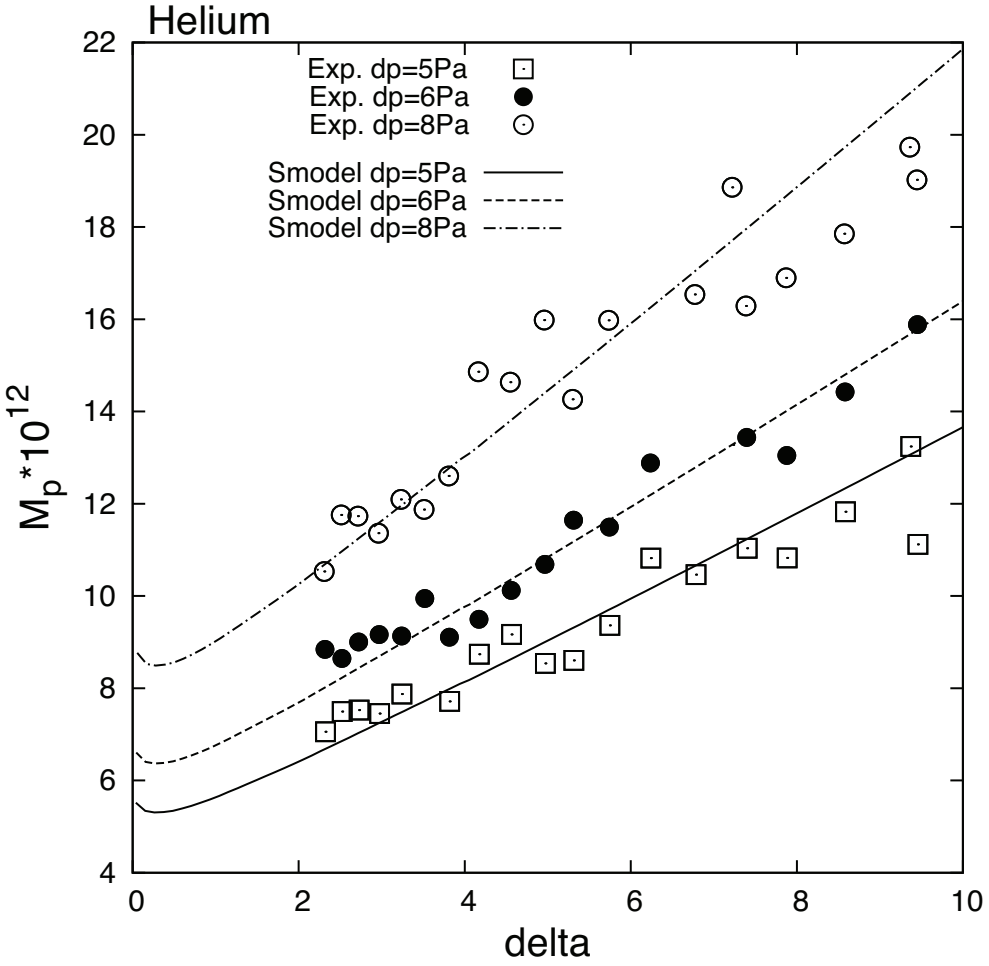

Figure 8.6: Dimensional mass flow rate in transitional regime. Experimental: $p_1 - p_2 = 8Pa$, empty circles [○]; $p_1 - p_2 = 6Pa$, black circles [●]; $p_1 - p_2 = 5Pa$, empty squares [□]. S-model: full black line [——], $p_1 - p_2 = 5Pa$; dashed black line [− − −], $p_1 - p_2 = 6Pa$; dot-dashed black line [− · −], $p_1 - p_2 = 8Pa$.

From Figure 8.6 it is possible to see the results for a dimensional mass flow rate in the case where the pressure differences imposed are in the order of some Pascals. Moreover the results, even if fluctuating, coincide with the S-model numerical results.

Let us notice that the mass flow rates engendered for this pressure differences imposed are really low, that is in the order of $10^{-12} kg/s$. As expected, the mass flow rates are higher for higher imposed pressure differences. It is also possible to see that the mass flow rate, for a fixed pressure difference imposed, increase with the density.

We would like to show this results since we will use them in the last section of this chapter, where we will see if it is possible to associate the thermal transpiration final zero-flow stage to two oppositely directed flows, one of which is a Poiseuille flow. We would like the reader to remember from this section essentially that the measured values of the pressure driven mass flow rate are in accordance with the numerical results obtained with the S-model.

8.2.3 Mass conservation

A good reference of the measurement accuracy can be given from testing the mass conservation along the tube at a given instant: the mass flow rate which enters reservoir n.2 has to be the same as the mass flow rate which leaves reservoir n.1, therefore $|\dot{M}_1| = \dot{M}_2$. From eq. (5.4) it is then possible to write

$$V_1 \left.\frac{dp_{iso}}{dt}\right|_1 = V_2 \left.\frac{dp_{iso}}{dt}\right|_2 , \tag{8.6}$$

where the derivative of the pressure variation with time with subscripts 1 and 2 correspond respectively to reservoir n.1 and n.2.

It is possible to observe from Figure 8.7 that the measurements in reservoir n.1 lose accuracy when the gas flow is near free molecular regime. In this regime the mass flow rate meaningfully decreases and therefore it is more difficult for the instrumentation to detect a pressure variation with time: in this regime, in reservoir n.1, the

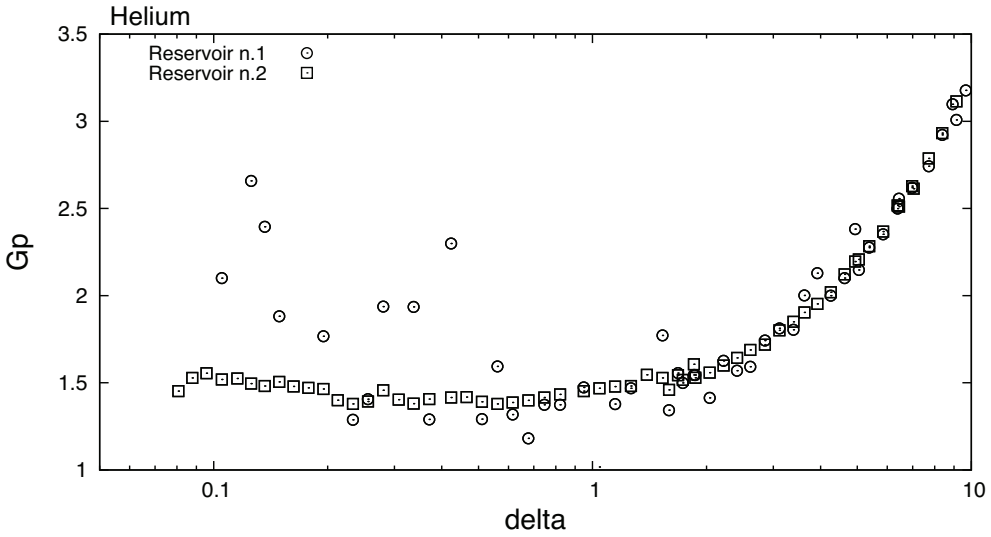

Figure 8.7: Comparison between measurements obtained in reservoir n.1 and n.2. The volume of reservoir n.1 is 10 times greater in respect to n.2 therefore it is more difficult to effectuate a dynamic measure. The measurement loses accuracy when the flow speed decreases.

pressure variation with time is of the same order as the instrumentation resolution.

In other words, in order to have an acceptable measurement, the pressure should significantly vary during the specific time interval chosen to effectuate the mass flow rate measurement. The difference of accuracy between the measurements effectuated in reservoir n.1 and n.2 derives from the disparity in the dimension of the reservoirs, since the ratio between the two volumes is approximately 10.

On the other hand, it is possible to observe that from the transitional to the hydrodynamic regime the measurements effectuated in reservoir n.1 coincide with the measurements effectuated in reservoir n.2.

8.3 Isothermal non-stationary experiments

Let us now show that it is possible to effectuate a non-stationary study of the isothermal experiments. As it can be seen from Figure 8.8 the pressure variation

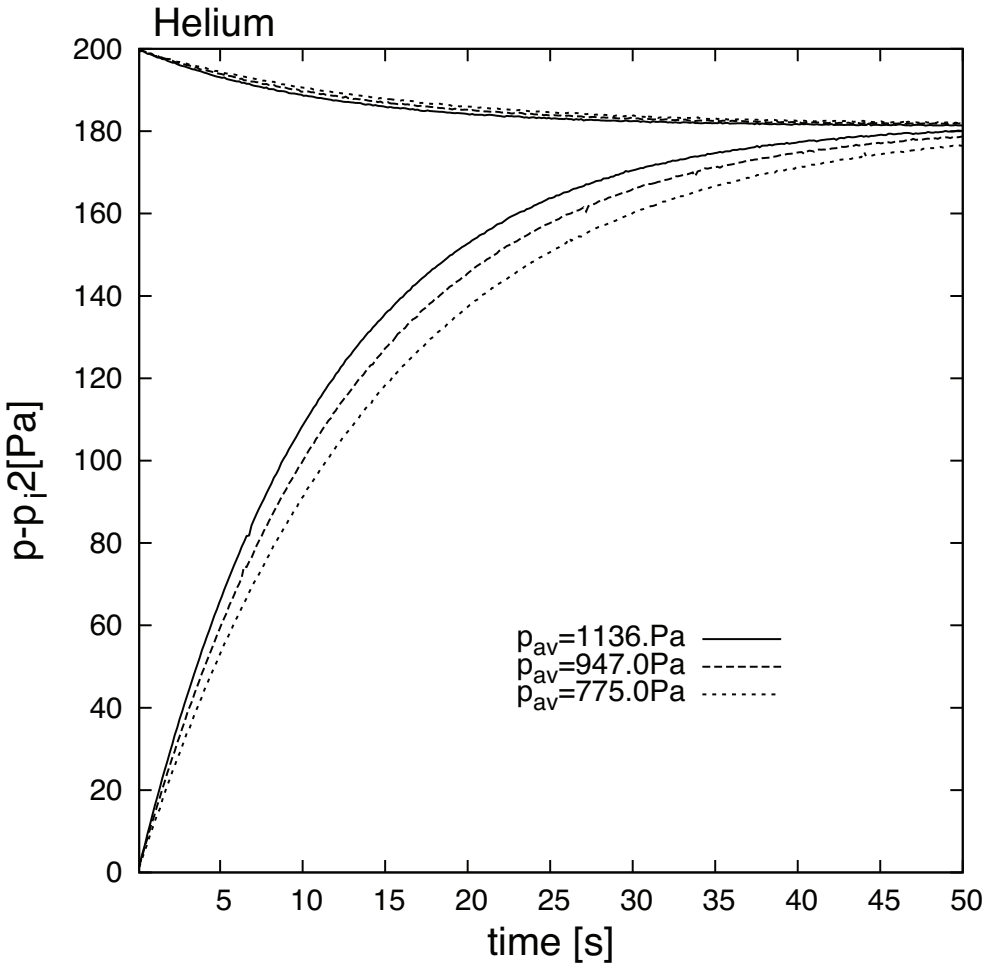

Figure 8.8: Non-stationary pressure variation with time for an isothermal experiment in the case of helium. Different pressure variation with time speed as a function of the average pressure at the initial time of the experiment. The initial pressure in reservoir n.2 was subtracted to the pressure variation with time inside both reservoirs. The initial pressure difference imposed was $200Pa$.

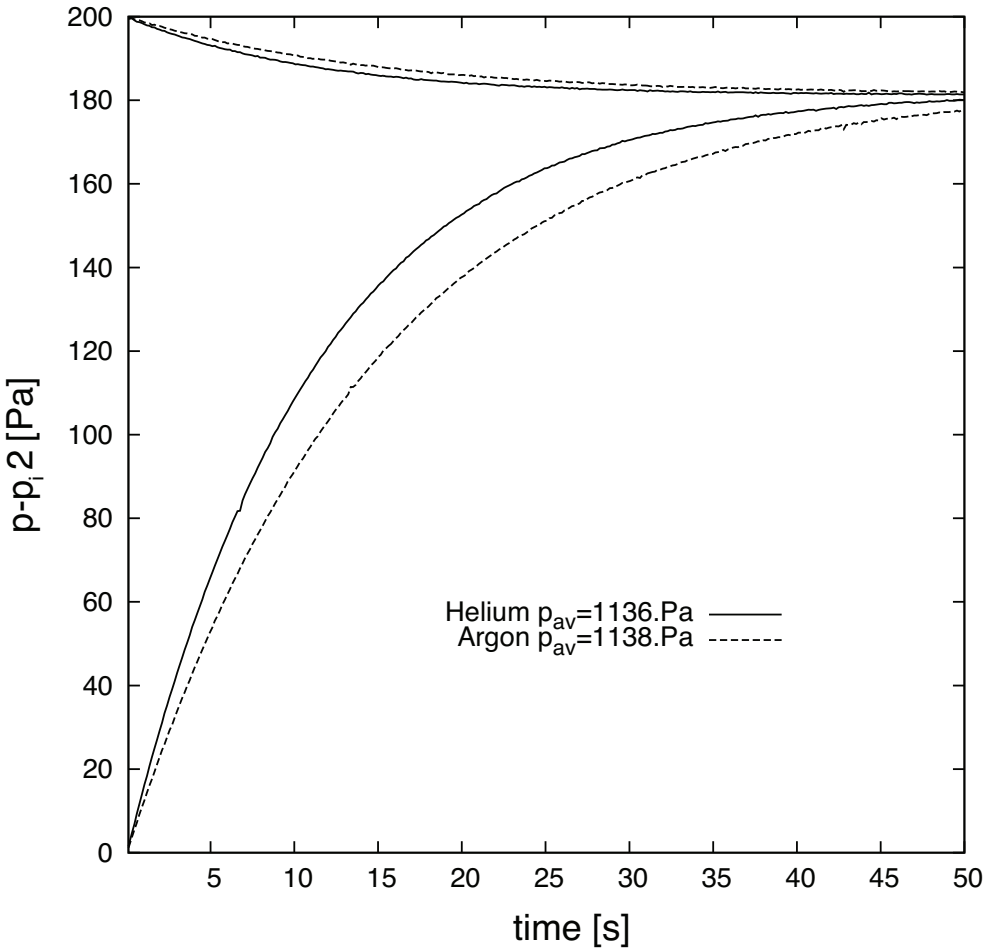

Figure 8.9: Non-stationary pressure variation with time for an isothermal experiment in the case of helium, full black line [——] and argon, dashed black line [− − −]. The initial pressure in reservoir n.2 was subtracted to the pressure variation with time inside both reservoirs. The initial pressure difference imposed was $200Pa$ and the initial average pressure was ~ 1137 for the two gases.

with time induced by applying an initial pressure difference between the inlet and outlet of the micro-tube is clearly influenced by the density of the gas. For a denser fluid, the pressure variation with time tends faster to the final equilibrium stage of zero flow.

In the presented case of helium, we show the same initial pressure difference as a departing point, but for the different cases the average density of the fluid is different. The pressure variation with time in the reservoir $n.1$ and the pressure variation with time in the reservoir $n.2$ have been subtracted of the initial pressure value in the reservoir at the outlet of the micro-tube.

From here on it could be possible to determine the characteristic time of the thermodynamic system and it could be possible to observe how this parameter is influenced by the rarefaction of the gas, the pressure difference applied and the gas nature.

In Figure 8.9 we show the pressure variation with time for the case of two gases, that is argon and helium, at the same initial difference of pressure and with the same initial average pressure. The rarefaction of the two presented conditions cannot be directly regarded since it is different due to the molecular weight difference between the gas.

It is anyhow possible to see from the example offered that helium, which is the lighter gas, tends more rapidly in respect to argon to the final zero-flow equilibrium stage. Since we previously saw that a denser gas tends more rapidly to the final equilibrium stage, if we had considered helium and argon at the same initial densities, for the same imposed difference of pressure, we would have found the same hierarchy for what concerns the speed of the pressure variation with time for the two gases. Therefore we can easily state that for the same densities helium would have been even faster in respect to argon.

Analogies can be found in the non-isothermal case of thermal transpiration, but in this case the driver of the pressure variation with time is not a temperature difference applied but a pressure difference applied.

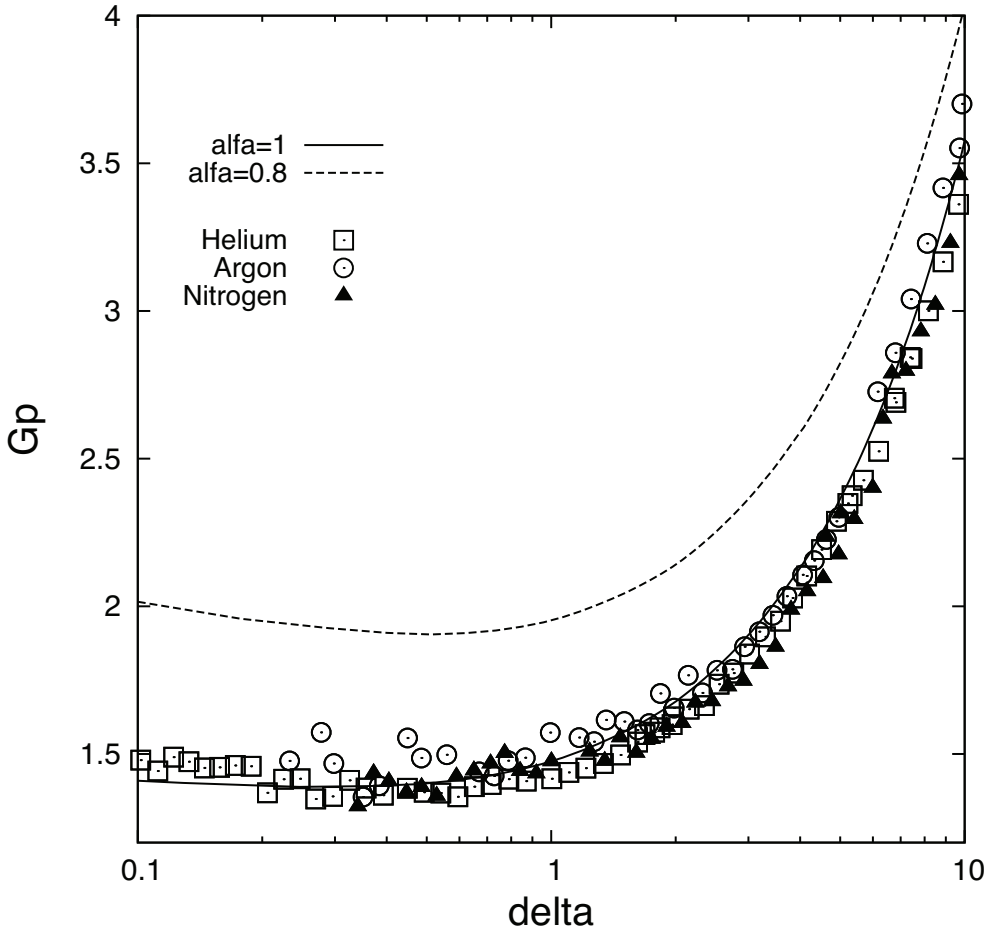

Figure 8.10: Non-dimensional mass flow rate in transitional regime. Experimental results: empty circles [○], argon; empty square [□], helium; filled triangle [▲], nitrogen. S-model numerical solution for a pressure driven flow: black full line [——], $\alpha = 1$; black dashed line [- - -], $\alpha = 0.8$.

8.4 Isothermal gas/surface interaction

We wanted to see if the gas/surface interaction corresponded to the same hierarchy found for the non-isothermal thermal transpiration case (Section 7.3.1.4). Therefore we compared the isothermal mass flow rate results obtained with the S-model numerical results by imposing different accommodation coefficients.

The isothermal mass flow rate hierarchy of the gas/surface interaction for argon, helium and nitrogen can be seen in Figure 8.10. It is possible to observe that the results for the three gases correspond to a fully diffuse reflection at the wall. If a fine analysis is done, we could consider helium at the top of the hierarchy as the gas with the best full accommodation to the wall and then successively nitrogen and argon. Similar results have been observed by Perrier *et al.* [2011], even if for their studied case the divergence for the different gases was slightly higher.

For what concerns the thermal transpiration experimental results obtained, we could observe an opposite tendency in the thermal molecular pressure exponent results in respect to the gas/surface interaction hierarchy of the isothermal results. In other words, for the non-isothermal case we found that the heavier the gas was, the better the gas was fully accommodated, while the lighter gas had an accommodation α in between 0.8 and 0.9. The accommodation coefficient for both the non-isothermal and isothermal case were neither accurately determined nor clearly defined, the values given can be considered as just preliminary observations.

At the present moment we have not elaborated a well founded prediction in order to explain this radical change of hierarchy, but this could be better studied if a different kernel was associated to the S-model kinetic equation, that is a kernel function that takes into consideration a momentum and an energy accommodation coefficient, as in the one proposed by Cercignani [1972].

8.5 Thermal transpiration zero-flow

Lets introduce the last section of this chapter. We found of a certain interest the zero-flow final equilibrium stage of the thermal transpiration experiments and therefore we tried to analyze it from a slightly different perspective.

Without entering in any details on further explanations lets just remind the reader that the zero-flow final equilibrium stage has been considered until now to be the balance of two oppositely directed flows, one induced by a temperature difference applied to the micro-tube and the other induced by a pressure difference that was generated by the pressure variation with time engendered by thermal transpiration (Section 5.2.1).

The totality of the papers which have studied thermal transpiration so far have referred to the assumption of Knudsen in order to explain this equilibrium stage, but until now no concrete proof has been given in order to be able to consider this assumption as completely satisfied.

Here we have tried to give a first demonstration of the validity of Knudsen's assumption, that is that there is a perfect balance between two oppositely directed flows at the final zero-flow equilibrium stage.

In order to do this we need to refer to the results obtained for the thermal transpiration mass flow rate in Section 6.2 and to the results obtained for the isothermal mass flow rate induced by small pressure differences in Section 8.2.2.

As can be seen in Figure 8.11, by simply superposing the results of the temperature difference induced flow and the pressure difference induced flow we can effectively see that, for a given temperature difference applied and by a given pressure difference applied, a common balance point for two fixed rarefaction conditions of the gas can be found.

In the example given in Figure 8.11, we presented the thermal transpiration mass flow rate results in the case of helium for $\Delta T = 71K$ and $\Delta T = 53.5K$ as a function of the rarefaction conditions of the gas; and the isothermal mass flow rates engendered by small pressure differences applied in between the inlet and outlet of the tube which are represented by the parametric lines, the pressure differences considered go from $\Delta p = 1Pa$ to $\Delta p = 7pa$.

As it was previously presented, the isothermal experimental results are well rep-

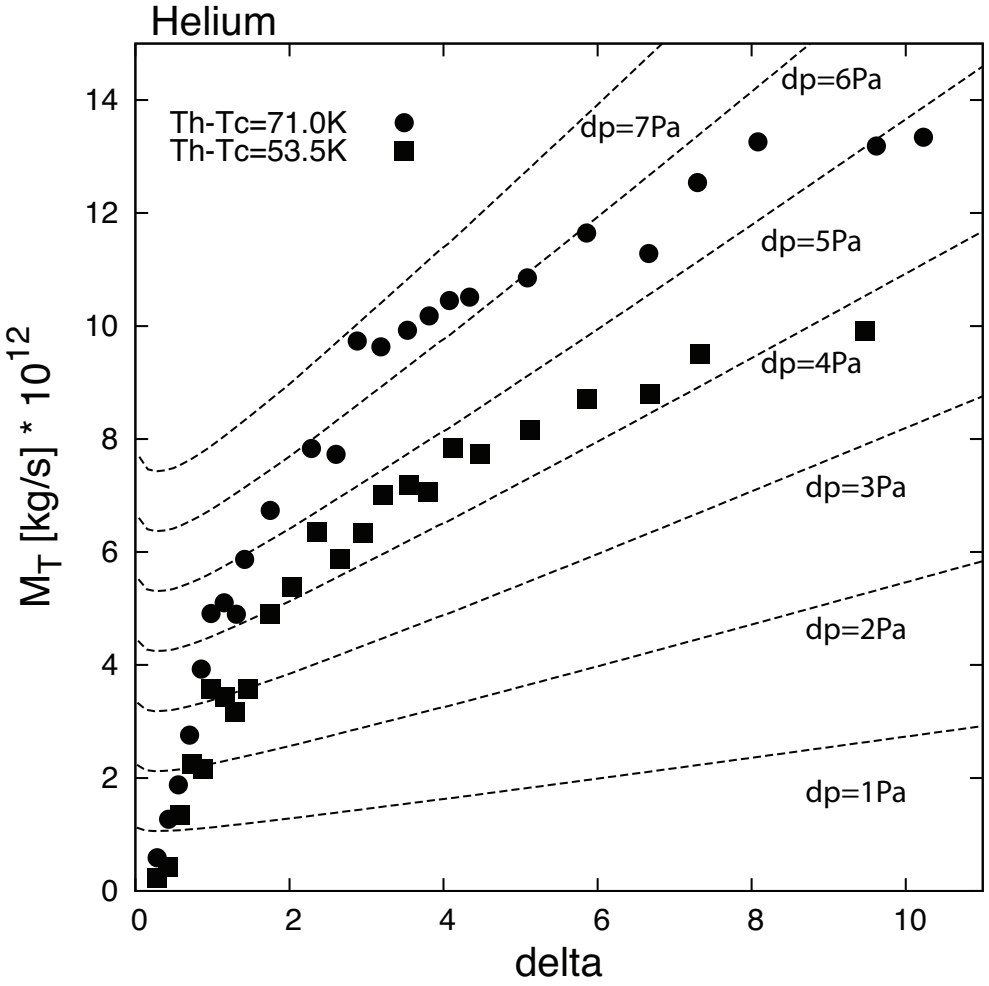

Figure 8.11: Dimensional mass flow rate in transitional regime. Thermal transpiration experiments: filled circles [○], $T_h - T_c = 71K$; filled squares [■], $T_h - T_c = 53.5K$. S-model: dashed black line [− − −] from $\Delta p = 1Pa$ to $\Delta p = 7Pa$

resented by the numerical results obtained by means of the S-model and therefore we decided to refer to the numerical results rather than to the experimental results obtained. This is due to the fact that at this stage of the measurements the experimental results for both the thermal transpiration mass flow rate and the pressure driven mass flow rate obtained for small pressure differences fluctuate too much and it would be difficult to obtain from them a precise analysis of the balance between the two flows.

Let us now extract, for a given pressure difference, the rarefaction parameter at which the balance between the isothermal Poiseuille flow and the thermal transpiration flow is reached. It is possible to see from Figure 8.11 that the balance, in the case of one pressure difference applied, is reached twice along the gas rarefaction spectrum considered. Therefore, if we consider the balance of the two flows at the point of intersection of the two curves, two solutions along the rarefaction spectrum can be found for a determined pressure driven flow of a given unique pressure difference imposed.

The intersecting points of the two flows correspond to a small pressure difference imposed at a precise rarefaction of the gas, for what concerns the Poiseuille flow, and correspond to a final pressure difference generated at a precise rarefaction condition of the gas, for what concerns the final stage of the thermal transpiration experiments (TPD).

Lets now refer to Figure 8.12 where the results obtained for TPD in the case of helium at $\Delta T = 53.5K$ are confronted to the results obtained from the balance of the two flows. It is then possible to see that effectively the two results have the same trend and they have values which we repute satisfyingly similar.

It is important to remember that the Poiseuille flow measured in the isothermal experiments was obtained at temperatures which do not correspond to the average temperature along the tube during the thermal transpiration experiments. Furthermore, we saw that the thermal transpiration mass flow rates of helium did not perfectly correspond to the numerical results found with the S-model, contrarily to the case of the mass flow rate results obtained for the heavier gases, that is argon and nitrogen, which match the S-model results. We think that the helium

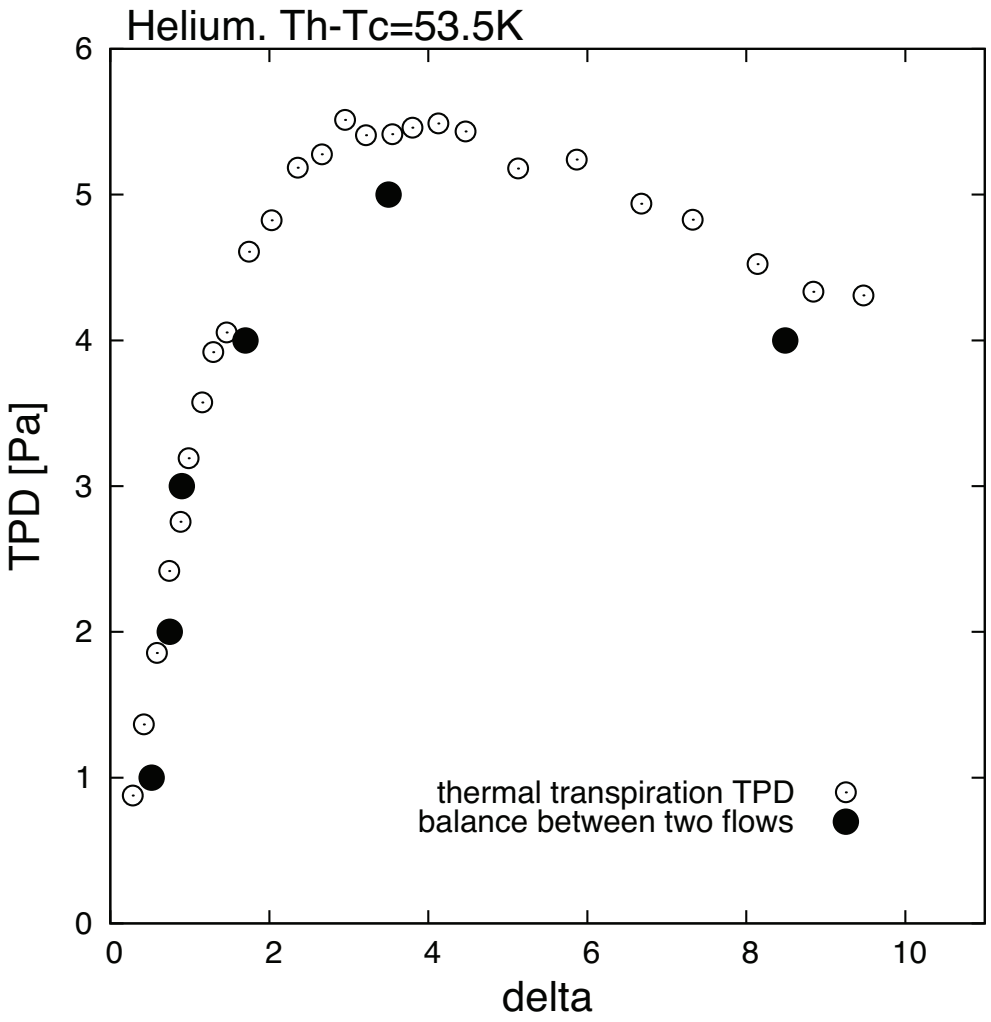

Figure 8.12: Comparison between thermal transpiration and the two flows balance results. Empty circles [○], thermal molecular pressure difference for the thermal transpiration experiment in the case of $\Delta T = 53.5K$. Filled circles [●] the two flows balance at a certain small pressure difference driven flow.

thermal transpiration mass flow rate results may be rapidly perturbed by a contrarily directed Poiseuille flow. Anyhow, we send the reader to Section 7.3.2.2 for the explanations regarding that divergence. We decided to, in any case pursue the comparison for helium and not for the heavier gases, since the TPD values which were found for helium were much higher in respect to the values found for argon and nitrogen, and therefore we assumed that it would be extremely difficult to measure an isothermal mass flow rate engendered by the low TPD values of argon and nitrogen, which are in the order of $2Pa$ and $3Pa$.

Nevertheless, if we consider that this is a first try and that both the thermal transpiration experiments and the isothermal experiments were not initially performed in order to open this kind of discussion, it is then possible to consider this preliminary results as sufficiently satisfying. By observing these preliminary results it could be possible to state that the initial assumption of Knudsen of a zero-flow stage which derives from the perfect balance of two oppositely directed flows can be considered as extremely pertinent.

These results could be of some interest since they partially explain the abrupt shifting at a given rarefaction parameter $\delta_T = 3.5$ of the tendency of the TPD, PV and PVS Section 6.3.4. To find a complete explanation would be of interest to explore the exact mechanisms behind the creation and propagation of an oppositely directed Poiseuille flow in respect to the thermal transpiration flow.

Right now, what can certainly be said on the subject is that this shift in the tendency is certainly promoted by the fact that the initial thermal transpiration mass flow rate tends to an asymptotic value at higher densities of the gas, while the Poiseuille flow grows considerably at higher densities if the same pressure difference is imposed in between the inlet and outlet of the tube.

Therefore, if the considered density of the fluid increases, the Poiseuille flow that balances the thermal transpiration flow will be engendered by continuously lower pressure differences. This could also be the explanation for the thermal transpiration phenomenon to be so difficult to measure at higher densities. Nevertheless, as it can be seen from Figure 8.11, if the thermal transpiration mass flow rate tends to a constant value going towards slip and hydrodynamic regime, the value of the

mass displaced per unit time along the inlet or outlet section of the tube could be measured at relatively high working pressures if the final TPD value stayed in the order of $1Pa$ or $2Pa$.

Chapter 9

Conclusions

The original idea behind this work was devoted to the analysis and characterization of the thermal transpiration induced mass flow rate along a micro-tube. The measurements were carried out on the basis of the constant volume technique. The measurements of the thermal transpiration mass flow rate were obtained by closely regarding the stationary phase of the transitional pressure variation with time induced by a shift in the configuration of the experimental apparatus, that is the passage from an ideal infinite reservoirs system to a finite reservoirs system. Then, by measuring the pressure variation with time and subsequently the pressure variation speed, namely at time $t = 0^+$, it was possible to deduce the stationary, fully-developed, uni-directed and not-perturbed thermal transpiration mass flow rate.

As we wanted to find a fine method to monitor the characteristic variation of pressure inside both reservoirs, we considered the exponential pressure variation with time in both reservoirs as a good starting point in order to capture the whole process, from the initial stationary transitional stage to the final zero-flow stage of the experiment. This was achieved by the successful fitting of the pressure variation with time by means of an exponential function. It was defined in within this exponential function a fitting parameter which we named the characteristic time of the thermodynamic system that was directly correlated to the timing needed by the pressure variation with time to reach its final stage of equilibrium. The characteristic time which was experimentally measured varied as a function of the rarefaction state of the gas, of the applied temperature difference, of the nature of

the analyzed gas and of the dimensions of the system itself. This pressure evolution with time appeared to us to have then a complex behavior which depended on all the before mentioned parameters.

From the pressure variation with time data analysis we concluded that it was of interest to study not only the stationary stages of the experiment, that is the initial thermal transpiration mass flow rate stage and the final zero-flow equilibrium stage, but also the whole ensemble of the time-dependent process. Particular attention was then dedicated to the manner in which the pressure variation with time depended on the stationary initial thermal transpiration mass flow rate and on the stationary final equilibrium zero-flow stage.

Furthermore, not only the pressure evolution, but also the pressure evolution speed was presented, which was a necessary element in order to relate the pressure variation with time to the macroscopic gas movement across the outlet or inlet section of the micro-tube at a given instant. Even if this method does not offer any insight in obtaining the velocity profiles along the tube, it can be considered as a first approach in order to develop an initial conception of stream line analysis which validates, in an efficient way, the initial idea of Knudsen of a zero-flow stage composed by two different and opposed flows of which the first is engendered by thermal transpiration and the other by the newly created difference of pressure.

We demonstrated through experimental measurements in which way the pressure variation speed depended on the molecular weight of the considered gas and also in which way the thermal molecular pressure exponent could be related to the accommodation of the gas to the surface of the tube.

It must be said that the accommodation of the gas to the wall can be considered of particular interest in the case where the driver of the gas movement acts only through the exchange of momentum and energy at the wall, as in the case of thermal transpiration. The gas/surface interaction becomes even more important when the number of molecular collisions with the walls is preponderant in respect to the number of intermolecular collisions, that is in free molecular or near free molecular regime. Therefore, the gas/surface interaction was considered to play a fundamental role in the experimental results obtained when comparing gases with

different molecular weights, specially in the transitional regime. From the experimental results obtained it could be possible to deduce differences in the nature of the gas/surface interaction, for the case of different gases.

Consequently, it is possible consider thermal transpiration to be an excellent test case in order to be able to extract gas/surface interaction information for what specially concerns the energy and momentum exchange at the wall which seems to depend strongly from the molecular weight of the gas.

In addition to the newly created concept of gas flows measurements for the case of thermal transpiration, we showed that with the same experimental methodology it was possible to measure also the final zero-flow equilibrium stage parameters, such as the thermal molecular pressure ratio, thermal molecular pressure difference and thermal molecular pressure exponent. We presented these parameters mainly in order to put into context our new experimental results and in order to show that the original measurement technique could offer a great package of information. Furthermore, we compared the experimental results found for the zero-flow case with the semi-empirical formulas found in the literature: we were able to state that we obtained zero-flow experimental results of relatively high quality which were in excellent agreement with the literature.

The last part of this thesis was devoted to the comparison of the stationary experimental results obtained with the numerical results obtained through the S-model kinetic equation and the direct simulation Monte Carlo method. We were able to see that effectively the experimental results matched the numerical results.

In particular we compared the thermodynamic parameter results along the tube of the DSMC method to the results of the S-model, during the initial thermal transpiration mass flow rate stage and during the final zero-flow equilibrium stage. We were able to see that the S-model and the DSMC method had a good agreement.

We would like to spend some words in particular for what concerns the results obtained for the thermal transpiration mass flow rate. The main comparison was done by regarding the experimental and the S-model results. Through this comparison and by observing the slight divergences that were present between the

experimental and the numerical results, we were able to understand in which direction our research will have to move in the future. The main problem encountered is the fact that in order to effectuate a proper comparison between experiments and numerical results we indeed need to be more aware of the temperature at which the gas effectively is at the hot-end of the tube. Let us stress the fact that in order to perform the measurement of a mass flow rate across the inlet section of the tube the temperature difference does not intervene directly and therefore none of the here proposed results could be considered in any manner to have a large margin of uncertainty.

Nevertheless, our research must move in the direction of acquiring additional knowledge on the manner on which the gas responds at the interaction with the walls of the hot-side region of the tube. Furthermore, by closely regarding the experimental results we strongly believe that this interaction is largely affected by the nature of the gas considered, where it would seem that the temperature would be better transmitted from the surface to the gas in the case of a heavy gas. A second element that deserves further investigation is the value of the heat flux as a function of the rarefaction parameter whose variation could influence the temperature at the outlet of the tube, that is in the hot-side region.

Let us conclude this chapter by giving a judgment on the efficiency of the DSMC method for the case of slow flows. We wanted to reproduce the thermal transpiration experimental results obtained by means of this method, since offered the possibility to work with the real geometry of the experimental apparatus used. Nevertheless, the dimensions of the experimental test-section used, that is the ensemble of the micro-tube and the two reservoirs, were far away of being practically realized in a DSMC frame-work, since the computations would had been excessively expensive in matter of time. Therefore, we were obliged to model the experimental test-section with dimensions which were not of the same order in respect of the ones used experimentally.

Hence, for what concerns the thermal transpiration mass flow rate results it is possible to state that even if the results obtained with the DSMC model are in good agreement with the results obtained with the S-model, it is largely more convenient to model the case which was studied experimentally by means of the

S-model approach. Nevertheless, it is necessary to keep in mind that the DSMC modeling part of this thesis had as objective to be a first step. In the future, computations will be realized for geometries that cannot be taken into account by the method used when solving the S-model kinetic equation at the present time.

References

Alexeenko, A., Gimelshein, S., Muntz, E. & Ketsdever, A. (2006). Kinetic modeling of temperature driven flows in short microchannels. *International Journal of Thermal Sciences*, **45**, 1045–1051. 53

Annis, B. (1972). Thermal creep in gases. *The Journal of Chemical Physics*, **57**, 2898. 51

Arkilic, E., Schmidt, M. & Breuer, K. (1997). Gaseous slip flow in long microchannels. *Microelectromechanical Systems, Journal of*, **6**, 167–178. 55, 82

Babovsky, H. & Illner, R. (1989). A convergence proof for nanbu's simulation method for the full boltzmann equation. *SIAM journal on numerical analysis*, 45–65. 34

Bennett, M. & Tompkins, F. (1957). Thermal transpiration: application of Liang's equation. *Transactions of the Faraday Society*, **53**, 185–192. 47, 49

Bernoulli, D. (1738). *Hydrodynamica: sive de viribus et motibus fluidorum commentarii*. 15

Bhatnagar, P., Gross, E. & Krook, M. (1954). A model for collision processes in gases. i. small amplitude processes in charged and neutral one-component systems. *Physical review*, **94**, 511. 31

Bird, G. (1963). Approach to translational equilibrium in a rigid sphere gas. *Physics of Fluids*, **6**, 1518. 33

Bird, G. (1965). Shock-wave structure in a rigid sphere gas. In *Rarefied Gas Dynamics, Volume 1*, vol. 1, 216. 33

Bird, G. (1995). Molecular gas dynamics and the direct simulation of gas flows(book). *Oxford, United Kingdom: Clarendon Press(Oxford Engineering Science Series,*. xxv, 5, 22, 33, 37, 161, 166

Boltzmann, L. (1872-1905). *Entropie und Wahrscheinlichkeit:(1872-1905)*, vol. 286. Harri Deutsch Verlag. 19

Brun, R. (1986). Transport et relaxation dans les écoulements gazeux. *Transport et relaxation dans les écoulements gazeux.. R. Brun. Masson, Paris, France. 208 pp. Price FF 180.00 (1986)*, **1**. 26

Cercignani, C. (1972). Scattering kernels for gas-surface interactions. *Transport Theory and Statistical Physics*, **2**, 27–53. xxv, 220

Cercignani, C. (2006). *Slow rarefied flows: theory and application to micro-electro-mechanical systems*, vol. 41. Springer Verlag. 27, 28, 31, 32

Cercignani, C. & Lampis, M. (1971). Kinetic models for gas-surface interactions. *transport theory and statistical physics*, **1**, 101–114. 30

Cercignani, C. & Sernagiotto, F. (1966). Cylindrical poiseuille flow of a rarefied gas. *Physics of Fluids*, **9**, 40. 50

Chapman, S. & Cowling, T. (1939). *The mathematical theory of non-uniform gases: an account of the kinetic theory of viscosity, thermal conduction, and diffusion in gases*. Cambridge Univ Pr. 19

Clausius, R. (1857). Xi. on the nature of the motion which we call heat. *The London, Edinburgh, and Dublin Philosophical Magazine and Journal of Science*, **14**, 108–127. 15

Colin, S., Lalonde, P. & Caen, R. (2004). Validation of a second-order slip flow model in rectangular microchannels. *Heat transfer engineering*, **25**, 23–30. 55, 82

Crookes, W. (1874). On attraction and repulsion resulting from radiation. *Philosophical Transactions of the Royal Society of London*, **164**, 501–527. 40

Dadzie, S. & Meolans, J. (2004). Anisotropic scattering kernel: Generalized and modified maxwell boundary conditions. *Journal of Mathematical Physics*, **45**, 1804. 30

Deryagin, B., Yalamov, Y. & Ivchenko, I. (1967). Application of the Method of Bhatnagar, Gross and Krook to the Determination of the Velocity of Thermal Slip of a Gas Past a Surface. In *Soviet Physics Doklady*, vol. 12, 362. 51

Edmonds, T. & Hobson, J. (1965). A study of thermal transpiration using ultrahigh-vacuum techniques. *Journal of Vacuum Science and Technology*, **2**, 182. 49, 108

Ewart, T., Perrier, P., Graur, I. & Gilbert Méolans, J. (2006). Mass flow rate measurements in gas micro flows. *Experiments in fluids*, **41**, 487–498. 55, 82

Ewart, T., Perrier, P., Graur, I. & Méolans, J. (2007). Tangential momentum accommodation in microtube. *Microfluidics and Nanofluidics*, **3**, 689–695. 149

Ewart, T., Firpo, J., Graur, I., Perrier, P. & Meolans, J. (2009). Dsmc simulation: Validation and application to low speed gas flows in microchannels. *Journal of Fluids Engineering*, **131**, 014501. 37, 169

Ferziger, J. (1967). Flow of a rarefied gas through a cylindrical tube. *Physics of Fluids*, **10**, 1448. 50

Graham, T. (1863). On the molecular mobility of gases. *Philosophical Transactions of the Royal Society of London*, **153**, 385–405. 15, 39

Graur, I. & Sharipov, F. (2009). Non-isothermal flow of rarefied gas through a long pipe with elliptic cross section. *Microfluidics and nanofluidics*, **6**, 267–275. 56, 161, 162, 185

Gupta, N. & Gianchandani, Y. (2008). Thermal transpiration in zeolites: A mechanism for motionless gas pumps. *Applied Physics Letters*, **93**, 193511. 54

Han, Y., Muntz, E.P., Alexeenko, A. & Young, M. (2007). Experimental and Computational Studies of Temperature Gradient–Driven Molecular Transport in Gas Flows through Nano/Microscale Channels. *Nanoscale and Microscale Thermophysical Engineering*, **11**, 151–175. 53, 55, 86, 152

Herapath, J. (1847). *Mathematical physics: or, The mathematical principles of natural philosophy: with a development of the causes of heat, gaseous elasticity, gravitation, and other great phenomena of nature*, vol. 1. Whittaker and co. 15

Huang, C., Tompson, R., Ghosh, T., Ivchenko, I. & Loyalka, S. (1999). Measurements of thermal creep in binary gas mixtures. *Physics of Fluids*, **11**, 1662. 55, 86

Joule, J. (1848). On the mechanical equivalent of heat and on the constitution of elastic fluids. *BAAS Report II*, **21**. 15

Knudsen, M. (1909). Eine revision der gleichgewichtsbedingung der gase. Thermische molekularstromung. *Annalen der Physik*, **336**, 205–229. xx, 2, 44, 152

Knudsen, M. (1935). The Kinetic Theory of Gases. Some Modern Aspects. *The Journal of Physical Chemistry*, **39**, 307–307. 14, 44

Liang, S. (1951). Some Measurements of Thermal Transpiration. *Journal of Applied Physics*, **22**, 148. 46, 49, 115, 178

Liang, S. (1953). On the calculation of thermal transpiration. *The Journal of Physical Chemistry*, **57**, 910–911. 45, 47, 49

Los, J. & Fergusson, R. (1952). Measurements of thermomolecular pressure differences on argon and nitrogen. *Transactions of the Faraday Society*, **48**, 730–738. 46, 49

Loyalka, S. (1969). Thermal transpiration in a cylindrical tube. *Physics of Fluids*, **12**, 2301. 50, 52

Loyalka, S. & Cipolla Jr, J. (1971). Thermal creep slip with arbitrary accommodation at the surface. *Physics of Fluids*, **14**, 1656. 51

Maxwell, J. (1860-1890). *The Scientific Papers of James Clerk Maxwell*, vol. 2. Dover Pubns. 16

Maxwell, J. (1867). On the dynamical theory of gases. *Philosophical Transactions of the Royal Society of London*, **157**, 49–88. 13, 16

Maxwell, J. (1873). Clerk-maxwell's kinetic theory of gases. *Nature*, **8**, 85. 16, 17

Maxwell, J. (1879). On stresses in rarified gases arising from inequalities of temperature. *Philosophical Transactions of the royal society of London*, **170**, 231–256. xix, 1, 16, 29, 41, 43, 84

McNamara, S. & Gianchandani, Y. (2005). On-chip vacuum generated by a micromachined knudsen pump. *Microelectromechanical Systems, Journal of*, **14**, 741–746. 54

Nanbu, K. (1980). Direct simulation scheme derived from the boltzmann equation. i. monocomponent gases. *J. Phys. Soc. Japan*, **49**, 2042–2049. 34

Nishizawa, S. & Hirata, M. (2002). Dsmc analysis of thermal transpiration of capacitance diaphragm gauge. *Vacuum*, **67**, 301–306. 70

Passian, A., Wig, A., Meriaudeau, F., Ferrell, T. & Thundat, T. (2002). Knudsen forces on microcantilevers. *Journal of applied physics*, **92**, 6326. 53

Passian, A., Warmack, R., Ferrell, T. & Thundat, T. (2003). Thermal transpiration at the microscale: a Crookes cantilever. *Physical review letters*, **90**, 124503. 53

Perrier, P., Graur, I., Ewart, T. & Méolans, J. (2011). Mass flow rate measurements in microtubes: From hydrodynamic to near free molecular regime. *Physics of Fluids*, **23**, 042004. 55, 82, 201, 220

Podgurski, H. & Davis, F. (1961). Thermal transpiration at low pressure. The vapor pressure of Xenon below 90K. *The Journal of Physical Chemistry*, **65**, 1343–1348. 49

Porodnov, B., Suetin, P., Borisov, S. & Akinshin, V. (1974). Experimental investigation of rarefied gas flow in different channels. *Journal of fluid mechanics*, **64**, 417–437. 55, 82

Porodnov, B., Kulev, A. & Tuchvetov, F. (1978). Thermal transpiration in a circular capillary with a small temperature difference. *Journal of Fluid Mechanics*, **88**, 609–622. 51

Reynolds, O. (1879). On certain dimensional properties of matter in the gaseous state. part i. and part ii. *Philosophical Transactions of the Royal Society of London*, **170**, 727–845. xx, 2, 39, 40

Rojas Cardenas, M., Graur, I., Perrier, P. & Meolans, J. (2011). Thermal transpiration flow: A circular cross-section microtube submitted to a temperature gradient. *Physics of Fluids*, **23**. 55

Rojas Cardenas, M., Graur, I., Perrier, P. & Meolans, J. (2012a). An experimental and numerical study of the final zero-flow thermal transpiration stage. *Journal of Thermal Science and Technology*, **7**. 55

Rojas Cardenas, M., Graur, I., Perrier, P. & Meolans, J. (2012b). Time-dependent experimental analysis of a thermal transpiration rarefied gas flow. *Journal of Fluid Mechanics - in revision*. 55

Ronney, P. (2004). Thermal transpiration pump for gaseous material driven by chemical reaction. US Patent App. 10/857,670. 53

Rosenberg, A. & Martel Jr, C. (1958). Thermal transpiration of gases at low pressures. *The Journal of Physical Chemistry*, **62**, 457–459. 48, 49

Shakov, E. (1968). Generalization of the krook kinetic equation. *Fluid Dynamics*, **3**, 95. 31

Sharipov, F. (1996). Rarefied gas flow through a long tube at any temperature ratio. *Journal of Vacuum Science & Technology A: Vacuum, Surfaces, and Films*, **14**, 2627–2635. 56

Sone, Y. (2002). *Kinetic theory and fluid dynamics*. Birkhauser. 26

Sone, Y. (2007). *Molecular gas dynamics: theory, techniques, and applications*. Birkhauser. xix, 1, 84, 149

Sone, Y. & Yamamoto, K. (1968). Flow of rarefied gas through a circular pipe. *Physics of Fluids*, **11**, 1672. 50

Sone, Y., Fukuda, T., Hokazono, T. & Sugimoto, H. (2001). Experiment on a one-way flow of a rarefied gas through a straight circular pipe without average temperature and pressure gradients. 54

Sugimoto, H. & Sone, Y. (2005). Vacuum pump without a moving part driven by thermal edge flow. In *AIP Conference Proceedings*, vol. 762, 168. 54

Sugimoto, H., Kawakami, S. & Moriuchi, K. (2008). Rarefied Gas Flows Induced through a Pair of Parallel Meshes with Different Temperatures. In *AIP Conference Proceedings*, vol. 1084, 1021. 54

Takaishi, T. & Sensui, Y. (1963). Thermal transpiration effect of hydrogen, rare gases and methane. *Transactions of the Faraday Society*, **59**, 2503–2514. 48, 49, 70, 115, 178

Van Itterbeek, A. & De Grande, E. (1947). Measurements on the thermomolecular pressure difference for hydrogen and deuterium gas at low temperatures. *Physica*, **13**, 289–304. 46

Vargo, S., Muntz, E., Shiflett, G. & Tang, W. (1999a). Knudsen compressor as a micro-and macroscale vacuum pump without moving parts or fluids. *Journal of Vacuum Science & Technology A: Vacuum, Surfaces, and Films*, **17**, 2308. 53

Vargo, S., Muntz, E. & Tang, W. (1999b). The MEMS Knudsen Compressor as a Vacuum Pump for Space Exploration Applications. In *2nd International Conference on Integrated Micro/Nanotechnology for Space Applications*. 53

Vargo, S., Green, A. & Muntz, E. (2000). Heat transfer implications in the first MEMS fabricated thermal transpiration-driven vacuum pump for gases. 53

Watkins, R., Taylor, W. & Haubach, W. (1967). Thermomolecular Pressure Difference Measurements for Precision Helium- 3 and Helium- 4 Vapor-Pressure Thermometry. *The Journal of Chemical Physics*, **46**, 1007. 49

Weber, S. & Schimdt, G. (1936). *Commun. Leiden. Rapp. et Commun.* 7^e *Congr. intern. du Froid*, **246c**, 72. 45

Welander, P. (1954). On the temperature jump in a rarefied gas. *Arkiv fysik*, **7**. 31

York, D., Chambers, A. & Chew, A. (2000). Thermal transpiration of helium and nitrogen in 50-[mu] m bore silica capillaries. *Vacuum*, **59**, 910–918. 48, 55

Young, M., Han, Y., Muntz, E., Shiflett, G., Ketsdever, A. & Green, A. (2003). Thermal transpiration in microsphere membranes. In *AIP Conference Proceedings*, 743–751, iop institute of physics publishing ltd. 53

Abstract - This thesis presents the study and analysis of rarefied gas flows induced by thermal transpiration. Thermal transpiration refers to the macroscopic movement of rarefied gas generated by a temperature gradient. The main aspect of this work is centered around the measurement of the mass flow rate engendered by subjecting a microtube to a temperature gradient along its axis. In this respect, an original experimental apparatus and an original time-dependent experimental methodology was developed. The experimental results for the initial stationary thermal transpiration mass flow rate and for the final zero-flow thermal molecular parameters were compared with the results obtained from the numerical solution of the Shakhov model kinetic equation and the direct simulation Monte Carlo method.

Keywords: thermal transpiration, MEMS, rarefied gas flow, kinetic theory